Pälike, H., Lyle, M., Nishi, H., Raffi, I., Gamage, K., Klaus, A., and the Expedition 320/321 Scientists
Proceedings of the Integrated Ocean Drilling Program, Volume 320/321

Site U1333[1]

Expedition 320/321 Scientists[2]

Chapter contents

Background and objectives

Integrated Ocean Drilling Program (IODP) Site U1333 (10°30.996′N, 138°25.159′W, 4853 meters below sea level [mbsl]) (Fig. F1; Table T1) is located about halfway between IODP Site U1332 to the northwest and the previously cored Ocean Drilling Program (ODP) Site 1218 to the southeast, both ~350 km away. This site is situated ~440 km north of the Clipperton Fracture Zone and 570 km south of the Clarion Fracture Zone (Fig. F1). Site U1333 is over seafloor basement with a estimated age of 46 Ma.

The primary coring objective at Site U1333 was to recover a complete sequence of carbonate sediments spanning the middle Eocene to Oligocene so we can evaluate changes in the temperature and structure of the near-surface ocean, bottom water temperatures, and the evolution of the calcium carbonate compensation depth (CCD).

One of the additional objectives of the Pacific Equatorial Age Transect (PEAT) program is to provide a depth transect for several Cenozoic key horizons, such as the Eocene–Oligocene transition (Coxall et al., 2005), which is being targeted at IODP Sites U1331–U1334. Site U1333 forms the third deepest paleodepth constraint, with an estimated crustal paleodepth of <4 km and a paleolatitude ~3° north of the paleoequator during the Eocene–Oligocene transition.

Good paleomagnetic stratigraphy at ODP Leg 199 sites allowed a significantly improved calibration of nannofossil and radiolarian biostratigraphic datums (Moore et al., 2004; Raffi et al., 2005; Pälike et al., 2005, 2006; Nigrini et al., 2006). From the combined information, a more detailed picture emerged of temporal variations in sediment accumulation through the middle and upper Eocene of the tropical Pacific. These data showed an increase of up to 2–3 times in accumulation rates of siliceous ooze during the middle Eocene (41–45 Ma).

There are also several notable periods of highly fluctuating CCD associated with intervals in which carbonate is preserved as deep as 4000 mbsl, or ~700 m deeper than the average Eocene CCD (Lyle, Wilson, Janecek, et al., 2002; Lyle et al., 2005; Rea and Lyle, 2005; Bohaty et al., 2009). These fluctuations occur immediately prior to the Middle Eocene Climatic Optimum (MECO), which is associated with CCD shoaling (Bohaty and Zachos, 2003; Bohaty et al., 2009). Such fluctuations in the CCD are similar in magnitude to those at the Eocene/Oligocene boundary (Coxall et al.,

[1] Expedition 320/321 Scientists, 2010. Site U1333. *In* Pälike, H., Lyle, M., Nishi, H., Raffi, I., Gamage, K., Klaus, A., and the Expedition 320/321 Scientists, *Proc. IODP,* 320/321: Tokyo (Integrated Ocean Drilling Program Management International, Inc.).
doi:10.2204/iodp.proc.320321.105.2010
[2] Expedition 320/321 Scientists' addresses.

2005). High siliceous sedimentation rates occur near an apparent short reversal in the middle Eocene cooling interval. It is difficult to interpret the cause of such a substantial change in silica flux during a very warm climatic regime.

Site U1333 is located in abyssal hill topography north of the Clipperton Fracture Zone (Fig. F1B), with a general deepening of the seafloor toward the north. Bathymetric relief across the abyssal hills is ~75–150 m, and sediment thickness is ~200 ms two-way traveltime (TWT), which coring determined to correspond to ~180 m of sediment.

The 48-channel stacked and migrated seismic reflection data (e.g., seismic Line PEAT-3C-sl-3 in Pälike et al., 2008) (Lyle et al., 2006) reveal a region where the sediment column that had been deposited is eroding away. Outcropping older horizons are common along seismic Line 1 and at the northern ends of the cross-lines. Site survey piston Core RR0603-09JC suggested that the surface sediments are composed of ~4 m of zeolitic clay and then 2 m of radiolarian clay overlying early Miocene carbonates. The carbonate section of the piston core consists of nannofossil ooze and radiolarian nannofossil ooze in meter-scale cycles. The base of the core is ~21 Ma based upon the combined radiolarian and nannofossil stratigraphy, with an average sedimentation rate of 7 m/m.y. for the cored section. We drilled Site U1333 slightly west of the intersection between seismic Lines 3 and 8 to maximize the thickness of the deeper section. The crossing point of the seismic lines was just south of a minor basement hill, and the drill site is a relatively small target, ~720 m across. The low amplitudes of the seismic reflections suggest that the sediment is not lithified, fitting in with the shallow depth to basement. An interpretation of the site survey seismic data (Fig. F2) indicated that Site U1333 might penetrate seismic reflectors P2 and P3 of Lyle et al. (2002), with P4 near the sediment surface.

We positioned Site U1333 and the other PEAT sites to the south of the estimated paleoequatorial position at a target age that would maximize the time that drill sites remain within the equatorial zone (i.e., ±2° of the equator). This allows for some southward bias of the equatorial sediment mound relative to the hotspot frame of reference (Knappenberger, 2000) and places the sediment interval of maximum interest above the basal hydrothermally altered sediments. To determine the site location, we used the digital age grid of seafloor ages from Müller et al. (1997), heavily modified and improved with additional magnetic anomaly picks from Petronotis (1991) and Petronotis et al. (1994), as well as Deep Sea Drilling Project (DSDP)/ODP basement ages. For this grid, each point is then backrotated in time to zero age, using the fixed-hotspot stage-poles from Koppers et al. (2001) and Engebretson et al. (1985) and the paleopole data from Sager and Pringle (1988). From the backtracked latitudes for each grid point we then obtained the paleoequator at the crustal age by contouring all backrotated latitudinal positions.

Science summary

Three holes were cored at Site U1333 (10°30.996′N, 138°25.159′W; 4853 mbsl) (Fig. F1; Table T1). At Site U1333, seafloor basalt is overlain by ~183 m of pelagic sediment, dominated by nannofossil and radiolarian ooze with varying amounts of clay (Fig. F3). The oldest sediment is of early middle Eocene age.

In Hole U1333A, advanced piston corer (APC)-cored sediments were recovered from ~3 m below the mudline (~4850 mbsl) to 95 m core depth below seafloor (CSF) (Core 320-U1333A-10H). Extended core barrel (XCB) coring advanced to 184.1 m drilling depth below seafloor (DSF) through an ~60 m thick sequence of lowermost Oligocene carbonate oozes and nannofossil-bearing Eocene sediments. Near the basal section, we recovered a 30 cm long interval of lithified carbonate in Core 320-U1333A-20X. The following Core 21X contained a limestone basalt breccia. A 6 cm piece of basalt was recovered in Core 320-U1333A-22X.

Coring in Hole U1333B started 5 m shallower than in Hole U1333A to recover the mudline and to span the core gaps from the first hole. A total of 7.73 m of carbonate-bearing ooze overlain by a few meters of clay were recovered in Core 320-U1333B-1H. Although the cores recovered from Hole U1333A showed significant porcellanite layers, we used the APC drillover strategy in Hole U1333B to obtain APC cores across and below the Eocene–Oligocene transition to 162.7 m CSF. We then XCB cored to basement and a total depth of 180.3 m CSF.

Hole U1333C was designed to provide stratigraphic overlap and confirm stratigraphic correlations made between Holes U1333A and U1333B. APC coring in Hole U1333C started 2.75 m shallower than in Hole U1333B and reached 163.2 m CSF before we had to switch to XCB coring. No downhole logging was conducted at Site U1333.

The sediment column at Site U1333 has a strong resemblance to that of Site 1218 (Lyle, Wilson, Janecek, et al., 2002) but with notably more carbonate-bearing sediments in the Eocene portion. The ~183 m of pelagic sediments has been divided into four major lithologic units (Fig. F4; Table T2). Unit I is ~7 m thick and contains an alternating sequence of clay, clayey radiolarian ooze, radiolarian clay, clayey nannofossil ooze, and nannofossil ooze of early Miocene age. Unit II is ~112 m thick and composed of alternating very pale brown nannofossil ooze and yellowish brown nannofossil ooze with radiolarians of early Miocene to latest Eocene age. Unit III is ~60 m thick and composed of Eocene biogenic sediments comprising clayey nannofossil ooze, nannofossil radiolarian ooze, nannofossil ooze, radiolarian nannofossil ooze, and porcellanite of latest Eocene to middle Eocene age (Unit III). Unit III is divided into two subunits, based on the absence (Subunit IIIa) or presence (Subunit IIIb) of porcellanite, which occurs between ~168 and 174 m CSF. Unit IV is a thin unit (~3.3 m) of lithified carbonate (partly limestone) and nannofossil ooze, overlying basalt (Unit V).

All major microfossil groups were found in sediments from Site U1333 and provide a consistent, coherent, and high-resolution biostratigraphic succession from basement to the top of lithologic Unit II. Shipboard biostratigraphy indicates that sediments recovered at Site U1333 span a near-continuous succession from around the lower Miocene boundary to the middle Eocene. Radiolarians are common and well preserved in the Eocene succession but less well preserved in the Oligocene sediments. A complete sequence of radiolarian zones from RN2 to RP14 (middle Eocene) was described. Initial assessment of the radiolarian assemblages across the Eocene/Oligocene boundary interval indicates a significant loss of diversity through this apparently complete succession. Although a few species from the Eocene carry through to the Oligocene, only one stratigraphic marker species (*Lithocyclia angusta*) first appears near the Eocene/Oligocene boundary. Calcareous nannofossils are present and moderately to well preserved through most of the succession, although there are some short barren intervals in the middle to upper Eocene. The succession spans a complete sequence of nannofossil zones from lower Miocene Zone NN1 to middle Eocene Zone NP15. The Oligocene/Miocene boundary is bracketed by the base of *Sphenolithus disbelemnos* in Sample 320-U1333A-2H-5, 70 cm (16.20 m CSF), and the presence of rare *Sphenolithus delphix* in Sample 320-U1332A-2H-CC (9.57 m CSF). Discoasters are very rare in basal assemblages, indicative of a eutrophic environment and consistent with the paleolatitude of this site in the early middle Eocene within the equatorial upwelling zone. Planktonic foraminifers are relatively abundant and well preserved from the lowest part of the Miocene to the lower Oligocene. Oligocene fauna is characterized by the common presence of *Catapsydrax* spp., *Dentoglobigerina* spp., and *Paragloborotalia* spp. In contrast, upper Eocene sediments contain poorly preserved specimens or are barren of planktonic foraminifers. Preservation and abundance slightly increased in some intervals of the middle Eocene, which is recognized by the presence of acarininids and clavigerinellids. The absence of the genera *Globigerinatheka* and *Morozovella* makes precise age determination of individual samples problematic. High abundances of *Clavigerinella* spp. have been linked to high-productivity environments, consistent with the paleogeographic location of this site (Coxall et al., 2007). Benthic foraminifers were almost continuously present and indicate lower bathyal to abyssal depths. Oligocene fauna is characterized by calcareous hyaline forms, such as *Nuttallides umbonifer, Oridorsalis umbonatus,* and *Cibicidoides mundulus*. *Nuttallides truempyi* and *O. umbonatus* often dominate the Eocene fauna. Benthic foraminifers are present through most of the section apart from an interval in the middle Eocene equivalent to radiolarian Zone RP16. They indicate lower bathyal to abyssal paleodepths.

Sedimentation rates at Site U1333 are ~5 m/m.y. in the middle Eocene section (~39–45 Ma), and ~4 m/m.y. between the early late Eocene and the early Oligocene (~31 Ma). In the early Oligocene, sedimentation rates increase to ~12 m/m.y. and then reach ~6 m/m.y. from the late Oligocene to the early Miocene in the upper sediment column.

Paleomagnetic results from measurements made along split-core sections and on discrete samples from Site U1333 provide a well-resolved magnetostratigraphy. Shipboard analyses suggest that a useful magnetic signal is preserved in most APC-cored intervals after removal of the drilling-induced overprint by partial alternating-field (AF) demagnetization at 20 mT. The overprint was nearly absent in those cores collected in nonmagnetic core barrels at Site U1333, whereas it was quite prominent for cores recovered in standard steel core barrels. Paleomagnetic directions from discrete samples agree well with those from split cores, confirming that AF demagnetization at 20 mT is generally sufficient to resolve the primary paleomagnetic direction regardless of which type of core barrel was used. Cleaned paleomagnetic data provide a series of distinct ~180° alternations in declination and subtle changes in inclination, which, when combined with biostratigraphic age constraints, allow a continuous magnetostratigraphy to be constructed that correlates well with the geomagnetic polarity timescale. The magnetostratigraphic record extends from the base of Chron C6n (19.722 Ma) at 1.7 m CSF in Hole U1333C to the top of Chron C20r (43.789 Ma) at 161.6 m CSF in Hole U1333C. Highlights include very high quality paleomagnetic data across Chrons C13r and C13n, which span the latest Eocene and earliest

Oligocene, and a newly recognized cryptochron within Chron 18n.1n.

Geochemistry results indicate that samples from the upper part of Site U1333 have modest $CaCO_3$ contents of 26–69 wt% between 0 and 4 m and have frequent variations between 58 wt% and up to 93 wt% in the interval between 4 and 35 m CSF. Calcium carbonate contents are consistently high (75.5–96 wt%) from 35 to 111 m CSF, whereas in the Eocene (between 111 and 171 m CSF) $CaCO_3$ contents vary abruptly between <1 and 74 wt%. The lowermost lithified carbonate rocks between 173 and 180 m CSF have high $CaCO_3$ contents between 76 and 90 wt%. TOC content, as determined by the acidification method, is generally very low. Pore water alkalinity values are never elevated, but alkalinity and dissolved strontium values are somewhat higher near the Eocene–Oligocene transition; these are generally consistent with carbonate dissolution or recrystallization processes. Dissolved silica increases with depth, with values always <1000 µM.

A full physical property program was run on cores from Holes U1333A–U1333C comprising Whole-Round Multisensor Logger (WRMSL) measurements of magnetic susceptibility, bulk density, and *P*-wave velocity; natural gamma radiation (NGR); and measurements of color reflectance, followed by discrete measurements of moisture and density properties, sound velocities, and thermal conductivity on Hole U1333A cores only. All track data show variability throughout the section, allowing a detailed correlation among holes primarily using magnetic susceptibility and density (magnetic susceptibility varies around 24×10^{-5} SI in radiolarian ooze–dominated sections and ~3×10^{-5} SI in more carbonate rich intervals). Magnetic susceptibility values gradually increase uphole. NGR measurements are elevated by an order of magnitude in the uppermost clays and increase near the lower Oligocene at ~115 m CSF (from 5 to 8 counts per second [cps]). *P*-wave velocity gradually increases downhole as we move from carbonate- to radiolarian-dominated successions. *P*-wave velocity generally varies between 1490 and 1560 m/s depending on lithology, with lower velocities corresponding more to carbonate-rich sections. Bulk density and grain density show a marked decrease at ~112 m CSF (~1.70 to 1.31 g/cm³ in bulk density), where carbonate content decreases rapidly. Porosity values are generally high in the radiolarian-rich sediments (80%) and decrease in the carbonate-rich section (~60%). Thermal conductivity measurements are increased in carbonate-rich intervals and range from ~0.8 W/(m·K) in lithologic Unit I to 1.2–1.3 W/(m·K) in lithologic Unit II.

Stratigraphic correlation indicated that a complete section was recovered to ~130 m CSF in the upper Eocene, equivalent to a composite depth of ~150 m CCSF-A (see **"Core composite depth scale"** in the "Methods" chapter). For Site U1333, a growth factor of 15% is estimated from the ratio between the CCSF-A and CSF (formerly meters composite depth [mcd] and meters below seafloor [mbsf]) depth scales. Stratigraphic correlation with Site 1218 suggests a complete stratigraphic section in the Oligocene to uppermost Eocene interval.

Five formation temperature measurements were conducted in Hole U1333B with the advanced piston corer temperature tool (APCT-3). These temperature measurements, when combined with thermal conductivity values obtained from the cores, indicate that Site U1333 has a heat flow of 42.3 mW/m² and a thermal gradient of 37.9°C/km.

Highlights

High carbonate fluctuations in middle Eocene sediments

Coring at Site U1333 was designed to capture a time interval when the CCD was slightly deeper within the middle Eocene interval that showed prominent fluctuations of carbonate content (Lyle et al., 2005). This interval occurs during the cooling that took place after the Early Eocene Climatic Optimum (EECO) (Zachos et al., 2001) and before the Eocene–Oligocene transition (e.g., Coxall et al., 2005). Unlike Site 1218, Site U1333 sediments show carbonate contents >75 wt% in this interval at a deeper water depth and apparently coeval with the CCD cycles described by Lyle et al. (2005). Basal lithologic Unit IV recovered partially lithified carbonates.

MECO, Eocene–Oligocene and Oligocene–Miocene transitions, and depth transects

Site U1333 forms the third oldest and deepest component of the PEAT depth transect component and can be directly compared with Site 1218, which will allow the study of critical intervals (such as the Eocene–Oligocene transition; see Coxall et al., 2005) and variations of the equatorial CCD. Site U1333 is estimated to have been ~3.8 km deep during the Eocene–Oligocene transition, ~1 km shallower than today and 200 m shallower at that time than Site U1332. Carbonate content in these sediments does not change as rapidly as at the deeper and older Sites U1332 and U1333. Some of these sediments appear to be Eocene–Oligocene transition sediments that are suitable for paleoceanographic studies using carbonate-based geochemical proxies and thus are an improvement over Site 1218. Of note, Site U1333 also contains high carbonate content–bearing sediments around the MECO event (Bohaty and Zachos, 2003; Bohaty et al., 2009), allowing a detailed study of the sequence of events linking carbonate preservation cycles (Lyle et al., 2005) with climatic oscillations.

Carbonate-bearing sediments across the Oligocene–Miocene transition were also recovered at Site U1333, adding important data to the study of this time interval in the context of the PEAT Oligocene/Miocene depth transect.

Age transect of seafloor basalt

At Site U1333 we recovered what appear to be fresh fragments of seafloor basalt overlain by sediments aged 45 to 46 Ma as estimated from biostratigraphic results. This material will, when combined with other PEAT basalt samples, provide important sample material for the study of seawater alteration of basalt.

Operations

Unless otherwise noted, times are local ship time, which was Hawaii Standard Time (UTC – 10 h) for Site U1333.

Transit to Site U1333

The 176 nmi voyage to Site U1333 took 18.3 h and was accomplished at an average speed of 9.6 kt. The journey required a little more than the allotted time because the speed was adversely affected by having to sail into a 22–26 kt wind and a strong current.

Site U1333

Hole U1333A

At 1400 h on 30 March 2009, the vessel began positioning over the site in dynamic positioning (DP) mode. Once the drilling assembly was deployed, the driller carefully lowered the bit and tagged the seafloor at ~4875 m drilling depth below rig floor (DRF). The bit was raised 10 m, and Hole U1333A was spudded at 1225 h on 31 March. The seafloor depth calculated from the recovery of the first core was 4865.0 m DRF (4853.7 mbsl) (Table T1); however, this depth measurement is questionable because the recovery was a full core (10.05 m).

APC Cores 320-U1333C-1H through 10H were taken from 0 to 95.0 m DSF, and we recovered 104 m (109%) (Table T1). We switched to XCB coring after the core barrel for Core 10H had to be drilled over to free the fully stroked core barrel from the sediment. All APC cores were obtained with nonmagnetic core barrels; the FlexIt orientation tool was not deployed since there were questions about its data reliability.

XCB Cores 11X through 22X penetrated from 95.0 to 184.1 m DSF, and we recovered 77.0 m (87%). Coring ended when we recovered basalt in Core 22X. The drill string was pulled out of the hole and cleared the seafloor at 1155 h on 1 April.

Hole U1333B

The vessel was offset 25 m east of Hole U1333A, and APC coring in Hole U1333B started at 1305 h on 1 April with the bit 5 m shallower than the first hole. We recovered 7.7 m in Core 1H, so the seafloor was established at 4861.8 DRF (4850.5 mbsl).

Based on drilling and coring data from the first hole, the drillers were confident that by drilling over stuck core barrels, the APC could safely be pushed deeper than the 95.0 m penetration that was realized in the first hole. This confidence was justified when APC Cores 1H through 18H were advanced to 162.7 m DSF and we recovered 166.4 m (102%). Nonmagnetic core barrels were used on Cores 1H through 9H, and standard steel core barrels were deployed on all subsequent piston cores. Formation temperature measurements were made with the APCT-3 tool at 26.7, 45.7, 64.7, and 83.7 m DSF (Cores 3H, 5H, 7H, and 9H, respectively). The FlexIt orientation tool was not used. Three stuck core barrels (Cores 13H, 16H, and 17H) required drilling over when they could not be released from the sediment despite 70,000 lb of overpull. Core 18H failed to achieve a full stroke of the core barrel, and no further APC coring was conducted.

Two XCB cores advanced the hole from 162.7 to the final depth of 180.3 m DSF, and we recovered 13.44 m (76%). Coring ended when we recovered basalt in Core 20X. The drill string was pulled out of the hole and cleared the seafloor at 1845 h on 2 April.

Hole U1333C

Hole U1333C was started 25 m east of and 2.75 m shallower than Hole U1333B. Core 320-U1333C-1H was shot at 2000 h on 2 April and we recovered 1.65 m, so the water depth for this hole is 4865.1 m DRF (4853.8 mbsl).

Cores 1H through 21H penetrated from 0 to 163.2 m DSF, and we recovered 176.1 m (108%). Seven core barrels (Cores 13H through 19H) required drilling over to release the barrels from the sediment when the application of 70,000 lb of overpull was not successful. Nonmagnetic core barrels were used on Cores 1H through 13H. Standard steel core barrels were used on all subsequent APC cores. The advancement of four cores was adjusted to maintain the overlap with previous holes: Cores 11H (6.0 m advance), 12H (5.0 m advance), 16H (4.5 m advance), and 19H (4.0 m advance). All other cores advanced the full 9.5 m except for Core 21H, which did not penetrate into the formation at all. We subsequently switched to XCB coring.

XCB Cores 22X through 24X penetrated from 163.0 to 177.0 m DSF, and we recovered 0.87 m (6%). Coring in this hole ended when we recovered basaltic basement in the last core.

Once the seafloor beacon was recovered on board, the drill string recovered on the rig floor, the thrusters raised, and the drilling equipment secured, the vessel departed for the Site U1334 at 1815 h on 4 April.

Lithostratigraphy

At Site U1333, Eocene seafloor basalt is overlain by ~183 m of pelagic sediments that are divided into four major lithologic units (Fig. **F4**). Lithostratigraphic Unit I is ~7 m thick and contains an alternating sequence of clay, clayey radiolarian ooze, radiolarian clay, clayey nannofossil ooze, and nannofossil ooze of early Miocene age (see **"Biostratigraphy"** and **"Paleomagnetism"**). These sediments overlie ~112 m of alternating very pale brown nannofossil ooze and yellowish brown nannofossil ooze with radiolarians of early Miocene to latest Eocene age (Unit II). Unit III consists of ~60 m of clayey radiolarian ooze and clayey nannofossil ooze, nannofossil radiolarian ooze, nannofossil ooze, radiolarian nannofossil ooze, and porcellanite of latest Eocene to middle Eocene age. Unit III is divided into two subunits (IIIa and IIIb) based on the occurrence of porcellanite (Subunit IIIb only). At the base of Hole U1333A a thin (~3.3 m thick) unit of nannofossil ooze and foraminifer-bearing limestone (Unit IV) overlies basalt of middle Eocene age (Unit V). Lithologic unit and subunit boundaries are also defined by differences in physical property data series. Lithologic differences, based on visual core descriptions and smear slide and thin section analysis (Table **T2;** Fig. **F4;** see **"Site U1333 smear slides"** in "Core descriptions"), are primarily attributable to varying distributions of biogenic components (e.g., nannofossils and radiolarians) and clay-sized lithogenic material. Lithologic descriptions are largely based on sediments recovered in Hole U1333A, supplemented with observations from Holes U1333B and U1333C.

Unit I

Intervals: 320-U1333A-1H-1, 0 cm, through 1H-3, 135 cm; 320-U1333B-1H-1, 0 cm, through at least 1H-CC, 18 cm (base not recovered); 320-U1333C-1H-1, 0 cm, through 2H-3, 40 cm
Depths: Hole U1333A = 0.0–4.35 m CSF; Hole U1333B = 0.0–7.66 m CSF; Hole U1333C = 0.0–5.00 m CSF
Age: early Miocene
Lithology: clay, clayey radiolarian ooze, radiolarian clay, clayey nannofossil ooze, and nannofossil ooze

The major lithologies in Unit I are dark brown (10YR 3/3) clay, dark brown (10YR 3/3) clayey radiolarian ooze, dark yellowish brown (10YR 4/4) radiolarian clay, dark brown (10YR 3/3) clayey nannofossil ooze, and very pale brown (10YR 7/3) to light yellowish brown (10YR 6/4) nannofossil ooze. Sometimes clay occurs with nannofossils and radiolarians, whereas both clayey radiolarian ooze and radiolarian clay occur with nannofossils. Both clayey nannofossil ooze and nannofossil ooze occur with radiolarians and clay. Unit I is characterized by a downhole alternation of dark brown clayey radiolarian ooze with nannofossils and very pale brown nannofossil ooze. Bioturbation intensity is minor in these sediments. Typically, Unit I is marked by higher magnetic susceptibility values, lower gamma ray attenuation (GRA) bulk densities, lower L* reflectance (lightness), and lower $CaCO_3$ content than Unit II (Fig. **F4;** see **"Physical properties"** and **"Geochemistry"**). The boundary between Unit I and underlying Unit II is defined by a downhole transition in lithology to an absence of clay as a major component.

Unit II

Intervals: 320-U1333A-1H-3, 135 cm, through 13X-4, 150 cm; 320-U1333B-3H-CC, 18 cm, through 13H-6, 55 cm; 320-U1333C-2H-3, 40 cm, through at least 14H-CC, 22 cm (base not recovered)
Depths: Hole U1333A = 4.35–116.30 m CSF; Hole U1333B = 7.66–120.25 m CSF; Hole U1333C = 5.00–117.57 m CSF
Age: early Miocene to late Eocene
Lithology: nannofossil ooze

Unit II is dominated by white (10YR 8/1) to very pale brown (10YR 7/3 and 10YR 8/2) to light yellowish brown (10YR 6/4) and yellowish brown (10YR 5/4) nannofossil ooze. Within the major lithology, alternations of predominantly very pale brown (10YR 8/2 to 10YR 7/4) nannofossil ooze and yellowish brown (10YR 5/4) nannofossil ooze with radiolarians occur in the uppermost part of the sequence (Cores 320-U1333A-2H through 4H). These sediments are deposited immediately above an alternating sequence of white (10YR 8/1), light gray (10YR 7/2), and very pale brown (10YR 7/3) nannofossil ooze (Cores 320-

U1333A-4H through 13H). At the base of Unit II, white nannofossil ooze shows increasing alternation with very pale brown (10YR 8/2) nannofossil ooze with diatoms and with very pale brown (10YR 7/4) nannofossil ooze with diatoms and radiolarians. Bioturbation intensity is typically minor to nonvisible within Unit II. Baseline magnetic susceptibility values are generally low in Unit II with greatest amplitude of variability in the uppermost part (Cores 320-U1333A-2H through 4H). GRA bulk density, L*, and $CaCO_3$ values are all high in Unit II relative to Unit I with significant variations in the uppermost part (Fig. F4; see "Physical properties"). The pronounced variability of physical property data in these sediments occurs in association with alternations of very pale brown (10YR 7/4) nannofossil ooze and yellowish brown (10YR 5/4) nannofossil ooze with radiolarians. Pumice clasts (0.5–2 cm) are occasionally found in Unit II. Thin section analysis indicates fine volcanic glass (shards typically 10–500 µm in diameter) with vesicules and plagioclase as a minor component (crystal size = 50–100 µm in diameter; Sample 320-U1333A-3H-6, 148–149 cm) (Fig. F5; see "Site U1333 smear slides" in "Core descriptions"). Pumice clast margins and some vesicules and pores are filled with nannofossil ooze. The boundary between Unit II and underlying Unit III is defined by the occurrence of clay as major component in the lithology in Unit III.

Unit III

Intervals: 320-U1333A-13X-4, 150 cm, through 20X-2, 82 cm; 320-U1333B-13H-6, 55 cm, through at least 20X-CC, 0 cm (boundary not recovered); 320-U1333C-14H-CC, 22 cm, through at least 23X-CC, 7 cm (boundary not recovered)

Depths: Hole U1333A = 116.30–179.92 m CSF; Hole U1333B = 120.25–178.17 m CSF; Hole U1333C = 117.57–172.87 m CSF

Age: late Eocene to middle Eocene

Lithology: clayey radiolarian ooze, clayey nannofossil ooze, nannofossil radiolarian ooze, nannofossil ooze, radiolarian nannofossil ooze, radiolarian ooze, nannofossil ooze, and porcellanite

The major lithologies in Unit III are dark yellowish brown (10YR 4/4) to very dark grayish brown (10YR 3/2) clayey radiolarian ooze, dark brown (10YR 3/3) clayey nannofossil ooze, very pale brown (10YR 7/3) to brown (10YR 5/3) nannofossil ooze, dark brown (10YR 3/3) nannofossil radiolarian ooze, grayish brown (10YR 5/2) to light yellowish brown (10YR 6/4) nannofossil ooze, pale brown (10YR 6/3) to brown (10YR 4/3 and 10YR 5/3) to yellowish brown (10YR 5/4) radiolarian nannofossil ooze, and brown (10YR 4/3) to dark brown (10YR 3/3) radiolarian ooze and porcellanite. In general, downhole changes in physical properties (magnetic susceptibility, GRA bulk density, and L*) correspond to changes in $CaCO_3$ content within Unit III (see Fig. F4). The Subunit IIIa/IIIb boundary is defined by the uppermost occurrence of porcellanite. The Unit III/IV boundary is defined by the uppermost occurrence of nannofossil ooze and limestone.

Subunit IIIa

Intervals: 320-U1333A-13X-4, 150 cm, through 19X-1, 10 cm; 320-U1333B-13H-6, 55 cm, through at least 18H-CC, 22 cm (boundary not recovered); 320-U1333C-14H-CC, 22 cm, through at least 22X-CC, 9 cm (boundary not recovered)

Depths: Hole U1333A = 116.30–168.10 m CSF; Hole U1333B = 120.25–162.94 m CSF; Hole U1333C = 117.57–163.29 m CSF

Age: late Eocene to middle Eocene

Lithology: clayey radiolarian ooze, nannofossil radiolarian ooze, radiolarian nannofossil ooze, radiolarian ooze, and nannofossil ooze

Subunit IIIa is distinguished from Subunit IIIb by the absence of porcellanite in Subunit IIIa. The major lithologies in Subunit IIIa are dark yellowish brown (10YR 4/4) to very dark grayish brown (10YR 3/2) clayey radiolarian ooze, very pale brown (10YR 7/3) to light yellowish brown (10YR 6/4) and brown (10YR 5/3) to grayish brown (10YR 5/2) nannofossil ooze, dark brown (10YR 3/3) nannofossil radiolarian ooze, pale brown (10YR 6/3) to brown (10YR 4/3 and 10YR 5/3) to yellowish brown (10YR 5/4) radiolarian nannofossil ooze, and brown (10YR 4/3) to dark brown (10YR 3/3) radiolarian ooze. Sometimes clayey radiolarian ooze occurs with nannofossils, nannofossil radiolarian ooze and radiolarian nannofossil ooze occur with clay, radiolarian ooze occurs with clay and nannofossils, and nannofossil ooze occurs with diatoms and radiolarians. On a decimeter to meter scale, three types of alternations are common:

1. Brown to pale brown radiolarian nannofossil ooze and brown to dark brown nannofossil radiolarian ooze,
2. Very dark grayish brown clayey radiolarian ooze and yellowish brown nannofossil radiolarian ooze, and
3. Very dark grayish brown clayey radiolarian ooze and brown clayey radiolarian ooze.

Bioturbation is moderate to intense in these sediments. GRA bulk density, L*, and $CaCO_3$ content show high-amplitude variations, with lowest values in Sections 320-U1333A-15X-4 through 16X-5 (Fig. F4; see "Physical properties"). Generally, magnetic susceptibility values in Subunit IIIa are ~30 × 10^{-5} SI higher than in Unit II (Fig. F4; see "Physical properties"). Microfaults occur in intervals 320-U1333A-18X-4, 80–87 cm, and 320-U1333B-18H-3, 26–28 cm, within stiff light yellowish brown (10YR 6/4) nannofossil ooze with radiolarians and dark yellowish brown (10YR 4/4) clayey radiolarian ooze. The boundary to underlying Subunit IIIb is defined by the uppermost occurrence of porcellanite.

Subunit IIIb

Intervals: 320-U1333A-19X-1, 10 cm, through 20X-2, 82 cm; 320-U1333B-19X-1, 0 cm, through at least 20X-CC, 0 cm (boundary not recovered); 320-U1333C-22X-CC, 9 cm, through at least 23X-CC, 7 cm (boundary not recovered)
Depths: Hole U1333A = 168.10–179.92 m CSF; Hole U1333B = 162.7–178.17 m CSF; Hole U1333C = 163.29–172.87 m CSF
Age: middle Eocene
Lithology: nannofossil ooze, radiolarian ooze, clayey nannofossil ooze, clayey radiolarian ooze, and porcellanite

Subunit IIIb is distinguished from Subunit IIa by the presence of porcellanite. The dominant lithologies in Subunit IIIb are yellowish brown (10YR 5/4) to brown (10YR 4/3) nannofossil ooze, dark brown (10YR 3/3) clayey nannofossil ooze, brown (10YR 3/3) radiolarian ooze, and brown porcellanite. Sometimes nannofossil ooze occurs with clay and radiolarians, radiolarian ooze occurs with clay, and clayey radiolarian ooze occurs with nannofossils. Bioturbation intensity in these sediments is minor. GRA bulk density, L*, $CaCO_3$ content, and magnetic susceptibility all increase downhole across the Subunit IIIb/Unit IV boundary. The boundary between Unit III and underlying Unit IV is defined by the uppermost occurrence of nannofossil ooze and limestone.

Unit IV

Intervals: 320-U1333A-20X-2, 82 cm, through at least 21X-CC, 0 cm (boundary not recovered); 320-U1333B-20X-CC, 0 cm, through at least 20X-CC, 17 cm (boundary not recovered); 320-U1333C-23X-CC, 7 cm, through at least 24X-CC, 16 cm (boundary not recovered)
Depths: Hole U1333A = 179.92–181.60 CSF; Hole U1333B = 178.17–178.34 CSF; Hole U1333C = 172.87–176.16 m CSF
Age: middle Eocene
Lithology: nannofossil ooze, limestone

The dominant lithology in Unit IV is white (10YR 8/1) to light gray (10YR 7/2) limestone with green flecks and very pale brown (10YR 7/4 and 10YR 8/2) nannofossil ooze. A small basalt fragment in Sample 320-U1333A-21X-CC, 2–5 cm, is found above an 11 cm thick white limestone with green flecks. GRA bulk density, L*, and $CaCO_3$ content are marked by lower values compared to Subunit IIIb (Fig. F4; see "Physical properties").

Unit V

Intervals: 320-U1333A-21X-CC, 0 cm, through at least 22X-CC, 5 cm (boundary not recovered); 320-U1333B-20X-CC, 17 cm, through at least 20X-CC, 40 cm (boundary not recovered); 320-U1333C-24X-CC, 16 cm, through at least 24X-CC, 38 cm (boundary not recovered)
Depths: Hole U1333A = 181.60–182.65 CSF; Hole U1333B = 178.34–178.57 m CSF; Hole U1333C = 176.16–176.38 m CSF
Age: middle Eocene
Lithology: basalt and breccia of limestone and basalt

Fine-grained fresh basalt fragments were recovered at the base of each hole drilled at Site U1333. A breccia of limestone and basalt was recovered in Section 320-U1333A-21X-CC.

Sediments across the Oligocene–Miocene transition

A complete record of the Oligocene–Miocene transition was recovered at Site U1333 (Fig. F6). In Hole U1333B the Oligocene–Miocene transition is captured in a single core (Core 320-U1333B-3H). The Oligocene/Miocene boundary is defined by the first occurrence of planktonic foraminifer *Paragloborotalia kugleri* (see "Biostratigraphy"). Both this datum and the last occurrence of the nannofossil datum *S. delphix* are observed in Core 320-U1333A-2H (see "Biostratigraphy"). The sediments across the Oligocene–Miocene transition at Site U1333 are marked by an alternating sequence of very pale brown (10YR 8/3 to 10YR 7/3) nannofossil ooze and yellowish brown (10YR 5/4) nannofossil ooze with radiolarians to brown (10YR 4/3) radiolarian nannofossil ooze with clay (Figs. F4, F6; see "Site U1333 smear slides" in "Core descriptions"). Holes U1333B and U1333C are marked by correlative variations of magnetic susceptibility (see "Physical properties;" Figs. F4, F6). An excellent magnetostratigraphy is available for Site U1333 (Fig. F6; see "Magnetostratigraphy"). In Hole U1333B the Oligocene–Miocene transition corresponds to magnetic Subchrons C6Cn.2n to C6Cn.3n. Section 320-U1333A-2H-5 is characterized by an interval of drilling disturbance (flow-in), obscuring the magnetic susceptibility signal.

Sediments across the Eocene–Oligocene transition

An Eocene–Oligocene transition was recovered in all three holes drilled at Site U1333 (Figs. F4, F7). The absence of the planktonic foraminifer biostratigraphic marker (*Hantkenina*) means that the Eocene/Oligocene boundary cannot be formally identified at Site U1333 (see "Biostratigraphy"). Radiolarian and nannofossil bio- and magnetostratigraphy provide excellent age control, however, indicating that the Eocene/Oligocene boundary falls between the base of Chron 13n and the Biozone RP20/RP19 boundary (within Cores 320-U1333C-14H and 320-U1333B-13H and between Cores 320-U1333A-12X and 13X) (Fig. F7).

The lithostratigraphy of the Eocene–Oligocene transition is well captured in all three holes at Site U1333, and in Holes U1333B and U1333C it falls within a single APC core. In Core 320-U1333B-13H a downhole transition takes place from white (10YR 8/1) to very pale brown (10YR 7/3) nannofossil ooze to alternations of very pale brown (10YR 7/4) nannofossil ooze with radiolarians (and between 5% and 10% diatoms) and yellowish brown (10YR 5/4) radiolarian ooze and finally to alternations of brown (10YR 5/3) radiolarian nannofossil ooze with clay and (10YR 4/2) dark grayish brown clayey radiolarian ooze (Figs. F5, F7). Thus, the Eocene–Oligocene transition is marked by a distinct stepwise color change from very pale brown nannofossil ooze to alternations of darker radiolarian nannofossil ooze and clayey radiolarian ooze. Associated pronounced downhole stepwise increases occur in magnetic susceptibility, a*, and b*, together with pronounced downhole decreases in GRA bulk density, L*, and $CaCO_3$ content (see "Physical properties;" Figs. F4, F7). These lithostratigraphic results for the Eocene–Oligocene transition at Site U1333 are broadly consistent with those obtained from Sites U1331 and U1332 and multiple sites drilled during ODP Leg 199, in particular with those of Site 1218 (Shipboard Scientific Party, 2002a, 2002b).

Porcellanite layers

Multiple distinct dark brown (10YR 3/3) to dark yellowish brown (10YR 4/4) porcellanite intervals occur in Subunit IIIb in all holes at Site U1333 interbedded with nannofossil ooze of Eocene age (calcareous nannofossil Zone NP15) (Figs. F4, F8; see "Site U1333 smear slides" in "Core descriptions"). Five porcellanite layers occur in Sections 320-U1333A-19X-4 (173.60–173.91 m CSF) and 320-U1333B-19X-1 (162.70–163.73 m CSF) with a typical thickness of 3 to 8 cm. Porcellanite fragments recovered in Sections 320-U1333C-19X-CC (169.45–169.84 m CSF) and 22X-CC (163.50–163.59 m CSF) are interpreted as drilling disturbance associated with penetration of similar layers (see "Site U1333 smear slides" in "Core descriptions").

Summary

At Site U1333, Eocene seafloor basalt (Unit V) is overlain by 183 m of pelagic sediments that are divided into four major lithologic units (I–IV), and Unit III is divided into two subunits. Site U1333 sediments are dominated by nannofossil and radiolarian ooze with varying amounts of clay and can be correlated with Site 1218 using biostratigraphic, magnetostratigraphic, and cyclostratigraphic (magnetic susceptibility and GRA density) results (see "Stratigraphic correlation and composite section"). Basal limestone and nannofossil ooze (Unit IV) of middle Eocene age is overlain by a clayey radiolarian ooze, clayey nannofossil ooze, and porcellanite, also of middle Eocene age. The immediately overlying sediments are dominated by alternations of clayey radiolarian ooze, nannofossil radiolarian ooze, radiolarian nannofossil ooze, radiolarian ooze, and nannofossil ooze of middle to late Eocene age. In turn, these sediments are overlain by alternating sequences of predominantly white and very pale brown nannofossil ooze, as well as yellowish brown nannofossil ooze with radiolarians of early Oligocene through early Miocene age. The uppermost sediments at Site U1333 comprise an alternating sequence of clay, clayey radiolarian ooze, radiolarian clay, clayey nannofossil ooze, and nannofossil ooze of early Miocene age.

Multiple distinct porcellanite layers were found at Site U1333 interbedded with nannofossil ooze of Eocene age. The Oligocene–Miocene transition at Site U1333 is marked by an alternating sequence of very pale brown nannofossil ooze and yellowish brown nannofossil ooze with radiolarians through brown radiolarian nannofossil ooze with clay. The Eocene–Oligocene transition at Site U1333 is marked by a distinct downhole color change from pale nannofossil ooze with radiolarians to alternations of brown radiolarian nannofossil ooze with clay and dark grayish brown clayey radiolarian ooze. A transition from Eocene siliceous sedimentation to Oligocene carbonate deposition is also observed in sediments from several other sites in the equatorial Pacific Ocean (e.g., ODP Sites 1218 and 1219 and DSDP Sites 161 and 162).

Biostratigraphy

At Site U1333, we recovered a 183 m thick sequence of lower Miocene to middle Eocene nannofossil ooze, radiolarian ooze, and radiolarian clays. The uppermost 2 m of clay is barren of calcareous microfossils but contains radiolarians of early Miocene age. Nannofossil ooze is dominant in the thick Oligocene section, and radiolarian clays and nannofossil ooze are dominant in the Eocene. Radiolarians are present through most of the section and are well preserved in the Eocene. They provide a coherent, high-resolution biochronology, and there appears to be a complete sequence of radiolarian zones from Zones RN1 (lower Miocene) to RP13 (middle Eocene). Calcareous nannofossils are present and moderately to well preserved through most of the succession, although there are some short barren intervals around the middle to upper Eocene boundary. The succession comprises an apparently complete sequence of nannofossil zones from the lower Miocene Zone NN1 to the middle Eocene Zone NP15. Nannofossil datum and zonal determinations agree well with radiolarian biostratigraphy. An integrated calcareous and siliceous microfossil biozonation is shown in Figure **F9.** A detailed age-depth plot including biostratigraphic and paleomagnetic datums is shown in Figure **F10.** Planktonic foraminifers are relatively abundant and well preserved from the lowest part of the Miocene to the lower Oligocene and less abundant but moderately preserved in the middle Eocene. They are poorly preserved or absent in the upper Eocene. Benthic foraminifers are present through most of the section and indicate lower bathyal to abyssal paleodepths.

Calcareous nannofossils

Calcareous nannofossil biostratigraphy is based on analysis of core catcher samples from all three holes and from samples from each core section, predominantly from Hole U1333A. Depth positions and age estimates of biostratigraphic marker events are shown in Table **T3.** Nannofossils are abundant in the nannofossil ooze of the Oligocene and are present, and often abundant, through the Eocene and Miocene. Barren intervals occur in the uppermost 2 m (Core 320-U1333B-1H) and the upper middle Eocene (Core 320-U1333A-16X). In nannofossil ooze lithologies, nannofossil preservation is moderate to good. Increased etching is observed in darker cycles that are dominated by radiolarians.

The interval from Samples 320-U1333A-1H-2, 110 cm, to 4H-CC (1.10–38.60 m CSF) consists of brown radiolarian nannofossil clay that contains low diversity but abundant and moderately preserved nannofossil assemblages dominated by *Discoaster deflandrei, Cyclicargolithus floridanus,* and *Triquetrorhabdulus carinatus*. Age-diagnostic taxa are rare, but the assemblages are typical of Zone NN1 (lower Miocene–upper Oligocene). The base of *S. disbelemnos* in Sample 320-U1333A-2H-5, 70 cm (16.20 m CSF), and the occurrence of rare *S. delphix* in Sample 320-U1333A-2H-CC (19.57 m CSF) bracket the Oligocene/Miocene boundary.

The Oligocene interval, Cores 320-U1333A-5H through 13H, is composed of white nannofossil ooze, which contains abundant nannofossil assemblages that are moderately to well preserved. Nannofossil Zones NP25 through NP22 are recognized using the top and base of *Sphenolithus ciperoensis* in Samples 320-U1333A-4H-6, 70 cm (36.70 m CSF), and 5H-4, 70 cm (43.20 m CSF), respectively; the top of *Reticulofenestra umbilicus* in Sample 320-U1333A-11X-CC (101.17 m CSF); and the top of *Coccolithus formosus* in Sample 320-U1333A-12X-4, 70 cm (105.90 m CSF). The crossover from *Triquetrorhabdulus longus* to *T. carinatus* is an intra–Zone NP25 event (24.7 Ma) and occurs between Samples 320-U1333A-3H-CC (28.87 m CSF) and 4H-1, 70 cm (29.20 m CSF). The top of *Sphenolithus predistentus* occurs in Sample 320-U1333A-5H-4, 70 cm (67.4 m CSF), and confirms the Zone NP24 designation. The base of *Sphenolithus distentus* is an intra–Zone NP23 datum and occurs in Sample 320-U1333A-9H-3, 50 cm (79.50 m CSF).

The Eocene/Oligocene boundary interval lies between the top of *C. formosus* (Sample 320-U1333A-12X-4, 70 cm; 105.90 m CSF) and the top of *Discoaster saipanensis* (Sample 320-U1333A-13X-3, 140 cm; 114.70 m CSF). The boundary interval yields nannofossils throughout and is apparently complete at the resolution provided by nannofossil biostratigraphy. This interval is associated with a lithologic change from white nannofossil ooze to a darker colored brown radiolarian clay.

Eocene nannofossil Zones NP18-20 through NP15 are recognized using the top of *Chiasmolithus grandis* in Sample 320-U1333A-14X-CC (129.80 m CSF); the top of *Chiasmolithus solitus* in Sample 320-U1333A-16X-5, 40 cm (145.60 m CSF); and the total range of *Nannotetrina fulgens* from Samples 320-U1333A-18X-CC (163.86 m CSF) to 20X-1, 73 cm (178.33 m CSF). The following datums were also useful in supporting these zonal determinations: base of *Dictyococcites bisectus,* total range of *Discoaster bifax* (Samples 320-U1333A-16X-6, 40 cm, to 18X-3, 88 cm; 147.10–161.62 m CSF), top and base of *Nannotetrina,* and top and base of *Sphenolithus furcatolithoides*. Middle Eocene assemblages are also characterized by the presence of common *Blackites* spines (including *Pseudotriquetrorhabdulus inversus* of many authors).

Basal sediments are composed of dolostone with green flecks in Holes U1333A and U1333C and dolomite nannofossil ooze in Hole U1333B. Nannofossil assemblages from these sediments are poor to moderately well preserved. The presence of *S. furcatolithoides* in Sample 320-U1333A-20X-2, 50 cm, suggests an age of Zone NP15 (45.8 Ma or younger), even though *N. fulgens* is absent from this sample to the base of the hole. The absence of *Nannotetrina* in this oldest time interval may be due to ecological exclusion; discoasters are very rare in these basal assemblages, indicative of a eutrophic environment, which is consistent with the site's paleolatitude at this time within the equatorial upwelling zone. It is therefore likely that the base of *N. fulgens* and *Nannotetrina* are both too high in the core, and the basal sediments have been tentatively assigned to Zone NP15.

Radiolarians

Radiolarian stratigraphy at Site U1333 (Table T4) spans the interval between Zone RN2 (near the base of the lower Miocene) and the upper part of Zone RP13 (middle Eocene) (Tables T5, T6, T7). The first core (Sample 320-U1333A-1-2H, 104–106 cm) recovered lower Miocene radiolarians in a moderately preserved assemblage with no detectable reworked older microfossils. This is very different from Sites U1331 and U1332, at which the uppermost cores were dominated by a highly mixed assemblage of Oligocene through Eocene radiolarians. Preservation in the upper part of Zone RP22 (Core 320-U1333A-3H; upper Oligocene) is generally poor to moderate but improves through the middle part of Zone RP20 (Cores 320-U1333A-4H through 8H), becomes poor again briefly in Core 320-U1333A-9H (Zone RP20), and then remains moderate to good through the remaining Oligocene and Eocene section.

Magnetic susceptibility records from Core 320-U1333A-13X show a "two-step" transition from Eocene to Oligocene sediments, with the base of Chron 13n occurring a few centimeters above the younger of these two steps. This pattern is indicative of an apparently complete Eocene/Oligocene boundary section, similar to that recovered at Site 1218. Initial assessment of radiolarian assemblages across the Eocene/Oligocene boundary interval indicates a significant loss of diversity through this transition. Although a few species from the Eocene carry through to the Oligocene, only one stratigraphic marker species (*L. angusta*) first appears near the Eocene/Oligocene boundary (Sample 320-U1333A-13X-3, 0–8 cm). Most of the lower Oligocene marker species make their first appearance in the middle part of Core 320-U1333A-12X, a few meters above the younger step in magnetic susceptibility. Between these first occurrences and the last occurrence of the Eocene marker species, there is a zone of relativity low radiolarian diversity, which commonly contains abundant diatoms in the >63 µm fraction.

There is a slight amount of reworked older Eocene species in the lower part of the Oligocene section. With the detailed sample coverage in this interval, the reworked forms clearly show a discontinuous appearance in the samples.

All the radiolarian zones down to Zone RP13 are present with moderate to good preservation of assemblages. Sample 320-U1333A-19X-CC and all of Core 320-U1333A-20X were barren of radiolarians.

Diatoms

Diatoms were examined in core catcher samples from Holes U1333A–U1333C and selected intermediate samples. The examined interval represents the *Rocella gelida* through *Coscinodiscus excavatus* Zones of Barron (1985, 2006) and Barron et al. (2004). Diatoms range in abundance from rare to abundant depending on the specific sample. Diatom preservation is variable but generally is poor to moderate.

Samples examined from Cores 320-U1333A-1H, 320-U1333B-1H, and 320-U1333C-1H and Sample 320-U1333C-2H-CC contain rare or no diatoms. No zonal assignment was made. The interval from Samples 320-U1333B-2H-CC through 320-U1333A-3H-2, 100–101 cm, is assigned to the *R. gelida* Zone based on the occurrence of *R. gelida*. Specimens of *Bogorovia veniamini, Rocella vigilans,* and *Cavitatus miocenica* also occur in Sample 320-U1333B-2H-CC.

The interval from Samples 320-U1333A-3H-4, 100–101 cm, through 5H-CC is assigned to the *B. veniamini* Zone based on the occurrence of *B. veniamini* in most samples examined from this interval. Supporting this zonal assignment is the occurrences of *Cestodiscus kugleri* in Samples 320-U1333A-4H-3, 100–101 cm, and 4H-5, 100–101 cm, and *Rossiella symmetrica* in Sample 4H-5, 100–101 cm. Other species typical of this interval, but not necessarily present in each sample are *R. vigilans, Azpeitia oligocenica, Cestodiscus pulchellus, Coscinodiscus rhombicus,* and *C. miocenica*.

The interval from Samples 320-U1333A-6H-2, 110–111 cm, through 8H-4, 115–116 cm, is assigned to the *R. vigilans* Zone based on the occurrence of *R. vigilans* without *B. veniamini*. Sample 320-U1333A-6H-5, 110–111 cm, is placed in Subzone A of this zone based on the occurrence of *Cavitatus jouseanus*. Sample 320-U1333A-7H-2, 100–101 cm, is placed into Subzone B based on the occurrence of *R. symmetrica* without *C. jouseanus*. The occurrence of *Cestodiscus trochus* without *R. symmetricus* in Sample 320-U1333A-7H-CC suggests placement of this sample into Subzone A; however, diatom preservation through this interval is poor to moderate.

Samples 320-U1333A-8H-CC and 9H-CC are assigned to the *C. trochus* Zone based on the occurrences of *C. miocenica* in Sample 8H-CC and *C. trochus* and *Cestodiscus robustus* in Sample 9H-CC without *C. excavatus*.

The *C. excavatus* Zone is represented by the occurrence of *C. excavatus* in the interval from Samples 320-U1333A-10H-2, 100–101 cm, through 13H-2, 100–101 cm. Typical of this interval is the occurrence of *C. trochus, C. excavatus, A. oligocenica,* and *C. robustus*.

Sample 320-U1333A-13H-4, 100–101 cm, and below typically contain rare diatoms or are barren of diatoms. The exceptions are Samples 320-U1333A-16X-CC and 320-U1333B-16X-CC, both of which contain fragments typified by *Hemiaulus*.

Planktonic foraminifers

Core catchers were sampled from all three holes at Site U1333, and additional samples were taken in Hole U1333A (two per core) to develop a high-resolution biostratigraphy. The early Miocene and much of the Oligocene is characterized by abundant and relatively well to moderately preserved planktonic foraminifers that delineate a sequence of lower Miocene (Zone M1) through Oligocene (Zone O2) zones. The record of planktonic foraminifers at this site indicate a relatively continuous succession of zones that agree well with calcareous nannofossil and radiolarian zonal determinations (Fig. **F9**). Preservation and abundance of planktonic foraminifers is poor in the earliest Oligocene and latest Eocene with many samples either barren or containing a few poorly preserved specimens. Preservation briefly improves in the late middle Eocene. Depth positions and age estimates of biostratigraphic marker events identified are shown in Table **T8.** Taxon preservation and occurrences are shown in Table **T9.**

Cores 320-U1333A-1H and 320-U1331C-2H were assigned to Zone M1a based on the co-occurrence of *P. kugleri* and *Paragloborotalia pseudokugleri* and the absence of *Globoquadrina dehiscens*. Early Miocene assemblages are characterized by the presence of *Dentoglobigerina* spp. and representatives of the *Paragloborotalia semivera–siakensis–mayeri* group. The Oligocene/Miocene boundary approximated by the first occurrence of *P. kugleri* is well constrained at this site and falls between Sample 320-U1333A-2H-2, 38–40 cm (11.38 m CSF), and Sample 2H-CC (19.57 m CSF), in excellent agreement with the estimate from calcareous nannofossils. A poorly preserved and scarce fauna in Sample 320-U1333A-2H-4, 38–40 cm, prevented closer constraints on the boundary. In Holes U1333B and U1333C, *P. kugleri* was rare or absent, as was *Globigerina ciperoensis,* the last occurrence of which falls directly above the Oligocene/Miocene boundary, hindering precise determination of the boundary in these holes. Samples 320-U1333A-2H-CC through 6H-CC (18.11–56.20 m CSF) are assigned to Zone O6 based on the last occurrence of *Paragloborotalia opima,* the sporadic presence of *G. ciperoensis* and *P. pseudokugleri,* and the absence of *P. kugleri*. The assemblage is dominated by paragloborotaliids, including the *P. opima–mayeri* group, *Paragloborotalia semivera,* and *Paragloborotalia pseudocontinousa*.

The presence of Zones O2–O5 is recognized by the top and base of *P. opima* between Samples 320-U1333A-6H-3, 38–40 cm (50.88 m CSF), and 10H-2, 38–40 cm (87.38 m CSF), respectively (see Table **T8** for further details). Differentiation between *P. opima* and *P. nana* is based on the size criterion proposed by Bolli and Saunders (1985). In addition, Spezzaferri (1994) noted that *P. opima* exhibits a more lobulate profile, larger final chamber, and higher arched aperture than observed in *P. nana;* these criteria were also used as a guide our identifications. Zones O4 and O5 were determined based on the overlapping ranges of *P. opima* and *Globigerina angulisuturalis*. *Chiloguembelina cubensis* was also identified in a single sample (320-U1333A-7H-5, 38–40 cm; 63.38 m CSF) but was not employed as a datum to distinguish Zones O4 and O5 because of its very low abundance and absence from the rest of the samples investigated. The presence of Zone O3 was identified between the base of *G. angulisuturalis* and the topmost occurrences of *Turborotalia ampliapertura* in Sample 320-U1333A-8H-CC (76.14 m CSF). However, the last occurrence of *T. ampliapertura* occurs somewhat shallower in the sedimentary record than expected (Fig. **F10**) and was too rare in Hole U1333B and U1333C core catchers to define. Furthermore, the topmost occurrence of *Subbotina angiporoides* in Sample 320-U1333A-9H-2, 52–53 cm (78.02 m CSF), should fall in Zone O3 but here occurs deeper than expected and falls in Zone O2; thus, caution is warranted.

As at the two previous drill sites, samples in the earliest Oligocene–latest Eocene (Cores 320-U1333A-13X through 16X, 320-U1333B-14H through 17H, and 320-U1333C-15H through 17H) are barren of planktonic foraminifers, preventing detection of the Eocene/Oligocene boundary. This barren interval directly coincides with a shift in sediment lithology from carbonate nannofossil ooze to radiolarian ooze. However, the FO of *Globoquadrina venezuelana* (~108 m CSF) can be used to roughly approximate the Eocene/Oligocene boundary (Wade and Pearson, 2008). The first consistent presence of *Catapsydrax unicarus* also occurs in Zone 01 following the Eocene/Oligocene boundary in Wade and Pearson (2008) and provides a good approximation of the boundary at ~108 m CSF but occurs much deeper in Hole U1333C (Sample 320-U1333B-13H-CC; ~122.14 m CSF).

Cores 320-U1333A-17X through 20X, 320-U1333B-18X through 20X, and 320-U1333C-18H through 20H are either barren or yield assemblages containing moderately to poorly preserved, dissolution-resistant planktonic foraminifers. The variable planktonic foraminifer abundance and preservation in the middle and late Eocene reflects shifts in the dominant sediment lithology between carbonate nannofossil and radiolarian oozes. The Eocene assemblage comprises parasubbotinids, paragloborotaliids, subbotinids, and broken but distinctive elongate chambers from *Clavigerinella eocaenica*. Species identified include *C. unicavus, Paragloborotalia griffinoides, Parasubbotina griffinae, Parasubbotina varianta, Subbotina corpulenta, Subbotina eocaena, Subbotina hagni, Subbotina linaperta,* and *Subbotina senni.* In samples where preservation is better (e.g., Sample 320-U1333A-20X-2, 42–44; 179.52 m CSF), *Acarinina praetopilensis, Acarinina bullbrooki,* and other small unidentified acarininids can also be found. The dominance of stratigraphically long-ranging Eocene taxa coupled with the absence of the genera *Globigerinatheka* and *Morozovella* makes precise age determination of individual samples problematic. However, the presence of *A. bullbrooki* in Sample 320-U1333A-20X-2, 42–44 cm (179.52 m CSF), indicates a basement age older than 40.8 Ma (below Zone E12), but better precision was given by the nannofossil biostratigraphic estimates (Zone NP15) (Fig. **F9**).

On an additional note, high abundances of *Clavigerinella* spp. are often linked to high-productivity environments (e.g., Coxall et al., 2003), which is consistent with the paleogeographic situation of this site within the high-productivity equatorial belt during the middle–late Eocene. Further evidence for this (although also a by-product of dissolution) is the dominance of globigerinid forms—parasubbotinids, subbotinids, paragloborotaliids—also associated with nutrient-rich surface waters.

Benthic foraminifers

Benthic foraminifers were examined semiquantitatively in all three holes of Site U1333. Benthic foraminifers occurred almost continuously in calcareous nannofossil ooze of the Oligocene and in radiolarian ooze of the Eocene. The occurrence of benthic foraminifers at this site is shown in Table **T10.**

In Samples 320-U1333A-1H-CC through 12X-CC (9.95–107.99 m CSF), *N. umbonifer, O. umbonatus, C. mundulus, Globocassidulina subglobosa, Gyroidinoides* spp., and *Pullenia* spp. were common and *Astrononion echolsi, Nonion havanensis, Siphonodosaria antillea,* and *Cibicidoides grimsdalei* were subordinate. *C. mundulus* and *G. subglobosa* were generally common in the lower part of the interval (maximum = 28% and 15%, respectively), whereas *N. umbonifer* was abundant in the upper part of the interval (maximum = 23%). A similar faunal transition was recognized in Holes U1333B (Samples 320-U1333B-1H-CC through 12H-CC; 7.69–112.32 m CSF) and U1333C (Samples 320-U1333C-2H-CC through 13H-CC; 36.54–75.94 m CSF). In addition, the abundance of *N. umbonifer* in Hole U1333C also varied continuously in the late Oligocene. Preservation of benthic foraminifer tests is good. These faunal compositions indicate lower bathyal and abyssal paleodepths during the Oligocene and the early Miocene, based on van Morkhoven et al. (1986). The Oligocene and early Miocene fauna at this site are basically similar to those observed at Site U1332 and in previous studies in the eastern equatorial Pacific (DSDP Site 573, Thomas, 1985; Sites 1218 and 1219, Takata and Nomura, 2005). *N. umbonifer* is a tolerant species to carbonate undersaturation and/or low food supply (e.g., Mackensen et al., 1990; Schmiedl et al., 1997). *O. umbonatus, Cibicidoides* spp., and *G. subglobosa* are common oligotrophic taxa in deep water (e.g., Nomura, 1995). This suggests that changes in carbonate undersaturation and/or food supply from the surface ocean may have occured in the late Oligocene.

Samples 320-U1333A-13X-CC through 19X-CC (119.96–174.73 m CSF) contained benthic foraminifers, except for Sample 320-U1333A-15X-CC (139.17 m CSF). *O. umbonatus, N. truempyi, Cibicidoides eocanus, C. grimsdalei, G. subglobosa,* and *S. antillea* were common in this interval. In addition, various taxa, such as *Abyssamina quadrata, Abyssamina poagi,* and *Alabamina dissonata,* were subordinate in Sample 320-U1333A-19X-CC (174.73 m CSF). Similar occurrences were also recognized in Samples 320-U1333B-13H-CC through 19X-CC (122.15–169.85 m CSF) and 320-U1333C-14H-CC through 20X-CC (117.59–155.10 m CSF). Test preservation of these calcareous foraminifers was generally poor, but well-preserved specimens were sometimes found in the lowermost part of the interval. These fauna suggest lower bathyal to abyssal paleodepth in the middle to late Eocene. Faunal associations of these calcareous taxa in the middle to late Eocene are similar to those recorded at Sites U1331 and U1332 and previous preliminary studies in the eastern equatorial Pacific (Site 1218; Shipboard Scientific Party, 2002b). Calcareous foraminifers at this site were more consistently present compared to those of Sites U1331 and U1332 (Fig. F11) and may be attributed to a shallower water depth at this site than at Sites U1331 and U1332. Common occurrences of *N. truempyi* and *O. umbonatus* were recognized in nannofossil Zone NP16 (e.g., Samples 320-U1331B-8H-CC, 320-U1332A-13H-CC, and 16X-CC), roughly coincide with the high-carbonate interval observed (see **"Lithostratigraphy"** and **"Geochemistry"**) at all three sites, and may correlate to deepening of the calcium carbonate compensation depth in the middle Eocene (Lyle et al., 2005).

Paleomagnetism

We conducted a paleomagnetic study of archive-half sections of 48 APC and 12 XCB cores from Holes U1333A–U1333C, with the primary objective of determining the magnetostratigraphy of the site and providing chronostratigraphic age constraints. To accomplish this we measured the natural remanent magnetization (NRM) of each section at 5 cm intervals before and after AF demagnetization of 20 mT. When time permitted, an additional 10 mT demagnetization step was measured. We processed the extracted data from the Laboratory Information Management System (LIMS) database by removing measurements made within 5 cm of section ends and data from disturbed intervals (Table T11). Cleaned data are presented in Tables T12, T13, T14, T15, T16, T17, T18, and T19.

Core orientation was estimated from paleomagnetic declination data as described in **"Paleomagnetism"** in the "Site U1331" chapter. The azimuthal core orientation was determined by correlating distinct reversal patterns as recorded by the paleomagnetic declination in each hole with the geomagnetic polarity timescale (GPTS). When distinct correlatable patterns are not easily recognized, this method could lead to a magnetic polarity ambiguity in which one might be unable to differentiate between magnetic north and magnetic south. Such ambiguities can be resolved in most cases by using biostratigraphic age estimates to guide the mapping of identifiable reversals in each hole. Once we had confidently identified a unique, unambiguous reversals pattern, the mean paleomagnetic directions for each hole were calculated using Fisher statistics (Table T20). Subsequently data were reoriented so that normal and reversed polarity magnetozones had declinations of ~0° and ~180°, respectively.

Magnetic susceptibilities were measured for 106 discrete samples. The data were mass and volume corrected using sediment moisture and density data (MAD) (see **"Physical properties"**) and are presented in Table T21. Of these samples, 72 were stepwise AF demagnetized and measured at 5 mT steps to a peak field of 40 mT and 10 mT steps to 60 mT. The remanence measurements and the characteristic remanent magnetization (ChRM) directions computed using principal component analysis (PCA) are given in Tables T22 and T23.

Results

Downhole paleomagnetic data for Holes U1333A–U1333C are presented in Figures F12, F13, and F14, respectively. NRM measurements indicate that the viscous isothermal remanent magnetization (IRM) drilling overprint (see **"Paleomagnetism"** in the "Site U1331" chapter) was weak for Hole U1333A; weak above 83 m CSF in Hole U1333B; and weak above ~107 m CSF in Hole U1333C. The increased strength of the drilling overprint in Hole U1333B below 83 m CSF and in Hole U1333C below ~107 m CSF coincides with the switch from nonmagnetic to standard steel core barrel. Figure F15 illustrates the effect of the steel core barrel and confirms the value of using nonmagnetic coring equipment. NRM inclinations before demagnetization reflected the patchy overprint with values of anywhere between –10° and 90°. The small and sometimes negative overprint may have been caused by the bottom-hole assembly (BHA) and drill string becoming magnetized by the local geomagnetic field, which is more or less horizontal. Declinations were typically less severely affected, and it was often possible to identify reversals before demagnetization. The patchy and sometimes shallow overprints also indicate that the BHA and drill string are probably contributing little to the drilling overprint at this site.

Demagnetization data from discrete samples (Fig. F16) indicate that the ChRM of the sediments is carried above 10–20 mT demagnetization steps and that in most cases 20 mT demagnetization effectively removed the drilling induced IRM. PCA directions of the ChRM component agree with measurements of coeval intervals from the archive halves (see Fig. F12), indicating that the magnetic directions after 20 mT demagnetization provide a reliable indicator of the ChRM of the sediments.

In a few isolated intervals, the inclinations remain steep after 20 mT demagnetization, indicating that the drilling overprint was not demagnetized fully. Between ~80 and ~105 m CSF in Hole U1333B is a noisy interval where declination and inclination vary considerably (Fig. F13). We remeasured the sections from this interval but found that the results were repeatable; therefore, the source of the noise is within the cores. Steel core barrels were used in Hole U1333B below ~83 m CSF. It is possible that the magnetization of the steel core barrels was passed onto the cored sediments or that the sediments were contaminated with rust or iron particles during coring.

Magnetostratigraphy

The relatively clear polarity reversal pattern and detailed biostratigraphic framework of key nannofossil, radiolarian, and foraminifer datums from core catcher and additional samples (see **"Biostratigraphy"**) allowed a relatively uncomplicated correlation of the magnetostratigraphy with the GPTS. The reversal depths for each core are provided in Table **T24.** The polarity interpretations for the three holes are provided in Figures **F12, F13,** and **F14,** and the summary of the magnetostratigraphy for this site is given in Figure **F17.**

At the top of Hole U1333A, our polarity assignments are constrained by clear declination and inclination records and by biostratigraphic data that indicate an age of ~21.5 Ma at the base of Core 320-U1333A-1H. Chron C6Ar was recovered twice (in Cores 320-U1333A-1H and 2H), which initially complicated our correlation. Most of Chron C7An is lost at a core break between Cores 320-U1333A-3H and 4H, Chron C8n.1r is absent, and the top of Chron C8r is lost in a break between Cores 320-U1333A-3H and 4H. Correlation of magnetozones with the GPTS is unambiguous for the remainder of the APC-cored portion of Hole U1333A to the base of Core 320-U1333A-10H, which records the upper part of Chron C12r. Extensive deformation and biscuiting of sediments associated with XCB coring below ~95 m CSF prohibits further identification of magnetozones.

The upper portion of Magnetozone N1 in Holes U1333B and U1333C is correlated with Chron C1n; however, biostratigraphic ages indicate ~21–22 Ma at ~10 m CSF. Therefore we correlate the lower portion of Magnetozone N1 with Chron C6n. Below this interval our interpretation is straightforward with one to one correlations with the GPTS to Chron C13r with a few exceptions where reversals were lost in core breaks.

In Hole U1333B, correlation of the magnetostratigraphy with the GPTS is relatively simple above Magnetozone N21. Chron C6Bn.2n is absent, and Chrons C11n.1r, C16n.2n, and C17n.2n are lost in core gaps between Cores 320-U1333B-8H and 9H, 13H and 14H, and 14H and 15H, respectively. Between ~80 and ~104 m CSF is an interval with unstable magnetic directions probably affected by a drilling-induced magnetic overprint. The reversal between Magnetozones R22 and N23 occurs within Section 320-U1333B-12H-6 and is correlated with the reversal between Chrons C12r and C13n. The Chron C13n/C13r boundary occurs in a break between Cores 320-U1333B-12H and 13H, so the true thickness of Chron C13n can not be determined in Hole U1333B.

At the base of Hole U1333B, correlation with the GPTS is more difficult because of coring gaps and infrequent reversals. Thick normal polarity Magnetozones N28 and N29 are correlated with Chron C18n.1n. The thin (~25 cm) reversed polarity interval R28 represents what is probably a newly recognized cryptochron within Chron C18n.1n. Our correlation to the bottom of Hole U1333B is aided by the lowest occurrence of *R. umbilicus,* which has an age of 42.5 Ma (see **"Biostratigraphy"**) and occurs between 158.3 and 162.94 m CSF. Consequently it is our preference to correlate Magnetozone N32 with Chron C20n, as this agrees most closely with the biostratigraphy and the polarity boundaries that are more completely recovered in Hole U1333C. XCB coring below ~162 m CSF prevents further interpretation of the magnetostratigraphy.

In Hole U1333C, Chron C7An is lost in a 3 m core break between Cores 320-U1333C-4H and 5H; therefore, the upper portion of Magnetozone R13 is correlated with Chron C7r and the lower portion with Chron C7Ar. The Magnetozone R20/N21 boundary is in a gap between Cores 320-U1333C-13H and 14H and is correlated with Chron C12r/C13n boundary. The Chron C13n/C13r boundary is, however, intact and occurs within Section 320-U1333C-14H-4. As is the case in Hole U1333B, Chron C13n is incompletely recovered, although the combined data from Holes U1333B and U1333C provide a complete record. Chron C15r is lost in a gap between Cores 320-U1333C-14H and 15H; therefore, the upper portion of Magnetozone N22 is correlated with Chron C15n and the lower portion with Chron C16n.1n. The cryptochron recognized within Chron C18n.1n in Hole U1333B is also recognized in Hole U1333C, where it spans ~30 cm. At the base of Hole U1333C, correlation with the GPTS is more difficult because of coring gaps and infrequent reversals. The Chron C18r/C19n boundary and the upper portion of Chron C19n fall within a break between Cores 320-U1333C-18H and 19H. The lowest reversal in Hole U1333C and for Site U1333 is the Chron C20n/C20r boundary, which occurs at 161.5 m CSF. Three XCB cores were collected below the last APC core (320-U1333C-21H), but these recovered only a small amount of material within core catchers and so were not measured.

Geochemistry

Sediment gases sampling and analysis

Headspace gas samples were taken at a frequency of one sample per core in Hole U1333A as part of the routine environmental protection and safety monitoring program. All headspace sample analyses resulted in nondetectable levels of methane (C_1; <1 ppmv), with no higher hydrocarbons, consistent with the low organic carbon content of these sediments.

Interstitial water sampling and chemistry

Twenty-five interstitial water samples were collected using the whole-round squeezing approach (Table T25). Chemical constituents were determined according to the procedures outlined in "Geochemistry" in the "Methods" chapter. Chlorinity shows relatively little variability with depth, with values ranging from 557 to 566 mM (Figs. F18). Chlorinity values slightly increase in the upper 50 m CSF and stay relatively constant below. Alkalinity ranges from 1.7 to 4.5 mM. Alkalinities increase in the uppermost 10 m CSF from ~2.1 to 2.8 mM and are relatively uniform to 50 m CSF downcore. Between 55 and 90 m CSF, alkalinity shows first a large increase to 4.5 mM followed by a local minimum of 1.6 mM. Between 130 and 140 m CSF, alkalinities are also reduced. Sulfate concentrations are relatively constant and near seawater values, ranging from 25 to 28 mM. Low alkalinities and high sulfate concentrations indicate that organic matter supply is not sufficient to drive redox conditions to sulfate reduction. The relatively low regeneration of organic carbon is also indicated by low dissolved phosphate concentrations, typically <1 µM. Because of the high sulfate concentrations, dissolved Ba concentrations are low and relatively homogeneous, with values between 1.0 and 1.6 µM. Concentrations of dissolved silicate increase with depth from ~400 to a maximum of ~800 µM at 135 m CSF, with a subsequent decrease to 730 µM.

Calcium concentrations increase slightly with depth, with values from 10 to 12 mM (Fig. F18). Magnesium concentrations are relatively constant, ranging from 50 to 53 mM, with minima around 20 and 120–140 m CSF.

Lithium concentrations decrease from ~28 to 22 µM in the upper 80 m CSF. Below 130 m CSF, Li concentrations increase again toward basement, except for the deepest sample. Strontium concentrations vary between 83 and 105 µM, showing an overall increase with depth and distinctly reduced concentrations between 130 and 140 m CSF. Boron concentrations range between 422 and 485 µM, showing reduced values between 130 and 140 m CSF.

Bulk sediment geochemistry: major and minor elements

At Site U1333, bulk sediment samples for minor and major element analyses were distributed over the core depth to characterize the major lithologic units (0–180 m CSF; Hole U1333A). We analyzed concentrations of silicon, aluminum, iron, manganese, magnesium, calcium, sodium, potassium, titanium, phosphorus, barium, copper, chromium, scandium, strontium, vanadium, yttrium, and zirconium (Table T26) in the sediment by inductively coupled plasma–atomic emission spectroscopy (ICP-AES).

SiO_2 ranges between 6 and 75 wt%, with values around 45 wt% in the top few meters and lower values (5–20 wt%) between 5 and 105 m CSF. Below 105 m CSF, SiO_2 concentrations vary mainly between 20 and 75 wt%, with concentrations <10 wt% near the basement. Concentrations of Al_2O_3 range from 0.2 to 6 wt%, with values decreasing in the upper few meters from 6 to <1 wt%. Below 5 m CSF, Al_2O_3 concentrations vary between 0.2 and 3 wt%. A distribution with depth similar to that of Al is shown by TiO_2 (0.01–0.3 wt%), K_2O (0.1–1.2 wt%), Zr (16–126 ppm), and Sc (up to 19 ppm).

Concentrations of Fe_2O_3 vary between 0.3 and 5 wt%, following the general pattern of SiO_2. Similar trends are also shown by MnO (0.04 to >0.2 wt%), MgO (0.3–2 wt%), copper (44 to >140 ppm), and vanadium (130 to >330 ppm). Peak concentrations of Mn, Cu, and V could not be quantified because they exceeded the calibrated range (Table T26).

Calcium (CaO) ranges from 0.5 to 40 wt%, with high values corresponding to the minimum in SiO_2 and Al_2O_3. Strontium concentrations range from 130 to >700 ppm, showing a similar pattern to CaO.

Bulk sediment geochemistry: sedimentary inorganic and organic carbon

$CaCO_3$, inorganic carbon (IC), and total carbon (TC) concentrations were determined on sediment samples from Hole U1333A (Table T27; Fig. F19). $CaCO_3$ concentrations ranged between <1 to 96 wt%. In the uppermost ~4 m CSF, $CaCO_3$ concentrations are relatively low (26–69 wt%) and then, from 4 to 35 m CSF, vary between 58 wt% and 93 wt%. $CaCO_3$ concentrations are consistently high (76–96 wt%) from 35 to 111 m CSF. From 111 to 171 m CSF, $CaCO_3$ concentrations exhibit large fluctuations ranging from <1 to 74 wt%. In the basal section (173–180 m CSF), $CaCO_3$ concentrations are high (76–90 wt%). Variations in $CaCO_3$ concentrations correspond to lithostratigraphic changes (see "Lithostratigraphy").

Total organic carbon (TOC) concentrations were determined by acidification (see **"Geochemistry"** in the "Methods" chapter) (Table **T27;** Fig. **F19**). TOC concentrations determined using the acidification method are very low throughout the sediment column, with a range from below the detection limit to 0.05 wt% (Fig. **F19**).

Physical properties

Physical properties at Site U1333 were measured on whole cores, split cores, and discrete samples. WRMSL (GRA bulk density, magnetic susceptibility, and *P*-wave velocity), thermal conductivity, and NGR measurements comprised the whole-core measurements. Compressional wave velocity measurements on split cores and MAD analyses on discrete core samples were made at a frequency of one per undisturbed section in Cores 320-U1333A-1H through 20X. Compressional wave velocities were measured toward the bottom of sections. MAD analyses were located 10 cm downsection from carbonate analyses (see **"Geochemistry"**). Lastly, the Section Half Multisensor Logger (SHMSL) was used to measure spectral reflectance on archive-half sections.

Density and porosity

Two methods were used to evaluate wet bulk density at Site U1333. GRA provided an estimate from whole cores (Fig. **F20**), and MAD samples gave a second, independent measure of wet bulk density, along with providing dry bulk density, grain density, water content, and porosity from discrete samples (Table **T28**). MAD and GRA bulk density measurements display the same trends and are also similar in absolute values through the entire section (Fig. **F21B**). Crossplots of wet and dry bulk density versus interpolated GRA density (Fig. **F22**) show excellent correlation between MAD and GRA data.

Generally, wet bulk density corresponds with changes in lithology. Density is highest in Unit II, which also has high $CaCO_3$ content (see **"Lithostratigraphy"**). Wet bulk density is ~1.3 g/cm^3 at the seafloor and increases sharply at the top of Unit II (~1.6 g/cm^3). In the upper part of Unit II, wet bulk density varies between 1.6 g/cm^3 and 1.2–1.3 g/cm^3, which is consistent with the occurrence of radiolarian-rich intervals within the nannofossil ooze in the upper part of Unit II (see **"Lithostratigraphy"**). From 40 to 100 m CSF, wet bulk density values are less variable. At the top of Subunit IIIa, density decreases to values of 1.2 g/cm^3, which coincide with the sudden drop in $CaCO_3$ (wt%) at the Eocene/Oligocene boundary (~116 m CSF). The transition from high to low density values at the Eocene/Oligocene boundary reveals a two-step transition that most likely covaries with $CaCO_3$ (wt%) (see **"Stratigraphic correlation and composite section"**). In Subunit IIIa, density varies from 1.2 to 1.6 g/cm^3. Limited data for Unit IV indicate higher density values of ~1.6 to 1.8 g/cm^3.

Variation in grain density in Hole U1333A generally matches changes in lithology (Fig. **F21C**). Grain density averages 2.7 g/cm^3 in Units I and II in Hole U1331A, indicating the presence of carbonate-dominated lithologies (calcite = 2.7 g/cm^3). Subunit IIIa shows increased variability and lower grain densities, consistent with a more radiolarian dominated lithology (see **"Lithostratigraphy"**). Subunit IIIb and Unit IV show a return to carbonate-dominated lithologies, with grain density averaging 2.7 g/cm^3.

Porosity averages 65% in Unit II and varies around 75% in the other units. Porosity and water content vary inversely with wet bulk density (Fig. **F21A**).

Magnetic susceptibility

Whole-core magnetic susceptibility measurements correlate well with the major differences in lithology and changes in bulk physical properties (Fig. **F20**). Magnetic susceptibility values in Unit I are 25 × 10^{-5} to 30 × 10^{-5} SI. As with wet bulk density, magnetic susceptibility values show a variable pattern in the upper part of Unit II, which reflects intervals of nannofossil ooze with radiolarians. Magnetic susceptibility values become more uniform in the lower part of Unit II (below 40 m CSF). Magnetic susceptibility values increase abruptly at the top of Subunit IIIa, reflecting a greater concentration of ferromagnetic minerals. As with wet bulk density measurements, the transition from low magnetic susceptibility values to high values at the Eocene/Oligocene boundary reveals a two-step transition that most likely covaries with $CaCO_3$ content (see **"Stratigraphic correlation and composite section"**). Magnetic susceptibility is higher and more variable in Subunits IIIa and IIIb and Unit IV compared to Unit II.

Compressional wave velocity

Shipboard results

Whole-core *P*-wave logger (PWL) and discrete velocity measurements made on split cores follow similar trends, with key transitions occurring at lithologic boundaries (Fig. **F23**). Discrete velocity measurements along the *y*- and *z*-axes are in excellent agreement with PWL measurements, although *x*-axis velocities are ~100 m/s faster than PWL velocities

(Table T29). Possibilities for this mismatch in absolute values are compression of the sediment during analysis with the *P*-wave *x*-axis caliper or an improper correction for the thickness of the core liner.

Slight downhole trends in velocity generally follow changes in lithology or bulk properties (Fig. F23). PWL velocity increases through Units I and II. In Subunit IIIa, the downhole increase in velocity becomes greater. Velocity measurements reach 1575 m/s in the lower part of Subunit IIIa.

Postcruise correction

During the initial sampling of Hole U1337A, it was observed that *x*-direction velocities are consistently higher than other velocities and that PWL velocities are consistently low for Hole U1337A and all holes drilled at Sites U1331–U1336. It was determined that the high *x*-directed velocities are the result of using an incorrect value for the system delay associated with the contact probe (see **"Physical properties"** in the "Site U1337" chapter). Critical parameters used in this correction are system delay = 19.811 µs, liner thickness = 2.7 mm, and liner delay = 1.26 µs. PWL velocities were corrected for Hole U1337A by adding a constant value that would produce a reasonable velocity of water (~1495 m/s) for the quality assurance/quality control (QA/QC) liner (see **"Physical properties"** in the "Site U1337" chapter). These corrections have not been applied to the velocity data presented in this chapter.

Natural gamma radiation

NGR was measured on all whole cores at Site U1333 (Fig. F20). The highest NGR values are present at the seafloor (~45 cps). NGR values decrease to the base of Unit I. NGR is uniform throughout Unit II and shows a slight increase across the lithologic transition into Subunit IIIa. NGR is slightly higher in Subunit IIIa.

Thermal conductivity

Thermal conductivity was measured on the third section of each core from Hole U1333A (Table T30). Thermal conductivity shows a strong dependence on porosity downhole through the succession (Figs. F24, F25). Decreased conductivity occurs with increasing porosity as increased interstitial spacing attenuates the applied current from the probe. Thermal conductivity is 0.8 W/(m·K) in Unit I and increases to a maximum value of 1.2–1.3 W/(m·K) in the middle of Unit II.

Reflectance spectroscopy

Spectral reflectance was measured on split archive-half sections from all three holes using the SHMSL (Fig. F26). The parameters L* (black–white), a* (green–red), and b* (blue–yellow) follow changes in lithology, with variations in L*, a*, and b* correlating very well to carbonate content, density, and magnetic susceptibility measurements (see Fig. F4). Carbonate-dominated sections, such as the interval of Unit II from 38 to 110 m CSF, are clearly recognized by an increase in L* values and a decrease in both a* and b* values, related to the paler color of these sediments. The boundary between Unit II and Subunit IIIa, marking the change from carbonate-dominated Unit II to radiolarian-dominated Unit III, is clearly marked by a sharp decrease in L* (from ~80 to 50). This boundary is also recognized in the a* and b* data as a peak, followed by a slight decrease in b* (from ~10 to ~6), whereas a* values remain fairly constant directly above and below this boundary peak (~4).

Stratigraphic correlation and composite section

Special Task Multisensor Logger (STMSL) data were collected at 5 cm intervals from Holes U1333B and U1333C and compared to the WRMSL data obtained at 2.5 cm intervals from Hole U1333A to monitor coring in Holes U1333B and U1333C in real time. Cores for the final composite section were depth-shifted on the basis of the magnetic susceptibility data at 2.5 cm resolution from the WRMSL track. Magnetic susceptibility and GRA density data were used for correlating among holes at Site U1333. The magnetic susceptibility data proved to be the most useful correlation parameter because of the higher signal-to-noise ratio compared to the GRA data. The high amplitude variations in magnetic susceptibility in the three holes drilled at Site U1333 permitted construction of a complete composite section to Core 320-U1333B-14H-7, 50 cm (131.20 m CSF), at a composite depth of ~150 m CCSF-A (Fig. F27). Offsets and composite depths are listed in Table T31, and the sections of core used for the splice are identified in Table T32. We avoided using intervals with significant disturbance or distortion for the composite record (see **"Paleomagnetism;"** Table T11). Very low magnetic susceptibility amplitudes made the splicing process challenging at ~115 m CCSF-A (at 220 revised meters composite depth [rmcd] in Fig. F28). However, preliminary correlation to the Site 1218 magnetic susceptibility record (Shipboard Scientific Party, 2002b) suggests a complete stratigraphic section and demonstrates that little, if any, material is missing (Fig. F28).

The Site U1333 splice can be used as a sampling guide to recover a single sedimentary sequence between 0 and 150 m CCSF-A, although it is advisable to overlap a few decimeters from different holes when sampling to accommodate anticipated ongoing development of the depth scale. Stretching and compression of sedimentary features in aligned cores indicates distortion of the cored sequence. Because much of the distortion occurs within individual cores on depth scales of <9 m, it was not possible to align every single feature in the magnetic susceptibility, GRA, NGR, and color reflectance records. However, at crossover points along the splice (Table T32) care was taken to align highly identifiable features from cores in each hole.

A growth factor of 1.15 was derived by linear regression for all holes at Site U1333, indicating a 15% increase in CCSF-A relative to CSF depth (Fig. F29). We used this value to calculate the CCSF-B (see **"Corrected core composite depth scale"** in the "Methods" chapter) depth presented in Table T31 to aid in the calculation of mass accumulation rates.

We calculated sedimentation rates using paleomagnetic and biostratigraphic datums (Table T33; Fig. F10; see **"Biostratigraphy"** and **"Paleomagnetism"**) on the CCSF-B depth scale to obtain values compatible with the actual recovered length. Paleomagnetic reversals are used to calculate the average linear sedimentation rates (LSRs) for Site U1333 through most of the section. Calcareous nannofossils, foraminifers, and radiolarians are present throughout the entire section and were used in addition to the magnetostratigraphy in establishing age control (Fig. F10).

The LSR at Site U1333 in the radiolarian and nannofossil oozes of lithologic Units II and III vary between ~4 and 6 m/m.y. in the middle and upper Eocene, increase to ~13 m/m.y. in the lower Oligocene, and remain at ~6.6 m/m.y. in the upper Oligocene and lower Miocene part of the section.

Downhole measurements

Heat flow

Four APCT-3 temperature measurements in Hole U1333B ranged from 2.52°C at 26.7 m to 4.55°C at 83.7 m (Table T34), giving a geothermal gradient of 37.9°C/km (Fig. F30). The bottom water temperature was 1.44°C, based on the average of the minimum temperature in the four APCT-3 temperature profiles. Thermal conductivity under in situ conditions was estimated from laboratory-determined thermal conductivity using the method of Hyndman et al. (1974) (see **"Physical properties"** in the "Methods" chapter). The calculated in situ values are up to 2.2% below the measured laboratory values. Thermal resistance was then calculated by cumulatively adding the inverse of the in situ thermal conductivity values over depth intervals downhole (Fig. F30). A heat flow of 42.3 mW/m² was obtained from the linear fit between temperature and thermal resistance (Fig. F30) (Pribnow et al., 2000), which is similar to Site 1220 to the west but roughly 20 mW/m² less than nearby Sites 1218, 1219, and U1332.

References

Amante, C., and Eakins, B.W., 2008. *ETOPO1 1 Arc-Minute Global Relief Model: Procedures, Data Sources and Analysis:* Washington, DC (DOC/NOAA/NESDIS/NGDC).

Barron, J.A., 1985. Late Eocene to Holocene diatom biostratigraphy of the equatorial Pacific Ocean, Deep Sea Drilling Project Leg 85. *In* Mayer, L., Theyer, F., Thomas, E., et al., *Init. Repts. DSDP,* 85: Washington, DC (U.S. Govt. Printing Office), 413–456. **doi:10.2973/dsdp.proc.85.108.1985**

Barron, J.A. 2006. Diatom biochronology for the early Miocene of the equatorial Pacific. *Stratigraphy,* 2(4):281–309.

Barron, J.A., Fourtanier, E., and Bohaty, S.M., 2004. Oligocene and earliest Miocene diatom biostratigraphy of ODP Leg 199 Site 1220, equatorial Pacific. *In* Wilson, P.A., Lyle, M., Janecek, T.R., and Firth, J.V. (Eds.), *Proc. ODP, Sci. Results,* 199: College Station (Ocean Drilling Program), 1–25. **doi:10.2973/odp.proc.sr.199.204.2004**

Barron, J.A. 2006. Diatom biochronology for the early Miocene of the equatorial Pacific. *Stratigraphy,* 2(4):281–309.

Bohaty, S.M., and Zachos, J.C., 2003. Significant Southern Ocean warming event in the late middle Eocene. *Geology,* 31(11):1017–1020. **doi:10.1130/G19800.1**

Bohaty, S.M., Zachos, J.C., Florindo, F., and Delaney, M.L., 2009. Coupled greenhouse warming and deep-sea acidification in the middle Eocene. *Paleoceanography,* 24(2):PA2207. **doi:10.1029/2008PA001676**

Bolli, H.M., and Saunders, J.B., 1985. Oligocene to Holocene low latitude planktic foraminifera. *In* Bolli, H.M., Saunders, J.B., and Perch-Nielsen, K. (Eds.), *Plankton Stratigraphy:* Cambridge (Cambridge Univ. Press), 155–262.

Busch, W.H., Vanden Berg, M.D., and Masau, P.E., 2006. Velocity and density of Paleogene equatorial sediments: variation with sediment composition. *In* Wilson, P.A., Lyle, M., and Firth, J.V. (Eds.), *Proc. ODP, Sci. Results,* 199: College Station, TX (Ocean Drilling Program), 1–31. **doi:10.2973/odp.proc.sr.199.226.2006**

Coxall, H.K., Wilson, P.A., Pearson, P.N., and Sexton, P.F., 2007. Iterative evolution of digital planktonic foraminafera. *Paleobiology,* 33(4):495–516. **doi:10.1666/06034.1**

Coxall, H.K., Huber, B.T., and Pearson, P.N., 2003. Origin and morphology of the Eocene planktonic foraminifer *Hantkenina. J. Foraminiferal Res.,* 33(3):237–261. **doi:10.2113/33.3.237**

Coxall, H.K., Wilson, P.A., Pälike, H., Lear, C.H., and Backman, J., 2005. Rapid stepwise onset of Antarctic glaciation and deeper calcite compensation in the Pacific

Ocean. *Nature (London, U. K.),* 433(7021):53–57. doi:10.1038/nature03135

Engebretson, D.C., Cox, A., and Gordon, R.G., 1985. *Relative Motions between Oceanic and Continental Plates in the Pacific Basin.* Spec. Pap.—Geol. Soc. Am., 206.

Hyndman, R.D., Erickson, A.J., and Von Herzen, R.P., 1974. Geothermal measurements on DSDP Leg 26. *In* Davies, T.A., Luyendyk, B.P., et al., *Init. Repts. DSDP,* 26: Washington, DC (U.S. Govt. Printing Office), 451–463. doi:10.2973/dsdp.proc.26.113.1974

Knappenberger, M., 2000. Sedimentation rates and Pacific plate motion calculated using seismic cross sections of the Neogene equatorial sediment bulge [M.Sc. thesis]. Boise State Univ., Idaho.

Koppers, A.A.P., Phipps Morgan, J., Morgan, J.W., and Staudigel, H., 2001. Testing the fixed hotspot hypothesis using $^{40}Ar/^{39}Ar$ age progressions along seamount trails. *Earth Planet. Sci. Lett.,* 185(3–4):237–252. doi:10.1016/S0012-821X(00)00387-3

Lyle, M., Wilson, P.A., Janecek, T.R., et al., 2002. *Proc. ODP, Init. Repts.,* 199: College Station, TX (Ocean Drilling Program). doi:10.2973/odp.proc.ir.199.2002

Lyle, M., Liberty, L., Moore, T.C., Jr., and Rea, D.K., 2002. Development of a seismic stratigraphy for the Paleogene sedimentary section, central tropical Pacific Ocean. *In* Lyle, M., Wilson, P.A., Janecek, T.R., et al., *Proc. ODP, Init. Repts.,* 199: College Station, TX (Ocean Drilling Program), 1–21. doi:10.2973/odp.proc.ir.199.104.2002

Lyle, M., Olivarez Lyle, A., Backman, J., and Tripati, A., 2005. Biogenic sedimentation in the Eocene equatorial Pacific—the stuttering greenhouse and Eocene carbonate compensation depth. *In* Lyle, M., Wilson, P.A., Janecek, T.R., et al., *Proc. ODP, Init. Repts.,* 199: College Station, TX (Ocean Drilling Program), 1–35. doi:10.2973/odp.proc.sr.199.219.2005

Lyle, M.W., Pälike, H., Moore, T.C., Mitchell, N., and Backman, J., 2006. *Summary Report of R/V Roger Revelle Site Survey AMAT03 to the IODP Environmental Protection and Safety Panel (EPSP) in Support for Proposal IODP626:* Southampton, U.K. (Univ. Southampton). http://eprints.soton.ac.uk/45921/

Mackensen, A., Grobe, H., Kuhn, G., and Fütterer, D.K., 1990. Benthic foraminiferal assemblages from the eastern Weddell Sea between 68° and 73°S: distribution, ecology and fossilization potential. *Mar. Micropaleontol.,* 16(3–4):241–283. doi:10.1016/0377-8398(90)90006-8

Moore, T.C., Jr., Backman, J., Raffi, I., Nigrini, C., Sanfilippo, A., Pälike, H., and Lyle, M., 2004. Paleogene tropical Pacific: clues to circulation, productivity, and plate motion. *Paleoceanography,* 19(3):PA3013. doi:10.1029/2003PA000998

Müller, R.D., Roest, W.R., Royer, J.-Y., Gahagan, L.M., and Sclater, J.G., 1997. Digital isochrons of the world's ocean floor. *J. Geophys. Res.,* 102(B2):3211–3214. doi:10.1029/96JB01781

Nigrini, C., Sanfilippo, A., and Moore, T.C., Jr., 2006. Cenozoic radiolarian biostratigraphy: a magnetobiostratigraphic chronology of Cenozoic sequences from ODP Sites 1218, 1219, and 1220, equatorial Pacific. *In* Wilson, P.A., Lyle, M., and Firth, J.V. (Eds.), *Proc. ODP, Sci. Results,* 199: College Station, TX (Ocean Drilling Program), 1–76. doi:10.2973/odp.proc.sr.199.225.2006

Nomura, R., 1995. Paleogene to Neogene deep-sea paleoceanography in the eastern Indian Ocean: benthic foraminifera from ODP Sites 747, 757, and 758. *Micropaleontology,* 41(3):251–290. doi:10.2307/1485862

Pälike, H., Lyle, M.W., Ahagon, N., Raffi, I., Gamage, K., and Zarikian, C.A., 2008. Pacific equatorial age transect. *IODP Sci. Prosp.,* 320/321. doi:10.2204/iodp.sp.320321.2008

Pälike, H., Moore, T., Backman, J., Raffi, I., Lanci, L., Parés, J.M., and Janecek, T., 2005. Integrated stratigraphic correlation and improved composite depth scales for ODP Sites 1218 and 1219. *In* Wilson, P.A., Lyle, M., and Firth, J.V. (Eds.), *Proc. ODP, Sci. Results,* 199: College Station, TX (Ocean Drilling Program), 1–41. doi:10.2973/odp.proc.sr.199.213.2005

Pälike, H., Norris, R.D., Herrle, J.O., Wilson, P.A., Coxall, H.K., Lear, C.H., Shackleton, N.J., Tripati, A.K., and Wade, B.S., 2006. The heartbeat of the Oligocene climate system. *Science,* 314(5807):1894–1898. doi:10.1126/science.1133822

Petronotis, K.E., 1991. Paleomagnetic studies of the skewness of Pacific plate marine magnetic anomalies 25–32R: implications for anomalous skewness and the motion of the Pacific plate and hotspots [Ph.D. thesis]. Northwestern Univ., Evanston, IL.

Petronotis, K.E., Gordon, R.G., and Acton, G.D., 1994. A 57 Ma Pacific plate paleomagnetic pole determined from a skewness analysis of crossings of marine magnetic anomaly 25r. *Geophys. J. Int.,* 118(3):529–554. doi:10.1111/j.1365-246X.1994.tb03983.x

Pribnow, D.F.C., Kinoshita, M., and Stein, C.A., 2000. *Thermal Data Collection and Heat Flow Recalculations for ODP Legs 101–180:* Hanover, Germany (Inst. Joint Geosci. Res., Inst. Geowiss. Gemeinschaftsauf. [GGA]). http://www-odp.tamu.edu/publications/heatflow/ODPReprt.pdf

Rea, D.K., and Lyle, M.W., 2005. Paleogene calcite compensation depth in the eastern subtropical Pacific: answers and questions. *Paleoceanography,* 20(1):PA1012. doi:10.1029/2004PA001064

Raffi, I., Backman, J., and Pälike, H., 2005. Changes in calcareous nannofossil assemblages across the Paleocene/Eocene transition from the paleo-equatorial Pacific Ocean. *Palaeogeogr., Palaeoclimatol., Palaeoecol.,* 226(1–2):93–126. doi:10.1016/j.palaeo.2005.05.006

Sager, W.W., and Pringle, M.S., 1988. Mid-Cretaceous to early Tertiary apparent polar wander path of the Pacific plate. *J. Geophys. Res., [Solid Earth],* 93(B10):11753–11771. doi:10.1029/JB093iB10p11753

Schmiedl, G., Mackensen, A., and Müller, P.J., 1997. Recent benthic foraminifera from the eastern South Atlantic Ocean: dependence on food supply and water masses. *Mar. Micropaleontol.,* 32(3–4):249–287. doi:10.1016/S0377-8398(97)00023-6

Shipboard Scientific Party, 2002a. Leg 199 summary. *In* Lyle, M., Wilson, P.A., Janecek, T.R., et al., *Proc. ODP,* *Init. Repts.,* 199: College Station, TX (Ocean Drilling Program), 1–87. doi:10.2973/odp.proc.ir.199.101.2002

Shipboard Scientific Party, 2002b. Site 1218. *In* Lyle, M., Wilson, P.A., Janecek, T.R., et al., *Proc. ODP, Init. Repts.,* 199: College Station, TX (Ocean Drilling Program), 1–125. doi:10.2973/odp.proc.ir.199.111.2002

Spezzaferri, S., 1994. Planktonic foraminiferal biostratigraphy and taxonomy of the Oligocene and lower Miocene in the oceanic record: an overview. *Palaeontographica Ital.,* 81:1–187.

Takata, H., and Nomura, R., 2005. Data report: Oligocene benthic foraminifers from the eastern equatorial Pacific, Sites 1218 and 1219, ODP Leg 199. *In* Wilson, P.A., Lyle, M., and Firth, J.V. (Eds.), *Proc. ODP, Sci. Results,* 199: College Station, TX (Ocean Drilling Program), 1–26. doi:10.2973/odp.proc.sr.199.224.2005

Thomas, E., 1985. Late Eocene to Recent deep-sea benthic foraminifers from the central equatorial Pacific Ocean. *In* Mayer, L., Theyer, F., Thomas, E., et al., *Init. Repts. DSDP,* 85: Washington, DC (U.S. Govt. Printing Office), 655–694. doi:10.2973/dsdp.proc.85.117.1985

Wade, B.S., and Pearson, P.N., 2008. Planktonic foraminiferal turnover, diversity fluctuations and geochemical signals across the Eocene/Oligocene boundary in Tanzania. *Mar. Micropaleontol.,* 68(3–4):244–255. doi:10.1016/j.marmicro.2008.04.002

van Morkhoven, F.P.C.M., Berggren, W.A., and Edwards, A.S., 1986. *Cenozoic Cosmopolitan Deep-Water Benthic Foraminifera*. Bull. Cent. Rech. Explor.—Prod. Elf-Aquitaine, Mem. 11.

Publication: 30 October 2010
MS 320321-105

Figure F1. A. ETOPO1 (Amante and Eakins, 2008) bathymetric overview map of Site U1333 and PEAT drilling locations, with previous ODP and DSDP sites. **B.** Swath map bathymetry for Site U1333 region from the AMAT-03 site survey. Black labels = seismic shotpoints, white labels = bathymetric contours. White line = part of the seismic reflection profile across Site U1333 (Fig. F2). F.Z. = fracture zone.

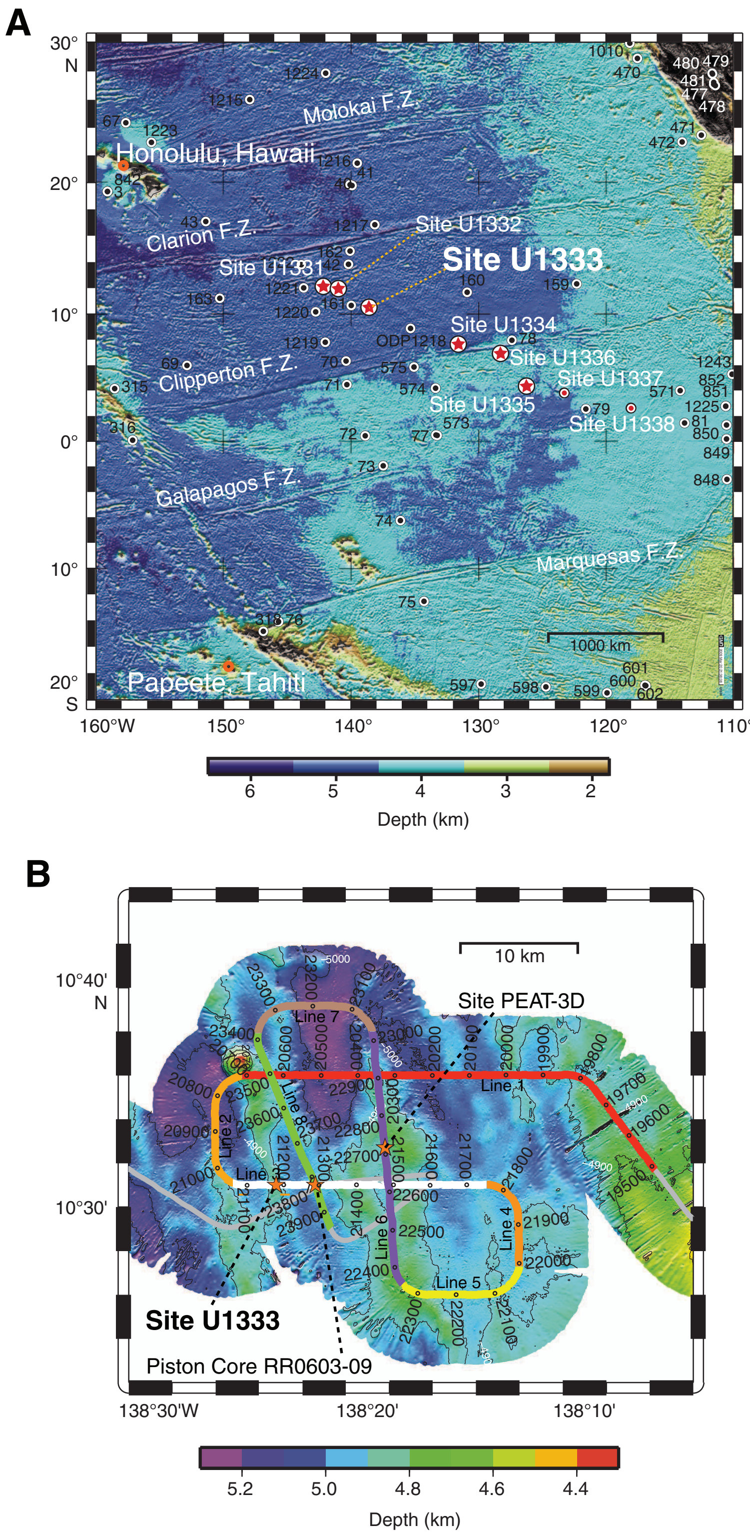

Figure F2. Seismic reflection profile PEAT-3C (Site U1333) Line 3 from the 48-channel seismic reflection survey, annotated in shotpoints (Lyle et al., 2006). Data are filtered, stacked, and migrated. Site was located where basal reflections appeared less strong to minimize possible cherts. Tentative conversion from two-way traveltime to depth uses velocity model of Busch et al. (2006). P2, P3 = seismic reflectors of Lyle et al., (2002). All times are Universal Time Coordinated (UTC). TD = total depth.

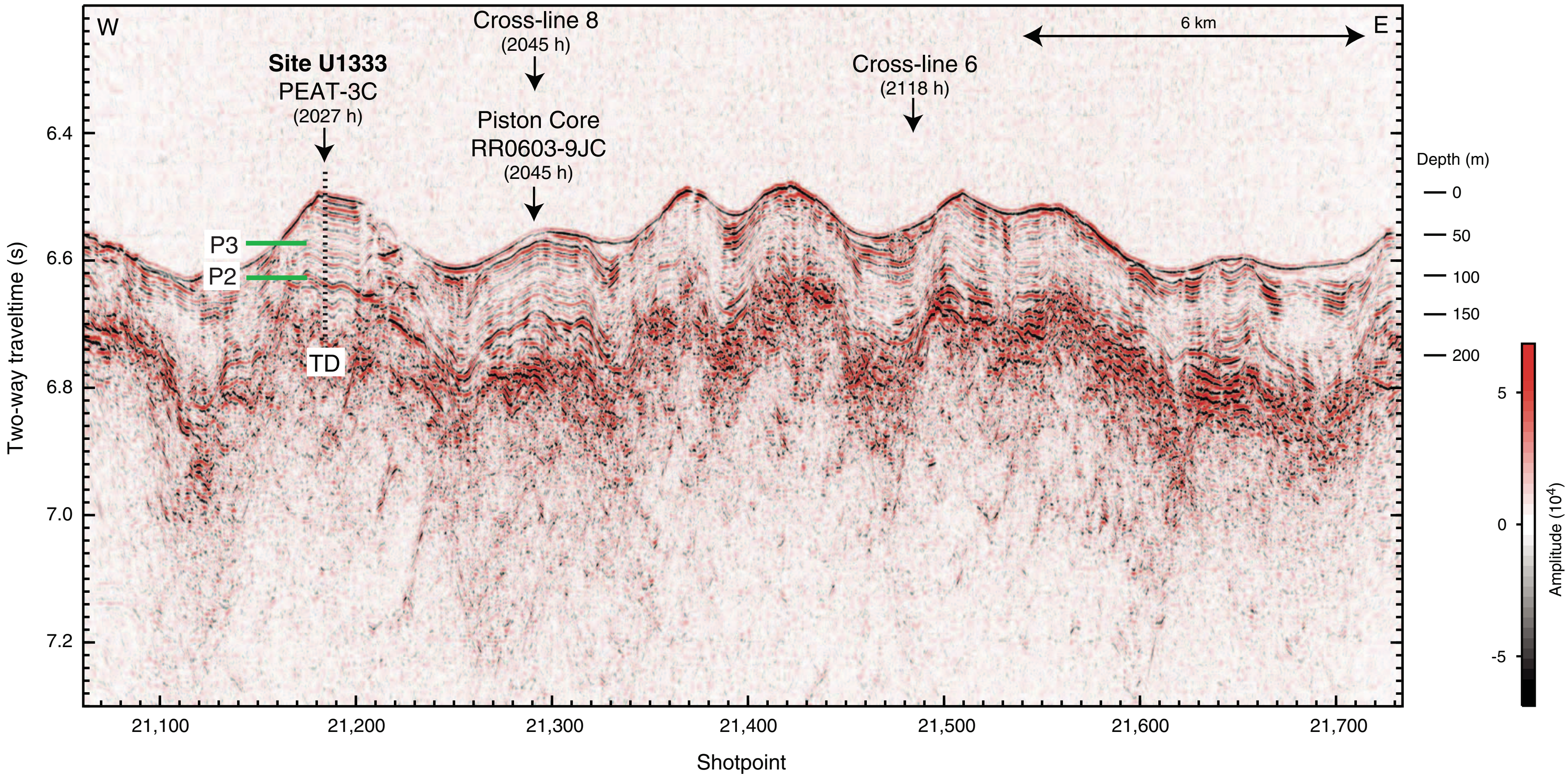

Figure F3. Site U1333 summary. At Site U1333, planktonic foraminifer Zones O3 and O6 are informally divided into an upper and lower part using the top of *Subbotina angiporoides* and base of *Paragloborotalia pseudokugleri,* respectively.

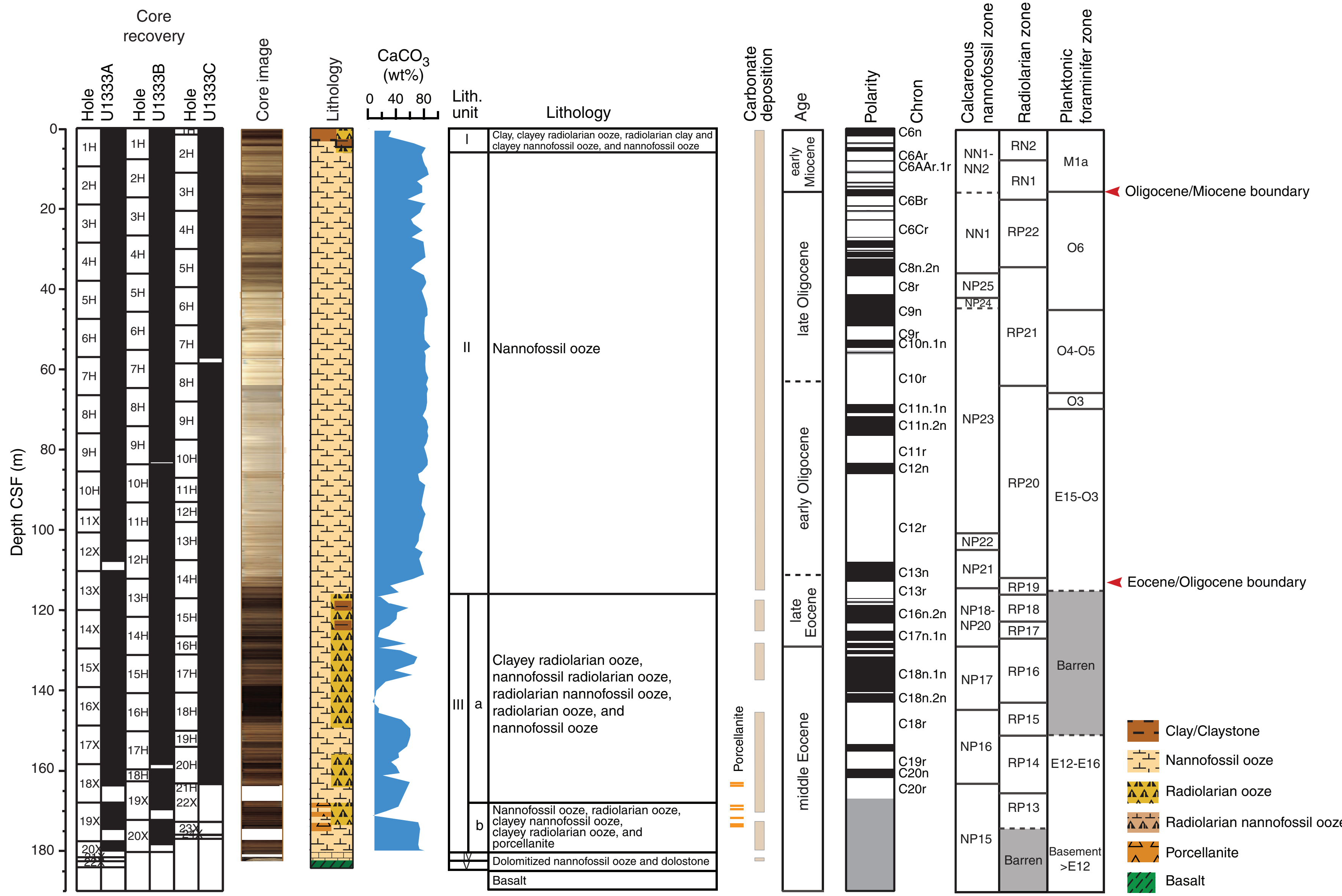

Figure F4. Lithologic summary, Site U1333. L* = reflectance value of sediment as defined in the LAB color model.

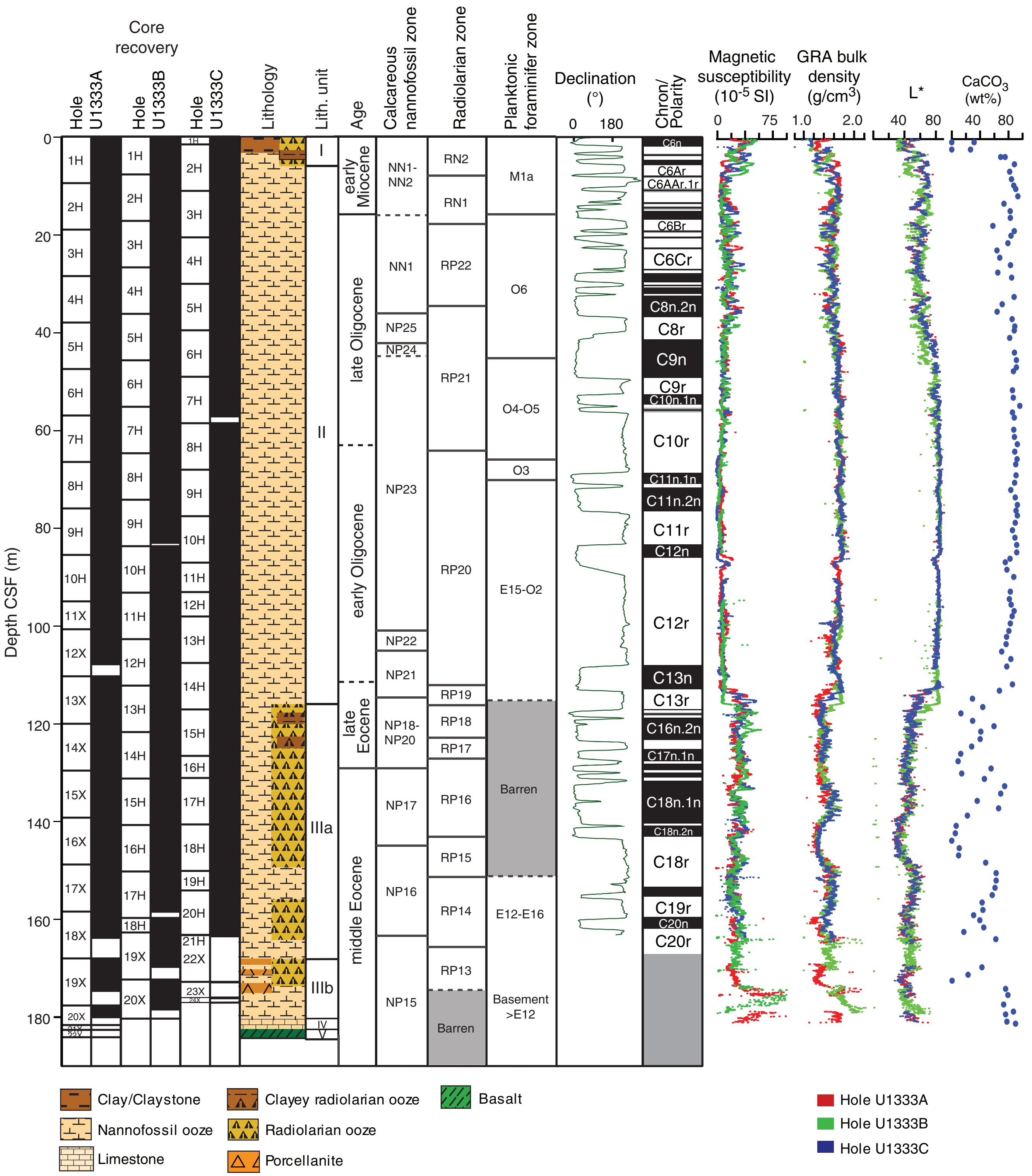

Figure F5. Photomicrographs of smear slides taken across the Eocene–Oligocene transition, Site U1333. Panels are arranged in stratigraphic order (increasing age top to bottom). See **"Site U1333 smear slides"** in "Core descriptions". **A.** Nannofossil ooze with radiolarians (and between 5% and 10% diatoms) (Sample 320-U1333B-13H-4, 114 cm). Left image = plane-polarized light, right image = cross-polarized light. **B.** Radiolarian ooze with clay (Sample 320-U1333C-14H-5, 85 cm). Left image = plane-polarized light, right image = cross-polarized light. **C, D.** Radiolarian nannofossil ooze (Sample 320-U1333B-13H-5, 2 cm) (plane-polarized light). Two fields of view. Note volcanic glass. **E.** Clayey radiolarian ooze with nannofossils (Sample 320-U1333C-16H-4, 23 cm). Left image = plane-polarized light, right image = cross-polarized light.

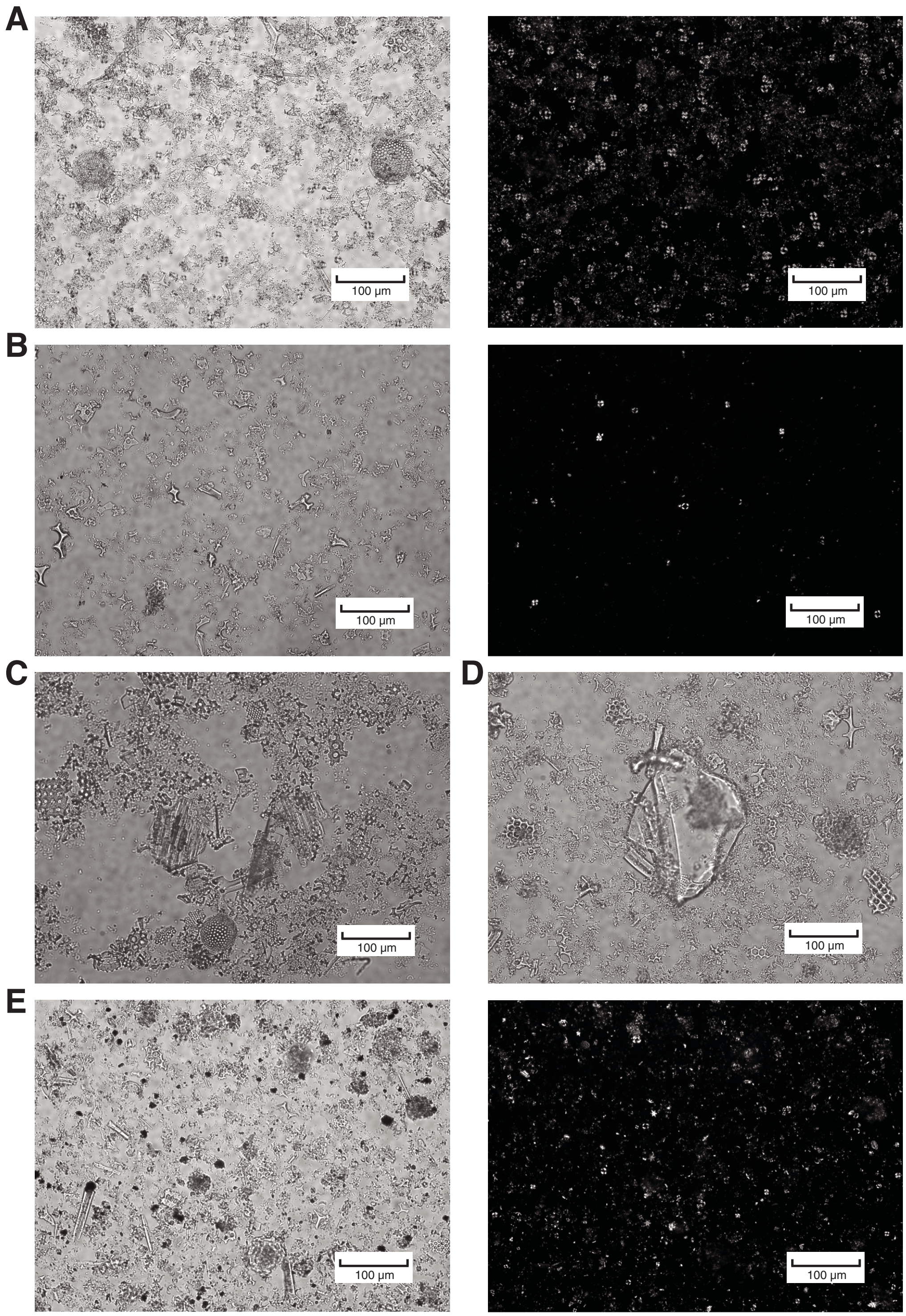

Figure F6. Line scan images of Oligocene–Miocene transition, Site U1333. First occurrence of *Paragloborotalia kugleri* indicated in Hole U1333A is the midpoint depth between samples (see **"Biostratigraphy"**). FO = first occurrence, LO = last occurrence. **A.** Hole U1333A. **B.** Hole U1333B. **C.** Hole U1333C.

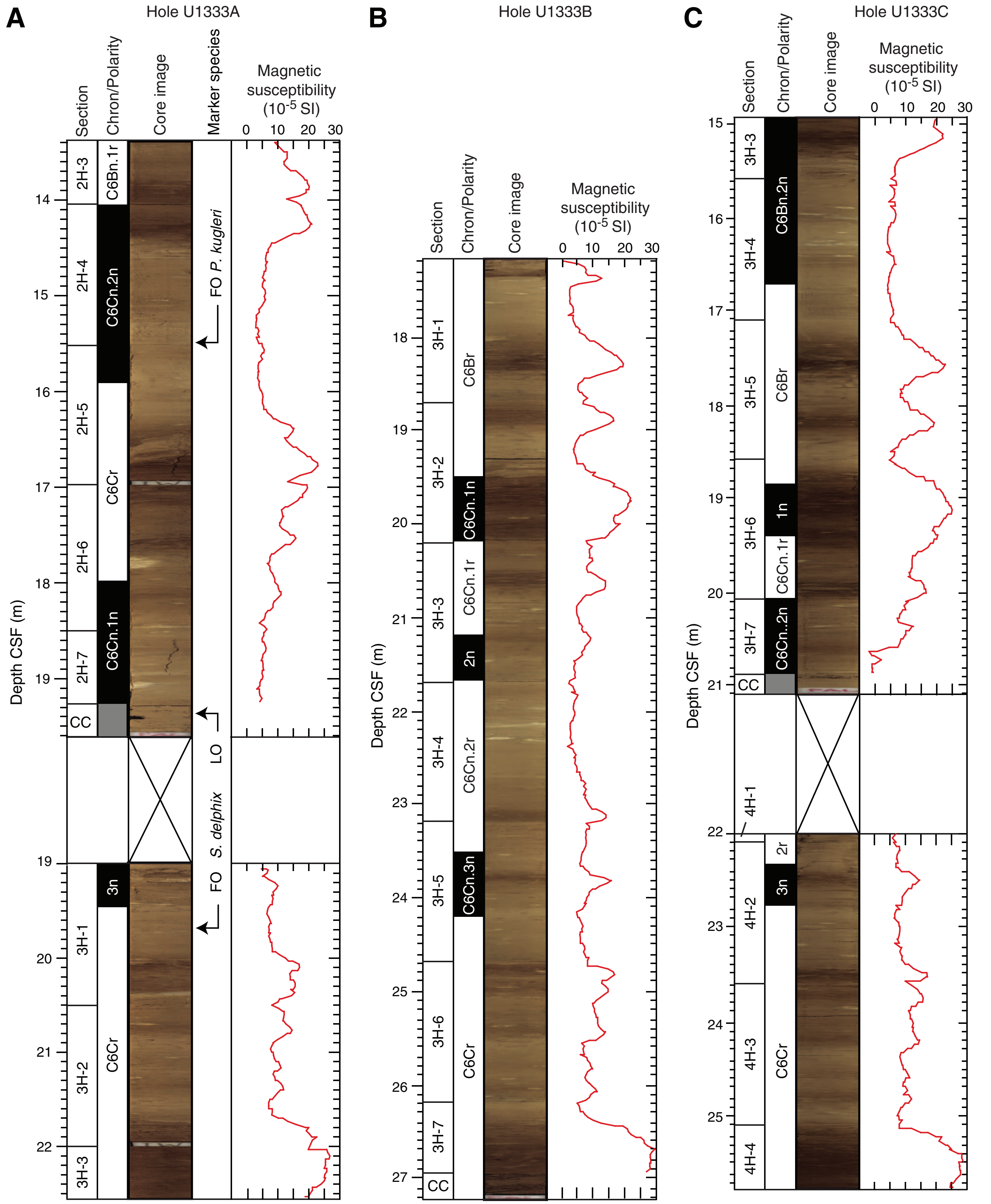

Figure F7. Line scan images of Eocene–Oligocene transition. **A.** Hole U1333A. **B.** Hole U1333B. **C.** Hole U1333C. L* = reflectance value of sediment as defined in the LAB color model.

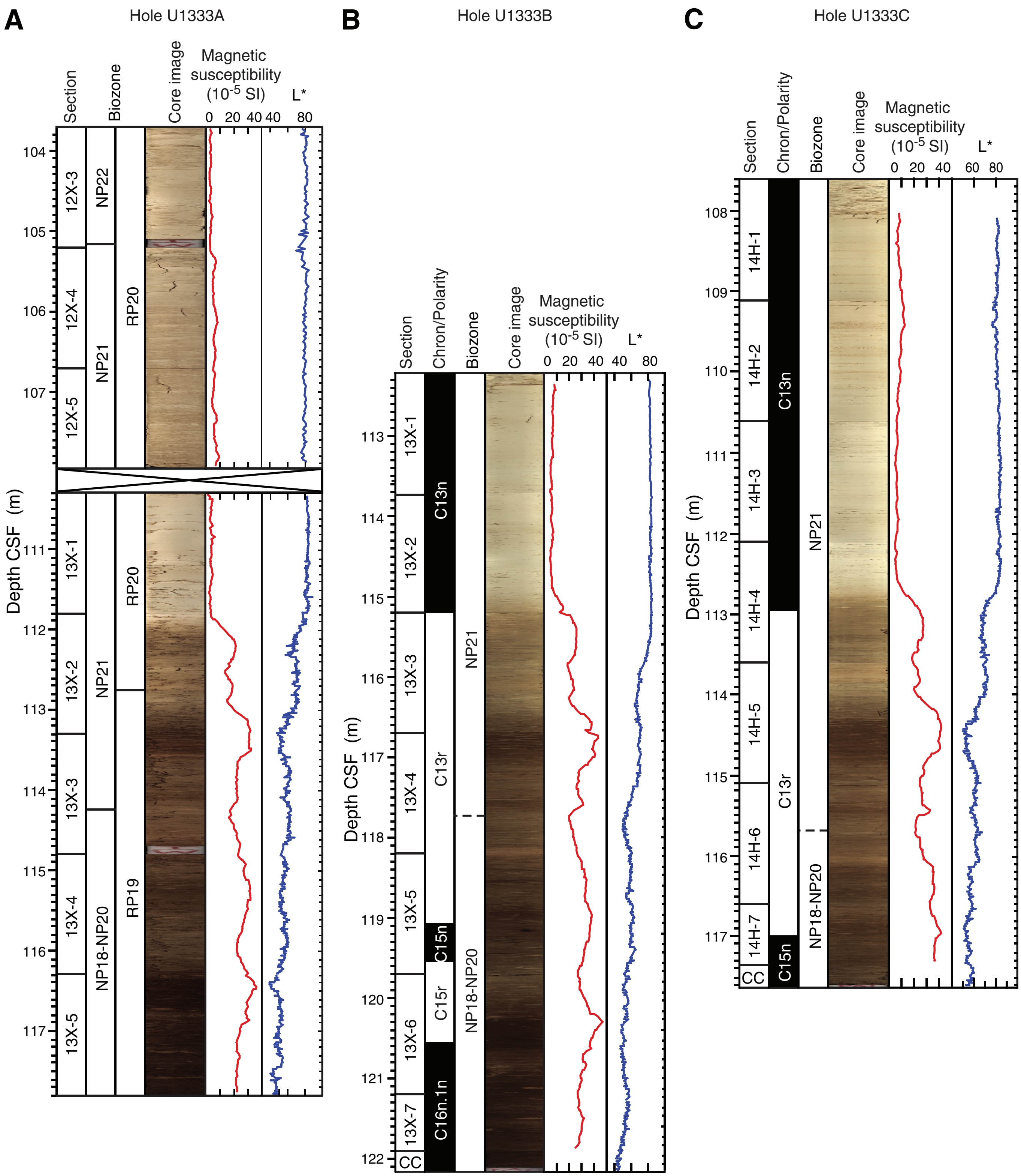

Figure F8. Line scan images of porcellanite layers. GRA = gamma ray attenuation. **A.** Hole U1333A. **B.** Hole U1333B.

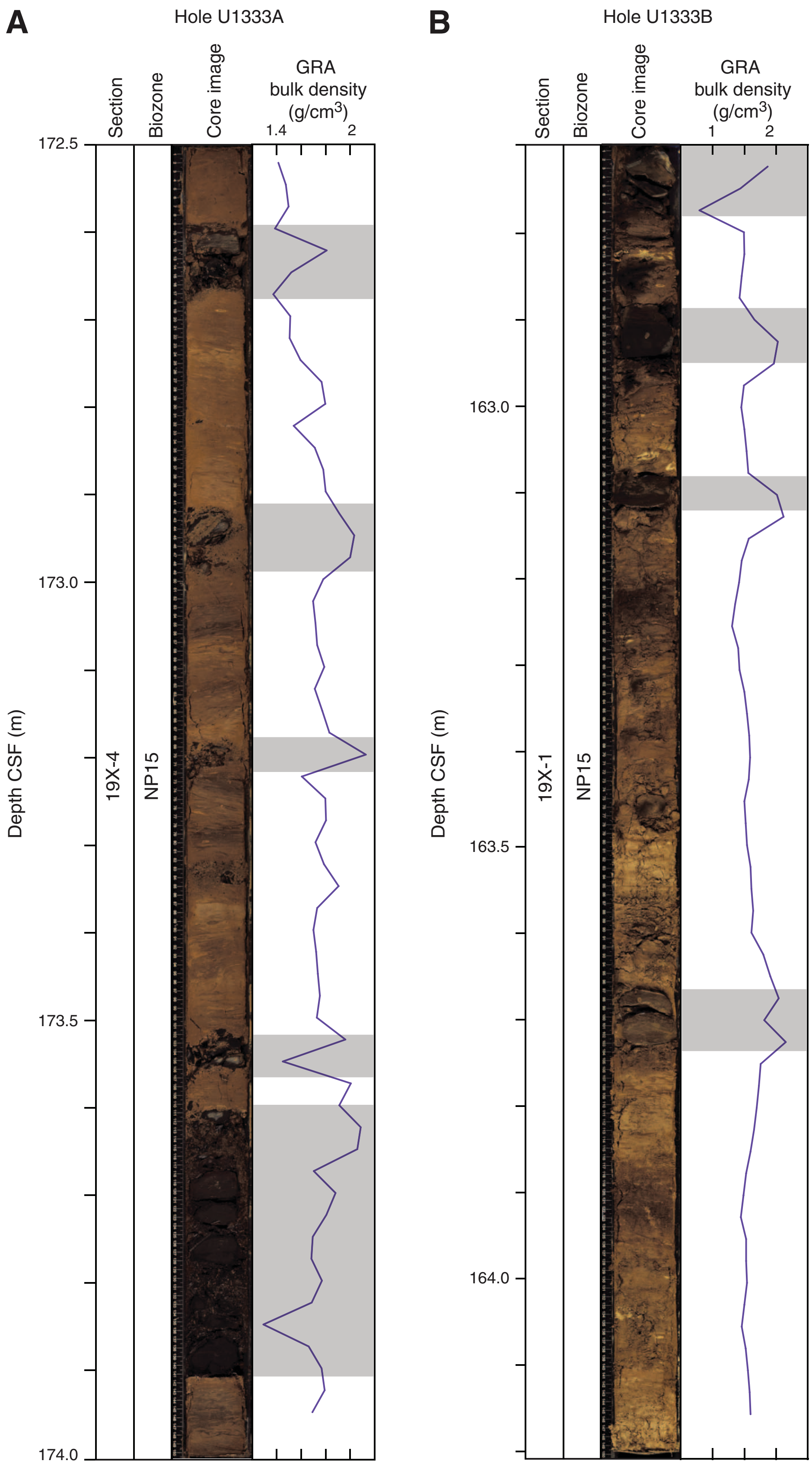

Figure F9. Integrated calcareous and siliceous microfossil biozonation, Site U1333. Calcareous microfossil zonation was limited by the presence of extensive barren intervals; dashed zonal boundaries indicate stratigraphic extent of calcareous microfossil assemblages consistent with a particular zonal assignment.

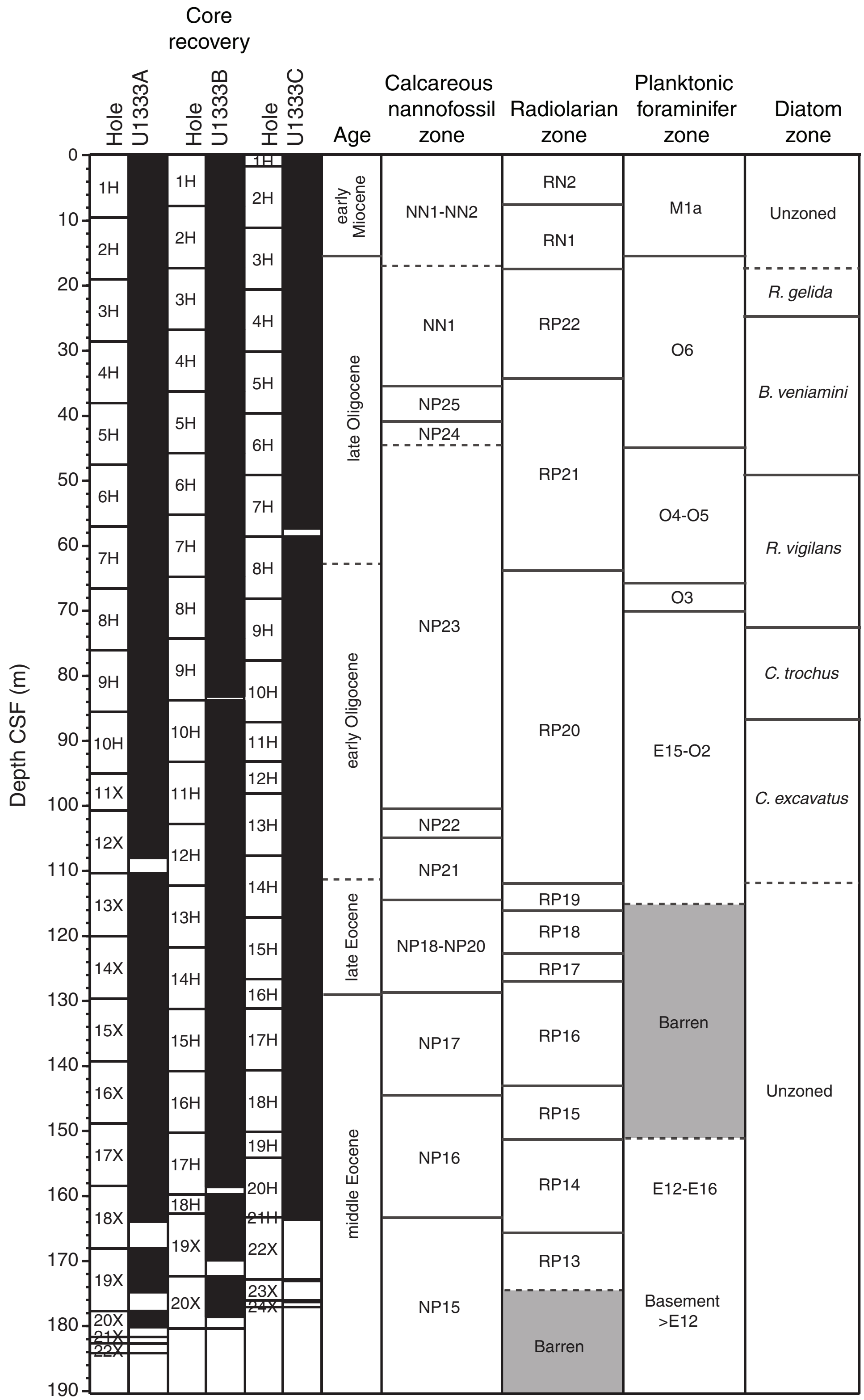

Figure F10. Linear sedimentation rates and chronostratigraphic markers, Site U1333. See Table T33 for data used.

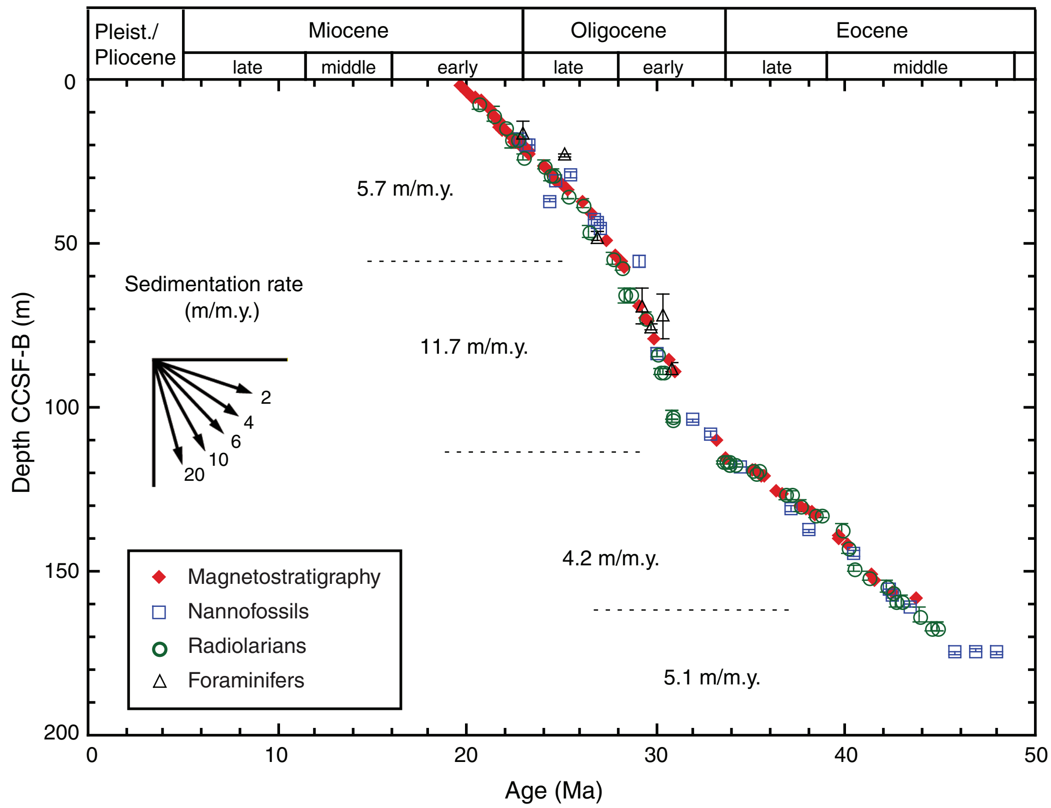

Figure F11. Stratigraphic distribution and abundance of *Nuttallides truempyi* and other benthic foraminifers (calcareous and agglutinated). High carbonate intervals (approximately >40%) in three holes of Sites (**A**) U1333, (**B**) U1332, and (**C**) U1331. Presence of other foraminifers indicates presence of calcareous hyaline foraminifers, except for *N. truempyi*.

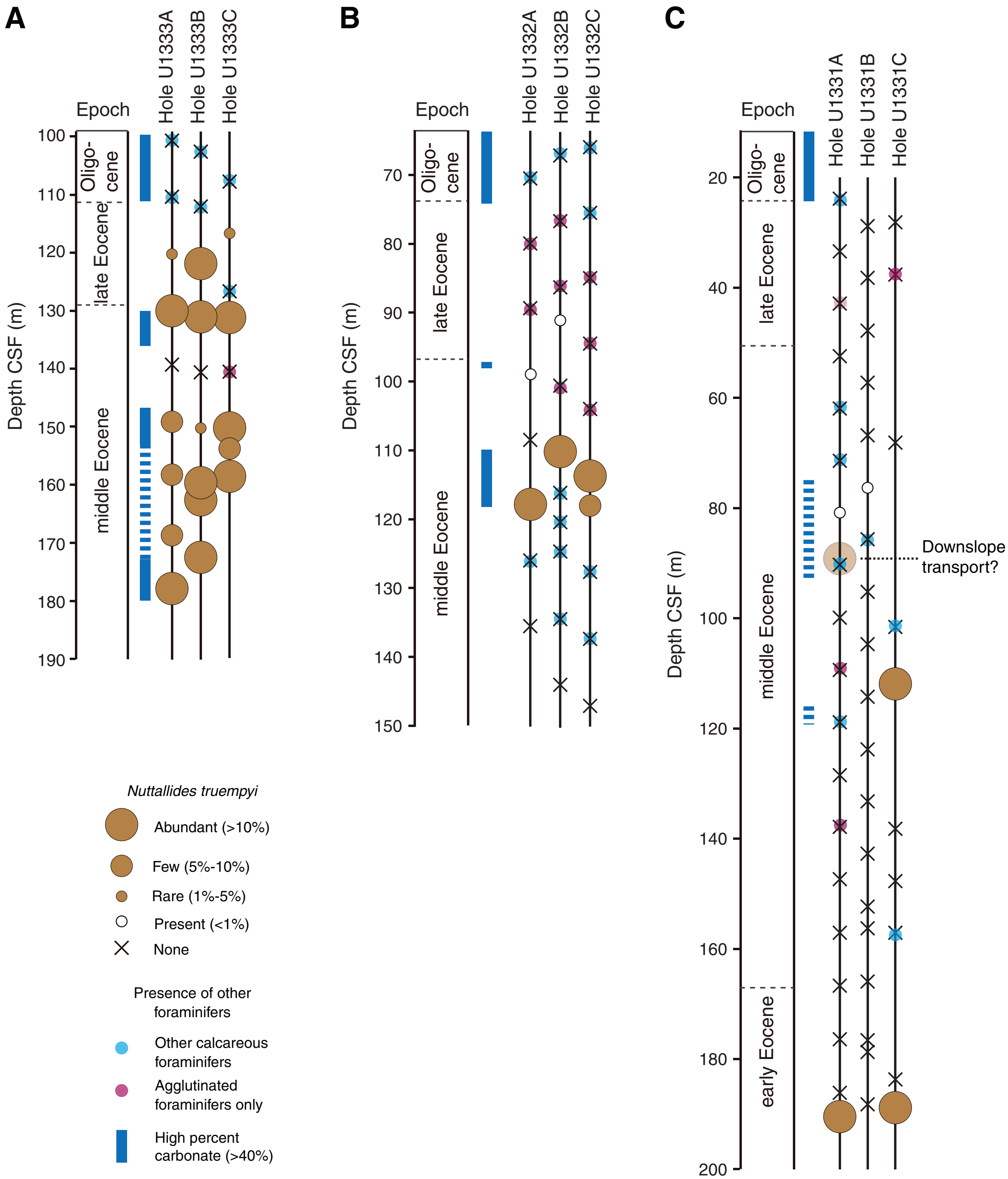

Figure F12. Summary of magnetic susceptibility and paleomagnetic results, Hole U1333A. NRM = natural remanent magnetization.

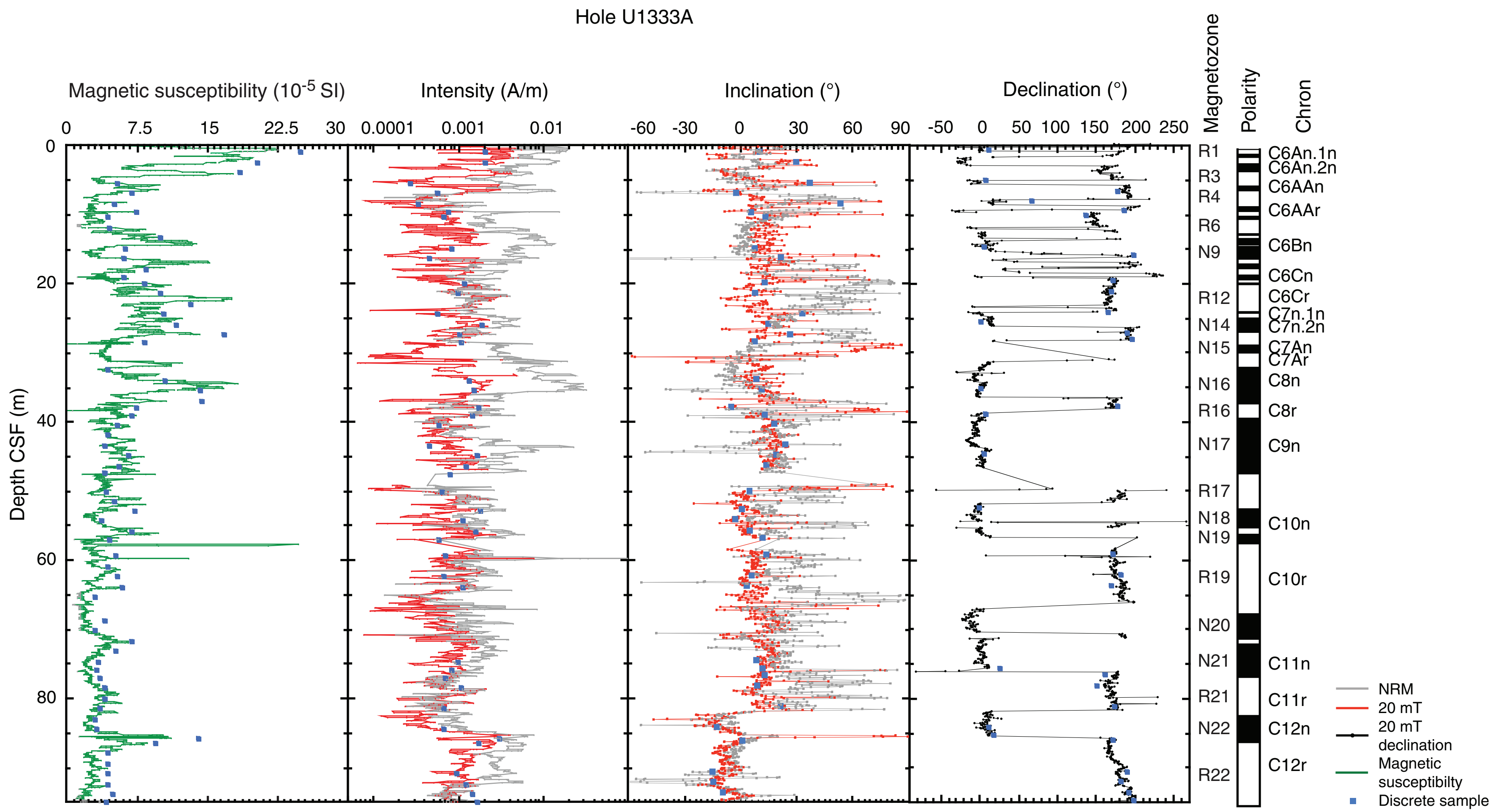

Figure F13. Summary of magnetic susceptibility and paleomagnetic results, Hole U1333B. * = position of the newly recognized cryptochron within Chron C18n.1n. NRM = natural remanent magnetization.

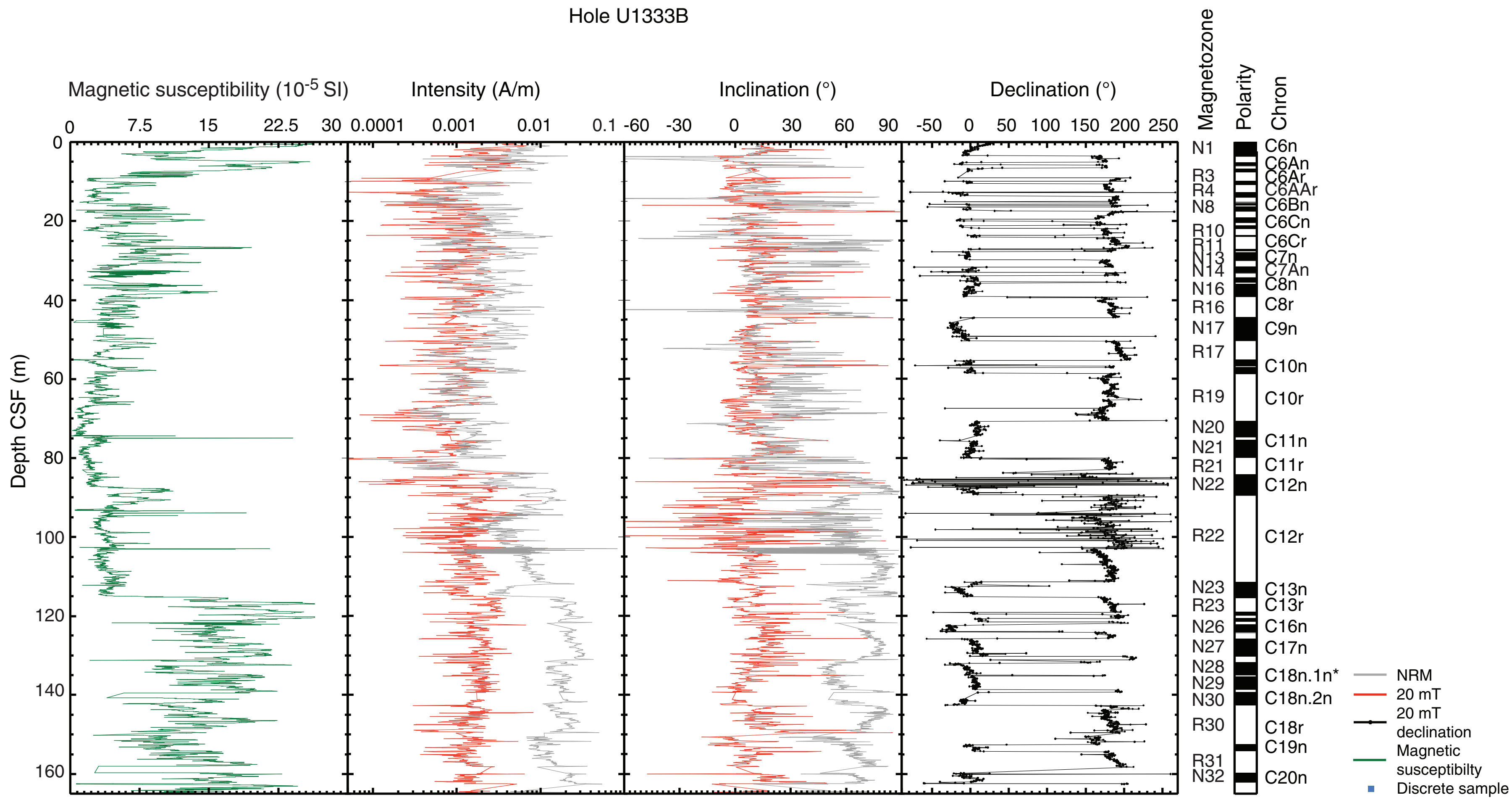

Figure F14. Summary of susceptibility and paleomagnetic results, Hole U1333C. * = position of the newly recognized cryptochron within Chron C18n.1n. NRM = natural remanent magnetization.

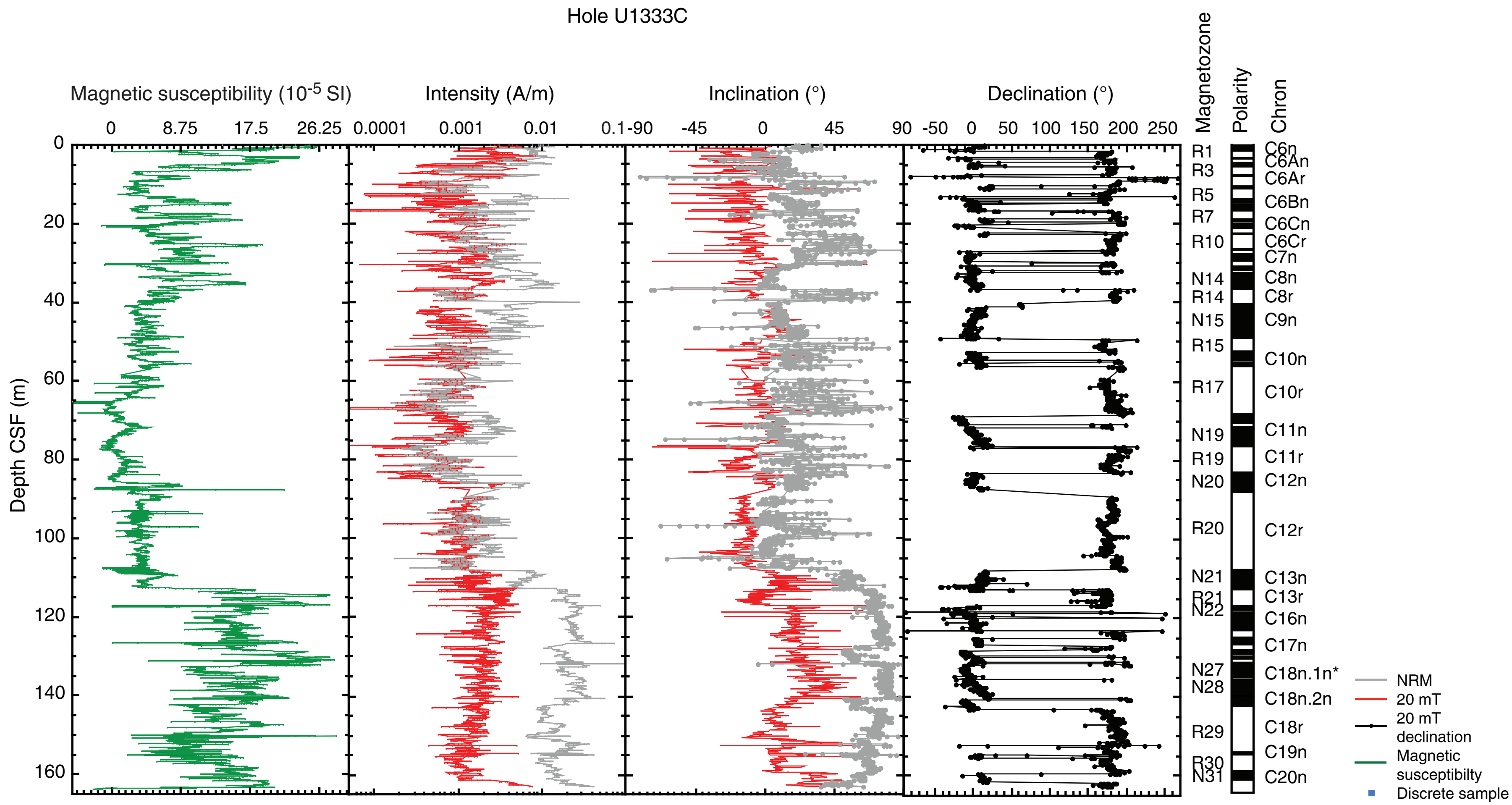

Figure F15. Natural remanent magnetization intensity from Holes U1333B and U1333C before demagnetization. Lithology from Hole U1333A (see "Lithostratigraphy"). Black arrows show increased magnetic overprinting and noise of sediments recovered using steel core barrel. E/O = Eocene/Oligocene.

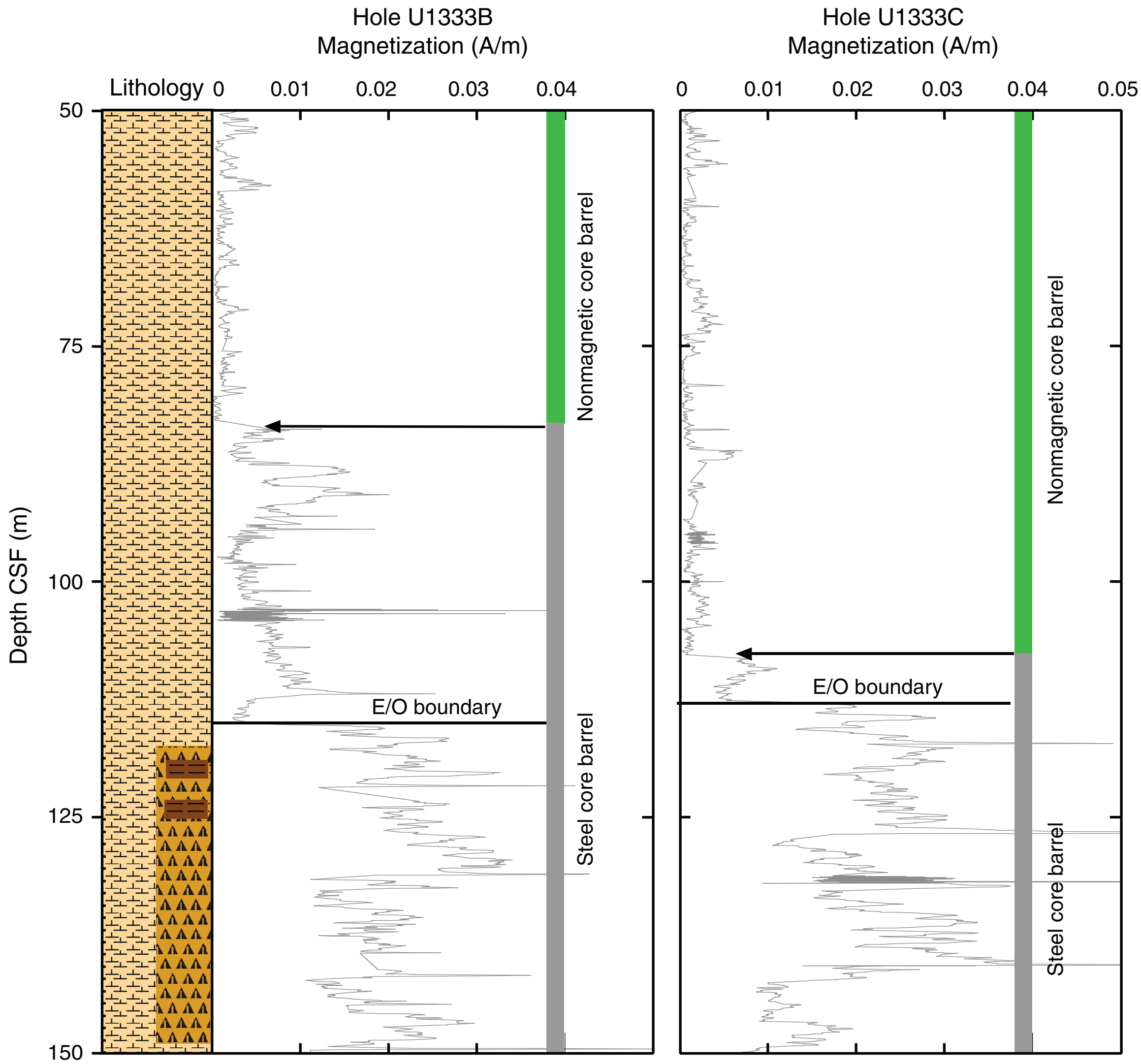

Figure F16. Alternating-field demagnetization (demag) results for two discrete samples. Left plot shows vector endpoints of paleomagnetic directions on vector demagnetization diagrams or modified Zijderveld plots (squares = inclinations, circles = declinations), right plot shows intensity variation with progressive demagnetization. Data illustrate removal of drilling overprint, which is small in these samples. Above the 10 mT demagnetization step, a stable component is observed, which we interpret as the ChRM. Vectors do not terminate at the origin of plots, which might indicate instrument noise. **A.** Sample 320-U1333A-1H-2, 85 cm (2.35 m CSF). **B.** Sample 320-U1333A-10H-6, 85 cm (93.85 CSF). NRM = natural remanent magnetization.

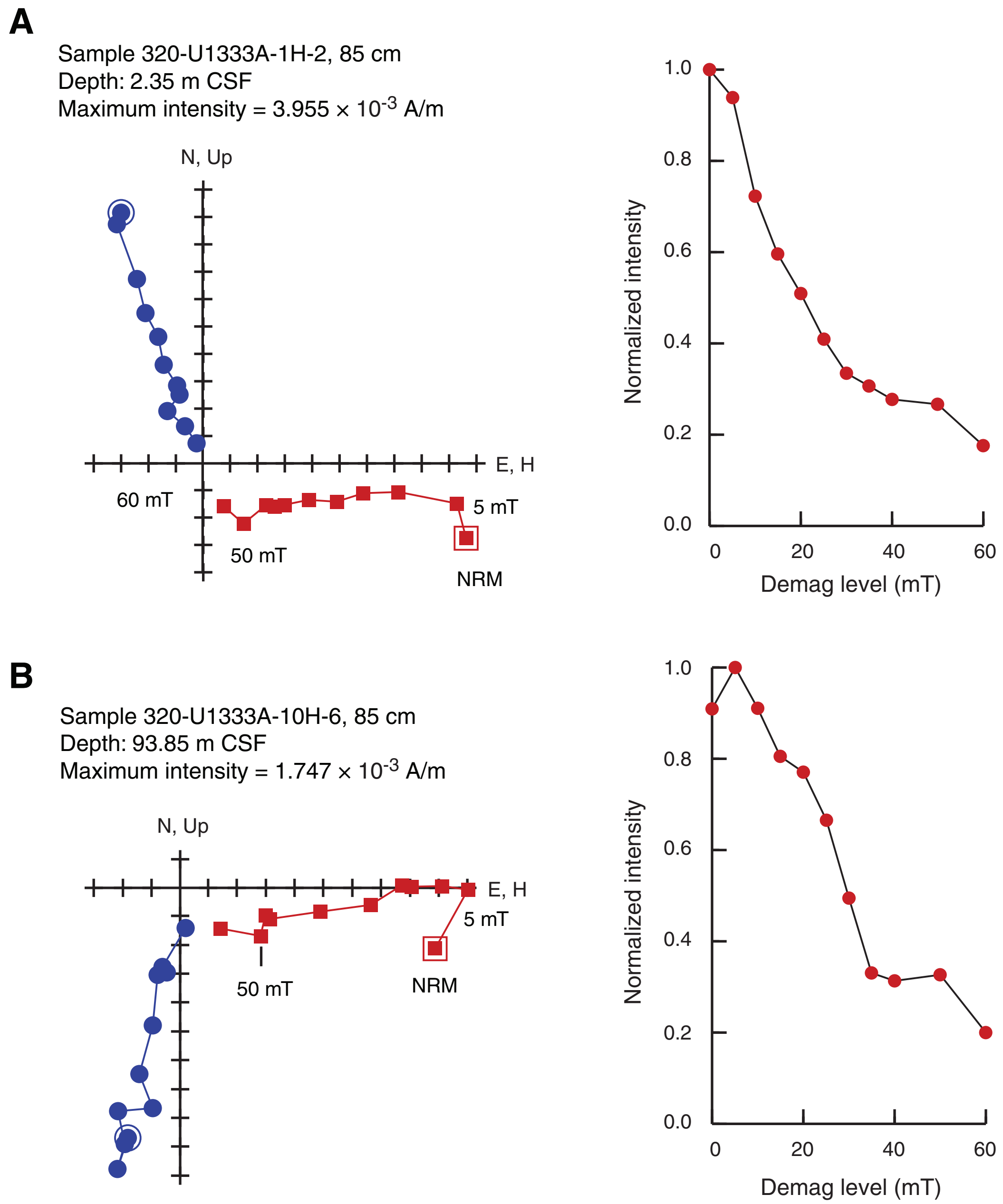

Figure F17. Latitude of the virtual geomagnetic pole (VGP), as determined from paleomagnetic directions. North latitudes = normal polarity, south latitudes = reversed polarity. Gray lines = core gaps.

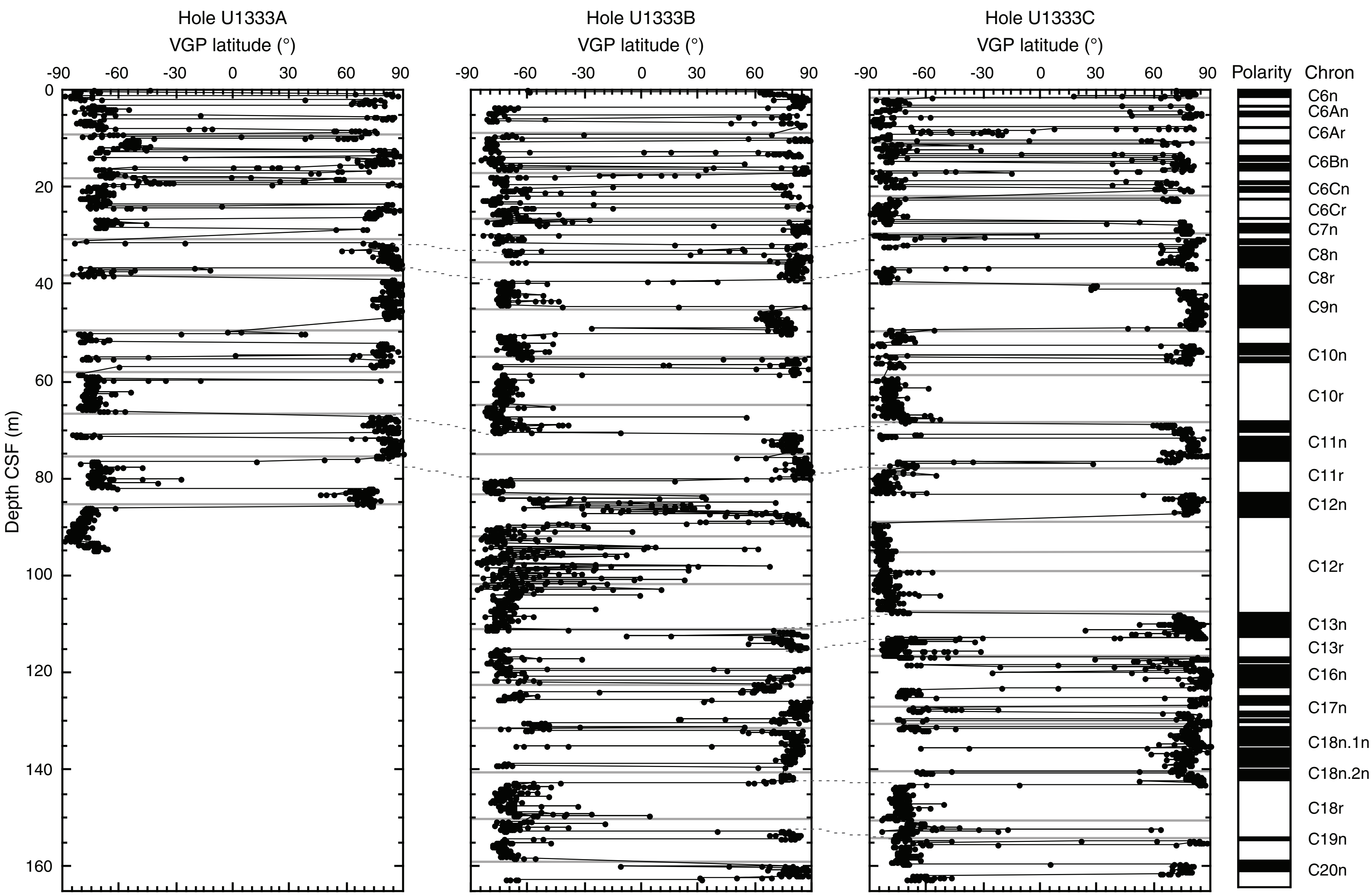

Figure F18. Interstitial water geochemical data, Hole U1333A. Values below the detection limit (see Table **T25**) are plotted as zero. (See **"Lithostratigraphy"** for information on unit boundaries.)

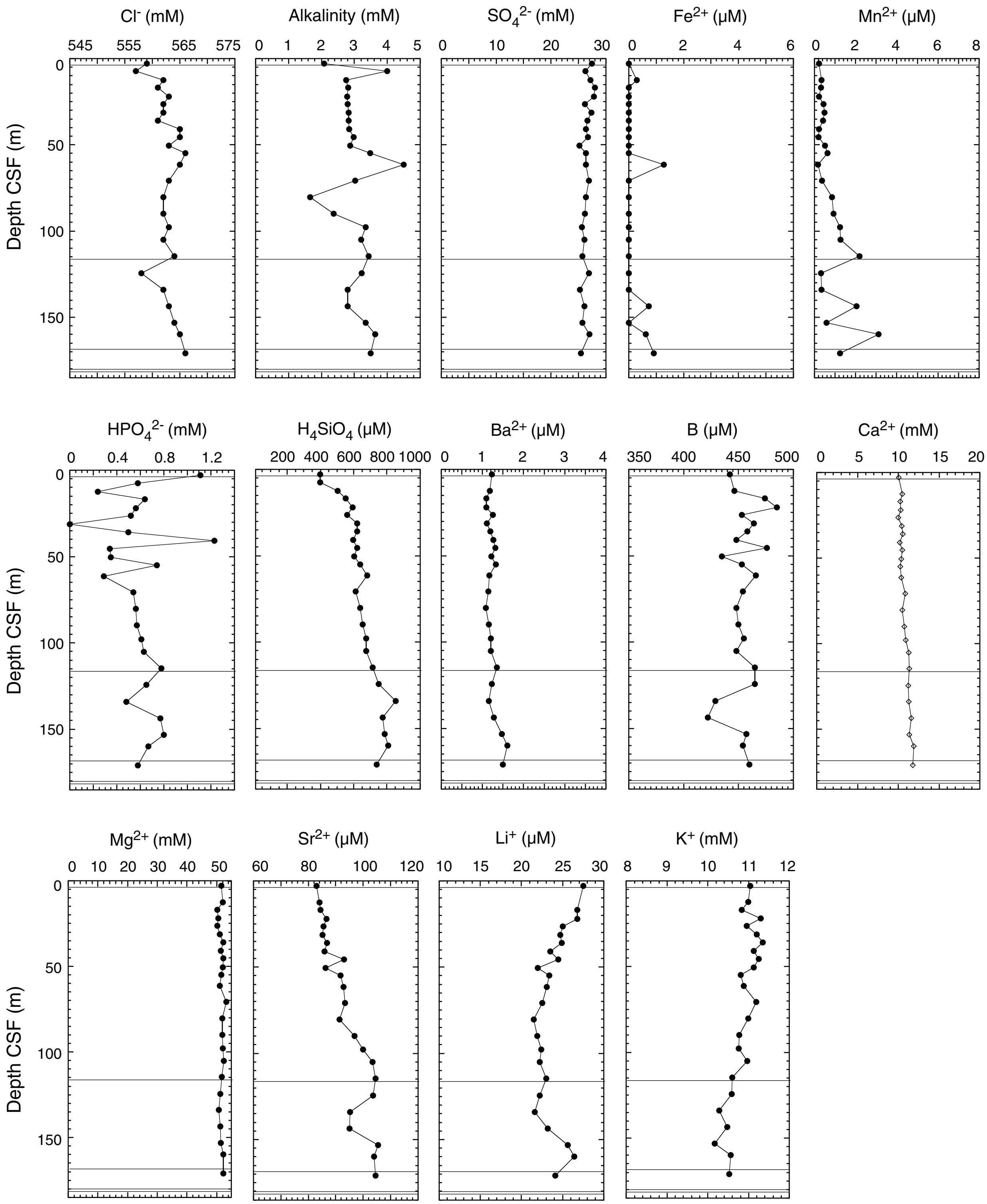

Figure F19. Calcium carbonate ($CaCO_3$), total carbon (TC), inorganic carbon (IC), and total organic carbon (TOC) determined by the acidification method in sediments from Hole U1333A.

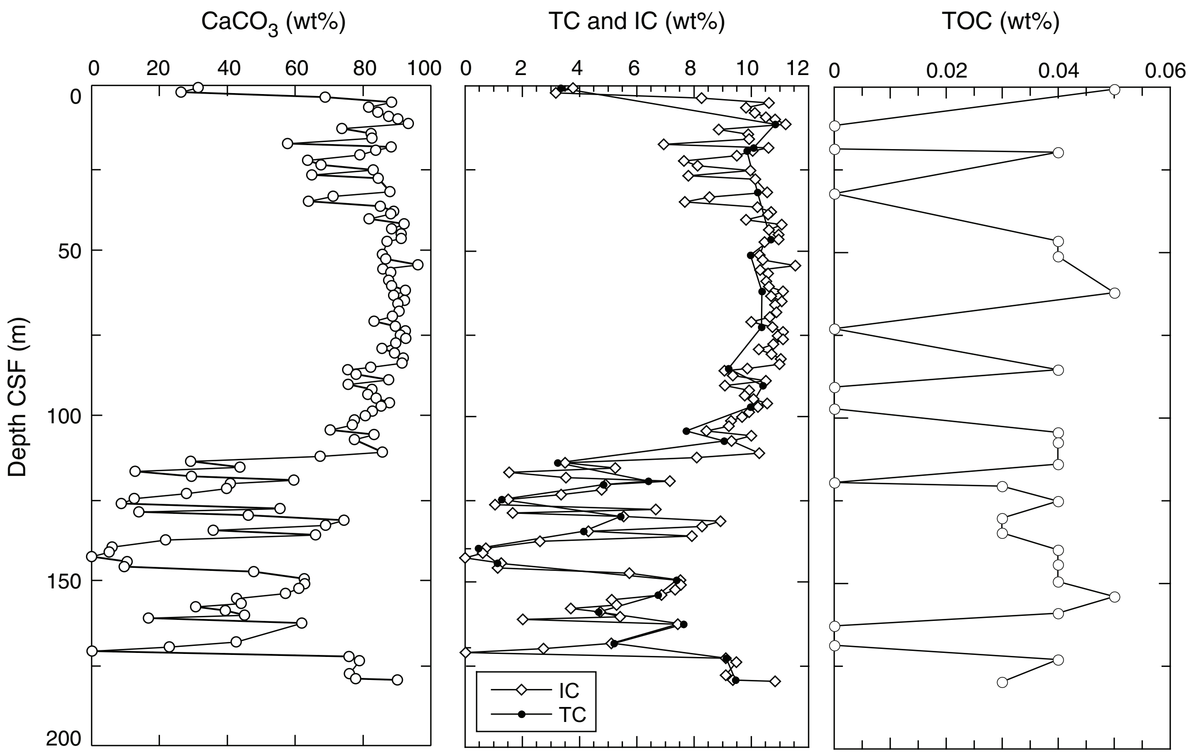

Figure F20. Whole-Round Multisensor Logger (WRMSL) and natural gamma radiation (NGR) data, Holes U1333A–U1333C. Hole U1333B and U1333C data are plotted using offsets (0.5 and 1.0 g/cm³ for gamma ray attenuation [GRA] bulk density; 10 and 20 × 10^{-5} SI for magnetic susceptibility; 100 and 200 m/s for *P*-wave velocity; 10 and 20 cps for NGR).

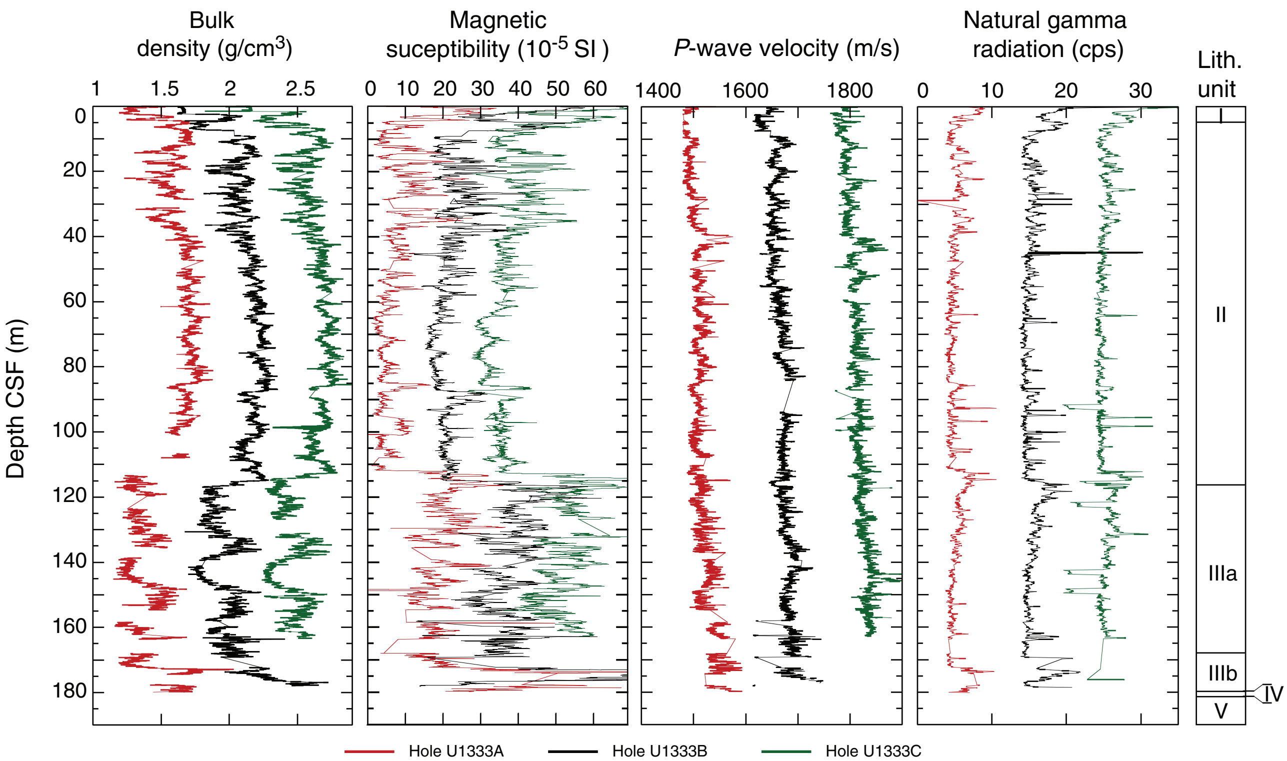

Figure F21. Moisture and density measurements, Hole U1333A. GRA = gamma ray attenuation. **A.** Porosity and water content. **B.** Bulk density, MAD, and GRA. **C.** Grain density.

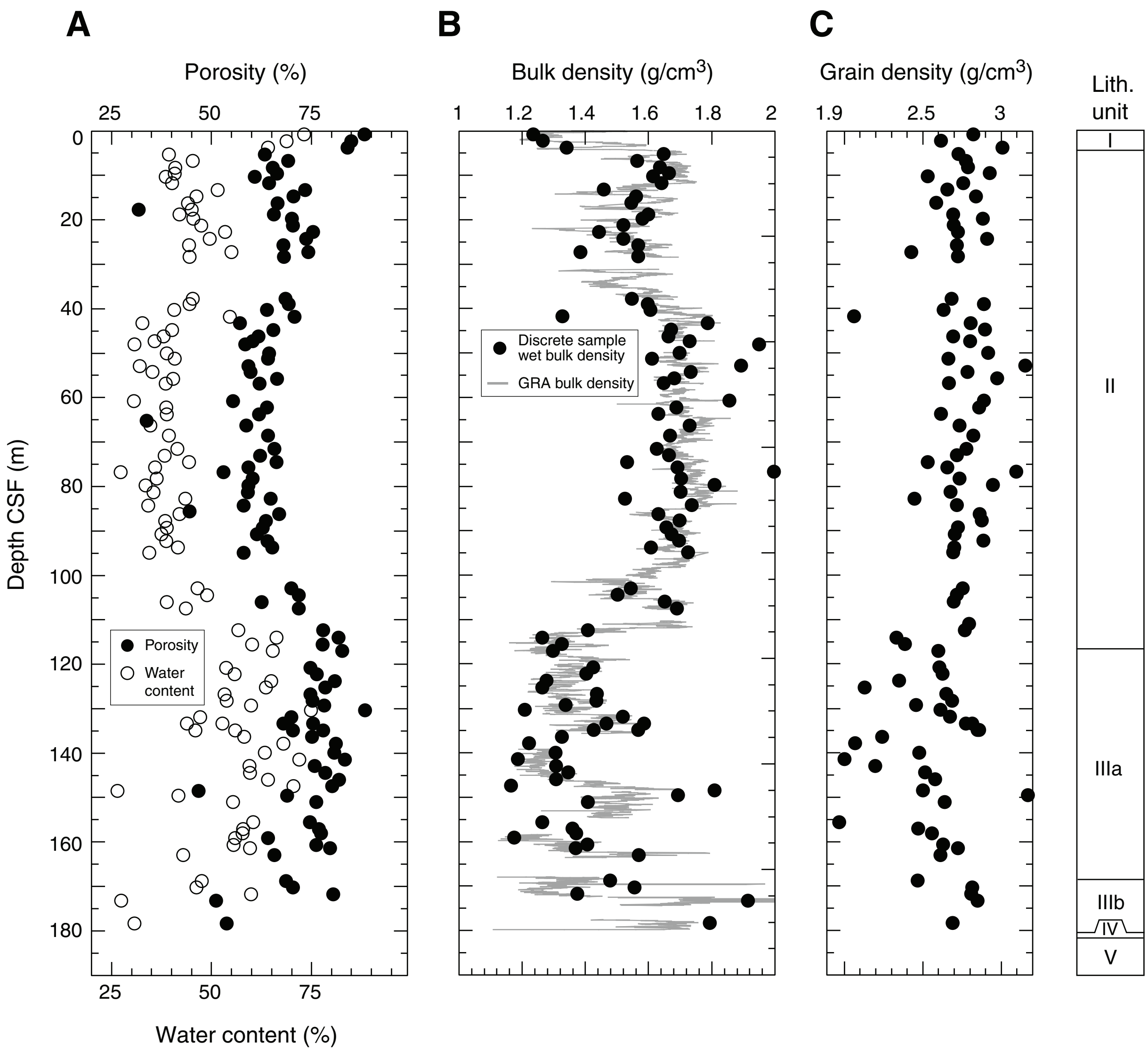

Figure F22. Moisture and density (MAD) analysis of discrete samples, Hole U1333A. Gamma ray attenuation (GRA) density interpolated with a 20 cm wide Gaussian window.

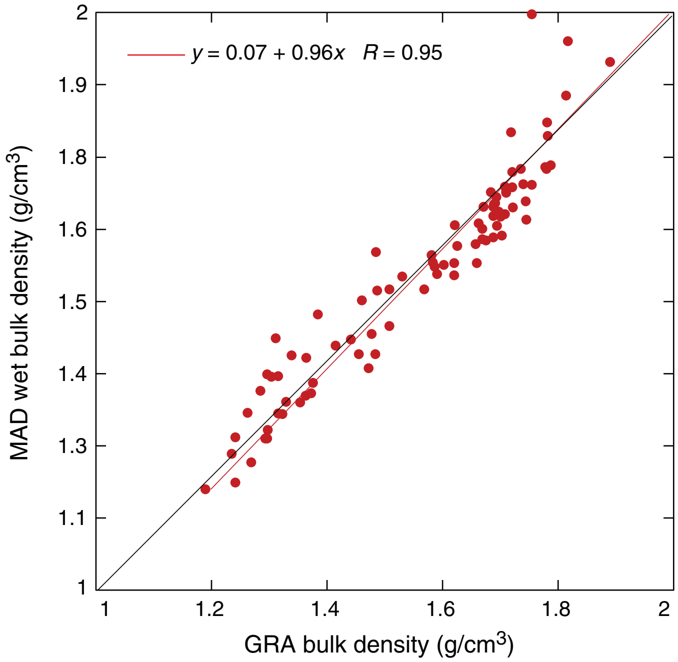

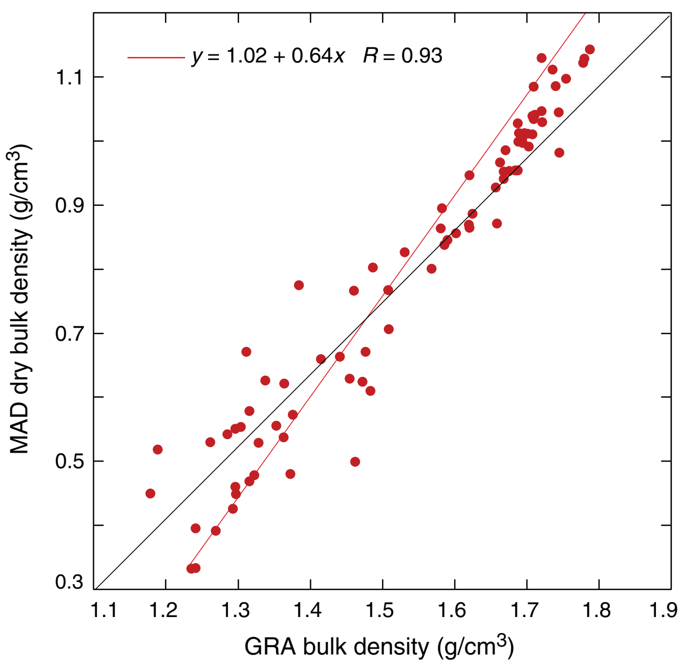

Figure F23. Compressional wave velocity from the *P*-wave logger (PWL) and discrete velocity measurements on split core from Hole U1333A, using the contact probe for *x*-axis measurements and insertion probes for *y*- and *z*-axis measurements. (see **"Compressional wave velocity"** for note on postcruise velocity correction.)

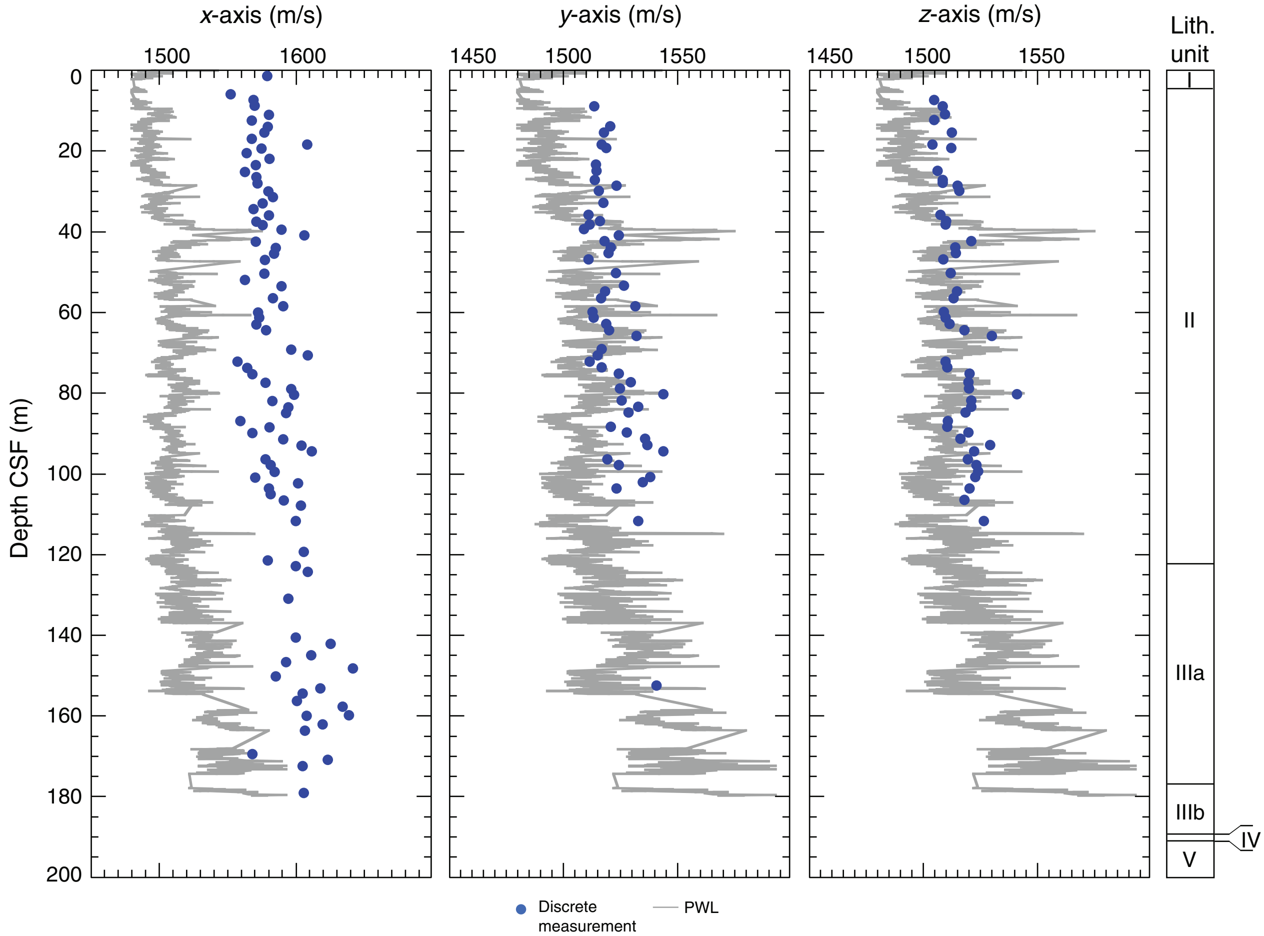

Figure F24. Porosity and thermal conductivity measurements, Hole U1333A.

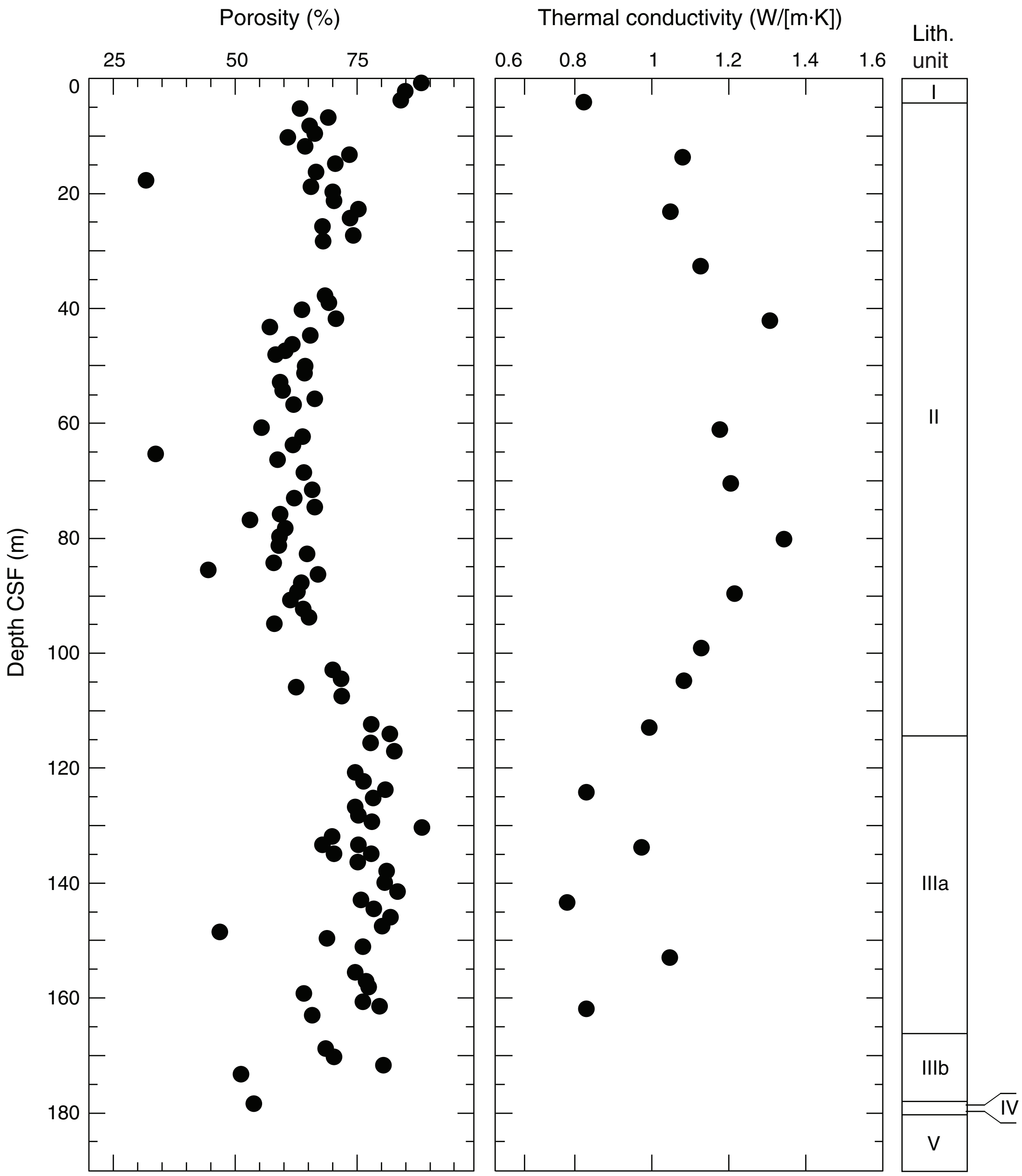

Figure F25. Thermal conductivity vs. porosity, from moisture and density analysis of discrete samples.

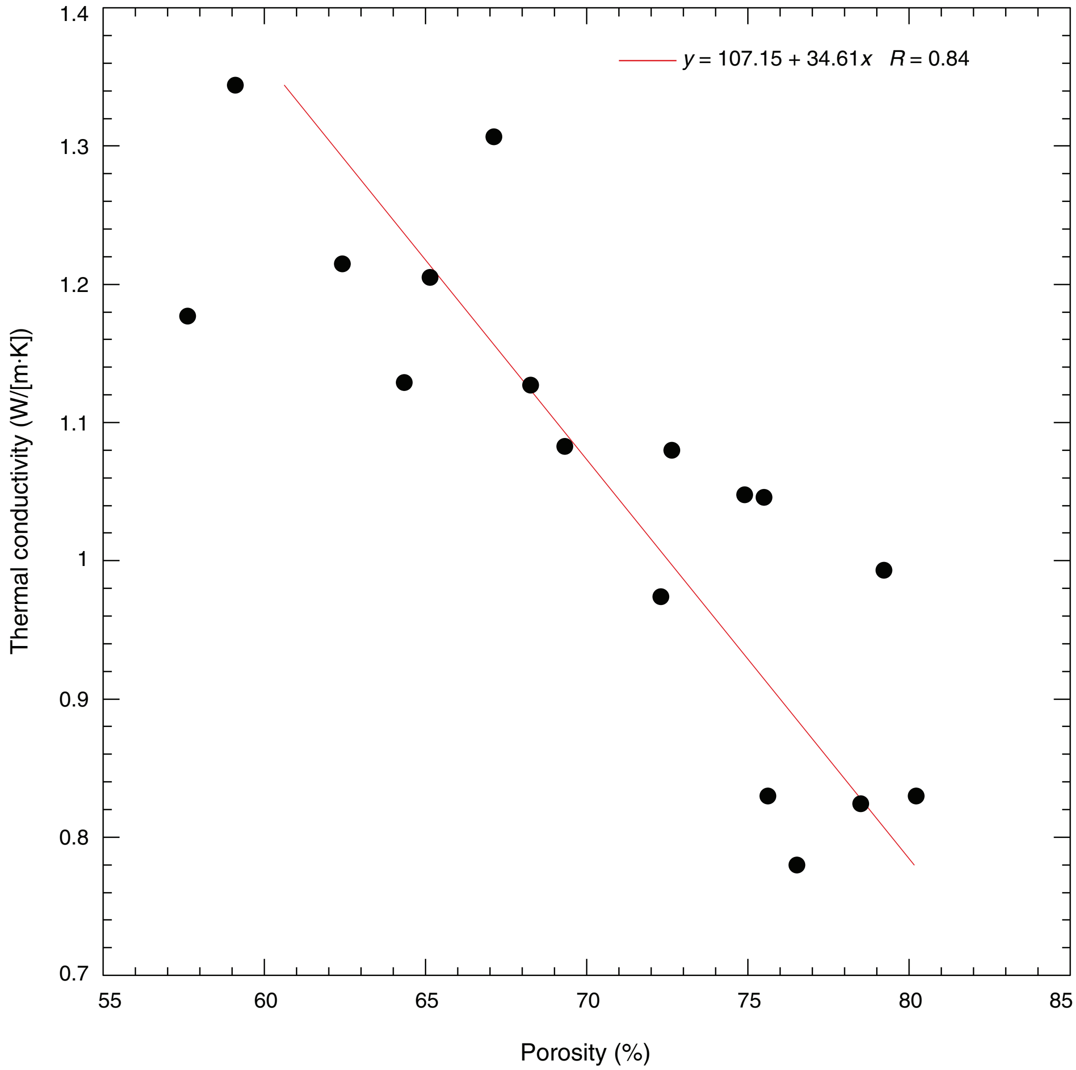

Figure F26. Reflectance spectrophotometer (RSC) data, Holes U1333A–U1333C. RSC for Holes U1333B and U1333C have been offset (20 and 40 for L*; 4 and 8 for a*; 8 and 16 for b*) for core to core comparison. L*, a*, b* = reflectance value of sediment as defined in the LAB color model.

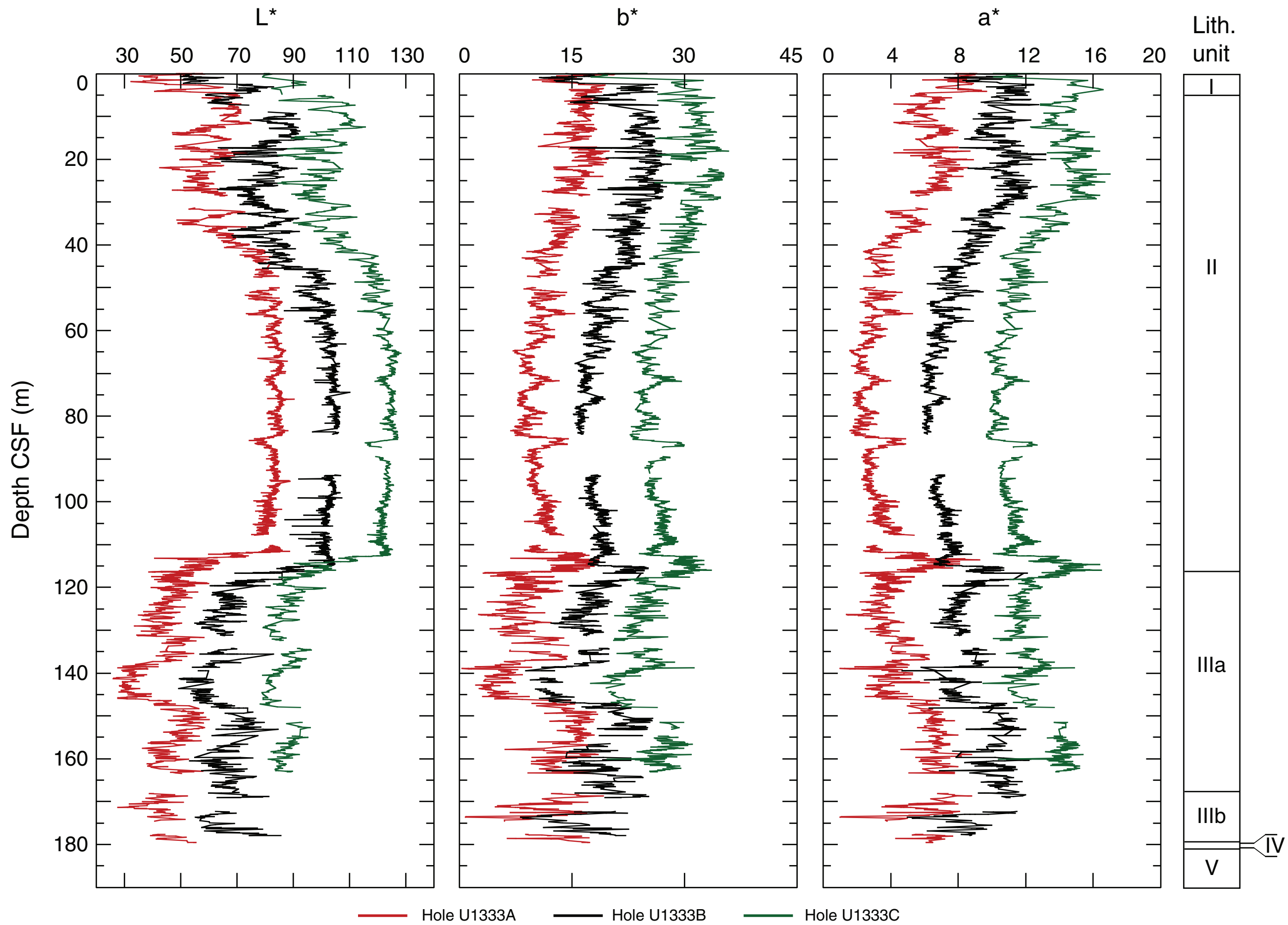

Figure F27. Magnetic susceptibility data, Site U1333. Top panel = spliced section with core breaks (triangles) and hole designations, bottom panel = Holes U1333A (red), U1333B (blue), and U1333C (green), offset from each other by a constant (300 × 10^{-6} SI). **A.** 0–50 CCSF-A. (**Continued on next three pages.**)

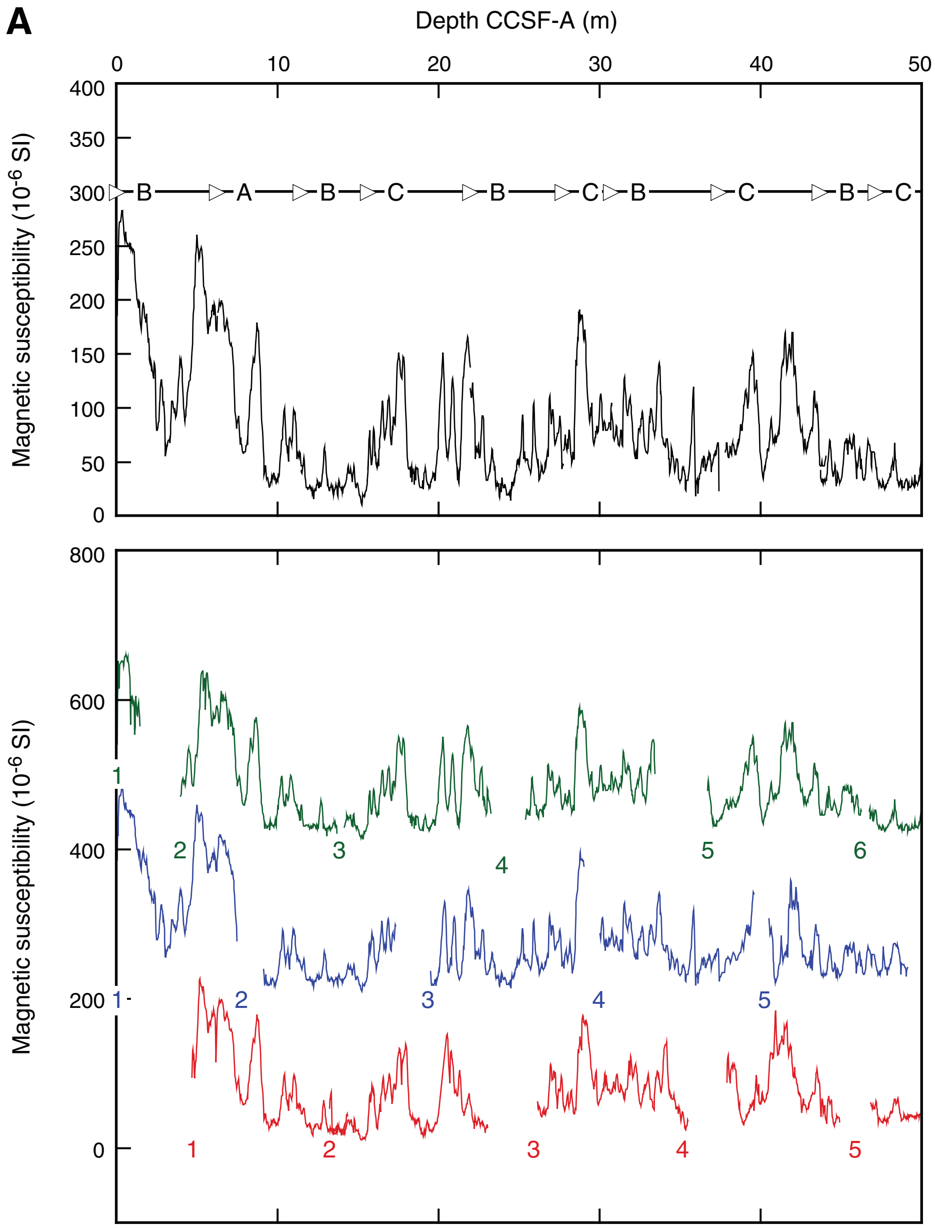

Figure F27 (continued). B. 50–100 CCSF-A. (**Continued on next page.**)

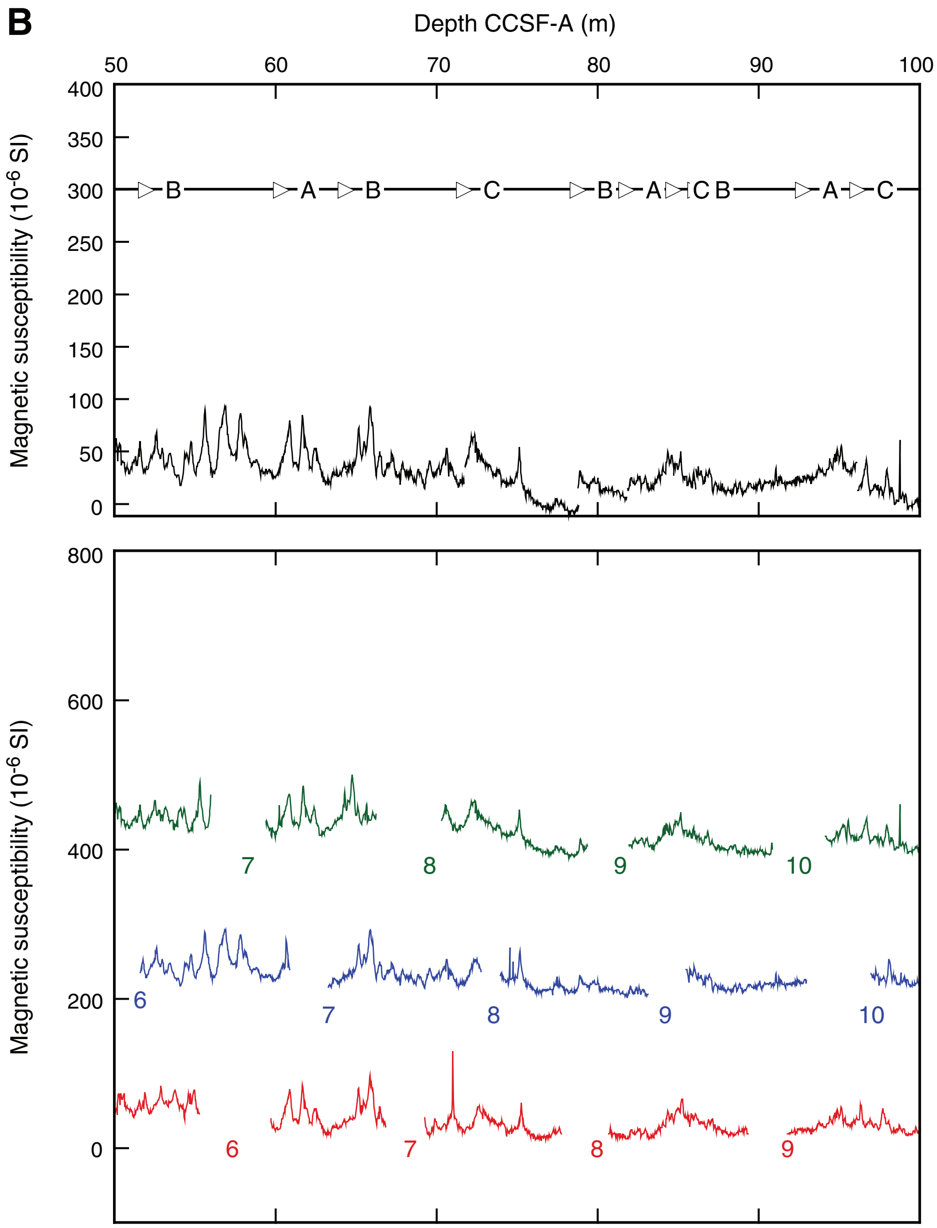

Figure F27 (continued). C. 100–150 CCSF-A. (**Continued on next page.**)

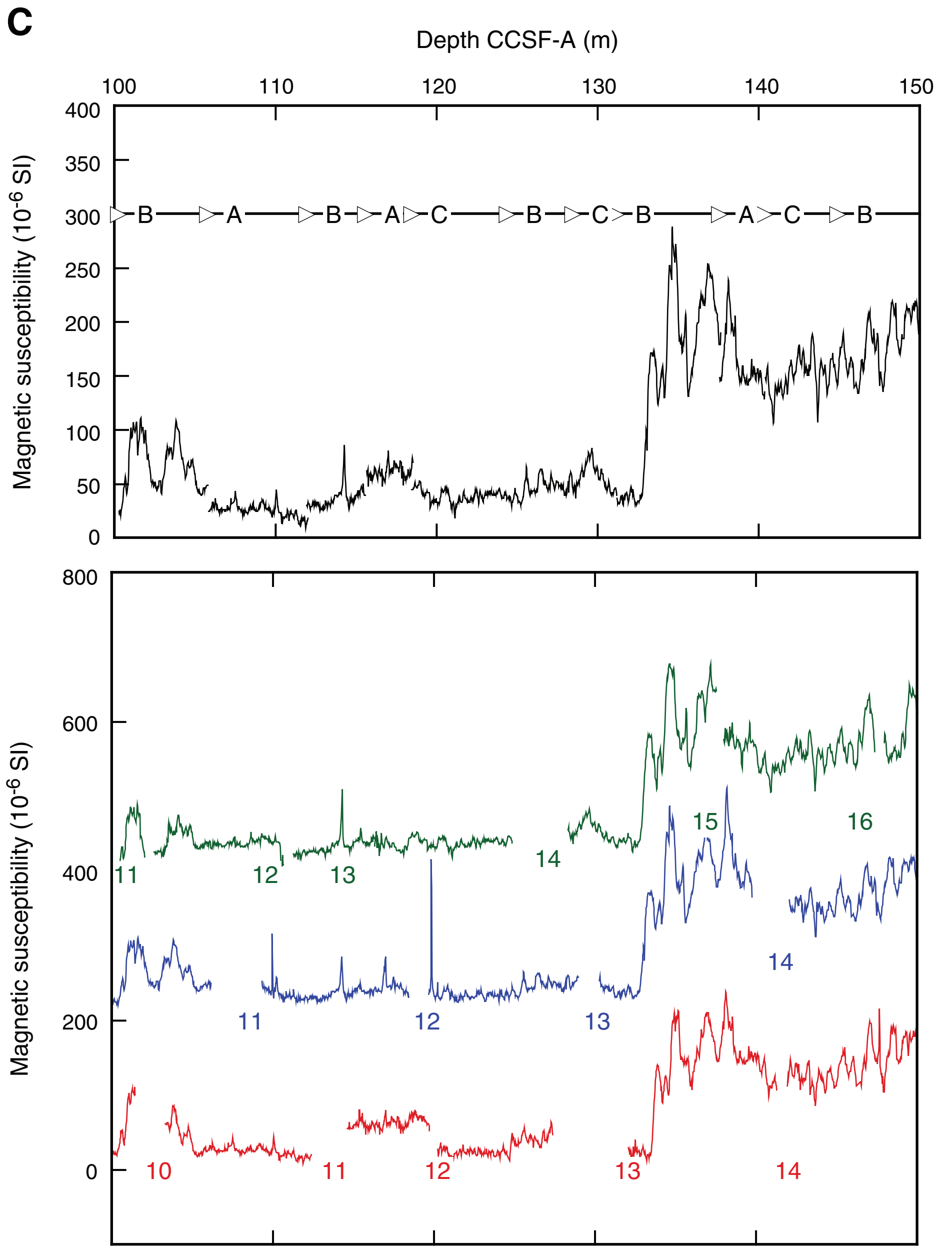

Figure F27 (continued). D. 150–200 CCSF-A.

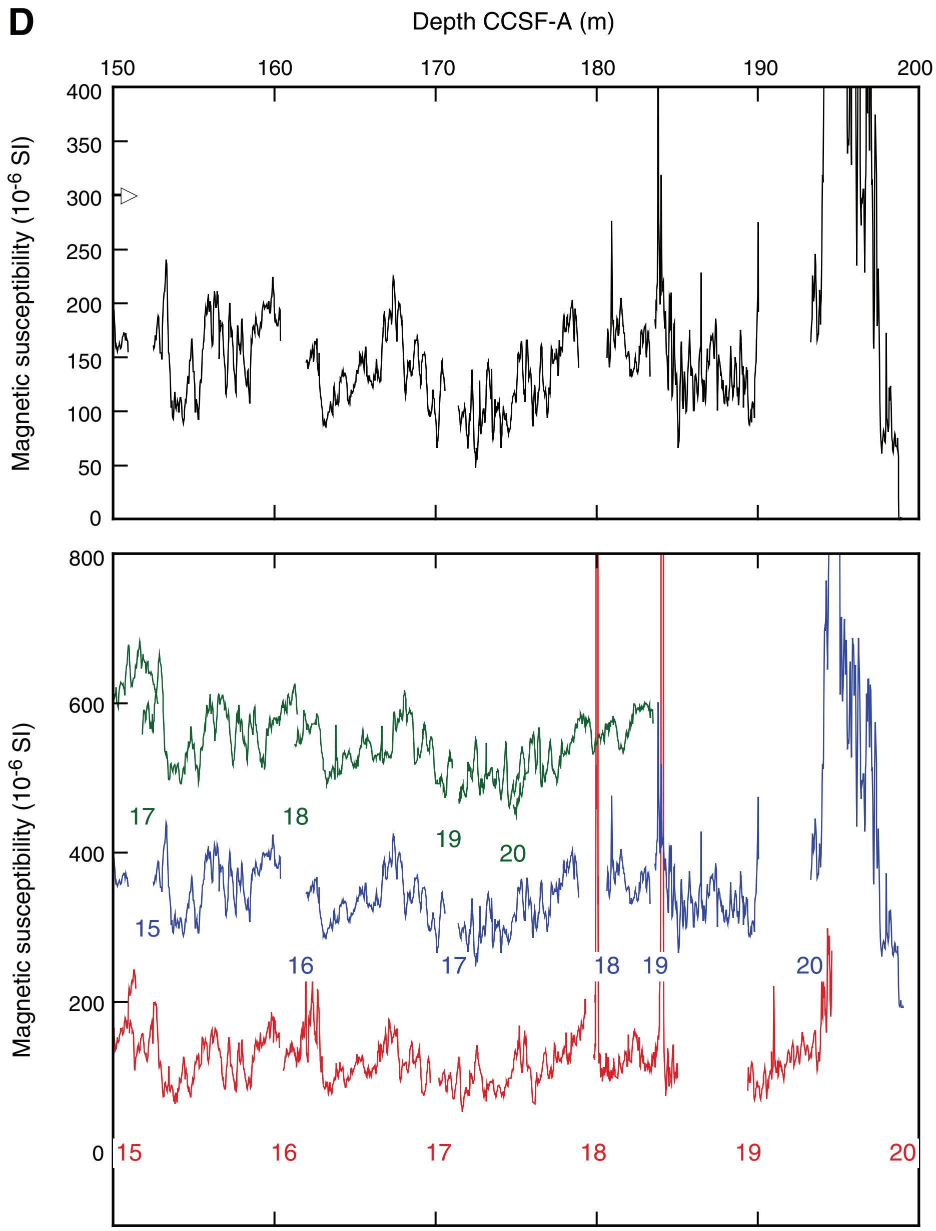

Figure F28. Comparison between magnetic susceptibility records, Sites 1218 and U1333. Site U1333 record is offset by 10 susceptibility units. Excellent correlation between the two records confirms Site U1333 splice at ~115 m CCSF-A is equivalent to ~220 rmcd on the common depth scale depicted.

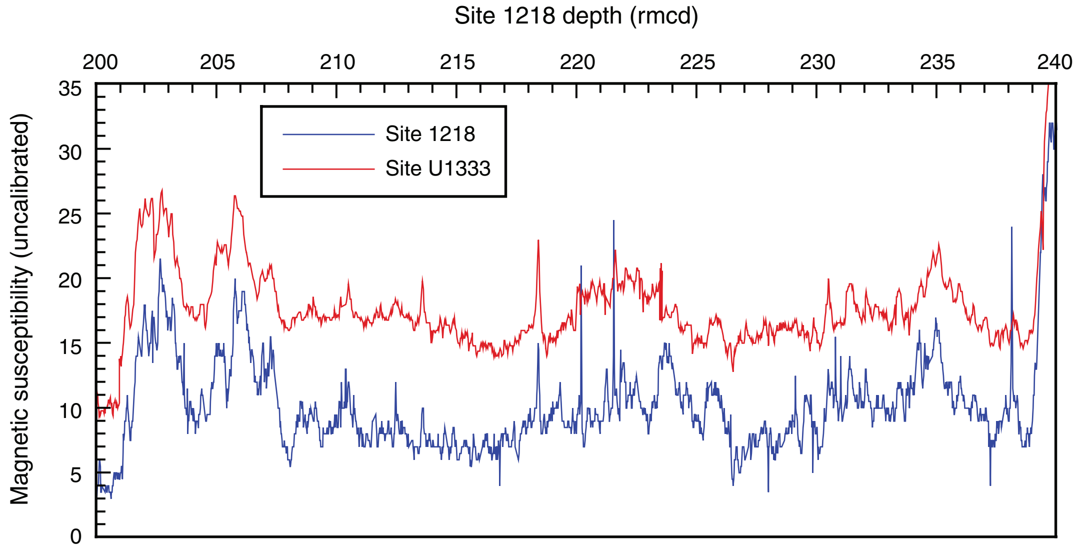

Figure F29. CSF depth vs. CCSF-A depth for tops of cores, Site U1333. Growth factor = slope of the regression line. On average, CCSF-A depth of spliced section is 15% greater than CSF depth.

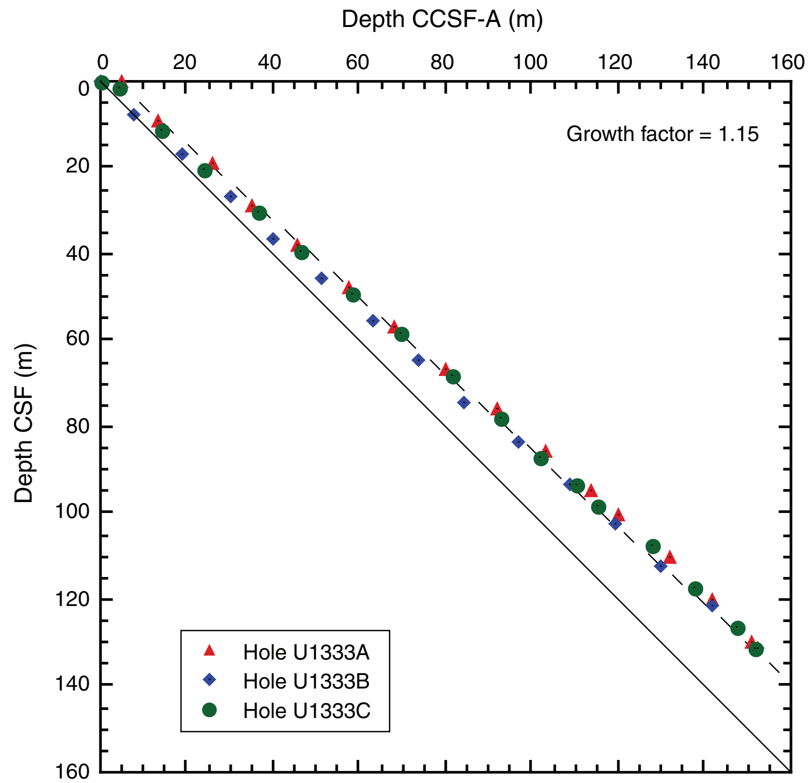

Figure F30. Heat flow calculation, Site U1333. **A.** Sediment temperatures, Hole U1333B. **B.** Thermal resistance based on laboratory thermal conductivity data, Hole U1333A. **C.** Bullard plot where heat flow is calculated from a linear fit of the temperature data. APCT-3 = advanced piston corer temperature tool.

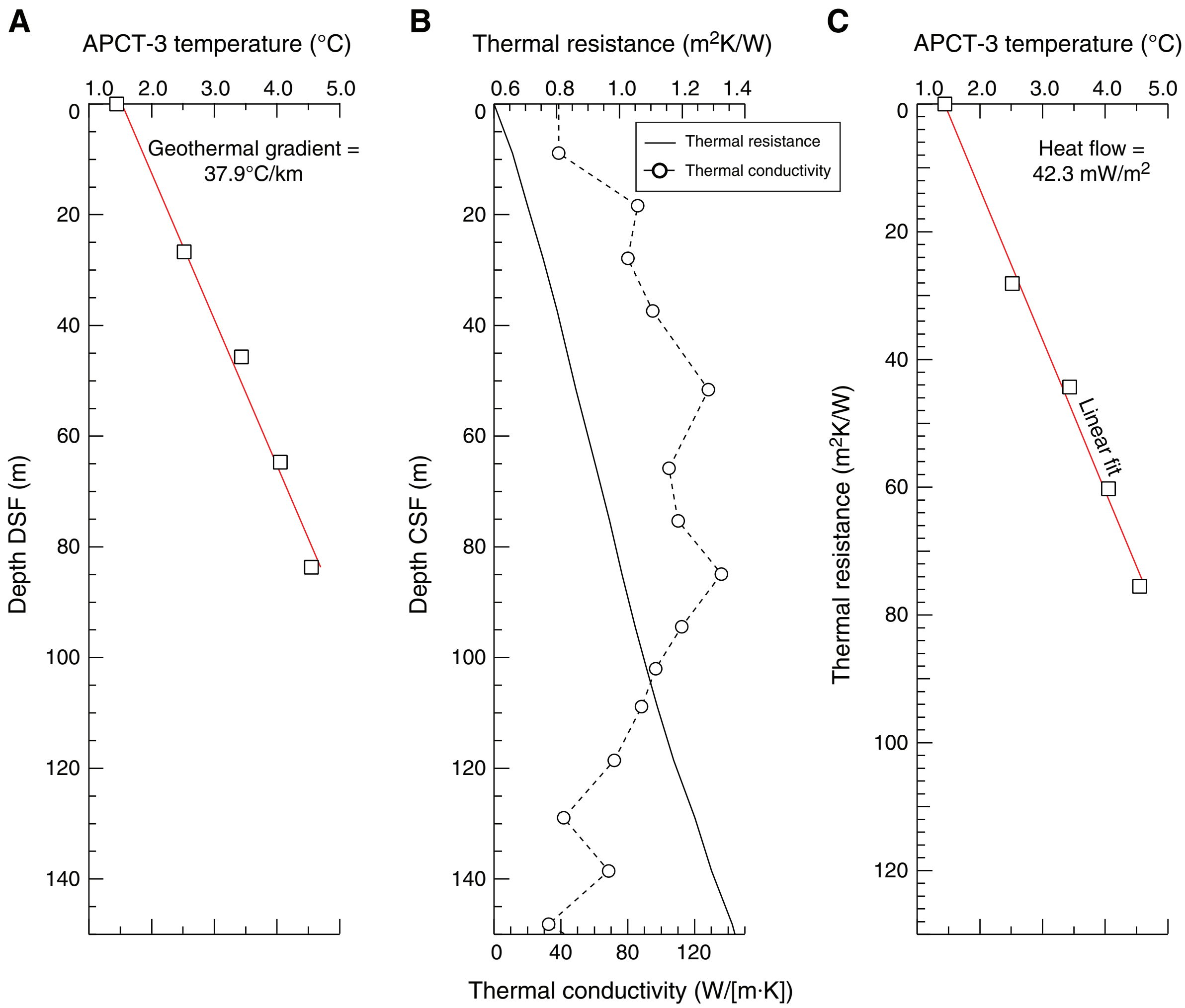

Table T1. Coring summary, Site U1333. (See table notes.) (Continued on next page.)

Site U1333
Time on site (h): 124.3 (1400 h, 30 March–1845 h, 4 April 2009)

Hole U1333A
Latitude: 10°30.995′N
Longitude: 138°25.173′W
Time on hole (h): 45.9 (1400 h, 30 March–1155 h, 1 April 2009)
Seafloor (drill pipe measurement below rig floor, m DRF): 4865.0
Distance between rig floor and sea level (m): 11.3
Water depth (drill pipe measurement from sea level, mbsl): 4853.7
Total depth (drill pipe measurement from rig floor, m DRF): 5049.1
Total penetration (drilling depth below seafloor, m DSF): 184.1
Total length of cored section (m): 184.1
Total number of cores: 22

Hole U1333B
Latitude: 10°30.996′N
Longitude: 138°25.160′W
Time on hole (h): 30.8 (1155 h, 1 April–1845 h, 2 April 2009)
Seafloor (drill pipe measurement below rig floor, m DRF): 4861.8
Distance between rig floor and sea level (m): 11.3
Water depth (drill pipe measurement from sea level, mbsl): 4850.5
Total depth (drill pipe measurement from rig floor, m DRF): 5042.1
Total penetration (drilling depth below seafloor, m DSF): 180.3
Total length of cored section (m): 180.3
Total core recovered (m): 179.9
Core recovery (%): 100
Total number of cores: 20

Hole U1333C
Latitude: 10°30.996′N
Longitude: 138°25.146′W
Time on hole (h): 47.5 (1845 h, 2 April–1815 h, 4 March 2009)
Seafloor (drill pipe measurement below rig floor, m DRF): 4865.1
Distance between rig floor and sea level (m): 11.3
Water depth (drill pipe measurement from sea level, mbsl): 4853.8
Total depth (drill pipe measurement from rig floor, m DRF): 5042.1
Total penetration (drilling depth below seafloor, m DSF): 177.0
Total length of cored section (m): 177.0
Total core recovered (m): 177.0
Core recovery (%): 100
Total number of cores: 24

			Depth DSF (m)			Depth CSF (m)			
Core	Date (2009)	Local time (h)	Top of cored interval	Bottom of cored interval	Interval advanced (m)	Top of cored interval	Bottom of cored interval	Length of core recovered (m)	Recovery (%)
320-U1333A-									
1H	31 Mar	0250	0.0	9.5	9.5	0.00	10.05	10.05	106
2H	31 Mar	0405	9.5	19.0	9.5	9.50	19.62	10.12	107
3H	31 Mar	0525	19.0	28.5	9.5	19.00	28.92	9.92	104
4H	31 Mar	0630	28.5	38.0	9.5	28.50	38.65	10.15	107
5H	31 Mar	0740	38.0	47.5	9.5	38.00	47.70	9.70	102
6H	31 Mar	0845	47.5	57.0	9.5	47.50	57.32	9.82	103
7H	31 Mar	1035	57.0	66.5	9.5	57.00	66.60	9.60	101
8H	31 Mar	1150	66.5	76.0	9.5	66.50	76.19	9.69	102
9H	31 Mar	1300	76.0	85.5	9.5	76.00	85.92	9.92	104
10H	31 Mar	1440	85.5	95.0	9.5	85.50	95.38	9.88	104
11X	31 Mar	1615	95.0	100.7	5.7	95.00	101.22	6.22	109
12X	31 Mar	1730	100.7	110.3	9.6	100.70	107.99	7.29	76
13X	31 Mar	1845	110.3	120.0	9.7	110.30	119.98	9.68	100
14X	31 Mar	1955	120.0	129.6	9.6	120.00	129.85	9.85	103
15X	31 Mar	2105	129.6	139.2	9.6	129.60	139.19	9.59	100
16X	31 Mar	2220	139.2	148.8	9.6	139.20	149.14	9.94	104
17X	31 Mar	2330	148.8	158.4	9.6	148.80	158.72	9.92	103
18X	1 Apr	0115	158.4	168.0	9.6	158.40	163.91	5.51	57
19X	1 Apr	0300	168.0	177.6	9.6	168.00	174.75	6.75	70
20X	1 Apr	0530	177.6	181.6	4.0	177.60	180.13	2.53	63

Table T1 (continued).

Core	Date (2009)	Local time (h)	Depth DSF (m) Top of cored interval	Depth DSF (m) Bottom of cored interval	Interval advanced (m)	Depth CSF (m) Top of cored interval	Depth CSF (m) Bottom of cored interval	Length of core recovered (m)	Recovery (%)
21X	1 Apr	0800	181.6	182.6	1.0	181.60	181.66	0.06	6
22X	1 Apr	1005	182.6	184.1	1.5	182.60	182.66	0.06	4
				Advanced total:	184.1			176.25	96
				Total interval cored:	184.1				
320-U1333B-									
1H	1 Apr	1330	0.0	7.7	7.7	0.00	7.73	7.73	100
2H	1 Apr	1440	7.7	17.2	9.5	7.70	17.65	9.95	105
3H	1 Apr	1600	17.2	26.7	9.5	17.20	27.23	10.03	106
4H	1 Apr	1700	26.7	36.2	9.5	26.70	36.66	9.96	105
5H	1 Apr	1830	36.2	45.7	9.5	36.20	45.90	9.70	102
6H	1 Apr	1950	45.7	55.2	9.5	45.70	55.60	9.90	104
7H	1 Apr	2125	55.2	64.7	9.5	55.20	65.16	9.96	105
8H	1 Apr	2240	64.7	74.2	9.5	64.70	74.55	9.85	104
9H	2 Apr	0020	74.2	83.7	9.5	74.20	83.16	8.96	94
10H	2 Apr	0125	83.7	93.2	9.5	83.70	93.46	9.76	103
11H	2 Apr	0230	93.2	102.7	9.5	93.20	103.31	10.11	106
12H	2 Apr	0340	102.7	112.2	9.5	102.70	112.34	9.64	101
13H	2 Apr	0525	112.2	121.7	9.5	112.20	122.17	9.97	105
14H	2 Apr	0635	121.7	131.2	9.5	121.70	131.46	9.76	103
15H	2 Apr	0745	131.2	140.7	9.5	131.20	141.34	8.64	107
16H	2 Apr	0920	140.7	150.2	9.5	140.70	150.05	9.35	98
17H	2 Apr	1100	150.2	159.7	9.5	150.20	158.56	8.36	88
18H	2 Apr	1220	159.7	162.7	3.0	159.70	162.99	3.29	110
19X	2 Apr	1445	162.7	172.3	9.6	162.70	169.87	7.17	75
20X	2 Apr	1740	172.3	180.3	8.0	172.30	178.57	6.27	78
				Advanced total:	180.3			178.36	99
				Total interval cored:	180.3				
320-U1333C-									
1H	2 Apr	2030	0.0	1.6	1.6	0.00	1.65	1.65	103
2H	2 Apr	2155	1.6	11.1	9.5	1.60	11.63	10.03	106
3H	2 Apr	2310	11.1	20.6	9.5	11.10	21.10	10.00	105
4H	3 Apr	0030	20.6	30.1	9.5	20.60	30.72	10.12	107
5H	3 Apr	0130	30.1	39.6	9.5	30.10	39.89	9.79	103
6H	3 Apr	0415	39.6	49.1	9.5	39.60	49.74	10.14	107
7H	3 Apr	0530	49.1	58.6	9.5	49.10	57.32	8.22	87
8H	3 Apr	0645	58.6	68.1	9.5	58.60	68.70	10.10	106
9H	3 Apr	0750	68.1	77.6	9.5	68.10	77.82	9.72	102
10H	3 Apr	0855	77.6	87.1	9.5	77.60	87.70	10.10	106
11H	3 Apr	1000	87.1	93.1	6.0	87.10	96.25	9.15	153
12H	3 Apr	1115	93.1	98.1	5.0	93.10	99.75	6.65	133
13H	3 Apr	1250	98.1	107.6	9.5	98.10	108.06	9.96	105
14H	3 Apr	1445	107.6	117.1	9.5	107.60	117.63	10.03	106
15H	3 Apr	1605	117.1	126.6	9.5	117.10	127.16	10.06	106
16H	3 Apr	1710	126.6	131.1	4.5	126.60	132.13	5.53	123
17H	3 Apr	1900	131.1	140.6	9.5	131.10	141.11	10.01	105
18H	3 Apr	2055	140.6	150.1	9.5	140.60	150.74	10.21	107
19H	3 Apr	2215	150.1	154.1	4.0	150.10	155.14	5.04	126
20H	3 Apr	2350	154.1	163.2	9.1	154.10	163.22	9.12	100
21H	4 Apr	0110	163.2	163.2	0.0	163.20	163.74	0.54	0
22X	4 Apr	0315	163.2	172.8	9.6	163.20	163.59	0.39	4
23X	4 Apr	0530	172.8	176.0	3.2	172.80	173.01	0.21	7
24X	4 Apr	0745	176.0	177.0	1.0	176.00	176.27	0.27	27
				Advanced total:	351.5			177.04	50
				Total interval cored:	351.5				

Notes: DRF = drilling depth below rig floor, DSF = drilling depth below seafloor, CSF = core depth below seafloor. H = APC core, X = XCB core. Local time = UTC – 10 h.

Table T2. Lithologic unit boundaries, Site U1333. (See table notes.)

Unit	Core, section, interval (cm)	Depth CSF (m)	Core, section, interval (cm)	Depth CSF (m)	Core, section, interval (cm)	Depth CSF (m)
	320-U1331A-		320-U1331B-		320-U1331C-	
I	1H-3,135	4.35	1H-CC, 18*	7.66	2H-3, 40	5.0
II	13H-4, 150	116.3	13H-6, 55	120.25	14H-CC, 22*	117.57
IIIa	19X-1, 10	168.1	18X-CC, 22*	162.7	22X-CC, 9*	163.29
IIIb	20X-2, 82	179.92	20X-CC, 0*	178.17	23H-CC, 7*	172.87
IV	21X-CC, 0*	181.6	20X-CC, 17*	178.34	24X-CC, 16*	176.16
V	22X-CC, 5*	182.65	20X-CC, 40*	178.57	24X-CC, 38*	176.38

Notes: Interval/depth are given for basal boundary of each unit. * = unit extends through at least given interval and depth, but boundary was not cored.

Table T3. Calcareous nannofossil datums, Site U1333. (See table note.)

Core, section, interval (cm)		Marker species	Age (Ma)	Depth CSF (m)			
Top	Bottom			Top	Bottom	Midpoint	±
320-U1333A-	320-U1333A-						
2H-5, 70	2H-6, 70	B *Sphenolithus disbelemnos*	22.8	16.20	17.70	16.95	0.75
2H-7, 70	2H-CC	T *Sphenolithus delphix*	23.1	19.20	19.57	19.39	0.19
2H-CC	3H-1, 70	B *Sphenolithus delphix*	23.2	19.57	19.70	19.64	0.06
4H-5, 70	4H-6, 70	T *Sphenolithus ciperoensis*	24.4	35.20	36.70	35.95	0.75
3H-CC	4H-1, 70	X *T. longus/T. carinatus*	24.7	28.87	29.20	29.04	0.16
3H-5, 70	3H-6, 70	Tc *Cyclicargolithus abisectus*	24.7	25.70	27.20	26.45	0.75
5H-2, 70	5H-3, 70	T *Sphenolithus distentus*	26.8	40.20	41.70	40.95	0.75
5H-3, 70	5H-4, 70	T *Sphenolithus predistentus*	26.9	41.70	43.20	42.45	0.75
5H-4, 70	5H-6, 70	B *Sphenolithus ciperoensis*	27.1	43.20	46.20	44.70	1.50
6H-4, 70	6H-6, 70	T *Sphenolithus pseudoradians*	28.8	52.70	55.70	54.20	1.50
9H-3, 50	9H-4, 50	B *Sphenolithus distentus*	30.0	79.50	81.00	80.25	0.75
11X-4, 70	11X-CC	T *Reticulofenestra umbilicus*	32.0	100.20	101.17	100.69	0.48
12X-3, 70	12X-4, 70	T *Coccolithus formosus*	32.9	104.40	105.90	105.15	0.75
13X-3, 70	13X-3, 140	T *Discoaster saipanensis*	34.4	114.00	114.70	114.35	0.35
14X-6, 70	14X-CC	T *Chiasmolithus grandis*	37.1	128.20	129.80	129.00	0.80
15X-5, 70	15X-6, 70	B *Dictyococcites bisectus*	38.0	136.30	137.80	137.05	0.75
16X-4, 40	16X-5, 40	T *Chiasmolithus solitus*	40.4	144.10	145.60	144.85	0.75
17X-6,110	17X-CC	T *Nannotetrina*	42.3	157.40	158.46	157.93	0.53
18X-1, 60	18X-2, 34	B *Reticulofenestra umbilicus* >14 µm	42.5	159.00	160.24	159.62	0.62
18X-4, 88	18X-CC	T *Nannotetrina fulgens*	43.4	163.12	163.86	163.49	0.37
20X-1, 73	20X-2, 50	B *Nannotetrina fulgens*	46.8	178.33	179.60	178.97	0.63
20X-2, 50	20X-CC	B *Sphenolithus furcatolithoides*	45.8	179.60	180.12	179.86	0.26
20X-2, 50	20X-CC	B *Nannotetrina*	48.0	179.60	180.12	179.86	0.26
320-U1332B-	320-U1332B-						
20X-1, 46	20X-2, 86	B *Sphenolithus furcatolithoides*	45.8	172.76	174.66	173.71	0.95
20X-3, 102	20X-4, 37	B *Nannotetrina*	48.0	176.32	177.17	176.75	0.42

Note: B = bottom, T = top, X = abundance crossover, Tc = top common.

Table T4. Radiolarian datums, Site U1333. (See table notes.) (Continued on next page.)

Geologic age	Zone	Marker species	Age (Ma)	Core, section interval (cm) Top	Bottom	Depth CSF (m) Top	Bottom	Midpoint	±
				320-U1333A-	320-U1333A-				
lower Miocene	RN2	B *S. delmontensis*	20.68	1H-2, 104–106	1H-4, 104–106	2.55	5.55	4.05	1.50
		T *L. pegetrum*	20.89	1H-4, 104–106	1H-CC	5.55	9.92	7.74	2.19
		T *T. annosa*	21.38	1H-4, 104–106	1H-CC	5.55	9.92	7.74	2.19
	RN1	B *C. virginis*	21.39	1H-4, 104–106	1H-CC	5.55	9.92	7.74	2.19
		B *L. leptetrum*	21.42	2H-4, 104–106	2H-CC	15.05	19.57	17.31	2.26
		T *E. mitodes*	21.95	2H-2, 104–106	2H-4, 104–106	12.05	15.04	13.55	1.50
		B *C. serrata*	22.04	1H-4, 104–106	1H-CC	5.55	9.92	7.74	2.19
		B *C. cornuta*	22.26	2H-4, 104–106	2H-CC	15.05	19.57	17.31	2.26
		B *C. tetrapera*	22.35	2H-4, 104–106	2H-CC	15.05	19.57	17.31	2.26
upper Oligocene	RP22	T *A. gracilis*	22.62	2H-4, 104–106	2H-CC	15.05	19.57	17.31	2.26
		B *D. bassanii*	22.93	2H-4, 104–106	2H-CC	15.05	19.57	17.31	2.26
		B *E. diaphanes*	22.95	3H-2, 105–107	3H-4, 105–107	21.56	24.56	23.06	1.50
		T *D. cyclacantha*	22.98	2H-CC	3H-2, 105–107	19.57	21.56	20.57	0.99
		T *D. riedeli*	23.01	4H-5, 106–108	4H-CC	35.57	38.60	37.09	1.52
		B *D. cyclacantha*	23.29	3H-2, 105–107	3H-4, 105–107	21.56	24.56	23.06	1.50
		T *D. papilio*	23.31	3H-2, 105–107	3H-4, 105–107	21.56	24.56	23.06	1.50
		T *L. longicornuta*	24.12	3H-2, 105–107	3H-4, 105–107	21.56	24.56	23.06	1.50
		T *A. octopylus*	24.38	3H-4, 105–107	3H-CC	24.56	28.87	26.72	2.16
		T *L. apodora*	24.5	3H-4, 105–107	3H-CC	24.56	28.87	26.72	2.16
		B *L. elongata*	25.05	4H-3, 106–108	4H-5, 106–108	32.57	35.57	34.07	1.50
	RP21	B *A. octopylus*	25.09	4H-5, 106–108	4H-CC	35.57	38.60	37.09	1.52
		B *D. praeforcipata*	25.27	5H-4, 105–107	5H-CC	43.55	47.65	45.60	2.05
		B *C. robusta*	25.27	4H-5, 106–108	4H-CC	35.57	38.60	37.09	1.52
		B *D. tubaria*	25.27	4H-5, 106–108	4H-CC	35.57	38.60	37.09	1.52
		B *L. longicornuta*	25.29	4H-3, 106–108	4H-5, 106–108	32.57	35.57	34.07	1.50
		B *D. scambos*	25.33	4H-3, 106–108	4H-5, 106–108	32.57	35.57	34.07	1.50
		B *L. apodora*	25.55	4H-5, 106–108	4H-CC	35.57	38.60	37.09	1.52
		T *D. circulus*	26.17	4H-5, 106–108	4H-CC	35.57	38.60	37.09	1.52
		B *D. riedeli*	26.2	5H-4, 105–107	5H-CC	43.56	47.65	45.61	2.04
		T *E. plesiodiaphanes*	26.4	5H-4, 105–107	5H-CC	43.56	47.65	45.61	2.04
		T *L. angusta*	27.68	6H-3, 95–97	6H-5, 95–97	51.46	54.46	52.96	1.50
		T *T. setanios*	28.21	6H-5, 95–97	6H-CC	54.46	57.27	55.87	1.41
lower Oligocene		B *T. annosa*	28.33	7H-4, 95–97	7H-CC	62.46	66.55	64.51	2.04
		B *D. ateuchus*		7H-4, 95–97	7H-CC	62.46	66.55	64.51	2.04
		T. triceros > *D. ateuchus*	28.60	7H-4, 95–97	7H-CC	62.46	66.55	64.51	2.04
	RP20	B *E. mitodes*	29.41	8H-2, 108–110	8H-4, 108–110	68.89	71.89	70.39	1.50
		B *T. setanios*	29.51	9H-2, 105–107	9H-4, 105–107	78.55	81.56	80.06	1.51
		B *D. circulus*	29.96	9H-2, 105–107	9H-4, 105–107	78.56	81.56	80.06	1.50
		T *T. tuberosa*	30.13	9H-CC	10H-2, 105–107	85.87	88.06	86.97	1.10
		T *L. crux*	30.13	9H-CC	10H-2, 105–107	85.87	88.06	86.97	1.10
		B *E. plesiodiaphanes*	30.37	9H-CC	10H-2, 105–107	85.87	88.06	86.97	1.10
		T *L. oberhaensliae*	30.74	9H-CC	10H-2, 105–107	85.87	88.06	86.97	1.10
		B *D. spinosa*	30.84	11X-2, 95–97	11X-4, 95–97	97.46	100.46	98.96	1.50
		T *D. pseudopaplilio*	30.84	11X-2, 95–97	11X-4, 95–97	97.46	100.46	98.96	1.50
		T *C. gravida*	30.89	11X-4, 95–97	11X-CC	100.46	101.17	100.82	0.36
		B *L.* cf. *L. elongata*		11X-CC	12X-2, 105–107	101.17	103.26	102.22	1.05
		B *L. crux*	31.00	12X-2, 105–107	12X-4, 105–107	103.26	106.26	104.76	1.50
		B *T. tuberosa*	31.00	12X-4, 105–107	12X-CC	106.26	107.99	107.13	0.86
		B *D. pseudopaplilio*	31.00	12X-2, 105–107	12X-4, 105–107	103.26	106.26	104.76	1.50
		B *C. gravida*	31.01	12X-2, 105–107	12X-4, 105–107	103.26	106.26	104.76	1.50
		T *T. triacantha*	33.34	13X-5, 8–16	13X-5, 96–104	116.42	117.30	116.86	0.44
		T *L. aristotelis* gr.	33.51	13X-2, 37–44	13X-2, 88–95	112.21	112.72	112.47	0.26
		T *C. hispida*	33.62	13X-2, 37–44	13X-2, 88–95	112.21	112.72	112.47	0.26
		T *C. ornatum*	33.62	13X-1, 127–134	13X-2, 37–44	111.61	112.21	111.91	0.30
		T *L. hadra*	33.75	13X-2, 105–107	13X-3, 0–8	112.86	113.20	113.03	0.17
		T *L. amphitrite*	33.75	13X-2, 37–44	13X-2, 88–95	112.21	112.72	112.47	0.26
		T *L. babylonis*	33.75	13X-2, 105–107	13X-3, 0–8	112.86	113.34	113.10	0.24
		L. aristotelis > *L. angusta*	33.82	13X-2, 88–95	13X-2, 105–107	112.72	112.86	112.79	0.07
upper Eocene	RP19	T *D. copetata*	33.84	12X-CC	13X-1, 127–134	107.99	111.57	109.78	1.79
		B *L. angusta*	34.13	13X-3, 0–8	13X-3, 122–129	113.34	114.07	113.71	0.36
		T *C. bandyca*	34.62	13X-4, 105–107	13X-4, 120–128	115.86	116.04	115.95	0.09
		T *C. turris*	34.83	13X-2, 105–107	13X-3, 0–8	112.86	113.20	113.03	0.17
		T *E. fistuligerum*	34.93	13X-CC	14X-2, 95–97	119.93	122.46	121.20	1.26
		T *T. bromia*	33.94	13X-4, 120–128	13X-5, 8–16	116.04	116.42	116.23	0.19
		T *T. lochites*	34.13	13X-4, 120–128	13X-5, 8–16	116.04	116.42	116.23	
		T *C. azyx*	35.07	13X-4, 105–107	13X-4, 120–128	114.07	116.04	115.06	0.99
		T *T. tetracantha*	35.30	13X-4, 120–128	13X-5, 8–16	116.04	116.42	116.23	0.19

Table T4 (continued).

Geologic age	Zone	Marker species	Age (Ma)	Core, section interval (cm) Top	Bottom	Depth CSF (m) Top	Bottom	Midpoint	±
upper Eocene	RP18	B *L. hadra*	35.34	13X-4, 72–80	13X-4, 96–104	115.52	115.76	115.64	0.12
		B *C. bandyca*	36.74	13X-CC	14X-2, 95–97	122.45	125.45	123.95	1.50
middle Eocene	RP17	B *L. jacchia*	37.06	14X-2, 95–97	14X-4, 95–97	122.46	125.46	123.96	1.50
		B *C. azyx*	37.52	14X-4, 95–97	14X-CC	125.46	129.80	127.63	2.17
	RP16	T *Anthocyrtoma* spp.	37.92	14X-CC	15X-2, 96–98	129.80	132.07	130.94	1.13
		B *T. bromia*	38.07	14X-CC	15X-2, 96–98	129.80	132.07	130.94	1.13
		B *T. tetracantha*	38.12	14X-CC	15X-2, 96–98	129.80	132.07	130.94	1.13
		T *D. anastasis*	38.45	14X-CC	15X-2, 96–98	129.80	132.07	130.94	1.13
		B *C. turris*	38.67	14X-CC	15X-2, 96–98	129.80	132.07	130.94	1.13
		B *L. aristotelis* gr.	39.73	15X-4, 96–98	15X-CC	135.07	139.14	137.11	2.03
		T *P. mitra*	39.85	15X-CC	16X-2, 104–106	139.14	141.75	140.45	1.31
		B *D. anastasis*	39.98	15X-CC	16X-2, 104–106	139.14	141.75	140.45	1.31
		B *P. goetheana*	40.16	16X-2, 104–106	16X-4, 104–106	141.75	144.75	143.25	1.50
	RP15	T *L. biaurita*	40.36	16X-CC	17X-2, 105–107	149.09	151.36	150.23	1.14
		P. mitra > *P. chalara*	40.70	17X-2, 105–107	17X-4, 105–107	151.36	154.36	152.86	1.50
	RP14	T *P. trachodes*	41.23	17X-2, 105–107	17X-4, 105–107	151.36	154.35	152.86	1.49
		B *P. chalara*	41.54	17X-4, 105–107	17X-CC	154.36	158.46	156.41	2.05
		B *C. ornatum*	42.10	17X-4, 105–107	17X-CC	154.36	158.46	156.41	2.05
		B *S. triconiscus*	42.40	17X-CC	18X-1, 95–97	158.46	159.36	158.91	0.45
		T *E. lagena*	42.69	18X-1, 95–97	18X-4, 95–97	159.36	163.20	161.28	1.92
		B *T. perpumila*	42.97	18X-1, 95–97	18X-4, 95–97	159.36	163.20	161.28	1.92
		B *P. trachodes*	43.22	18X-1, 95–97	18X-4, 95–97	159.36	163.20	161.28	1.92
		B *Z. cimelium*	43.35	18X-1, 95–97	18X-4, 95–97	159.36	163.20	161.28	1.92
		P. sinuosa > *P. mitra*	43.84	18X-CC	19X-1, 104–106	163.86	169.05	166.46	2.59
	RP13	T *P. phyxis*	44.44	19X-1, 104–106	19X-3, 104–106	169.05	172.30	170.68	1.63
		B *P. ampla*	44.77	19X-1, 104–106	19X-3, 104–106	169.05	172.30	170.68	1.63
		P. phyxis > *P. ampla*	44.77	19X-1, 104–106	19X-3, 104–106	169.05	172.30	170.68	1.63

Notes: B = bottom, T = top.

Table T5. Preservation and relative abundance of radiolarians, Hole U1333A. This table is available in an **over-sized format.**

Table T6. Preservation and relative abundance of radiolarians, Hole U1333B. (See table notes.) (Continued on next page.)

Core, section, interval (cm)	Radiolarian zone	Abundance	Preservation	Mixing	*Anthocyrtoma* spp.	*Artophormis gracilis*	*Calocyclas hispida*	*Calocyclas turris*	*Calocycloma ampulla*	*Calocycloma castum*	*Carpocanopsis cingulata*	*Cryptocarpium azyx*	*Cryptocarpium ornatum*	*Cyrtocapsella cornuta*
320-U1333B-														
1H-CC	B	B												
2H-CC	RN1	C	M				F				R			C
3H-CC	RP22	C	M			R	F							
4H-CC		C	M			R	R							
5H-CC	RP21	C	M			R								
6H-CC		A	M			R								
7H-CC		A	M			R								
8H-CC	RP20	A	M			R								
9H-CC		C	M											
10H-CC		C	M			R								
11H-CC		C	M			R								
12H-CC		C	M			R								
13H-CC	RP18	C	M			—	R						R	
14H-CC	RP17	A	M				R	R				R	R	
15H-CC	RP16	C	M										R	
16X-CC	RP15	C	M		VR				R	R			R	
17X-CC	RP14	C	M											
17X-CC		C	M											
18X-CC	—	B												
19X-CC		B												
19X-CC	B	B												
20X-CC	—	B												
20X-CC	B	B												

Core, section, interval (cm)	*Cyrtocapsella tetrapera*	*Dictyophimus craticula*	*Dictyoprora armadillo*	*Dictyoprora mongolfieri*	*Didymocyrtis prismatica*	*Dorcadospyris anastasis*	*Dorcadospyris ateuchus*	*Dorcadospyris circulus*	*Dorcadospyris copelata*	*Dorcadospyris ombros* (upper)	*Dorcadospyris papilio*	*Dorcadospyris praeforcipata*	*Dorcadospyris quadripes*	*Dorcadospyris scambos*	*Dorcadospyris spinosa*
320-U1333B-															
1H-CC															
2H-CC	R				R		R					R		R	
3H-CC					R		R				R	R			
4H-CC					R		R				R	R			
5H-CC					R		R	R			—	R			
6H-CC					R		R	R			—				
7H-CC					R		R	R							
8H-CC							—	R							
9H-CC					R			R							
10H-CC													R		R
11H-CC													R		R
12H-CC													R		R
13H-CC				R											
14H-CC			R	R					R	R					
15H-CC			R	F		R									
16X-CC		R	R	F						R					
17X-CC															
17X-CC															
18X-CC															
19X-CC															
19X-CC															
20X-CC															
20X-CC															

Core, section, interval (cm)	*Eucyrtidium diaphanes*	*Eucyrtidium mitodes*	*Eucyrtidium plesiodiaphanes*	*Eusyringium fistuligerum*	*Liriospyris longicornuta*	*Lithocyclia angusta*	*Lithocyclia aristotelis* gr.	*Lithocyclia crux*	*Lithocyclia ocellus* gr.	*Lophocyrtis jacchia*	*Lophocyrtis oberhaensliae*	*Lophocyrtis pegetrum*	*Lychnocanoma amphitrite*	*Lychnocanoma babylonis*	*Lychnocanoma elongata*	*Lychnocanoma turgidum*	*Podocyrtis apeza*	*Podocyrtis chalara*	*Podocyrtis goetheana*	*Podocyrtis mitra*
320-U1333B-																				
1H-CC																				
2H-CC	R														R					
3H-CC	—	R										R			R					
4H-CC		R			R							R			R					
5H-CC		R	R									R			R					
6H-CC		R	R									R			R					
7H-CC		R	R									R								
8H-CC		—	R																	
9H-CC			R					—												
10H-CC			—			R		R												
11H-CC						R		R			VR									
12H-CC						R		R												
13H-CC							R		R	R				R						
14H-CC				R			R		R							R				
15H-CC				R												R	R	R	R	R
16X-CC				R												R	R	R		R
17X-CC																				
17X-CC																				
18X-CC																				
19X-CC																				
19X-CC																				
20X-CC																				
20X-CC																				

Notes: Abundance: A = abundant, C = common, F = frequent, R = rare, VR = very rare, B = barren, — = undetermined. Preservation: M = moderate. Mixing: blank = no mixing of older specimens detected.

Table T6 (continued).

Core, section, interval (cm)	Radiolarian zone	Abundance	Preservation	Mixing	*Podocyrtis papalis*	*Podocyrtis trachodes*	*Rhopalocanium ornatum*	*Sethochytris triconiscus*	*Spongatractus pachystylus*	*Theocorys anaclasta*	*Theocyrtis annosa*	*Theocyrtis careotuberosa*	*Theocyrtis perpumila*	*Theocyrtis perysinos*	*Theocyrtis setanios*	*Theocyrtis tuberosa*	*Thyrsocyrtis bromia*	*Thyrsocyrtis krooni*	*Thyrsocyrtis lochites*	*Thyrsocyrtis orthotenes*	*Thyrsocyrtis triacantha*	*Tristylospyris triceros*	*Zygocircus cimelium*
320-U1333B-																							
1H-CC	B	B																					
2H-CC	RN1	C	M								R												
3H-CC	RP22	C	M								R												
4H-CC		C	M								R												
5H-CC	RP21	C	M								R												
6H-CC		A	M								R												
7H-CC		A	M								R				R								
8H-CC	RP20	A	M								—				R								
9H-CC		C	M											R	R	—						R	
10H-CC		C	M													C							
11H-CC		C	M									R				C							
12H-CC		C	M									R				C							
13H-CC	RP18	C	M									R					R		R		R	R	
14H-CC	RP17	A	M									R	F				R	R	R	R	R	R	
15H-CC	RP16	C	M		R		R						R								F		R
16X-CC	RP15	C	M		R	R	R	R	R	R			R								F		R
17X-CC	RP14	C	M																				
17X-CC		C	M																				
18X-CC	—	B																					
19X-CC		B																					
19X-CC	B	B																					
20X-CC	—	B																					
20X-CC	B	B																					

Table T7. Preservation and relative abundance of radiolarians, Hole U1333C. (See table notes.) (Continued on next page.)

Core, section, interval (cm)	Radiolarian zone	Abundance	Preservation	Mixing	*Anthocyrtoma* spp.	*Artophormis gracilis*	*Calocyclas bandyca*	*Calocyclas turris*	*Calocycletta anekathen*	*Calocycletta robusta*	*Calocycletta serrata*	*Calocycletta virginis*	*Carpocanopsis cingulata*	*Centrobotrys gravida*	*Centrobotrys petrushevskayae*	*Cryptocarpium azyx*	*Cryptocarpium ornatum*	*Cyrtocapsella cornuta*	*Cyrtocapsella tetrapera*	*Dictyoprora armadillo*	*Dictyoprora mongolfieri*	*Didymocyrtis bassanii*	*Didymocyrtis prismatica*	*Didymocyrtis tubaria*	*Dorcadospyris anastasis*	*Dorcadospyris ateuchus*	*Dorcadospyris circulus*	*Dorcadospyris copelata*	*Dorcadospyris ombros* (upper)	*Dorcadospyris papilio*	*Dorcadospyris praeforcipata*	*Dorcadospyris pseudopapilio*	*Dorcadospyris quadripes*	*Dorcadospyris riedeli*	*Dorcadospyris scambos*	*Dorcadospyris spinosa*	*Eucyrtidium diaphanes*	*Eucyrtidium mitodes*	*Eucyrtidium plesiodiaphanes*	*Eusyringium fistuligerum*	*Eusyringium lagena*	*Lithocyclia angusta*	*Lithocyclia aristotelis* gr.	*Lithocyclia crux*	*Lophocyrtis exitelus*	*Lophocyrtis hadra*	*Lophocyrtis jacchia*	*Lophocyrtis milowi*	*Lophocyrtis oberhaensliae*
320-U1333C-																																																	
1H-CC	RN2	C	M							R	R	VR	R					F	R			R	R												R		R												
2H-CC	RN1	C	M							F			R					F	R			R	R	R		R					R				R		R											R	
3H-CC	RP22	C	M			R				F								—	—				R	R		R					R				R		—	R										R	
4H-CC		C	M			R				F													R	R		R				R	R				VR			R										R	
5H-CC	RP21	C	M			R				—													R			R				—	—			R				R										R	
6H-CC		C	M			R																	R			R	VR											R	R									R	
7H-CC		C	M			R									R								R			R	R											R	R			R							
8H-CC		C	M			R									R								R			VR	R											R	R			R							
9H-CC		C	M			R									R								R			—	R											—	R			R		—					
10H-CC		C	M			R									R								—				—												R			R		R					
11H-CC		A	G			R																											R			R						R		R				R	
12H-CC		A	G			F																										R	R			R						R		R				R	VR
13H-CC		A	G			R								R																		R	R									R		R				R	
14H-1, 50–58	RP20	A	G	1		F																						R														R		R				R	
14H-1, 70–78		A	G	1		F			VR																			R														R		R				R	
14H-2, 0–8		C	M			F																						R														R		R				R	
14H-3, 100–108		F	P			F																						R														R							
14H-4, 70–78		F	P			R																						R														R						VR	
14H-4, 140–148		C	M	1		R		VR									F																									R						VR	
14H-5, 40–48		C	M			R			F								F			R	F																					R	R						
14H-5, 50–58		F	M	1					F								F			R	R							R															R						
14H-5, 110–118		C	M	1		R			F								F			R	R							R															R						
14H-5, 130–138		A	M						F								F			R	R							R	R														R		R	R	R		
14H-6, 20–24		A	M			R			F								R			R	R							R	R														R			R	R		
14H-6, 50–58		A	M			R			F								F			R	R							R	R														R			R	R		
14H-6, 80–88	RP19	A	M	1		R			F								F			R	R							R	R											VR			R			R	R		
14H-6, 120–128		A	M			R			F							VR	F			R	R							R	R														R				R		
14H-7, 30–38		A	M	1		R	VR		F								F			R	R							R	R											VR			R			R	R		
14H-7, 60–68		A	M	1		R			F								F			R	R							R	R														R			R	R		
14H-7, 67–75		A	G	1		R			F								F			R	R							R	R														R				R		
14H-CC		A	G	1		R	VR	R	F								R			R	F							R	R														R				R		
15H-CC	RP18	A	G			R		R								F	R			R	R								R														R				R		
16H-CC	RP16	A	G														R				F																			R									
17H-CC		A	G														R			R	F				R															R									
18H-CC	RP15	A	G														R				R																			R									
19H-CC	RP14	A	G		VR												R				R																			R	—								
20H-CC		A	G														—				R																			R	R								

Notes: Abundance: A = abundant, C = common, F = frequent, R = rare, VR = very rare, — = undetermined. Preservation: G = good, M = moderate, P = poor. Mixing: blank = no mixing of older specimens detected, 1 = 1–3 reworked specimens detected.

Table T7 (continued).

Core, section, interval (cm)	Radiolarian zone	Abundance	Preservation	Mixing	*Lophocyrtis leptetrum*	*Lophocyrtis pegetrum*	*Lychnocanoma amphitrite*	*Lychnocanoma babylonis*	*Lychnocanoma turgidum*	*Lychnodictyum audax*	*Podocyrtis apeza*	*Podocyrtis chalara*	*Podocyrtis mitra*	*Podocyrtis papalis*	*Podocyrtis trachodes*	*Rhopalocanium ornatum*	*Sethochytris triconiscus*	*Spongatractus balbis*	*Spongatractus pachystylus*	*Theocyrtis annosa*	*Theocyrtis careotuberosa*	*Theocyrtis perpumila*	*Theocyrtis perysinos*	*Theocyrtis setanios*	*Theocyrtis tuberosa*	*Thyrsocyrtis bromia*	*Thyrsocyrtis lochites*	*Thyrsocyrtis orthotenes*	*Thyrsocyrtis tetracantha*	*Thyrsocyrtis triacantha*	*Tristylospyris triceros*	*Zealithapium mitra*	*Zygocircus cimelium*
320-U1333C-																																	
1H-CC	RN2	C	M		R				R												—												
2H-CC	RN1	C	M			R			F												R												
3H-CC	RP22	C	M			R			R												R												
4H-CC	RP21	C	M			R			—												R												
5H-CC		C	M			R															R												
6H-CC		C	M			R															R												
7H-CC		C	M			R				R										R				VR									
8H-CC	RP20	C	M			R				R										—			R	R							R		
9H-CC		C	M			R				R													R	R	—						R		
10H-CC		C	M			R				R													—	—	VR						R		
11H-CC		A	G																		F				C						R		
12H-CC		A	G																		F				C						R		
13H-CC		A	G																		F		R	R	F						R		
14H-1, 50–58		A	G	1																	F				R								
14H-1, 70–78		A	G	1																	F				R						R		
14H-2, 0–8		C	M																		F				R						R		
14H-3, 100–108		F	P																		F										R		
14H-4, 70–78		F	P																		F										R		
14H-4, 140–148		C	M	1			VR														F										R		
14H-5, 40–48		C	M				R														F	VR				R					R		
14H-5, 50–58	RP19	F	M	1																	R										R		
14H-5, 110–118		C	M	1				R													R										R		
14H-5, 130–138		A	M																		R									VR	R		
14H-6, 20–24		A	M																		R										R		
14H-6, 50–58		A	M				R														R										R		
14H-6, 80–88		A	M	1			R														R					VR				VR	R		
14H-6, 120–128		A	M				R														R						VR				R		
14H-7, 30–38		A	M	1			R	VR						VR							R							VR			R		
14H-7, 60–68		A	M	1			F	R	VR					VR							R					VR	VR			VR	R		
14H-7, 67–75		A	G	1			R	R													R					VR				VR	R		
14H-CC		A	G	1			R	R													F					R				VR	R		
15H-CC	RP18	A	G					R													F	R				R	R		R	R	R		
16H-CC	RP16	A	G						R			R				R		R	R			R						R		F			R
17H-CC		A	G									R				R		R	R			R						R		F			R
18H-CC	RP15	A	G								R	R				R	R	R	R			R						R		F			R
19H-CC	RP14	A	G						R			VR	R		—	R	R	R	R			R						R		F			R
20H-CC		A	G									—	R		R		—	R	R			R						R		R			

Table T8. Planktonic foraminifer datums, Site U1333. (**See table note.**)

Core, section, interval (cm)		Marker species	Age (Ma)	Depth CSF (m)			
Top	Bottom			Top	Bottom	Midpoint	±
320-U1333A-	320-U1333A-						
2H-2, 38–40	2H-CC	B *Paragloborotalia kugleri*	23.0	11.38	19.57	15.48	4.10
2H-CC	3H-2, 38–40	B *Paragloborotalia pseudokugleri*	25.2	19.57	20.88	20.23	0.66
5H-CC	6H-3, 38–40	T *Paragloborotalia opima*	26.9	47.65	50.88	49.27	1.62
8H-2, 38–40	8H-4, 38–40	B *Globigerina angulisuturalis*	29.2	60.38	71.18	65.78	5.40
8H-CC	9H-2, 52–53	T *Subbotina angiporoides*	29.8	76.14	78.02	77.08	0.94
7H-5, 38–40	8H-CC	T *Turborotalia ampliapertura*	30.3	63.39	76.14	69.76	6.38
10H-2, 38–40	10H-4, 38–40	B *Paragloborotalia opima*	30.8	87.38	90.38	88.88	1.50
320-U1333B-	320-U1333B-						
5H-CC	6H-CC	T *Paragloborotalia opima*	26.9	45.85	55.55	50.70	4.85
9H-CC	10H-CC	B *Paragloborotalia opima*	30.8	83.21	93.43	88.32	5.11
320-U1333C-	320-U1333C-						
3H-CC	4H-CC	B *Paragloborotalia pseudokugleri*	25.2	21.15	30.59	25.87	4.72
5H-CC	6H-CC	T *Paragloborotalia opima*	26.9	39.86	49.63	44.75	4.89
8H-CC	9H-CC	T *Subbotina angiporoides*	29.8	65.58	77.78	71.68	6.10
9H-CC	10H-CC	B *Paragloborotalia opima*	30.8	77.78	87.67	82.73	4.94

Note: B = bottom, T = top.

Table T9. Distribution of planktonic foraminifers, Site U1333. This table is available in an **oversized format.**

Table T10. Distribution of benthic foraminifers, Site U1333. This table is available in an **oversized format.**

Table T11. Coring-disturbed intervals and gaps, Site U1333. (See table notes.)

Core, section, interval (cm)	Type of disturbance
320-U1333A-	
1H-2, 145–150	Interstitial water
1H-5, 145–150	Interstitial water
2H-2, 145–150	Interstitial water
2H-5, 93–127	Flow-in
2H-5, 145–150	Interstitial water
3H-1, 0–24	Top of core
3H-2, 145–150	Interstitial water
3H-5, 145–150	Interstitial water
4H-1, 0–150	Flow-in(?)
4H-2, 0–122	Flow-in
4H-2, 145–150	Interstitial water
4H-5, 145–150	Interstitial water
5H-1, 0–100	Top of core
5H-2, 145–150	Interstitial water
5H-5, 145–150	Interstitial water
6H-1, 0–150	Top of core
6H-2, 0–90	Top of core
6H-2, 145–150	Interstitial water
6H-5, 145–150	Interstitial water
7H-1, 0–94	Top of core
7H-3, 140–150	Interstitial water
8H-1, 0–76	Top of core
8H-3, 140–150	Interstitial water
9H-1, 0–22	Minor disturbance
9H-3, 140–150	Interstitial water
10H-1, 0–44	Top of core
10H-3, 140–150	Interstitial water
11X-1, 0–80	Disturbed
11X-2, 140–150	Interstitial water
11X-4, 44–53	Slightly disturbed
12X-3, 140–150	Interstitial water
13X-3, 140–150	Interstitial water
14X-3, 140–150	Interstitial water
15X-3, 140–150	Interstitial water
16X-3, 140–150	Interstitial water
17X-3, 140–150	Interstitial water
17X-4, 140–150	Interstitial water
18X-1, 140–150	Interstitial water
18X-4, 28–72	Disturbed
19X-2, 140–150	Interstitial water
320-U1333B-	
1H-1, 0–10	Slightly disturbed mudline
2H-1, 0–130	Top of core
3H-1, 0–20	Flow-in
5H-1, 0–40	Top of core
7H-2, 140–150	Whole-round sample
8H-1, 0–46	Top of core
9H-1, 0–132	Top of core
10H-1, 0–54	Top of core
11H-1, 0–67	Top of core
12H-1, 0–15	Top of core
13H-1, 0–16	Top of core
14H-1, 0–57	Top of core
15H-1, 0–39	Top of core
16H-1, 0–31	Top of core
16H-1, 31–43	Disturbed
17H-1, 0–30	Disturbed
320-U1333C-	
1H-1, 0–10	Slightly disturbed mudline
3H-1, 0–34	Flow-in
4H-1, 0–150	Top of core
6H-1, 0–57	Top of core
7H-1, 0–112	Top of core
8H-1, 0–77	Top of core
9H-1, 0–29	Top of core
9H-1, 29–60	Fragmented
10H-1, 0–57	Top of core
10H-1, 57–80	Fragmented
11H-1, 0–150	Top of core
11H-2, 0–80	Top of core
12H-1, 0–100	Top of core
13H-1, 0–117	Top of core
14H-1, 0–50	Top of core
15H-1, 0–42	Top of core
16H-1, 0–66	Top of core
17H-4, 140–150	Whole-round sample
19H-1, 0–87	Top of core
20H-1, 0–40	Top of core

Notes: When interval listed is 0–150 cm, entire section is included even if true section length is <150 cm. Top of core = myriad forms of voids, disturbance, and debris from uphole that affect top portion of most cores. For that reason, probably the top 20 cm or so of all cores should be avoided.

Table T12. Paleomagnetic data from archive-half sections, Hole U1333A, at 0 mT AF demagnetization. (See table notes.)

Core, section	Offset (m)	Depth CSF (m)	Declination (°)	Inclination (°)	Intensity (Am)	Time (s)
320-U1333A-						
1H-1	0.10	0.10	331.0	71.4	1.401E–02	3321383392.88037
1H-1	0.15	0.15	339.0	44.9	6.138E–03	3321383398.19287
1H-1	0.20	0.20	325.1	41.7	4.816E–03	3321383403.52100
1H-1	0.25	0.25	21.4	23.4	1.360E–02	3321383408.84912
1H-1	0.30	0.30	51.8	17.1	1.899E–02	3321383414.17725
1H-1	0.35	0.35	15.1	22.8	5.429E–03	3321383419.48975
1H-1	0.40	0.40	355.1	19.2	5.510E–03	3321383424.81787
1H-1	0.45	0.45	357.5	19.3	5.527E–03	3321383430.14600
1H-1	0.50	0.50	349.4	21.8	4.290E–03	3321383435.47412
1H-1	0.55	0.55	7.1	4.9	8.149E–03	3321383440.78662
1H-1	0.60	0.60	6.5	7.7	1.540E–02	3321383446.11475
1H-1	0.65	0.65	1.3	10.0	1.716E–02	3321383451.44287
1H-1	0.70	0.70	358.6	8.6	1.883E–02	3321383456.77100
1H-1	0.75	0.75	359.8	8.3	1.868E–02	3321383462.08350
1H-1	0.80	0.80	1.4	8.9	1.541E–02	3321383467.41162
1H-1	0.85	0.85	0.3	9.1	1.441E–02	3321383472.73975
1H-1	0.90	0.90	4.5	8.5	1.605E–02	3321383478.08350
1H-1	0.95	0.95	1.6	6.7	1.581E–02	3321383483.41162
1H-1	1.00	1.00	355.4	9.7	1.365E–02	3321383488.73975
1H-1	1.05	1.05	1.2	10.7	1.277E–02	3321383494.06787
1H-1	1.10	1.10	0.9	10.5	1.193E–02	3321383499.39600
1H-1	1.15	1.15	357.4	15.4	8.490E–03	3321383504.73975
1H-1	1.20	1.20	1.4	13.4	6.706E–03	3321383510.06787
1H-1	1.25	1.25	353.8	6.5	6.500E–03	3321383515.39600
1H-1	1.30	1.30	354.9	–1.2	5.726E–03	3321383520.70850
1H-1	1.35	1.35	1.7	–5.2	4.958E–03	3321383526.03662
1H-1	1.40	1.40	1.9	–4.0	5.634E–03	3321383531.36475
1H-2	0.10	1.60	356.2	1.1	7.368E–03	3321385687.95850
1H-2	0.15	1.65	356.9	–0.2	7.475E–03	3321385693.28662
1H-2	0.20	1.70	355.5	–1.2	7.072E–03	3321385698.59912
1H-2	0.25	1.75	358.8	–4.2	5.624E–03	3321385703.92725
1H-2	0.30	1.80	0.5	–10.3	3.975E–03	3321385709.25537
1H-2	0.35	1.85	3.5	–10.9	4.272E–03	3321385714.58350
1H-2	0.40	1.90	1.6	0.8	9.983E–03	3321385719.91162
1H-2	0.45	1.95	359.3	8.9	1.178E–02	3321385725.23975
1H-2	0.50	2.00	0.6	6.7	9.347E–03	3321385730.55225
1H-2	0.55	2.05	353.7	5.3	1.087E–02	3321385735.88037
1H-2	0.60	2.10	351.0	7.5	1.368E–02	3321385741.20850
1H-2	0.65	2.15	348.7	7.1	1.493E–02	3321385746.53662
1H-2	0.70	2.20	348.7	7.5	1.517E–02	3321385751.84912
1H-2	0.75	2.25	349.9	6.2	1.480E–02	3321385757.17725
1H-2	0.80	2.30	352.0	5.9	1.445E–02	3321385762.50537
1H-2	0.85	2.35	353.8	7.6	1.365E–02	3321385767.83350
1H-2	0.90	2.40	351.9	8.6	1.389E–02	3321385773.16162
1H-2	0.95	2.45	348.2	8.7	1.427E–02	3321385778.48975
1H-2	1.00	2.50	347.9	9.4	1.306E–02	3321385783.80225
1H-2	1.05	2.55	347.4	11.0	1.139E–02	3321385789.13037
1H-2	1.10	2.60	11.5	18.1	1.113E–02	3321385794.45850
1H-2	1.15	2.65	336.3	25.1	1.272E–02	3321385799.78662
1H-2	1.20	2.70	336.4	14.1	6.389E–03	3321385805.09912
1H-2	1.25	2.75	355.3	8.5	4.884E–03	3321385810.42725
1H-2	1.30	2.80	354.9	10.0	5.345E–03	3321385815.75537
1H-2	1.35	2.85	349.4	7.9	5.645E–03	3321385821.08350
1H-2	1.40	2.90	353.2	5.8	6.653E–03	3321385826.41162
1H-3	0.10	3.10	1.2	–1.2	4.961E–03	3321387082.66162
1H-3	0.15	3.15	358.0	1.5	3.765E–03	3321387087.98975
1H-3	0.20	3.20	21.0	2.3	3.512E–03	3321387093.31787
1H-3	0.25	3.25	13.8	2.9	3.496E–03	3321387098.64600
1H-3	0.30	3.30	354.2	3.5	3.561E–03	3321387103.97412
1H-3	0.35	3.35	14.0	14.8	3.933E–03	3321387109.28662
1H-3	0.40	3.40	39.1	2.2	4.272E–03	3321387114.61475
1H-3	0.45	3.45	11.5	–9.6	2.346E–03	3321387119.94287
1H-3	0.50	3.50	24.7	–15.5	2.591E–03	3321387125.27100

Notes: Time = since 1 January 1904. Only a portion of this table appears here. The complete table is available in ASCII.

Table T13. Paleomagnetic data from archive-half sections, Hole U1333A, at 20 mT AF demagnetization. (See table notes.)

Core, section	Offset (m)	Depth CSF (m)	Declination (°)	Inclination (°)	Intensity (A/m)	Time (s)	Declination: Core mean (°)	Declination: Reoriented 0°–360°	Declination: Reoriented –90°–270°	Depth CCSF-A (m)	VGP (°) Latitude	VGP (°) Longitude
320-U1333A-												
1H-1	0.10	0.10	214.6	21.4	1.912E–03	3321384967.33350	353.50	221.1	221.1	4.7552	–43.8	158.3
1H-1	0.15	0.15	167.6	8.8	1.042E–03	3321384972.66162	353.50	174.1	174.1	4.8052	–73.9	243.3
1H-1	0.20	0.20	174.4	–4.6	1.354E–03	3321384977.97412	353.50	180.9	180.9	4.8552	–81.7	215.3
1H-1	0.25	0.25	169.0	–12.0	1.958E–03	3321384983.30225	353.50	175.5	175.5	4.9052	–83.7	266.9
1H-1	0.30	0.30	168.0	–8.5	2.165E–03	3321384988.63037	353.50	174.5	174.5	4.9552	–81.7	263.1
1H-1	0.35	0.35	177.7	–8.8	2.346E–03	3321384993.95850	353.50	184.2	184.2	5.0052	–82.6	186.9
1H-1	0.40	0.40	178.1	–5.2	4.094E–03	3321384999.28662	353.50	184.6	184.6	5.0552	–80.9	191.3
1H-1	0.45	0.45	183.2	1.3	4.705E–03	3321385004.59912	353.50	189.7	189.7	5.1052	–75.2	180.2
1H-1	0.50	0.50	188.2	4.9	5.595E–03	3321385009.92725	353.50	194.7	194.7	5.1552	–70.4	172.3
1H-1	0.55	0.55	187.2	3.2	4.054E–03	3321385015.25537	353.50	193.7	193.7	5.2052	–71.8	172.4
1H-1	0.60	0.60	327.8	30.3	5.581E–04	3321385020.58350	353.50	334.3	–25.7	5.2552	64.4	147.4
1H-1	0.65	0.65	1.3	13.0	3.078E–03	3321385025.91162	353.50	7.8	7.8	5.3052	81.3	338.0
1H-1	0.70	0.70	357.2	11.0	4.174E–03	3321385031.22412	353.50	3.7	3.7	5.3552	83.8	4.9
1H-1	0.75	0.75	355.8	8.8	4.494E–03	3321385036.55225	353.50	2.3	2.3	5.4052	83.5	20.9
1H-1	0.80	0.80	355.7	9.2	3.139E–03	3321385041.88037	353.50	2.2	2.2	5.4552	83.7	21.1
1H-1	0.85	0.85	356.8	9.6	2.437E–03	3321385047.20850	353.50	3.3	3.3	5.5052	83.4	11.4
1H-1	0.90	0.90	356.9	7.7	3.089E–03	3321385052.53662	353.50	3.4	3.4	5.5552	82.5	14.4
1H-1	0.95	0.95	358.1	6.5	3.678E–03	3321385057.86475	353.50	4.6	4.6	5.6052	81.4	9.1
1H-1	1.00	1.00	356.7	10.6	2.338E–03	3321385063.17725	353.50	3.2	3.2	5.6552	83.9	9.8
1H-1	1.05	1.05	354.6	14.9	1.462E–03	3321385068.50537	353.50	1.1	1.1	5.7052	86.9	21.2
1H-1	1.10	1.10	359.3	23.5	5.714E–04	3321385073.83350	353.50	5.8	5.8	5.7552	84.1	293.9
1H-1	1.15	1.15	180.3	7.0	1.395E–03	3321385079.16162	353.50	186.8	186.8	5.8052	–74.4	195.5
1H-1	1.20	1.20	176.8	–8.2	2.996E–03	3321385084.47412	353.50	183.3	183.3	5.8552	–82.8	194.2
1H-1	1.25	1.25	174.4	–18.6	3.186E–03	3321385089.80225	353.50	180.9	180.9	5.9052	–88.7	178.9
1H-1	1.30	1.30	174.7	–13.7	3.261E–03	3321385095.13037	353.50	181.2	181.2	5.9552	–86.2	203.1
1H-1	1.35	1.35	174.7	–11.5	4.007E–03	3321385100.45850	353.50	181.2	181.2	6.0052	–85.1	207.3
1H-1	1.40	1.40	173.3	–12.3	3.885E–03	3321385105.78662	353.50	179.8	179.8	6.0552	–85.7	224.2
1H-2	0.10	1.60	173.0	–8.6	2.508E–03	3321386181.23975	353.50	179.5	179.5	6.2552	–83.8	226.2
1H-2	0.15	1.65	170.7	–8.1	2.437E–03	3321386186.56787	353.50	177.2	177.2	6.3052	–83.0	245.1
1H-2	0.20	1.70	166.3	–8.6	2.777E–03	3321386191.89600	353.50	172.8	172.8	6.3552	–80.6	271.2
1H-2	0.25	1.75	158.5	–12.0	3.336E–03	3321386197.22412	353.50	165.0	165.0	6.4052	–74.5	296.1
1H-2	0.30	1.80	164.3	–9.6	4.326E–03	3321386202.53662	353.50	170.8	170.8	6.4552	–79.3	280.3
1H-2	0.35	1.85	165.7	–10.7	5.043E–03	3321386207.86475	353.50	172.2	172.2	6.5052	–80.7	278.6
1H-2	0.40	1.90	153.3	–17.7	2.717E–03	3321386213.19287	353.50	159.8	159.8	6.5552	–70.0	309.2
1H-2	0.45	1.95	45.4	9.9	7.555E–04	3321386218.52100	353.50	51.9	51.9	6.6052	38.3	313.5
1H-2	0.50	2.00	12.6	21.3	1.069E–03	3321386223.84912	353.50	19.1	19.1	6.6552	71.2	308.2
1H-2	0.55	2.05	11.5	36.5	7.741E–04	3321386229.17725	353.50	18.0	18.0	6.7052	70.1	280.0
1H-2	0.60	2.10	343.4	31.4	1.278E–03	3321386234.48975	353.50	349.9	–10.1	6.7552	78.3	166.0
1H-2	0.65	2.15	338.0	23.3	1.810E–03	3321386239.81787	353.50	344.5	–15.5	6.8052	74.7	139.2
1H-2	0.70	2.20	326.9	25.9	2.180E–03	3321386245.14600	353.50	333.4	–26.6	6.8552	63.8	141.2
1H-2	0.75	2.25	334.8	20.8	2.456E–03	3321386250.45850	353.50	341.3	–18.7	6.9052	71.6	134.1
1H-2	0.80	2.30	333.3	22.2	2.393E–03	3321386255.78662	353.50	339.8	–20.2	6.9552	70.2	136.4
1H-2	0.85	2.35	337.1	29.3	2.673E–03	3321386261.11475	353.50	343.6	–16.4	7.0052	73.2	151.2
1H-2	0.90	2.40	343.3	19.0	3.372E–03	3321386266.44287	353.50	349.8	–10.2	7.0552	79.9	128.2
1H-2	0.95	2.45	336.3	18.4	3.218E–03	3321386271.77100	353.50	342.8	–17.2	7.1052	73.0	129.5

Notes: Time = since 1 January 1904. VGP = virtual geomagnetic pole. Only a portion of this table appears here. The complete table is available in ASCII.

Table T14. Paleomagnetic data from archive-half sections, Hole U1333B, at 0 mT AF demagnetization. (See table notes.)

Core, section	Offset (m)	Depth CSF (m)	Declination (°)	Inclination (°)	Intensity (A/m)	Time (s)
320-U1333B-						
1H-1	0.15	0.15	343.9	–6.5	4.736E–03	3321589173.98437
1H-1	0.20	0.20	281.0	–11.7	1.907E–03	3321589179.31250
1H-1	0.25	0.25	231.4	3.1	4.907E–03	3321589184.64062
1H-1	0.30	0.30	219.9	8.5	5.495E–03	3321589189.95312
1H-1	0.35	0.35	206.3	11.3	8.530E–03	3321589195.28125
1H-1	0.40	0.40	202.7	11.2	1.008E–02	3321589200.60937
1H-1	0.45	0.45	202.4	11.1	9.943E–03	3321589205.93750
1H-1	0.50	0.50	202.7	10.4	9.227E–03	3321589211.26562
1H-1	0.55	0.55	206.2	10.8	8.597E–03	3321589216.57812
1H-1	0.60	0.60	204.6	11.8	8.097E–03	3321589221.90625
1H-1	0.65	0.65	203.3	14.2	7.674E–03	3321589227.23437
1H-1	0.70	0.70	197.8	14.3	9.019E–03	3321589232.56250
1H-1	0.75	0.75	196.0	12.8	9.989E–03	3321589237.89062
1H-1	0.80	0.80	196.1	14.5	9.842E–03	3321589243.21875
1H-1	0.85	0.85	190.8	12.8	1.042E–02	3321589248.53125
1H-1	0.90	0.90	184.9	11.4	1.110E–02	3321589253.85937
1H-1	0.95	0.95	186.1	11.8	1.209E–02	3321589259.18750
1H-1	1.00	1.00	181.4	12.2	1.280E–02	3321589264.51562
1H-1	1.05	1.05	183.2	13.0	1.121E–02	3321589269.82812
1H-1	1.10	1.10	181.8	12.0	1.032E–02	3321589275.15625
1H-1	1.15	1.15	177.1	13.3	9.453E–03	3321589280.48437
1H-1	1.20	1.20	177.0	13.0	9.754E–03	3321589285.81250
1H-1	1.25	1.25	178.1	11.2	8.555E–03	3321589291.14062
1H-1	1.30	1.30	177.9	13.4	6.886E–03	3321589296.45312
1H-1	1.35	1.35	174.9	14.3	6.019E–03	3321589301.78125
1H-1	1.40	1.40	171.7	14.8	5.235E–03	3321589307.10937
1H-2	0.10	1.60	182.2	13.4	5.783E–03	3321590405.34375
1H-2	0.15	1.65	180.9	7.8	6.469E–03	3321590410.67187
1H-2	0.20	1.70	176.4	5.4	8.249E–03	3321590416.00000
1H-2	0.25	1.75	170.5	6.1	8.526E–03	3321590421.31250
1H-2	0.30	1.80	170.2	8.9	8.621E–03	3321590426.64062
1H-2	0.35	1.85	168.1	15.6	6.093E–03	3321590431.96875
1H-2	0.40	1.90	167.7	20.6	4.391E–03	3321590437.29687
1H-2	0.45	1.95	169.4	20.4	3.951E–03	3321590442.62500
1H-2	0.50	2.00	168.8	18.9	4.288E–03	3321590447.95312
1H-2	0.55	2.05	168.9	17.2	4.855E–03	3321590453.28125
1H-2	0.60	2.10	169.7	18.4	6.994E–03	3321590458.59375
1H-2	0.65	2.15	163.2	16.3	8.103E–03	3321590463.92187
1H-2	0.70	2.20	164.7	15.6	8.247E–03	3321590469.25000
1H-2	0.75	2.25	162.7	13.7	7.150E–03	3321590474.57812
1H-2	0.80	2.30	161.7	17.3	5.390E–03	3321590479.89062
1H-2	0.85	2.35	159.8	17.8	4.470E–03	3321590485.21875
1H-2	0.90	2.40	157.9	18.5	3.581E–03	3321590490.54687
1H-2	0.95	2.45	160.4	12.4	3.878E–03	3321590495.85937
1H-2	1.00	2.50	157.8	13.0	3.861E–03	3321590501.18750
1H-2	1.05	2.55	157.3	14.3	3.986E–03	3321590506.51562
1H-2	1.10	2.60	155.5	13.9	4.658E–03	3321590511.84375
1H-2	1.15	2.65	152.8	13.3	5.740E–03	3321590517.17187
1H-2	1.20	2.70	147.6	12.7	5.868E–03	3321590522.50000
1H-2	1.25	2.75	144.2	13.0	5.363E–03	3321590527.81250
1H-2	1.30	2.80	146.5	9.3	5.289E–03	3321590533.14062
1H-2	1.35	2.85	152.2	8.5	5.584E–03	3321590538.46875
1H-2	1.40	2.90	155.3	7.2	6.211E–03	3321590543.79687
1H-3	0.10	3.10	166.0	12.3	3.423E–03	3321591601.81250
1H-3	0.15	3.15	165.8	12.7	3.442E–03	3321591607.14062
1H-3	0.20	3.20	162.8	9.8	4.097E–03	3321591612.45312
1H-3	0.25	3.25	163.1	7.8	3.815E–03	3321591617.78125
1H-3	0.30	3.30	166.1	9.6	4.014E–03	3321591623.10937
1H-3	0.35	3.35	164.9	17.9	6.286E–03	3321591628.43750
1H-3	0.40	3.40	158.1	28.4	7.555E–03	3321591633.76562
1H-3	0.45	3.45	46.0	33.0	8.112E–03	3321591639.09375
1H-3	0.50	3.50	27.3	7.3	2.012E–02	3321591644.40625
1H-3	0.55	3.55	26.5	–4.6	2.117E–02	3321591649.73437

Notes: Time = since 1 January 1904. Only a portion of this table appears here. The complete table is available in ASCII.

Table T15. Paleomagnetic data from archive-half sections, Hole U1333B, at 10 mT AF demagnetization. (See table notes.)

Core, section	Offset (m)	Depth CSF (m)	Declination (°)	Inclination (°)	Intensity (A/m)	Time (s)
320-U1333B-						
1H-1	0.15	0.15	18.8	–10.1	5.133E–03	3321589595.28125
1H-1	0.20	0.20	29.2	–18.0	2.597E–03	3321589600.60937
1H-1	0.25	0.25	191.7	–27.6	6.166E–04	3321589605.93750
1H-1	0.30	0.30	204.0	5.7	2.662E–03	3321589611.26562
1H-1	0.35	0.35	194.0	11.0	4.156E–03	3321589616.59375
1H-1	0.40	0.40	191.3	9.2	6.973E–03	3321589621.90625
1H-1	0.45	0.45	192.5	9.5	6.737E–03	3321589627.23437
1H-1	0.50	0.50	192.5	8.8	6.158E–03	3321589632.56250
1H-1	0.55	0.55	194.9	8.4	5.185E–03	3321589637.89062
1H-1	0.60	0.60	194.5	7.7	5.171E–03	3321589643.20312
1H-1	0.65	0.65	194.3	8.8	5.226E–03	3321589648.53125
1H-1	0.70	0.70	191.4	10.8	5.848E–03	3321589653.85937
1H-1	0.75	0.75	190.2	11.7	7.075E–03	3321589659.18750
1H-1	0.80	0.80	189.2	12.6	7.620E–03	3321589664.51562
1H-1	0.85	0.85	187.1	11.3	7.852E–03	3321589669.82812
1H-1	0.90	0.90	185.6	10.2	8.420E–03	3321589675.15625
1H-1	0.95	0.95	184.9	10.2	9.312E–03	3321589680.48437
1H-1	1.00	1.00	182.5	11.5	9.325E–03	3321589685.81250
1H-1	1.05	1.05	181.5	10.9	8.770E–03	3321589691.14062
1H-1	1.10	1.10	181.2	11.4	6.788E–03	3321589696.45312
1H-1	1.15	1.15	179.5	10.0	6.675E–03	3321589701.78125
1H-1	1.20	1.20	176.1	10.0	5.931E–03	3321589707.10937
1H-1	1.25	1.25	178.5	9.6	4.882E–03	3321589712.43750
1H-1	1.30	1.30	177.6	8.4	4.161E–03	3321589717.75000
1H-1	1.35	1.35	175.3	12.0	3.199E–03	3321589723.07812
1H-1	1.40	1.40	172.5	9.1	3.179E–03	3321589728.40625
1H-2	0.10	1.60	177.4	6.4	2.360E–03	3321590815.75000
1H-2	0.15	1.65	177.4	–0.4	2.236E–03	3321590821.07812
1H-2	0.20	1.70	173.6	–2.9	4.810E–03	3321590826.40625
1H-2	0.25	1.75	165.3	–1.0	5.842E–03	3321590831.71875
1H-2	0.30	1.80	170.4	2.5	5.788E–03	3321590837.04687
1H-2	0.35	1.85	169.2	8.7	3.331E–03	3321590842.35937
1H-2	0.40	1.90	166.6	22.9	1.541E–03	3321590847.68750
1H-2	0.45	1.95	179.7	20.8	1.510E–03	3321590853.01562
1H-2	0.50	2.00	172.1	18.6	1.640E–03	3321590858.32812
1H-2	0.55	2.05	169.9	14.7	2.257E–03	3321590863.65625
1H-2	0.60	2.10	173.8	14.8	4.186E–03	3321590868.98437
1H-2	0.65	2.15	170.3	15.2	5.103E–03	3321590874.31250
1H-2	0.70	2.20	165.6	13.9	5.476E–03	3321590879.64062
1H-2	0.75	2.25	166.1	10.3	4.588E–03	3321590884.95312
1H-2	0.80	2.30	164.6	13.2	2.483E–03	3321590890.28125
1H-2	0.85	2.35	165.3	20.4	1.680E–03	3321590895.60937
1H-2	0.90	2.40	164.6	16.2	1.679E–03	3321590900.93750
1H-2	0.95	2.45	165.1	9.9	2.101E–03	3321590906.26562
1H-2	1.00	2.50	163.2	9.8	2.223E–03	3321590911.59375
1H-2	1.05	2.55	161.9	11.3	2.240E–03	3321590916.90625
1H-2	1.10	2.60	166.8	7.7	3.453E–03	3321590922.23437
1H-2	1.15	2.65	162.5	8.6	3.376E–03	3321590927.56250
1H-2	1.20	2.70	161.1	8.6	3.366E–03	3321590932.89062
1H-2	1.25	2.75	160.0	9.9	2.639E–03	3321590938.21875
1H-2	1.30	2.80	161.4	9.0	2.710E–03	3321590943.53125
1H-2	1.35	2.85	163.8	6.8	3.145E–03	3321590948.85937
1H-2	1.40	2.90	163.0	5.3	3.522E–03	3321590954.18750
1H-2	0.10	3.10	165.8	8.9	1.923E–03	3321592030.54687
1H-2	0.15	3.15	167.9	8.5	1.790E–03	3321592035.87500
1H-2	0.20	3.20	163.8	5.6	2.040E–03	3321592041.20312
1H-2	0.25	3.25	162.2	1.6	2.165E–03	3321592046.53125
1H-2	0.30	3.30	164.7	1.4	1.973E–03	3321592051.85937
1H-2	0.35	3.35	151.0	4.4	3.514E–03	3321592057.18750
1H-2	0.40	3.40	164.5	5.1	6.034E–03	3321592062.50000
1H-2	0.45	3.45	161.8	5.4	4.270E–03	3321592067.82812
1H-2	0.50	3.50	188.0	–27.6	6.071E–04	3321592073.15625

Notes: Time = since 1 January 1904. Only a portion of this table appears here. The complete table is available in ASCII.

Table T16. Paleomagnetic data from archive-half sections, Hole U1333B, at 20 mT AF demagnetization. (See table notes.)

Core, section	Offset (m)	Depth CSF (m)	Declination (°)	Inclination (°)	Intensity (A/m)	Time (s)	Declination: Core mean (°)	Declination: Reoriented 0°–360°	Declination: Reoriented –90°–270°	Depth CCSF-A (m)	VGP (°) Latitude	VGP (°) Longitude
320-U1333B-												
1H-1	0.15	0.15	19.2	–4.5	3.792E–03	3321590013.95312	171.00	208.2	208.2	0.1500	–60.8	146.1
1H-1	0.20	0.20	20.9	–4.7	2.275E–03	3321590019.28125	171.00	209.9	209.9	0.2000	–59.2	144.9
1H-1	0.25	0.25	196.1	25.6	5.462E–04	3321590024.60937	171.00	25.1	25.1	0.2500	65.3	302.2
1H-1	0.30	0.30	198.8	21.5	1.403E–03	3321590029.92187	171.00	27.8	27.8	0.3000	62.7	307.6
1H-1	0.35	0.35	196.3	18.1	3.449E–03	3321590035.25000	171.00	25.3	25.3	0.3500	65.1	312.2
1H-1	0.40	0.40	194.4	15.9	4.316E–03	3321590040.57812	171.00	23.4	23.4	0.4000	66.8	315.5
1H-1	0.45	0.45	193.5	14.1	4.839E–03	3321590045.90625	171.00	22.5	22.5	0.4500	67.5	318.3
1H-1	0.50	0.50	194.6	14.3	4.215E–03	3321590051.23437	171.00	23.6	23.6	0.5000	66.5	317.6
1H-1	0.55	0.55	195.9	15.4	3.504E–03	3321590056.56250	171.00	24.9	24.9	0.5500	65.3	315.7
1H-1	0.60	0.60	196.0	14.2	3.552E–03	3321590061.87500	171.00	25.0	25.0	0.6000	65.1	317.1
1H-1	0.65	0.65	196.3	14.6	3.658E–03	3321590067.20312	171.00	25.3	25.3	0.6500	64.8	316.5
1H-1	0.70	0.70	193.2	15.1	4.115E–03	3321590072.53125	171.00	22.2	22.2	0.7000	67.9	317.1
1H-1	0.75	0.75	191.2	13.7	5.021E–03	3321590077.85937	171.00	20.2	20.2	0.7500	69.7	320.1
1H-1	0.80	0.80	189.6	14.7	5.284E–03	3321590083.17187	171.00	18.6	18.6	0.8000	71.4	319.4
1H-1	0.85	0.85	188.1	14.5	5.439E–03	3321590088.50000	171.00	17.1	17.1	0.8500	72.8	320.7
1H-1	0.90	0.90	186.3	13.8	5.834E–03	3321590093.82812	171.00	15.3	15.3	0.9000	74.5	323.4
1H-1	0.95	0.95	185.5	13.9	6.768E–03	3321590099.15625	171.00	14.5	14.5	0.9500	75.3	324.0
1H-1	1.00	1.00	183.1	14.6	6.640E–03	3321590104.48437	171.00	12.1	12.1	1.0000	77.7	325.1
1H-1	1.05	1.05	183.3	14.5	6.230E–03	3321590109.79687	171.00	12.3	12.3	1.0500	77.5	325.1
1H-1	1.10	1.10	182.4	15.3	5.108E–03	3321590115.12500	171.00	11.4	11.4	1.1000	78.4	324.2
1H-1	1.15	1.15	180.4	14.2	4.782E–03	3321590120.45312	171.00	9.4	9.4	1.1500	80.1	330.4
1H-1	1.20	1.20	178.9	14.7	4.295E–03	3321590125.78125	171.00	7.9	7.9	1.2000	81.6	332.2
1H-1	1.25	1.25	179.2	12.3	3.986E–03	3321590131.10937	171.00	8.2	8.2	1.2500	80.8	338.8
1H-1	1.30	1.30	179.2	15.1	3.081E–03	3321590136.43750	171.00	8.2	8.2	1.3000	81.4	330.2
1H-1	1.35	1.35	176.3	18.7	2.528E–03	3321590141.75000	171.00	5.3	5.3	1.3500	84.7	321.0
1H-1	1.40	1.40	172.2	15.5	2.217E–03	3321590147.07812	171.00	1.2	1.2	1.4000	87.1	17.2
1H-2	0.10	1.60	180.4	20.9	1.460E–03	3321591242.93750	171.00	9.4	9.4	1.6000	80.8	308.9
1H-2	0.15	1.65	180.9	13.7	1.521E–03	3321591248.26562	171.00	9.9	9.9	1.6500	79.6	330.8
1H-2	0.20	1.70	173.2	3.8	3.054E–03	3321591253.57812	171.00	2.2	2.2	1.7000	81.1	27.2
1H-2	0.25	1.75	171.1	3.6	4.145E–03	3321591258.90625	171.00	0.1	0.1	1.7500	81.3	40.9
1H-2	0.30	1.80	171.1	5.5	4.268E–03	3321591264.23437	171.00	0.1	0.1	1.8000	82.2	40.8
1H-2	0.35	1.85	170.3	17.8	2.538E–03	3321591269.56250	171.00	359.3	–0.7	1.8500	88.4	67.9
1H-2	0.40	1.90	173.0	31.5	1.489E–03	3321591274.89062	171.00	2.0	2.0	1.9000	83.2	237.9
1H-2	0.45	1.95	180.1	48.0	9.430E–04	3321591280.20312	171.00	9.1	9.1	1.9500	69.6	245.0
1H-2	0.50	2.00	176.2	34.2	1.209E–03	3321591285.53125	171.00	5.2	5.2	2.0000	80.3	252.3
1H-2	0.55	2.05	172.8	25.9	1.597E–03	3321591290.85937	171.00	1.8	1.8	2.0500	86.4	250.7
1H-2	0.60	2.10	174.1	23.7	2.616E–03	3321591296.18750	171.00	3.1	3.1	2.1000	86.4	279.8
1H-2	0.65	2.15	172.4	18.3	4.443E–03	3321591301.51562	171.00	1.4	1.4	2.1500	88.2	350.7
1H-2	0.70	2.20	167.1	17.9	3.944E–03	3321591306.82812	171.00	356.1	–3.9	2.2000	85.9	112.7
1H-2	0.75	2.25	166.5	13.4	3.344E–03	3321591312.15625	171.00	355.5	–4.5	2.2500	84.2	92.0
1H-2	0.80	2.30	163.8	29.0	1.665E–03	3321591317.48437	171.00	352.8	–7.2	2.3000	81.4	167.7
1H-2	0.85	2.35	170.5	28.0	1.316E–03	3321591322.81250	171.00	359.5	–0.5	2.3500	85.6	215.3
1H-2	0.90	2.40	168.8	28.5	1.205E–03	3321591328.14062	171.00	357.8	–2.2	2.4000	84.9	197.2
1H-2	0.95	2.45	166.4	11.1	1.481E–03	3321591333.45312	171.00	355.4	–4.6	2.4500	83.3	84.8
1H-2	1.00	2.50	163.9	15.9	1.577E–03	3321591338.78125	171.00	352.9	–7.1	2.5000	82.6	113.2

Notes: Time = since 1 January 1904. VGP = virtual geomagnetic pole. Only a portion of this table appears here. The complete table is available in ASCII.

Table T17. Paleomagnetic data from archive-half sections, Hole U1333C, at 0 mT AF demagnetization. (See table notes.)

Core, section	Offset (m)	Depth CSF (m)	Declination (°)	Inclination (°)	Intensity (A/m)	Time (s)
320-U1333C-						
1H-1	0.15	0.15	59.1	35.7	7.712E–03	3321763840.82812
1H-1	0.20	0.20	55.5	28.2	9.651E–03	3321763846.15625
1H-1	0.25	0.25	53.6	26.9	9.910E–03	3321763851.48437
1H-1	0.30	0.30	52.7	28.1	9.371E–03	3321763856.81250
1H-1	0.35	0.35	52.9	21.7	1.054E–02	3321763862.12500
1H-1	0.40	0.40	46.7	20.0	1.196E–02	3321763867.45312
1H-1	0.45	0.45	48.6	22.0	1.261E–02	3321763872.78125
1H-1	0.50	0.50	48.9	21.5	1.218E–02	3321763878.10937
1H-1	0.55	0.55	43.5	17.4	1.335E–02	3321763883.43750
1H-1	0.60	0.60	40.8	20.6	1.411E–02	3321763888.75000
1H-1	0.65	0.65	40.9	22.5	1.327E–02	3321763894.07812
1H-1	0.70	0.70	40.5	24.6	1.218E–02	3321763899.40625
1H-1	0.75	0.75	43.5	23.3	1.124E–02	3321763904.71875
1H-1	0.80	0.80	42.8	23.0	9.887E–03	3321763910.04687
1H-1	0.85	0.85	40.1	35.7	5.248E–03	3321763915.37500
1H-1	0.90	0.90	37.4	28.3	6.710E–03	3321763920.68750
1H-1	0.95	0.95	42.2	24.9	8.647E–03	3321763926.01562
1H-1	1.00	1.00	41.7	26.4	8.081E–03	3321763931.34375
1H-1	1.05	1.05	43.7	27.6	7.324E–03	3321763936.67187
1H-1	1.10	1.10	40.7	33.3	5.099E–03	3321763942.00000
1H-1	1.15	1.15	347.5	24.8	2.658E–03	3321763947.32812
1H-1	1.20	1.20	34.1	14.1	4.949E–03	3321763952.65625
1H-1	1.25	1.25	47.3	23.1	7.711E–03	3321763957.98437
1H-1	1.30	1.30	34.0	27.1	7.774E–03	3321763963.31250
1H-1	1.35	1.35	45.4	24.6	8.051E–03	3321763968.62500
1H-1	1.40	1.40	55.5	29.8	6.708E–03	3321763973.95312
2H-1	0.10	1.70	299.9	24.4	1.076E–02	3321770259.48437
2H-1	0.15	1.75	295.7	16.3	1.085E–02	3321770264.81250
2H-1	0.20	1.80	279.9	9.4	8.314E–03	3321770270.14062
2H-1	0.25	1.85	266.5	4.2	7.233E–03	3321770275.45312
2H-1	0.30	1.90	270.9	4.5	7.232E–03	3321770280.78125
2H-1	0.35	1.95	268.3	5.4	7.368E–03	3321770286.10937
2H-1	0.40	2.00	267.7	5.6	7.791E–03	3321770291.43750
2H-1	0.45	2.05	266.5	1.9	8.597E–03	3321770296.76562
2H-1	0.50	2.10	256.2	–4.0	8.692E–03	3321770302.09375
2H-1	0.55	2.15	249.5	–6.0	8.309E–03	3321770307.40625
2H-1	0.60	2.20	242.0	–6.5	8.094E–03	3321770312.73437
2H-1	0.65	2.25	243.6	–7.9	7.739E–03	3321770318.06250
2H-1	0.70	2.30	254.0	–5.0	7.000E–03	3321770323.39062
2H-1	0.75	2.35	258.9	–4.9	7.203E–03	3321770328.70312
2H-1	0.80	2.40	259.3	–4.5	7.321E–03	3321770334.03125
2H-1	0.85	2.45	261.7	–4.1	7.434E–03	3321770339.35937
2H-1	0.90	2.50	256.8	–4.2	7.558E–03	3321770344.68750
2H-1	0.95	2.55	237.7	–6.6	6.994E–03	3321770350.01562
2H-1	1.00	2.60	240.3	–7.0	7.265E–03	3321770355.34375
2H-1	1.05	2.65	261.0	–2.7	7.844E–03	3321770360.65625
2H-1	1.10	2.70	266.8	–0.6	8.660E–03	3321770365.98437
2H-1	1.15	2.75	254.5	–4.3	7.569E–03	3321770371.31250
2H-1	1.20	2.80	247.4	–6.8	8.111E–03	3321770376.64062
2H-1	1.25	2.85	248.8	–6.1	8.998E–03	3321770381.96875
2H-1	1.30	2.90	247.6	–6.6	9.895E–03	3321770387.28125
2H-1	1.35	2.95	238.9	–7.5	1.075E–02	3321770392.60937
2H-1	1.40	3.00	231.3	–8.1	1.169E–02	3321770397.93750
2H-2	0.10	3.20	302.8	8.5	9.032E–03	3321771594.33187
2H-2	0.15	3.25	309.8	10.8	1.332E–02	3321771599.65999
2H-2	0.20	3.30	316.5	11.0	1.435E–02	3321771604.98812
2H-2	0.25	3.35	320.9	11.3	1.330E–02	3321771610.31624
2H-2	0.30	3.40	314.0	12.8	1.234E–02	3321771615.64437
2H-2	0.35	3.45	315.6	14.3	1.243E–02	3321771620.95687
2H-2	0.40	3.50	319.5	13.0	1.339E–02	3321771626.28499
2H-2	0.45	3.55	318.9	14.2	1.037E–02	3321771631.59749
2H-2	0.50	3.60	318.3	16.0	7.920E–03	3321771636.92562

Notes: Time = since 1 January 1904. Only a portion of this table appears here. The complete table is available in ASCII.

Table T18. Paleomagnetic data from archive-half sections, Hole U1333C, at 10 mT AF demagnetization. (See table notes.) (Continued on next two pages.)

Core, section	Offset (m)	Depth CSF (m)	Declination (°)	Inclination (°)	Intensity (A/m)	Time (s)
320-U1333C-						
1H-1	0.15	0.15	50.7	2.5	4.633E–03	3321764261.35937
1H-1	0.20	0.20	50.9	3.3	4.635E–03	3321764266.68750
1H-1	0.25	0.25	46.3	4.1	4.941E–03	3321764272.00000
1H-1	0.30	0.30	46.5	6.0	4.656E–03	3321764277.32812
1H-1	0.35	0.35	44.9	8.7	5.696E–03	3321764282.65625
1H-1	0.40	0.40	46.9	8.2	7.350E–03	3321764287.98437
1H-1	0.45	0.45	43.1	7.5	7.785E–03	3321764293.29687
1H-1	0.50	0.50	45.4	7.0	7.704E–03	3321764298.62500
1H-1	0.55	0.55	39.4	5.1	8.496E–03	3321764303.95312
1H-1	0.60	0.60	37.2	5.8	8.699E–03	3321764309.28125
1H-1	0.65	0.65	37.3	7.0	8.324E–03	3321764314.60937
1H-1	0.70	0.70	37.0	7.9	7.454E–03	3321764319.93750
1H-1	0.75	0.75	37.6	8.4	6.365E–03	3321764325.25000
1H-1	0.80	0.80	42.4	7.8	5.357E–03	3321764330.57812
1H-1	0.85	0.85	28.2	13.3	2.543E–03	3321764335.90625
1H-1	0.90	0.90	28.7	8.1	3.347E–03	3321764341.23437
1H-1	0.95	0.95	35.1	6.5	4.724E–03	3321764346.54687
1H-1	1.00	1.00	33.6	7.2	4.219E–03	3321764351.87500
1H-1	1.05	1.05	38.2	9.0	3.118E–03	3321764357.20312
1H-1	1.10	1.10	3.9	6.4	2.232E–03	3321764362.53125
1H-1	1.15	1.15	333.8	–32.1	1.635E–03	3321764367.85937
1H-1	1.20	1.20	359.0	–36.1	1.859E–03	3321764373.18750
1H-1	1.25	1.25	31.7	–5.7	3.567E–03	3321764378.50000
1H-1	1.30	1.30	27.6	3.2	4.807E–03	3321764383.82812
1H-1	1.35	1.35	33.7	3.1	4.215E–03	3321764389.15625
1H-1	1.40	1.40	45.6	–4.4	3.420E–03	3321764394.48437
9H-1	0.65	68.75	234.9	8.5	3.285E–04	3321838295.25000
9H-1	0.70	68.80	230.8	–0.4	3.941E–04	3321838300.57812
9H-1	0.75	68.85	230.4	2.2	5.755E–04	3321838305.90625
9H-1	0.80	68.90	233.5	4.6	8.506E–04	3321838311.21875
9H-1	0.85	68.95	234.9	3.4	1.088E–03	3321838316.54687
9H-1	0.90	69.00	238.6	0.4	1.064E–03	3321838321.87500
9H-1	0.95	69.05	239.1	–4.6	9.486E–04	3321838327.20312
9H-1	1.00	69.10	217.6	–1.1	1.478E–03	3321838332.51562
9H-1	1.05	69.15	231.5	0.8	1.506E–03	3321838337.84375
9H-1	1.10	69.20	229.7	2.4	1.153E–03	3321838343.17187
9H-1	1.15	69.25	232.4	1.1	7.849E–04	3321838348.50000
9H-1	1.20	69.30	228.8	0.8	7.963E–04	3321838353.82812
9H-1	1.25	69.35	229.3	2.2	9.278E–04	3321838359.14062
9H-1	1.30	69.40	233.2	2.3	8.754E–04	3321838364.46875
9H-1	1.35	69.45	234.3	6.8	7.085E–04	3321838369.79687
9H-1	1.40	69.50	234.2	11.6	7.590E–04	3321838375.12500
9H-2	0.10	69.70	243.6	4.4	7.939E–04	3321839498.07812
9H-2	0.15	69.75	243.2	15.2	1.007E–03	3321839503.40625
9H-2	0.20	69.80	245.4	16.1	1.503E–03	3321839508.73437
9H-2	0.25	69.85	242.3	14.5	1.241E–03	3321839514.04687
9H-2	0.30	69.90	244.2	17.0	8.049E–04	3321839519.37500
9H-2	0.35	69.95	246.0	17.2	7.447E–04	3321839524.68750
9H-2	0.40	70.00	245.7	12.5	9.881E–04	3321839530.01562
9H-2	0.45	70.05	245.4	10.3	1.232E–03	3321839535.34375
9H-2	0.50	70.10	242.1	10.2	1.346E–03	3321839540.67187
9H-2	0.55	70.15	240.9	9.2	1.340E–03	3321839546.00000
9H-2	0.60	70.20	240.7	7.8	1.095E–03	3321839551.32812
9H-2	0.65	70.25	240.3	7.3	8.621E–04	3321839556.65625
9H-2	0.70	70.30	238.3	9.6	8.425E–04	3321839561.96875
9H-2	0.75	70.35	234.4	15.2	1.127E–03	3321839567.29687
9H-2	0.80	70.40	237.7	19.3	1.329E–03	3321839572.62500
9H-2	0.85	70.45	240.9	16.5	1.395E–03	3321839577.95312
9H-2	0.90	70.50	234.8	12.2	1.866E–03	3321839583.28125
9H-2	0.95	70.55	240.0	10.9	1.846E–03	3321839588.59375
9H-2	1.00	70.60	240.8	0.2	1.781E–03	3321839593.92187
9H-2	1.05	70.65	240.6	2.8	1.612E–03	3321839599.25000
9H-2	1.10	70.70	244.4	6.3	1.407E–03	3321839604.57812
9H-2	1.15	70.75	244.3	7.1	1.280E–03	3321839609.89062
9H-2	1.20	70.80	243.7	6.3	8.909E–04	3321839615.21875
9H-2	1.25	70.85	101.0	–28.9	1.746E–04	3321839620.54687

Table T18 (continued). (Continued on next page.)

Core, section	Offset (m)	Depth CSF (m)	Declination (°)	Inclination (°)	Intensity (A/m)	Time (s)
9H-2	1.30	70.90	42.2	–24.3	5.124E–04	3321839625.87500
9H-2	1.35	70.95	46.2	–26.8	6.280E–04	3321839631.20312
9H-2	1.40	71.00	61.7	–16.5	1.243E–03	3321839636.53125
9H-3	0.10	71.20	68.0	–10.8	1.265E–03	3321840757.25000
9H-3	0.15	71.25	67.8	–11.7	1.407E–03	3321840762.57812
9H-3	0.20	71.30	65.8	–19.2	1.222E–03	3321840767.90625
9H-3	0.25	71.35	63.7	–21.3	1.269E–03	3321840773.23437
9H-3	0.30	71.40	66.0	–22.6	1.313E–03	3321840778.56250
9H-3	0.35	71.45	71.4	–15.9	2.043E–03	3321840783.89062
9H-3	0.40	71.50	70.5	–14.4	1.854E–03	3321840789.20312
9H-3	0.45	71.55	56.1	–14.2	3.451E–04	3321840794.53125
9H-3	0.50	71.60	252.5	–0.2	5.484E–04	3321840799.85937
9H-3	0.55	71.65	248.6	20.4	7.678E–04	3321840805.18750
9H-3	0.60	71.70	257.7	4.9	1.587E–03	3321840810.50000
9H-3	0.65	71.75	252.2	9.1	1.435E–03	3321840815.82812
9H-3	0.70	71.80	255.9	7.1	2.635E–03	3321840821.15625
9H-3	0.75	71.85	245.3	10.0	2.277E–03	3321840826.48437
9H-3	0.80	71.90	247.8	0.4	1.805E–03	3321840831.81250
9H-3	0.85	71.95	249.5	2.9	1.268E–03	3321840837.14062
9H-3	0.90	72.00	248.4	6.5	1.372E–03	3321840842.45312
9H-3	0.95	72.05	248.3	7.6	1.709E–03	3321840847.78125
9H-3	1.00	72.10	248.5	8.7	1.432E–03	3321840853.10937
9H-3	1.05	72.15	241.8	15.6	9.771E–04	3321840858.43750
9H-3	1.10	72.20	245.4	13.6	1.399E–03	3321840863.76562
9H-3	1.15	72.25	243.7	12.7	1.603E–03	3321840869.07812
9H-3	1.20	72.30	245.0	14.8	1.361E–03	3321840874.40625
9H-3	1.25	72.35	248.7	17.3	1.077E–03	3321840879.73437
9H-3	1.30	72.40	247.8	15.5	1.314E–03	3321840885.04687
9H-3	1.35	72.45	249.8	11.3	1.794E–03	3321840890.37500
9H-3	1.40	72.50	251.0	11.1	1.691E–03	3321840895.70312
9H-4	0.10	72.70	255.5	7.9	1.805E–03	3321841990.17187
9H-4	0.15	72.75	249.7	5.4	1.607E–03	3321841995.50000
9H-4	0.20	72.80	252.2	3.5	1.854E–03	3321842000.82812
9H-4	0.25	72.85	255.0	6.1	1.965E–03	3321842006.15625
9H-4	0.30	72.90	257.3	8.3	1.649E–03	3321842011.46875
9H-4	0.35	72.95	253.4	10.2	1.202E–03	3321842016.79687
9H-4	0.40	73.00	257.2	8.5	1.385E–03	3321842022.12500
9H-4	0.45	73.05	260.0	9.0	1.232E–03	3321842027.43750
9H-4	0.50	73.10	262.5	7.6	1.146E–03	3321842032.76562
9H-4	0.55	73.15	261.7	6.7	1.219E–03	3321842038.09375
9H-4	0.60	73.20	260.3	8.2	1.559E–03	3321842043.42187
9H-4	0.65	73.25	259.6	8.2	1.882E–03	3321842048.75000
9H-4	0.70	73.30	262.0	7.2	1.549E–03	3321842054.07812
9H-4	0.75	73.35	262.9	7.7	1.296E–03	3321842059.40625
9H-4	0.80	73.40	258.5	8.6	1.772E–03	3321842064.71875
9H-4	0.85	73.45	254.7	8.1	2.116E–03	3321842070.04687
9H-4	0.90	73.50	253.0	7.8	1.753E–03	3321842075.37500
9H-4	0.95	73.55	257.2	6.2	1.296E–03	3321842080.70312
9H-4	1.00	73.60	261.1	4.7	9.945E–04	3321842086.01562
9H-4	1.05	73.65	260.5	5.4	1.054E–03	3321842091.34375
9H-4	1.10	73.70	258.4	7.4	1.339E–03	3321842096.67187
9H-4	1.15	73.75	260.2	7.5	1.561E–03	3321842102.00000
9H-4	1.20	73.80	259.4	6.1	1.709E–03	3321842107.32812
9H-4	1.25	73.85	259.9	5.6	1.849E–03	3321842112.65625
9H-4	1.30	73.90	259.3	6.3	1.759E–03	3321842117.98437
9H-4	1.35	73.95	258.9	7.9	1.401E–03	3321842123.29687
9H-4	1.40	74.00	255.5	13.4	3.506E–04	3321842128.62500
9H-5	0.10	74.20	261.4	6.2	9.495E–04	3321843270.25000
9H-5	0.15	74.25	257.9	9.3	8.680E–04	3321843275.57812
9H-5	0.20	74.30	259.5	9.0	1.117E–03	3321843280.90625
9H-5	0.25	74.35	260.2	7.2	1.347E–03	3321843286.21875
9H-5	0.30	74.40	261.9	8.1	1.061E–03	3321843291.54687
9H-5	0.35	74.45	266.7	8.8	5.185E–04	3321843296.87500
9H-5	0.40	74.50	274.3	1.2	2.849E–04	3321843302.20312
9H-5	0.45	74.55	268.4	–3.7	2.353E–04	3321843307.51562
9H-5	0.50	74.60	272.7	–1.0	2.228E–04	3321843312.84375
9H-5	0.55	74.65	266.5	0.4	2.743E–04	3321843318.17187
9H-5	0.60	74.70	268.5	1.0	3.402E–04	3321843323.50000

Table T18 (continued).

Core, section	Offset (m)	Depth CSF (m)	Declination (°)	Inclination (°)	Intensity (A/m)	Time (s)
9H-5	0.65	74.75	267.3	4.2	4.429E–04	3321843328.82812
9H-5	0.70	74.80	265.6	1.4	6.503E–04	3321843334.15625
9H-5	0.75	74.85	267.5	–7.3	7.203E–04	3321843339.46875
9H-5	0.80	74.90	271.4	–8.6	5.926E–04	3321843344.79687
9H-5	0.85	74.95	267.6	–0.3	5.955E–04	3321843350.12500
9H-5	0.90	75.00	265.1	5.0	5.555E–04	3321843355.45312
9H-5	0.95	75.05	268.4	8.2	7.564E–04	3321843360.76562
9H-5	1.00	75.10	269.5	10.5	1.099E–03	3321843366.09375
9H-5	1.05	75.15	264.7	11.9	1.242E–03	3321843371.42187
9H-5	1.10	75.20	264.2	10.9	1.045E–03	3321843376.75000
9H-5	1.15	75.25	260.0	13.1	9.387E–04	3321843382.07812
9H-5	1.20	75.30	255.2	19.3	9.947E–04	3321843387.39062
9H-5	1.25	75.35	256.3	20.8	9.404E–04	3321843392.71875
9H-5	1.30	75.40	258.6	20.5	8.805E–04	3321843398.04687
9H-5	1.35	75.45	257.0	15.6	9.268E–04	3321843403.37500
9H-5	1.40	75.50	259.3	8.9	9.897E–04	3321843408.70312
9H-6	0.10	75.70	266.3	5.3	9.732E–04	3321844510.79687
9H-6	0.15	75.75	271.7	8.9	1.134E–03	3321844516.12500
9H-6	0.20	75.80	271.8	2.8	1.368E–03	3321844521.45312
9H-6	0.25	75.85	268.7	2.4	1.099E–03	3321844526.76562
9H-6	0.30	75.90	269.4	5.6	1.033E–03	3321844532.09375
9H-6	0.35	75.95	269.7	8.4	8.713E–04	3321844537.42187
9H-6	0.40	76.00	268.9	6.3	8.131E–04	3321844542.75000
9H-6	0.45	76.05	270.1	5.1	7.806E–04	3321844548.07812
9H-6	0.50	76.10	269.2	6.5	5.529E–04	3321844553.39062
9H-6	0.55	76.15	271.1	7.4	3.223E–04	3321844558.71875
9H-6	0.60	76.20	273.3	2.6	3.549E–04	3321844564.04687
9H-6	0.65	76.25	273.0	1.6	2.669E–04	3321844569.37500
9H-6	0.70	76.30	172.5	78.5	2.380E–05	3321844574.70312
9H-6	0.75	76.35	233.7	17.5	1.246E–04	3321844580.01562
9H-6	0.80	76.40	252.2	6.2	1.967E–04	3321844585.34375
9H-6	0.85	76.45	271.2	10.7	1.660E–04	3321844590.67187
9H-6	0.90	76.50	152.7	29.1	4.077E–05	3321844596.00000
9H-6	0.95	76.55	94.3	–8.0	4.005E–04	3321844601.32812
9H-6	1.00	76.60	93.0	–11.2	5.664E–04	3321844606.64062
9H-6	1.05	76.65	93.8	–21.2	3.135E–04	3321844611.96875
9H-6	1.10	76.70	135.3	–49.1	9.872E–05	3321844617.29687
9H-6	1.15	76.75	231.7	–40.2	8.153E–05	3321844622.62500
9H-6	1.20	76.80	100.5	–16.8	1.105E–04	3321844627.95312
9H-6	1.25	76.85	93.1	2.3	3.310E–04	3321844633.26562
9H-6	1.30	76.90	92.9	7.8	3.780E–04	3321844638.59375
9H-6	1.35	76.95	93.1	6.8	3.478E–04	3321844643.92187
9H-6	1.40	77.00	91.4	0.1	4.288E–04	3321844649.25000
9H-7	0.10	77.20	98.2	–18.9	4.233E–04	3321845696.50000
9H-7	0.15	77.25	101.2	–25.9	2.608E–04	3321845701.82812
9H-7	0.20	77.30	90.2	–36.7	1.330E–04	3321845707.14062
9H-7	0.25	77.35	88.7	–14.1	2.697E–04	3321845712.46875
9H-7	0.30	77.40	92.8	–6.6	4.901E–04	3321845717.79687
9H-7	0.35	77.45	94.9	–4.0	5.009E–04	3321845723.12500
9H-7	0.40	77.50	95.1	–6.4	5.485E–04	3321845728.45312
9H-7	0.45	77.55	100.7	–9.2	6.743E–04	3321845733.76562
9H-7	0.50	77.60	96.6	–6.5	7.753E–04	3321845739.09375
10H-1	0.85	78.45	116.4	–3.8	5.677E–04	3321846826.68750
10H-1	0.90	78.50	117.7	4.5	4.953E–04	3321846832.01562
10H-1	0.95	78.55	117.5	8.8	2.968E–04	3321846837.32812
10H-1	1.00	78.60	97.5	–0.2	1.407E–03	3321846842.65625
10H-1	1.05	78.65	108.2	–6.0	7.983E–04	3321846847.98437
10H-1	1.10	78.70	109.5	–5.3	7.223E–04	3321846853.31250
10H-1	1.15	78.75	110.3	–3.7	5.198E–04	3321846858.62500
10H-1	1.20	78.80	109.0	–3.5	3.640E–04	3321846863.95312
10H-1	1.25	78.85	111.1	–2.8	2.716E–04	3321846869.28125
10H-1	1.30	78.90	128.9	–6.5	1.257E–04	3321846874.60937
10H-1	1.35	78.95	140.1	–14.3	1.270E–04	3321846879.93750
10H-1	1.40	79.00	122.5	–6.2	2.147E–04	3321846885.25000

Notes: Time = since 1 January 1904. This table is also available in **ASCII.**

Table T19. Paleomagnetic data from archive-half sections, Hole U1333C, at 20 mT AF demagnetization. (See table notes.)

Core, section	Offset (m)	Depth CSF (m)	Declination (°)	Inclination (°)	Intensity (A/m)	Time (s)	Declination			Depth CCSF-A (m)	VGP (°)	
							Core mean (°)	Reoriented				
								0°–360°	–90°–270°		Latitude	Longitude
320-U1333C-												
1H-1	0.15	0.15	49.7	–1.2	2.439E–03	3321768857.04687	34.6	15.1	15.1	0.1500	71.3	347.2
1H-1	0.20	0.20	47.9	–4.9	2.974E–03	3321768862.37500	34.6	13.3	13.3	0.2000	71.5	355.3
1H-1	0.25	0.25	44.4	–3.0	3.094E–03	3321768867.70312	34.6	9.8	9.8	0.2500	74.5	2.0
1H-1	0.30	0.30	43.5	–1.3	2.758E–03	3321768873.01562	34.6	8.9	8.9	0.3000	75.7	2.6
1H-1	0.35	0.35	34.6	3.0	4.020E–03	3321768878.34375	34.6	0.0	0.0	0.3500	81.0	41.6
1H-1	0.40	0.40	42.6	3.6	4.363E–03	3321768883.67187	34.6	8.0	8.0	0.4000	78.2	358.7
1H-1	0.45	0.45	42.2	4.8	5.209E–03	3321768888.98437	34.6	7.6	7.6	0.4500	78.9	358.1
1H-1	0.50	0.50	42.4	3.3	4.931E–03	3321768894.31250	34.6	7.8	7.8	0.5000	78.2	359.9
1H-1	0.55	0.55	39.6	2.0	5.202E–03	3321768899.64062	34.6	5.0	5.0	0.5500	79.3	13.7
1H-1	0.60	0.60	34.9	2.5	5.730E–03	3321768904.96875	34.6	0.3	0.3	0.6000	80.7	39.7
1H-1	0.65	0.65	35.2	3.6	5.384E–03	3321768910.29687	34.6	0.6	0.6	0.6500	81.3	37.6
1H-1	0.70	0.70	35.1	4.4	4.746E–03	3321768915.62500	34.6	0.5	0.5	0.7000	81.7	38.1
1H-1	0.75	0.75	32.8	4.1	3.955E–03	3321768920.93750	34.6	358.2	–1.8	0.7500	81.3	53.6
1H-1	0.80	0.80	34.0	2.5	3.725E–03	3321768926.26562	34.6	359.4	–0.6	0.8000	80.7	45.3
1H-1	0.85	0.85	34.1	0.4	1.756E–03	3321768931.59375	34.6	359.5	–0.5	0.8500	79.7	44.4
1H-1	0.90	0.90	27.5	0.3	2.107E–03	3321768936.92187	34.6	352.9	–7.1	0.9000	77.5	76.3
1H-1	0.95	0.95	32.1	1.2	2.876E–03	3321768942.25000	34.6	357.5	–2.5	0.9500	79.8	55.8
1H-1	1.00	1.00	30.4	1.1	2.732E–03	3321768947.57812	34.6	355.8	–4.2	1.0000	79.2	64.6
1H-1	1.05	1.05	29.3	0.3	2.121E–03	3321768952.89062	34.6	354.7	–5.3	1.0500	78.4	68.9
1H-1	1.10	1.10	12.4	–1.5	1.525E–03	3321768958.21875	34.6	337.8	–22.2	1.1000	65.2	105.9
1H-1	1.15	1.15	327.7	–37.5	1.045E–03	3321768963.54687	34.6	293.1	–66.9	1.1500	17.1	105.6
1H-1	1.20	1.20	3.4	–42.9	1.197E–03	3321768968.87500	34.6	328.8	–31.2	1.2000	43.3	81.8
1H-1	1.25	1.25	24.9	–8.8	2.554E–03	3321768974.20312	34.6	350.3	–9.7	1.2500	72.2	74.9
1H-1	1.30	1.30	29.9	–1.1	2.708E–03	3321768979.51562	34.6	355.3	–4.7	1.3000	78.0	64.8
1H-1	1.35	1.35	30.4	–2.5	2.806E–03	3321768984.84375	34.6	355.8	–4.2	1.3500	77.5	61.4
1H-1	1.40	1.40	35.0	–13.5	2.309E–03	3321768990.17187	34.6	0.4	0.4	1.4000	72.6	40.3
2H-1	0.10	1.70	316.8	1.9	8.752E–04	3321771181.40999	341.7	335.1	–24.9	4.0000	63.5	112.1
2H-1	0.15	1.75	162.8	–61.7	1.009E–03	3321771186.72249	341.7	181.1	181.1	4.0500	–57.6	43.1
2H-1	0.20	1.80	147.5	–33.9	1.393E–03	3321771192.05062	341.7	165.8	165.8	4.1000	–74.1	343.6
2H-1	0.25	1.85	148.7	–30.0	1.208E–03	3321771197.37874	341.7	167.0	167.0	4.1500	–76.2	336.8
2H-1	0.30	1.90	152.6	–21.1	1.381E–03	3321771202.70687	341.7	170.9	170.9	4.2000	–81.1	315.0
2H-1	0.35	1.95	159.1	–21.8	1.465E–03	3321771208.03499	341.7	177.4	177.4	4.2500	–87.3	329.1
2H-1	0.40	2.00	146.3	–24.1	2.646E–03	3321771213.34749	341.7	164.6	164.6	4.3000	–74.8	321.0
2H-1	0.45	2.05	156.8	–29.1	3.464E–03	3321771218.67562	341.7	175.1	175.1	4.3500	–83.1	358.6
2H-1	0.50	2.10	154.0	–25.9	3.600E–03	3321771224.00374	341.7	172.3	172.3	4.4000	–81.8	334.9
2H-1	0.55	2.15	153.1	–21.2	4.395E–03	3321771229.33187	341.7	171.4	171.4	4.4500	–81.5	315.5
2H-1	0.60	2.20	150.3	–23.1	3.916E–03	3321771234.65999	341.7	168.6	168.6	4.5000	–78.7	320.4
2H-1	0.65	2.25	148.4	–25.8	2.659E–03	3321771239.97249	341.7	166.7	166.7	4.5500	–76.6	326.2
2H-1	0.70	2.30	154.6	–26.7	2.343E–03	3321771245.30062	341.7	172.9	172.9	4.6000	–82.2	339.7
2H-1	0.75	2.35	155.3	–26.2	2.164E–03	3321771250.62874	341.7	173.6	173.6	4.6500	–82.9	340.1
2H-1	0.80	2.40	153.8	–27.1	2.262E–03	3321771255.95687	341.7	172.1	172.1	4.7000	–81.4	338.8
2H-1	0.85	2.45	150.5	–25.2	3.446E–03	3321771261.28499	341.7	168.8	168.8	4.7500	–78.7	326.6
2H-1	0.90	2.50	143.2	–16.2	4.887E–03	3321771266.61312	341.7	161.5	161.5	4.8000	–71.6	306.1
2H-1	0.95	2.55	146.5	–18.8	4.081E–03	3321771271.94124	341.7	164.8	164.8	4.8500	–75.0	309.7
2H-1	1.00	2.60	151.9	–23.4	2.367E–03	3321771277.25374	341.7	170.2	170.2	4.9000	–80.2	322.5

Notes: Time = since 1 January 1904. VGP = virtual geomagnetic pole. Only a portion of this table appears here. The complete table is available in ASCII.

Table T20. Mean paleomagnetic direction for each core, Site U1333. (See table notes.)

Core	Inclination (°)	Declination (°)	*N*	*R*	*k*	α95
320-U1333A-						
1H	8.6	353.5	166	156.123	16.7	2.8
2H	–1.3	29.5	133	119.490	9.8	4.1
3H	–2.2	48.3	165	154.998	16.4	2.8
4H	–7.8	11.6	121	117.828	37.8	2.1
5H	–16.2	12.6	143	141.621	102.9	1.2
6H	1.5	61.6	119	116.740	52.2	1.8
7H	6.2	162.4	133	130.846	61.3	1.6
8H	–12.8	57.2	153	150.418	58.9	1.5
9H	11.5	141.6	165	159.973	32.6	2.0
10H	8.5	161.2	162	158.836	50.9	1.6
11X	2.5	40.2	45	40.345	9.5	7.3
12X	1.4	72.1	58	51.411	8.7	6.7
13X	0.1	142.8	77	68.826	9.3	5.6
14X	–1.6	69.5	71	61.815	7.6	6.5
15X	4.0	41.7	75	67.043	9.3	5.7
16X	–3.3	165.8	84	75.307	9.5	5.3
17X	1.9	86.6	76	67.685	9.0	5.7
18X	–5.3	147.8	55	47.806	7.5	7.5
19X	–16.1	163.3	44	38.602	8.0	8.1
20X	4.7	24.8	20	17.721	8.3	12.0
320-U1333B-						
1H	10.6	171.0	133	128.305	28.1	2.3
2H	–4.7	96.2	140	135.457	30.6	2.2
3H	3.9	31.9	160	153.033	22.8	2.4
4H	–4.7	42.3	160	151.902	19.6	2.6
5H	–6.2	104.3	138	133.601	31.1	2.2
6H	2.4	129.3	169	158.240	15.6	2.8
7H	–5.5	29.1	163	159.252	43.2	1.7
8H	0.3	109.2	163	158.055	32.8	2.0
9H	–11.2	47.4	132	127.956	32.4	2.2
10H	–4.1	11.4	115	106.312	13.1	3.8
11H	–0.5	79.4	122	112.487	12.7	3.7
12H	7.1	158.4	173	166.889	28.1	2.1
13H	–2.8	19.0	164	156.794	22.6	2.4
14H	8.2	139.2	149	137.395	12.8	3.4
15H	–4.1	162.4	139	135.326	37.6	2.0
16H	13.1	163.7	151	145.065	25.3	2.3
17H	2.5	79.2	137	131.362	24.1	2.5
18H	19.7	103.0	48	46.198	26.1	4.1
19X	7.5	42.8	42	36.597	7.6	8.6
20X	26.1	44.0	53	48.773	12.3	5.8
320-U1333C-						
1H	0.0	34.6	23	22.739	84.4	3.3
2H	–17.5	161.7	153	145.993	21.7	2.5
3H	3.4	109.4	158	151.060	22.6	2.4
4H	6.3	73.0	146	142.655	43.3	1.8
5H	–0.6	65.9	167	163.297	44.8	1.6
6H	–8.8	25.5	149	147.013	74.5	1.3
7H	–5.8	102.6	121	117.562	34.9	2.2
8H	–3.2	160.2	163	159.525	46.6	1.6
9H	–6.5	75.3	157	150.231	23.0	2.4
10H	–9.1	113.7	159	154.909	38.6	1.8
11H	–13.8	75.5	120	119.535	255.8	0.8
12H	–8.0	101.6	89	88.122	100.2	1.5
13H	–14.1	71.4	147	144.171	51.6	1.6
14H	–7.3	89.6	910	887.146	39.8	0.7
15H	14.1	133.8	160	151.450	18.6	2.7
16H	7.9	33.3	80	73.893	12.9	4.6
17H	29.9	156.7	163	156.959	26.8	2.2
18H	0.4	139.4	175	169.272	30.4	2.0
19H	–15.2	56.4	66	63.619	27.3	3.4
20H	–0.9	126.3	139	126.805	11.3	3.7

Notes: Mean paleomagnetic directions and statistics were calculated using Fisher statistics for each core, using data from stable polarity intervals. Reversed polarity intervals were inverted prior to computing the mean directions and statistics. Inclination = mean paleomagnetic inclination from stable polarity intervals in a core. Declination = mean paleomagnetic declination from stable polarity intervals in a core. By subtracting this value from the observed paleomagnetic declinations measured along the core, the core can be approximately reoriented back into geographic coordinates. After this reorientation, the normal polarity intervals will have ~0° declination and the reversed polarity intervals will have ~180° declination. *N* = number of paleomagnetic observations used in calculating the mean, *R* = resultant vector length from summing the *N* vectors (directions or poles), *k* = precision parameter from Fisher statistical calculations, α95 = 95% confidence angle for the mean direction.

Table T21. Magnetic susceptibility data for discrete samples, Hole U1333A. (See table notes.) (Continued on next page.)

Core, section	Depth CSF (m)	LIMS ID	Susceptibility (SI)	Total mass (g)	Bulk density (g/cm³)	Volume (cm³)	Susceptibility: Volume normalized (SI)	Susceptibility: Mass normalized (m³/kg)
320-U1333A-								
1H-1	0.84	CUBE613391	1.787E–04	11.56	1.252	5.57	2.248E–04	1.082E–07
1H-2	2.34	CUBE613401	1.518E–04	12.05	1.263	5.90	1.800E–04	8.818E–08
1H-3	3.84	CUBE613411	1.117E–04	10.97	1.319	4.84	1.617E–04	7.128E–08
1H-4	5.34	CUBE613451	2.597E–05	15.09	1.692	6.20	2.930E–05	1.205E–08
1H-5	6.84	CUBE613421	3.725E–05	13.78	1.610	5.71	4.569E–05	1.892E–08
1H-6	8.34	CUBE613431	2.047E–05	13.93	1.687	5.54	2.589E–05	1.029E–08
1H-7	9.64	CUBE613441	3.825E–05	13.53	1.663	5.37	4.982E–05	1.979E–08
2H-1	10.34	CUBE615271	1.716E–05	14.88	1.717	5.99	2.005E–05	8.073E–09
2H-2	11.84	CUBE615311	1.524E–05	13.02	1.709	4.93	2.163E–05	8.194E–09
2H-3	13.34	CUBE615321	6.613E–05	14.16	1.557	6.15	7.533E–05	3.269E–08
2H-4	14.84	CUBE615331	3.128E–05	13.70	1.601	5.69	3.849E–05	1.598E–08
2H-5	16.14	CUBE615281	3.328E–05	14.64	1.610	6.24	3.733E–05	1.591E–08
2H-6	17.94	CUBE615291	5.400E–05	14.68	1.610	6.27	6.033E–05	2.575E–08
2H-7	18.89	CUBE615301	3.224E–05	14.70	1.675	6.03	3.740E–05	1.535E–08
3H-1	19.84	CUBE615921	4.517E–05	13.12	1.602	5.32	5.940E–05	2.410E–08
3H-2	21.34	CUBE615941	6.659E–05	14.02	1.544	6.11	7.634E–05	3.325E–08
3H-3	22.84	CUBE615951	9.138E–05	13.30	1.473	5.91	1.082E–04	4.809E–08
3H-4	24.34	CUBE615961	7.199E–05	14.44	1.549	6.36	7.926E–05	3.490E–08
3H-5	25.84	CUBE615971	7.808E–05	14.30	1.642	5.91	9.245E–05	3.822E–08
3H-6	27.34	CUBE615981	1.310E–04	14.19	1.513	6.34	1.446E–04	6.462E–08
3H-7	28.39	CUBE615931	5.049E–05	14.22	1.612	5.97	5.917E–05	2.485E–08
4H-3	32.34	CUBE616971	1.418E–05	13.16	1.650	5.19	1.912E–05	7.543E–09
4H-4	33.84	CUBE616981	7.152E–05	13.64	1.475	6.13	8.161E–05	3.670E–08
4H-5	35.34	CUBE616991	1.093E–04	14.37	1.514	6.46	1.185E–04	5.324E–08
4H-6	36.84	CUBE617001	1.113E–04	14.47	1.520	6.50	1.199E–04	5.384E–08
4H-7	37.89	CUBE617011	4.902E–05	15.47	1.603	6.79	5.057E–05	2.218E–08
5H-1	39.04	CUBE618131	4.043E–05	14.78	1.630	6.25	4.528E–05	1.915E–08
5H-2	40.34	CUBE618141	2.550E–05	14.74	1.659	6.12	2.918E–05	1.211E–08
5H-3	41.84	CUBE618151	1.641E–05	15.09	1.782	5.89	1.950E–05	7.612E–09
5H-4	43.34	CUBE618161	1.491E–05	15.41	1.735	6.24	1.674E–05	6.773E–09
5H-5	44.84	CUBE618171	3.742E–05	14.81	1.660	6.16	4.255E–05	1.769E–08
5H-6	46.34	CUBE618181	2.700E–05	14.78	1.699	6.00	3.152E–05	1.279E–08
5H-7	47.41	CUBE618191	1.446E–05	15.40	1.776	6.09	1.633E–05	6.573E–09
6H-2	50.09	CUBE619531	1.590E–05	15.30	1.731	6.19	1.799E–05	7.275E–09
6H-3	51.34	CUBE619541	2.275E–05	15.09	1.717	6.11	2.605E–05	1.055E–08
6H-4	52.74	CUBE619551	4.360E–05	14.90	1.664	6.19	4.927E–05	2.048E–08
6H-5	54.14	CUBE619561	1.041E–05	15.12	1.758	5.99	1.217E–05	4.819E–09
6H-6	55.84	CUBE619571	4.060E–05	15.20	1.685	6.30	4.514E–05	1.870E–08
6H-7	56.89	CUBE619581	1.914E–05	15.56	1.729	6.34	2.112E–05	8.611E–09
7H-2	59.34	CUBE620161	2.194E–05	13.56	1.665	5.39	2.851E–05	1.133E–08
7H-3	60.84	CUBE620171	1.748E–05	15.16	1.699	6.22	1.967E–05	8.071E–09
7H-4	62.34	CUBE620181	2.700E–05	15.08	1.682	6.24	3.031E–05	1.253E–08
7H-5	63.84	CUBE620191	2.826E–05	13.98	1.664	5.64	3.506E–05	1.415E–08
7H-6	65.34	CUBE620201	5.559E–06	14.64	1.768	5.68	6.847E–06	2.658E–09
8H-2	68.64	CUBE621401	1.552E–05	15.23	1.665	6.39	1.700E–05	7.133E–09
8H-3	70.14	CUBE621411	3.122E–06	11.05	1.715	3.77	5.804E–06	1.978E–09
8H-4	71.64	CUBE621421	3.383E–05	13.35	1.664	5.26	4.499E–05	1.774E–08
8H-5	73.14	CUBE621431	2.486E–05	15.38	1.715	6.29	2.766E–05	1.131E–08
8H-6	74.64	CUBE621441	8.027E–06	15.82	1.747	6.43	8.743E–06	3.552E–09
8H-7	75.84	CUBE621451	6.958E–06	14.24	1.713	5.63	8.648E–06	3.420E–09
9H-1	76.84	CUBE622071	9.847E–06	15.41	1.751	6.18	1.116E–05	4.473E–09
9H-2	78.34	CUBE622091	1.474E–05	15.94	1.754	6.47	1.595E–05	6.473E–09
9H-3	79.84	CUBE622111	1.528E–05	16.14	1.809	6.38	1.676E–05	6.627E–09
9H-4	81.34	CUBE622121	7.903E–06	12.80	1.749	4.69	1.179E–05	4.322E–09
9H-5	82.84	CUBE622131	5.965E–06	15.29	1.761	6.07	6.873E–06	2.731E–09
9H-6	84.34	CUBE622141	7.390E–06	15.38	1.797	6.00	8.617E–06	3.363E–09
9H-7	85.64	CUBE622151	9.891E–05	14.38	1.658	5.90	1.173E–04	4.815E–08
10H-1	86.34	CUBE622491	6.397E–05	14.68	1.608	6.27	7.138E–05	3.050E–08
10H-2	87.84	CUBE622501	1.386E–05	13.23	1.708	5.06	1.918E–05	7.333E–09
10H-3	89.34	CUBE622511	1.661E–05	14.30	1.693	5.73	2.028E–05	8.131E–09
10H-4	90.84	CUBE622521	1.676E–05	14.87	1.710	6.01	1.952E–05	7.890E–09
10H-5	92.34	CUBE622531	1.747E–05	15.15	1.704	6.20	1.974E–05	8.072E–09
10H-6	93.84	CUBE622541	2.289E–05	15.27	1.680	6.36	2.521E–05	1.049E–08
10H-7	94.99	CUBE622551	1.471E–05	14.97	1.763	5.89	1.749E–05	6.878E–09

Table T21 (continued).

Core, section	Depth CSF (m)	LIMS ID	Susceptibility (SI)	Total mass (g)	Bulk density (g/cm³)	Volume (cm³)	Susceptibility: Volume normalized (SI)	Susceptibility: Mass normalized (m³/kg)
11X-1	95.84	CUBE623001	1.238E–05	14.12	1.742	5.47	1.584E–05	6.137E–09
11X-2	97.34	CUBE623011	2.223E–05	14.00	1.670	5.63	2.762E–05	1.112E–08
11X-3	98.84	CUBE623021	2.303E–05	14.33	1.552	6.27	2.569E–05	1.125E–08
11X-4	100.34	CUBE623031	3.526E–05	14.81	1.610	6.35	3.889E–05	1.667E–08
12X-2	103.04	CUBE623421	2.178E–05	14.02	1.641	5.75	2.654E–05	1.087E–08
12X-3	104.19	CUBE623451	1.869E–05	12.93	1.570	5.31	2.463E–05	1.012E–08
12X-4	106.04	CUBE623461	4.887E–05	14.82	1.570	6.51	5.251E–05	2.308E–08
12X-5	107.54	CUBE623471	3.276E–05	13.65	1.616	5.61	4.091E–05	1.680E–08
13X-1	110.89	CUBE624511	2.095E–05	14.49	1.501	6.59	2.224E–05	1.012E–08
13X-2	112.54	CUBE624521	1.278E–04	14.34	1.570	6.21	1.441E–04	6.238E–08
13X-3	114.24	CUBE624531	1.195E–04	13.19	1.320	6.51	1.284E–04	6.342E–08
13X-4	115.44	CUBE624541	2.048E–04	11.97	1.306	5.65	2.538E–04	1.198E–07
13X-5	117.14	CUBE624551	1.707E–04	12.72	1.273	6.38	1.871E–04	9.394E–08
13X-6	118.64	CUBE624561	1.115E–04	12.36	1.381	5.62	1.388E–04	6.315E–08
13X-7	119.49	CUBE624571	1.170E–04	12.56	1.444	5.52	1.484E–04	6.521E–08
14X-1	120.84	CUBE627551	1.239E–04	13.01	1.404	6.00	1.447E–04	6.666E–08
14X-2	122.34	CUBE627561	1.023E–04	12.68	1.570	5.15	1.390E–04	5.647E–08
14X-3	123.84	CUBE627571	1.227E–04	12.02	1.317	5.64	1.523E–04	7.146E–08
14X-4	125.34	CUBE627581	1.611E–04	11.92	1.303	5.62	2.005E–04	9.461E–08
14X-5	126.84	CUBE627591	1.254E–04	12.40	1.329	5.88	1.494E–04	7.079E–08
14X-6	128.34	CUBE627601	1.469E–04	13.18	1.467	5.85	1.757E–04	7.802E–08
14X-7	129.39	CUBE627611	2.391E–04	12.58	1.361	5.87	2.851E–04	1.330E–07
15X-1	130.44	CUBE628741	1.654E–04	13.06	1.309	6.47	1.790E–04	8.865E–08
15X-2	131.94	CUBE628751	8.848E–05	13.50	1.489	5.98	1.035E–04	4.588E–08
15X-3	133.44	CUBE628761	6.286E–05	12.85	1.545	5.34	8.232E–05	3.424E–08
15X-3	133.44	CUBE628771	1.753E–04	12.30	1.570	4.91	2.499E–04	9.976E–08
15X-5	136.44	CUBE628781	1.346E–04	12.58	1.574	5.07	1.857E–04	7.490E–08
15X-6	137.94	CUBE628791	1.536E–04	11.51	1.480	4.67	2.300E–04	9.341E–08
16X-1	140.04	CUBE629731	1.379E–04	12.62	1.249	6.43	1.502E–04	7.649E–08
16X-2	141.54	CUBE629741	8.084E–05	12.11	1.196	6.29	9.002E–05	4.673E–08
16X-3	143.14	CUBE629751	8.761E–05	11.84	1.218	5.95	1.031E–04	5.180E–08
16X-4	144.54	CUBE629761	1.430E–04	12.15	1.273	5.94	1.685E–04	8.236E–08
16X-5	146.24	CUBE629771	1.460E–04	11.23	1.330	4.99	2.048E–04	9.101E–08
16X-6	147.67	CUBE629781	9.451E–05	10.28	1.414	4.02	1.645E–04	6.436E–08
16X-7	148.62	CUBE629791	9.332E–05	11.88	1.559	4.67	1.397E–04	5.499E–08
17X-1	149.65	CUBE630761	4.435E–05	9.89	1.557	3.40	9.124E–05	3.139E–08
17X-2	151.15	CUBE630771	1.171E–04	12.83	1.416	5.82	1.408E–04	6.386E–08
17X-3	152.65	CUBE630781	7.026E–05	12.63	1.473	5.46	9.012E–05	3.894E–08
17X-4	154.16	CUBE630791	1.437E–04	13.26	1.426	6.08	1.655E–04	7.586E–08
17X-5	155.66	CUBE630801	8.859E–05	13.10	1.511	5.63	1.101E–04	4.734E–08

Notes: Depth = depth to middle of discrete sample measured in meters using the core depth below seafloor, method A (CSF), depth scale. LIMS ID = sample identification within the Laboratory Information Management System (LIMS) database. Susceptibility = volume magnetic susceptibility of discrete sample measured in KappaBridge with volume of cube assumed to be 7 cm^3. Mass = mass of sample including mass of plastic cube, which has a mean of 4.5921 g. Bulk density = density from moisture and density (MAD) measurements. When these were not available or were obviously anomalous, we used a density of 1.2 m^3/kg. Volume = volume of sediments, calculated by subtracting mass of plastic cube from total mass and then dividing by bulk density. Volume normalized susceptibility = susceptibility of discrete samples normalized by true sample volume. These are unitless in the SI unit system. Mass normalized susceptibility = susceptibility of discrete samples normalize by mass of sediment in each sample cube.

Table T22. Paleomagnetic results for discrete samples, Hole U1333A. (See table notes.)

Core, section, interval (cm)	Depth CSF (m)	Demag (mT)	Declination: Azimuthally unoriented (°)	Declination: Geographical coordinates 0°–360°	Declination: Geographical coordinates –90°–270°	Inclination (°)	Intensity (A/m)
320-U1333A-							
1H-1, 85	0.85	0	3.7	10.2	10.2	7.6	3.840E–03
1H-1, 85	0.85	5	0.7	7.2	7.2	–0.3	3.637E–03
1H-1, 85	0.85	10	2.8	9.3	9.3	–2.5	2.798E–03
1H-1, 85	0.85	15	0.5	7.0	7.0	0.9	2.490E–03
1H-1, 85	0.85	20	0.1	6.6	6.6	8.2	2.028E–03
1H-1, 85	0.85	25	–0.5	6.0	6.0	12.2	1.741E–03
1H-1, 85	0.85	30	–2.9	3.6	3.6	17.3	1.128E–03
1H-1, 85	0.85	35	–2.0	4.5	4.5	25.4	1.113E–03
1H-1, 85	0.85	40	–14.2	–7.7	–7.7	37.5	6.901E–04
1H-1, 85	0.85	50	–11.9	–5.4	–5.4	45.6	7.752E–04
1H-1, 85	0.85	60	–13.5	–7.0	–7.0	57.0	8.971E–04
1H-2, 85	2.35	0	–24.6	–18.1	–18.1	15.9	3.955E–03
1H-2, 85	2.35	5	–26.3	–19.8	–19.8	9.1	3.712E–03
1H-2, 85	2.35	10	–26.3	–19.8	–19.8	8.4	2.854E–03
1H-2, 85	2.35	15	–27.5	–21.0	–21.0	10.6	2.357E–03
1H-2, 85	2.35	20	–26.0	–19.5	–19.5	16.1	2.012E–03
1H-2, 85	2.35	25	–28.3	–21.8	–21.8	19.3	1.619E–03
1H-2, 85	2.35	30	–25.0	–18.5	–18.5	27.0	1.325E–03
1H-2, 85	2.35	35	–25.3	–18.8	–18.8	31.3	1.216E–03
1H-2, 85	2.35	40	–40.9	–34.4	–34.4	33.3	1.097E–03
1H-2, 85	2.35	50	–32.4	–25.9	–25.9	56.1	1.055E–03
1H-2, 85	2.35	60	–24.9	–18.4	–18.4	64.2	6.954E–04
1H-4, 85	5.35	0	–30.9	–24.4	–24.4	28.4	5.110E–04
1H-4, 85	5.35	5	–27.9	–21.4	–21.4	18.5	3.940E–04
1H-4, 85	5.35	10	21.1	27.6	27.6	31.5	1.621E–04
1H-4, 85	5.35	15	–1.7	4.8	4.8	24.7	3.121E–04
1H-4, 85	5.35	20	1.4	7.9	7.9	42.4	2.629E–04
1H-4, 85	5.35	25	–1.3	5.2	5.2	39.3	3.123E–04
1H-4, 85	5.35	30	16.8	23.3	23.3	64.1	2.320E–04
1H-4, 85	5.35	35	–36.7	–30.2	–30.2	73.9	2.311E–04
1H-4, 85	5.35	40	–124.6	–118.1	241.9	62.7	1.980E–04
1H-4, 85	5.35	50	–1.9	4.6	4.6	80.8	3.137E–04
1H-4, 85	5.35	60	–19.1	–12.6	–12.6	81.4	1.956E–04
1H-5, 85	6.85	0	167.3	173.8	173.8	–1.7	6.034E–04
1H-5, 85	6.85	5	164.2	170.7	170.7	–11.4	6.169E–04
1H-5, 85	6.85	10	159.7	166.2	166.2	–14.5	5.485E–04
1H-5, 85	6.85	15	168.0	174.5	174.5	–11.1	6.254E–04
1H-5, 85	6.85	20	160.9	167.4	167.4	–5.0	5.594E–04
1H-5, 85	6.85	25	142.3	148.8	148.8	0.5	3.509E–04
1H-5, 85	6.85	30	150.8	157.3	157.3	6.5	2.907E–04
1H-5, 85	6.85	35	139.8	146.3	146.3	13.2	2.386E–04
1H-5, 85	6.85	40	174.2	180.7	180.7	18.0	1.501E–04
1H-5, 85	6.85	50	106.4	112.9	112.9	36.0	2.128E–04
1H-5, 85	6.85	60	88.6	95.1	95.1	31.0	1.627E–04
1H-6, 85	8.35	0	2.7	9.2	9.2	34.3	6.028E–04
1H-6, 85	8.35	5	0.7	7.2	7.2	30.5	4.395E–04
1H-6, 85	8.35	10	12.9	19.4	19.4	28.8	3.700E–04
1H-6, 85	8.35	15	12.9	19.4	19.4	37.4	3.034E–04
1H-6, 85	8.35	20	60.1	66.6	66.6	48.5	3.322E–04
1H-6, 85	8.35	25	50.6	57.1	57.1	55.7	3.204E–04
1H-6, 85	8.35	30	4.0	10.5	10.5	82.6	2.203E–04
1H-6, 85	8.35	35	20.6	27.1	27.1	76.2	2.127E–04
1H-6, 85	8.35	40	78.7	85.2	85.2	75.1	2.089E–04
1H-6, 85	8.35	50	–0.6	5.9	5.9	64.3	2.425E–04
1H-6, 85	8.35	60	–0.9	5.6	5.6	65.3	2.122E–04
1H-7, 65	9.65	0	–177.2	–170.7	189.3	34.0	8.387E–04
1H-7, 65	9.65	5	–175.1	–168.6	191.4	18.4	8.586E–04
1H-7, 65	9.65	10	–175.6	–169.1	190.9	8.7	9.020E–04
1H-7, 65	9.65	15	–172.5	–166.0	194.0	6.8	8.419E–04
1H-7, 65	9.65	20	–179.5	–173.0	187.0	14.3	7.359E–04
1H-7, 65	9.65	25	–175.7	–169.2	190.8	19.7	6.492E–04
1H-7, 65	9.65	30	–168.5	–162.0	198.0	22.1	5.599E–04

Notes: Only a portion of this table appears here. The complete table is available in ASCII.

Table T23. Principal component analysis (PCA) results for paleomagnetic data, Holes U1333A and U1333B. (See table notes.) (Continued on next page.)

		PCA						Archive half section at 20 mT AF demagnetization		
		Declination								
Core, section, interval (cm)	Depth CSF (m)	Azimuthally Unoriented (°)	Geographical Coordinates (0°–360°)	Inclination (°)	MAD (°)	Range (mT)	NRM 20 mT (A/m)	Declination (°)	Inclination (°)	NRM (A/m)
320-U1333A-										
1H-1, 85	0.85	4.8	11.3	–7.1	6.0	20–50	2.028E–03	356.8	9.6	2.437E–03
1H-2, 85	2.35	332.8	339.3	–6.8	3.6	10–35	2.012E–03	337.1	29.3	2.673E–03
1H-4, 85	5.35	2.0	8.5	–17.7	16.7	15–35	2.629E–04	342.4	36.6	1.908E–04
1H-5, 85	6.85	171.1	177.6	–21.8	18.0	10–40	5.594E–04	186.9	–3.0	1.068E–03
1H-6, 85	8.35	61.2	67.7	14.8	14.8	20–40	3.322E–04	357.7	53.1	1.339E–04
1H-7, 65	9.65	179.7	186.2	–13.5	10.8	10–35	7.359E–04	189.5	4.9	1.162E–03
2H-1, 85	10.35	166.9	137.4	–28.4	11.5	10–35	6.461E–04	174.6	12.9	7.526E–04
2H-2, 85	11.85	NA	NA	NA	NA	NA	3.993E–04	181.5	28.8	3.820E–04
2H-4, 85	14.85	36.5	7.0	–1.6	19.1	5–30	8.218E–04	32.6	7.0	7.332E–04
2H-5, 65	16.15	227.4	197.9	–31.2	16.5	5–25	4.494E–04	206.1	21.0	3.787E–04
2H-6, 95	17.95	NA	NA	NA	NA	NA	1.040E–04	215.0	45.9	1.627E–04
2H-7, 40	18.90	NA	NA	NA	NA	NA	7.740E–04	254.7	15.1	4.695E–04
3H-1, 85	19.85	221.0	172.7	–3.1	11.9	5–25	1.140E–03	223.4	12.4	1.037E–03
3H-2, 85	21.35	217.8	169.5	–0.3	10.7	10–30	9.560E–04	214.8	7.2	1.190E–03
3H-4, 85	24.35	214.3	166.0	–22.2	13.5	5–25	5.500E–04	195.7	32.6	3.189E–04
3H-5, 85	25.85	50.1	1.8	–2.7	7.7	10–50	1.880E–03	63.1	14.3	1.203E–03
3H-6, 85	27.35	238.8	190.5	–15.4	15.6	10–30	9.960E–04	236.5	26.0	9.179E–04
3H-7, 40	28.40	243.8	195.5	–13.7	5.2	10–30	1.060E–03	241.9	7.0	8.139E–04
4H-4, 85	33.85	174.2	342.6	1.7	5.8	5–25	1.320E–03	185.6	7.9	1.544E–03
4H-5, 85	35.35	193.1	1.5	–14.0	2.3	5–25	1.520E–03	198.5	10.7	1.750E–03
4H-6, 85	36.85	NA	NA	NA	NA	NA	2.338E–04	307.1	30.9	1.186E–04
4H-7, 40	37.90	9.5	177.9	5.9	10.8	5–25	1.714E–03	2.0	–5.7	5.930E–04
5H-1, 105	39.05	200.8	8.2	5.4	10.7	5–25	1.415E–03	196.7	12.3	1.294E–03
5H-2, 85	40.35	182.9	350.3	–6.5	11.8	5–40	5.871E–04	184.2	17.5	5.832E–04
5H-4, 85	43.35	182.6	350.0	0.4	11.0	5–30	4.455E–04	186.5	23.3	7.426E–04
5H-5, 85	44.85	197.5	4.9	7.8	3.3	5–25	1.608E–03	199.4	18.3	1.457E–03
5H-6, 85	46.35	192.1	359.5	–16.0	7.0	10–40	1.184E–03	198.1	13.4	9.367E–04
5H-7, 42	47.42	178.2	345.6	–25.2	8.4	5–35	7.742E–04			
6H-2, 110	50.10	334.4	272.8	–24.9	14.4	5–30	6.170E–04	7.3	4.2	4.656E–04
6H-4, 75	52.75	62.1	0.4	–0.2	6.7	5–35	1.786E–03	58.5	0.1	1.567E–03
6H-5, 65	54.15	58.1	356.5	3.7	4.3	5–25	1.120E–03	55.2	–3.5	7.770E–04
6H-6, 85	55.85	55.9	354.3	–2.2	12.8	5–50	1.554E–03	61.8	4.4	1.146E–03
6H-7, 40	56.90	36.0	334.4	–0.8	13.2	10–50	5.853E–04	77.0	11.1	3.474E–04
7H-2, 85	59.35	155.2	172.8	–1.9	10.2	5–25	6.845E–04	159.9	13.4	7.664E–04
7H-4, 85	62.35	164.4	182.0	–16.9	17.5	5–25	6.584E–04	162.0	5.4	6.517E–04
7H-5, 85	63.85	151.6	169.2	–8.3	11.1	10–40	1.123E–03	167.9	2.7	9.507E–04
7H-6, 85	65.35	NA	NA	NA	NA	NA	4.183E–04	167.6	5.1	1.990E–04
8H-2, 85	68.65	NA	NA	NA	NA	NA	8.316E–04	224.0	3.8	7.151E–04
8H-4, 85	71.65	NA	NA	NA	NA	NA	6.129E–04	244.8	5.7	6.180E–04
8H-5, 85	73.15	NA	NA	NA	NA	NA	8.203E–04	239.1	15.6	8.021E–04
8H-6, 85	74.65	237.0	359.8	–6.7	8.1	5–30	9.735E–04	240.1	7.8	8.695E–04
8H-7, 55	75.85	263.7	26.4	15.5	16.6	5–60	8.076E–04	248.9	11.2	1.217E–03
9H-1, 85	76.85	123.4	161.8	3.1	18.2	5–40	6.978E–04	139.4	12.3	4.312E–04
9H-2, 85	78.35	113.1	151.5	–16.4	15.4	5–60	1.042E–03	124.9	8.4	6.609E–04
9H-4, 85	81.35	135.1	173.5	–9.3	10.9	10–30	6.524E–04	131.9	20.9	4.959E–04
9H-5, 85	82.85	NA	NA	NA	NA	NA	3.319E–04	330.2	–7.4	4.157E–04
9H-6, 85	84.35	333.7	12.1	23.2	16.7	0–30	6.538E–04	330.3	–13.5	5.630E–04
9H-7, 65	85.65	340.35	18.8	5.7	4.3	10–30	3.002E–03			
10H-1, 85	86.35	333.17	172.0	–8.0	8.7	5–50	1.739E–03	329.7	0.4	1.480E–03
10H-2, 85	87.85	NA	NA	NA	NA	NA	6.318E–04	327.5	–11.4	7.892E–04
10H-4, 85	90.85	352.6	191.4	–1.9	11.4	5–50	9.124E–04	337.6	–15.6	7.944E–04
10H-5, 85	92.35	343.7	182.5	–16.4	6.4	15–40	1.226E–03	343.1	–15.3	8.461E–04
10H-6, 85	93.85	353.88	192.7	–10.0	7.9	5–40	1.406E–03	350.1	–10.2	9.468E–04
10H-7, 50	95.00	359.64	198.4	–0.1	6.1	10–30	1.657E–03			
11X-1, 85	95.85	NA		NA	NA	NA	6.360E–04	339.7	19.8	3.427E–04
11X-2, 85	97.35	NA		NA	NA	NA	6.688E–04	346.6	16.3	8.341E–04
12X-2, 85	103.05	72.8		28.6	11.4	10–60	1.123E–03	64.8	13.0	1.534E–03
12X-4, 85	106.05	186.3		–9.8	9.0	5–25	2.233E–03	186.2	–1.4	2.138E–03
12X-5, 85	107.55	57.4		–1.4	9.4	5–25	1.302E–03	21.4	–0.8	6.361E–04
13X-1, 60	110.90	302.3		–1.5	13.2	5–40	1.566E–03	48.8	9.4	2.095E–03
13X-5, 85	117.15	46.9		2.7	11.6	5–25	2.727E–03	282.9	45.0	3.523E–04
14X-1, 85	120.85	244.96		9.4	5.7	5–25	1.546E–03	293.8	21.3	1.249E–03
14X-5, 85	126.85	125.2		0.3	14.9	5–40	1.875E–03	159.9	5.9	9.784E–04

Table T23 (continued).

Core, section, interval (cm)	Depth CSF (m)	PCA: Declination: Azimuthally Unoriented (°)	PCA: Declination: Geographical Coordinates (0°–360°)	PCA: Inclination (°)	PCA: MAD (°)	PCA: Range (mT)	NRM 20 mT (A/m)	Archive half section at 20 mT AF demagnetization: Declination (°)	Archive half section at 20 mT AF demagnetization: Inclination (°)	Archive half section at 20 mT AF demagnetization: NRM (A/m)
15X-1, 85	130.45	NA		NA	NA	NA	7.920E–04	69.9	18.3	1.264E–03
15X-5, 85	136.45	313.9		–1.1	9.7	10–40	1.746E–03	317.4	–5.6	1.806E–03
16X-1, 85	140.05	0.2		–6.6	4.8	15–35	2.307E–03	22.5	–2.4	1.621E–03
16X-4, 85	144.55	289.2		–7.2	16.7	10–50	1.802E–03	311.3	6.8	1.475E–03
16X-5, 105	146.25	119.9		4.8	6.7	10–30	1.738E–03	86.0	9.5	2.183E–03
320-U1333B-										
1H-1, 85	0.85	184.4	13.4	10.7	3.9	5–50	6.372E–03	188.1	14.5	5.439E–03
17H-5, 85	157.05	NA		NA	NA	NA	1.107E–03	90.4	4.4	1.378E–03

Notes: MAD = maximum angular deviation, NRM = natural remanent magnetization. NA = not applicable.

Table T24. Magnetostratigraphy, Site U1333. (See table note.) (Continued on next two pages.)

Polarity chron	Age (Ma)	Hole U1333A Range CSF (m)	Best estimate CSF (m)	Best estimate core, section, interval (cm)	Measurement type
C6n–C6r	19.722				
C6r–C6An.1n	20.040	0.55–0.65	0.600	1H-1, 60.0	Split core
C6An.1n–C6An.1r	20.213	1.10–1.15	1.125	1H-1, 112.5	Split core
C6An.1r–C6An.2n	20.439	2.00–2.10	2.050	1H-2, 55.0	Split core
C6An.2n–C6Ar	20.709	3.20–3.30	3.250	1H-3, 25.0	Split core
C6Ar–C6AAn	21.083	5.25–5.35	5.300	1H-4, 80.0	Split core
C6AAn–C6AAr.1r	21.159	5.90–6.10	6.000	Between Sections 1H-4 and 5	Split core
C6AAr.1r–C6AAr.1n	21.403	8.00–8.15	8.075	1H-6, 57.5	Split core
C6AAr.1n–C6AAr.2r	21.483	8.90–9.10	9.000	Between Sections 1H-6 and 7	Split core
C6AAr.2r–C6AAr.2n	21.659	9.65–9.70	9.675	Between Cores 1H and 2H	Split core
C6AAr.2n–C6AAr.3r	21.688	12.05–12.25	12.150	2H-2, 115.0	Split core
C6AAr.3r–C6Bn.1n	21.767	12.85–12.90	12.875	2H-3, 37.5	Split core
C6Bn.1n–C6Bn.1r	21.936	13.70–13.80	13.750	2H-3, 125.0	Split core
C6Bn.1r–C6Bn.2n	21.992	13.90–14.15	14.025	Between Sections 2H-3 and 4	Split core
C6Bn.2n–C6Br	22.268	15.75–16.20	15.975	2H-5, 47.5	Split core
C6Br–C6Cn.1n	22.564	18.05–18.15	18.100	2H-6, 110.0	Split core
C6Cn.1n–C6Cn.1r	22.754			Not identified	
C6Cn.1r–C6Cn.2n	22.902			Not identified	
C6Cn.2n–C6Cn.2r	23.030			Not identified	
C6Cn.2r–C6Cn.3n	23.278			Not identified	
C6Cn.3n–C6Cr	23.340	19.40–19.50	19.450	3H-1, 45.0	Split core
C6Cr–C7n.1n	24.022	23.40–23.60	23.500	Between Sections 3H-3 and 4	Split core
C7n.1n–C7n.1r	24.062	23.70–23.80	23.750	3H-4, 25.0	Split core
C7n.1r–C7n.2n	24.147	24.30–24.50	24.400	3H-4, 90.0	Split core
C7n.2n–C7r	24.459	26.40–26.60	26.500	Between Sections 3H-5 and 6	Split core
C7r–C7An	24.756	28.45–28.50	28.475	3H-7, 47.5	Split core
C7An–C7Ar	24.984			Not identified	
C7Ar–C8n.1n	25.110	31.30–31.60	31.450	4H-2, 145.0	Split core
C8n.1n–C8n.1r	25.248			Not identified	
C8n.1r–C8n.2n	25.306			Not identified	
C8n.2n–C8r	26.032	36.70–37.00	36.850	4H-6, 85.0	Split core
C8r–C9n	26.508	38.30–39.05	38.675	Between Cores 4H and 5H	Split core
C9n–C9r	27.412	46.90–50.20	48.550	Between Cores 5H and 6H	Split core
C9r–C10n.1n	27.886	51.90–51.90	51.900	6H-3, 140.0	Split core
C10n.1n–C10n.1r	28.126	54.60–54.90	54.750	6H-5, 125.0	Split core
C10n.1r–C10n.2n	28.164	55.50–55.60	55.550	6H-6, 55.0	Split core
C10n.2n–C10r	28.318	56.95–57.00	56.975	6H-7, 50.0	Split core
C10r–C11n.1n	29.166	66.35–67.30	66.825	Between Cores 7H and 8H	Split core
C11n.1n–C11n.1r	29.467	70.60–70.95	70.775	Between Sections 8H-3 and 4	Split core
C11n.1r–C11n.2n	29.536	71.50–71.60	71.550	8H-4, 75.0	Split core
C11n.2n–C11r	29.957	76.30–76.40	76.350	9H-1, 35.0	Split core
C11r–C12n	30.617	81.90–82.10	82.000	Between Sections 9H-4 and 5	Split core
C12n–C12r	31.021	85.60–85.95	85.775	Between Cores 9H and 10H	Split core
C12r–C13n	33.232			Not identified, XCB coring disturbance	
C13n–C13r	33.705			Not identified, XCB coring disturbance	
C13r–C15n	35.126			Not identified, XCB coring disturbance	
C15n–C15r	35.254			Not identified, XCB coring disturbance	
C15r–C16n.1n	35.328			Not identified, XCB coring disturbance	
C16n.1n–C16n.1r	35.554			Not identified, XCB coring disturbance	
C16n.1r–C16n.2n	35.643			Not identified, XCB coring disturbance	
C16n.2n–C16r	36.355			Not identified, XCB coring disturbance	
C16r–C17n.1n	36.668			Not identified, XCB coring disturbance	
C17n.1n–C17n.1r	37.520			Not identified, XCB coring disturbance	
C17n.1r–C17n.2n	37.656			Not identified, XCB coring disturbance	
C17n.2n–C17n.2r	37.907			Not identified, XCB coring disturbance	
C17n.2r–C17n.3n	37.956			Not identified, XCB coring disturbance	
C17n.3n–C17r	38.159			Not identified, XCB coring disturbance	
C17r–C18n.1n	38.449			Not identified, XCB coring disturbance	
C18n.1n–C18n.1r	39.554			Not identified, XCB coring disturbance	
C18n.1r–C18n.2n	39.602			Not identified, XCB coring disturbance	
C18n.2n–C18r	40.084			Not identified, XCB coring disturbance	
C18r–C19n	41.358			Not identified, XCB coring disturbance	
C19n–C19r	41.510			Not identified, XCB coring disturbance	
C19r–C20n	42.536			Not identified, XCB coring disturbance	
C20n–C20r	43.789			Not identified, XCB coring disturbance	

Note: When the location of a reversal is listed as between sections, it could occur anywhere within 10 cm of the juxtaposing ends of the two sections listed.

Table T24 (continued). (Continued on next page.)

Polarity chron	Age (Ma)	Hole U1333B Range CSF (m)	Best estimate CSF (m)	Best estimate core, section, interval (cm)	Measurement type
C6n–C6r	19.722	3.45–3.55	3.500	1H-3, 50.0	Split core
C6r–C6An.1n	20.040	5.10–5.20	5.150	1H-4, 65.0	Split core
C6An.1n–C6An.1r	20.213	5.70–5.80	5.750	1H-4, 125.0	Split core
C6An.1r–C6An.2n	20.439	6.60–6.85	6.725	1H-4, 72.5	Split core
C6An.2n–C6Ar	20.709	7.400-9.050		Between Sections 1H-5 and 2H-1	Split core
C6Ar–C6AAn	21.083	9.90–10.00	9.950	2H-2, 75.0	Split core
C6AAn–C6AAr.1r	21.159	10.50–10.55	10.525	2H-2, 132.5	Split core
C6AAr.1r–C6AAr.1n	21.403	12.65–12.85	12.750	2H-4, 55.0	Split core
C6AAr.1n–C6AAr.2r	21.483	13.60–13.80	13.700	Between Sections 2H-4 and 5	Split core
C6AAr.2r–C6AAr.2n	21.659	15.70–15.80	15.750	2H-6, 55.0	Split core
C6AAr.2n–C6AAr.3r	21.688	16.00–16.10	16.050	2H-6, 85.0	Split core
C6AAr.3r–C6Bn.1n	21.767	16.45–16.55	16.500	2H-6, 130.0	Split core
C6Bn.1n–C6Bn.1r	21.936			Not identified	
C6Bn.1r–C6Bn.2n	21.992			Not identified	
C6Bn.2n–C6Br	22.268			Not identified	
C6Br–C6Cn.1n	22.564	19.50–19.55	19.525	3H-2, 82.5	Split core
C6Cn.1n–C6Cn.1r	22.754	20.00–20.30	20.150	Between Sections 3H-2 and 3	Split core
C6Cn.1r–C6Cn.2n	22.902	21.15–21.20	21.175	3H-3, 97.5	Split core
C6Cn.2n–C6Cn.2r	23.030	21.60–21.90	21.750	Between Sections 3H-3 and 4	Split core
C6Cn.2r–C6Cn.3n	23.278	23.55–23.65	23.600	3H-5, 40.0	Split core
C6Cn.3n–C6Cr	23.340	24.10–24.20	24.150	3H-5, 95.0	Split core
C6Cr–C7n.1n	24.022	27.00–27.10	27.050	4H-1, 35.0	Split core
C7n.1n–C7n.1r	24.062	27.20–27.30	27.250	4H-1, 55.0	Split core
C7n.1r–C7n.2n	24.147	27.75–27.85	27.800	4H-1, 110.0	Split core
C7n.2n–C7r	24.459	29.80–29.90	29.850	4H-3, 15.0	Split core
C7r–C7An	24.756	31.65–31.80	31.725	4H-4, 52.5	Split core
C7An–C7Ar	24.984	32.95–33.15	33.050	4H-5, 35.0	Split core
C7Ar–C8n.1n	25.110	33.85–33.95	33.900	4H-5, 120.0	Split core
C8n.1n–C8n.1r	25.248	35.40–35.45	35.425	4H-6, 122.5	Split core
C8n.1r–C8n.2n	25.306	35.60–35.80	35.700	Between Sections 4H-6 and 7	Split core
C8n.2n–C8r	26.032	39.10–39.45	39.275	Between Sections 5H-2 and 3	Split core
C8r–C9n	26.508	44.45–44.60	44.525	5H-6, 82.5	Split core
C9n–C9r	27.412	50.35–50.45	50.400	6H-4, 20.0	Split core
C9r–C10n.1n	27.886	55.25–55.30	55.275	Between Sections 6H-7 and 7H-1	Split core
C10n.1n–C10n.1r	28.126	56.55–56.80	56.675	Between Sections 7H-1 and 2	Split core
C10n.1r–C10n.2n	28.164	57.15–57.25	57.200	7H-2, 50.0	Split core
C10n.2n–C10r	28.318	58.50–58.65	58.575	7H-3, 37.5	Split core
C10r–C11n.1n	29.166	70.50–70.80	70.650	Between Sections 8H-4 and 5	Split core
C11n.1n–C11n.1r	29.467			Not identified	
C11n.1r–C11n.2n	29.536			Not identified	
C11n.2n–C11r	29.957	80.30–80.40	80.350	9H-5, 15.0	Split core
C11r–C12n	30.617	84.90–87.65	86.275	Between Sections 10H-1 and 3	Split core
C12n–C12r	31.021	89.25–89.40	89.325	10H-4, 112.5	Split core
C12r–C13n	33.232	111.35–111.40	111.375	12H-6, 117.5	Split core
C13n–C13r	33.705	115.10–115.30	115.200	Between Sections 13H-2 and 3	Split core
C13r–C15n	35.126	119.05–119.15	119.100	13H-5, 90.0	Split core
C15n–C15r	35.254	119.50–119.60	119.550	13H-5, 135.0	Split core
C15r–C16n.1n	35.328	120.60–120.70	120.650	13H-6, 95.0	Split core
C16n.1n–C16n.1r	35.554	121.45–121.50	121.475	13H-7, 27.5	Split core
C16n.1r–C16n.2n	35.643	121.85–122.30	122.075	Between Cores 13H-7 and 14H-1	Split core
C16n.2n–C16r	36.355	124.10–124.15	124.125	14H-2, 92.5	Split core
C16r–C17n.1n	36.668	125.70–125.85	125.775	14H-3, 107.5	Split core
C17n.1n–C17n.1r	37.520	130.20–130.25	130.225	14H-6, 102.5	Split core
C17n.1r–C17n.2n	37.656			Not identified	
C17n.2n–C17n.2r	37.907			Not identified	
C17n.2r–C17n.3n	37.956			Not identified	
C17n.3n–C17r	38.159			Not identified	
C17r–C18n.1n	38.449	131.90–132.00	131.950	15H-1, 75.0	Split core
C18n.1n–C18n.1r	39.554	138.60–138.80	138.700	Between Sections 15H-5 and 6	Split core
C18n.1r–C18n.2n	39.602	139.30–139.40	139.350	15H-6, 65.0	Split core
C18n.2n–C18r	40.084	142.55–142.75	142.650	16H-2, 45.0	Split core
C18r–C19n	41.358	152.55–152.65	152.600	17H-2, 90.0	Split core
C19n–C19r	41.510	154.30–154.35	154.325	17H-3, 112.5	Split core
C19r–C20n	42.536	158.25–159.80	159.025	Between Cores 17H-6 and 18H-1	Split core
C20n–C20r	43.789			Not identified	

Table T24 (continued).

Polarity chron	Age (Ma)	Hole U1333C Range CSF (m)	Best estimate CSF (m)	Best estimate core, section, interval (cm)	Measurement type
C6n–C6r	19.722	1.70–1.75	1.725	2H-1, 12.5	Split core
C6r–C6An.1n	20.040	3.00–3.25	3.125	Between Sections 2H-1 and 2	Split core
C6An.1n–C6An.1r	20.213	3.70–3.75	3.725	2H-2, 62.5	Split core
C6An.1r–C6An.2n	20.439	4.40–4.50	4.450	2H-2, 135.0	Split core
C6An.2n–C6Ar	20.709	5.50–5.60	5.550	2H-3, 95.0	Split core
C6Ar–C6AAn	21.083	7.45–7.70	7.575	Between Sections 2H-4 and 5	Split core
C6AAn–C6AAr.1r	21.159	8.00–8.40	8.200	2H-5, 60.0	Split core
C6AAr.1r–C6AAr.1n	21.403	10.15–10.30	10.225	2H-6, 112.5	Split core
C6AAr.1n–C6AAr.2r	21.483	11.05–11.15	11.100	2H-7, 50.0	Split core
C6AAr.2r–C6AAr.2n	21.659			Not identified	
C6AAr.2n–C6AAr.3r	21.688			Not identified	
C6AAr.3r–C6Bn.1n	21.767	13.85–13.95	13.900	3H-2, 130.0	Split core
C6Bn.1n–C6Bn.1r	21.936	14.65–14.70	14.675	3H-3, 57.5	Split core
C6Bn.1r–C6Bn.2n	21.992	14.90–14.95	14.925	3H-3, 82.5	Split core
C6Bn.2n–C6Br	22.268	16.70–16.75	16.725	3H-4, 112.5	Split core
C6Br–C6Cn.1n	22.564	18.80–18.85	18.825	3H-6, 22.5	Split core
C6Cn.1n–C6Cn.1r	22.754	19.45–19.45	19.450	3H-6, 85.0	Split core
C6Cn.1r–C6Cn.2n	22.902	20.00–20.20	20.100	Between Sections 3H-6 and 7	Split core
C6Cn.2n–C6Cn.2r	23.030			Not identified	Split core
C6Cn.2r–C6Cn.3n	23.278	22.30–22.30	22.300	4H-2, 20.0	Split core
C6Cn.3n–C6Cr	23.340	22.80–22.85	22.825	4H-2, 72.5	Split core
C6Cr–C7n.1n	24.022	26.85–26.85	26.850	4H-5, 25.0	Split core
C7n.1n–C7n.1r	24.062	27.05–27.10	27.075	4H-5, 47.5	Split core
C7n.1r–C7n.2n	24.147	27.60–27.65	27.625	4H-5, 102.5	Split core
C7n.2n–C7r	24.459	29.50–29.70	29.600	Between Sections 4H-6 and 7	Split core
C7r–C7An	24.756			Not identified	
C7An–C7Ar	24.984			Not identified	
C7Ar–C8n.1n	25.110	30.55–30.60	30.575	5H-1, 47.5	Split core
C8n.1n–C8n.1r	25.248	31.90–32.00	31.950	5H-2, 35.0	Split core
C8n.1r–C8n.2n	25.306	32.25–32.30	32.275	5H-2, 67.5	Split core
C8n.2n–C8r	26.032	36.60–36.80	36.700	5H-5, 60.0	Split core
C8r–C9n	26.508	41.00–41.35	41.175	Between Sections 6H-1 and 2	Split core
C9n–C9r	27.412	49.20–49.20	49.200	6H-7, 60.0	Split core
C9r–C10n.1n	27.886	52.50–52.55	52.525	7H-3, 42.5	Split core
C10n.1n–C10n.1r	28.126	54.55–54.65	54.600	7H-4, 100.0	Split core
C10n.1r–C10n.2n	28.164	55.00–55.25	55.125	Between Sections 7H-4 and 5	Split core
C10n.2n–C10r	28.318	56.10–56.15	56.125	7H-5, 102.5	Split core
C10r–C11n.1n	29.166	68.40–68.75	68.575	Between Cores 8H and 9H	Split core
C11n.1n–C11n.1r	29.467	70.80–70.85	70.825	9H-2, 122.5	Split core
C11n.1r–C11n.2n	29.536	71.55–71.60	71.575	9H-3, 47.5	Split core
C11n.2n–C11r	29.957	76.45–76.50	76.475	9H-6, 87.5	Split core
C11r–C12n	30.617	83.15–83.20	83.175	10H-4, 107.5	Split core
C12n–C12r	31.021			Not identified	
C12r–C13n	33.232	107.75–108.15	107.950	Between Cores 13H and 14H	Split core
C13n–C13r	33.705	112.92–112.98	112.950	14H-4, 85.0	Split core
C13r–C15n	35.126	116.98–116.99	116.985	14H-7, 38.0	Split core
C15n–C15r	35.254			Not identified	
C15r–C16n.1n	35.328			Not identified	
C16n.1n–C16n.1r	35.554	118.25–118.35	118.300	15H-1, 120.0	Split core
C16n.1r–C16n.2n	35.643	118.50–118.80	118.650	Between Sections 15H-1 and 2	Split core
C16n.2n–C16r	36.355	123.25–123.40	123.325	15H-5, 22.5	Split core
C16r–C17n.1n	36.668	125.05–125.15	125.100	15H-6, 50.0	Split core
C17n.1n–C17n.1r	37.520			Not identified	
C17n.1r–C17n.2n	37.656	128.00–128.20	128.100	Between Sections 16H-1 and 2	Split core
C17n.2n–C17n.2r	37.907	129.45–129.50	129.475	16H-2, 137.5	Split core
C17n.2r–C17n.3n	37.956	129.85–129.90	129.875	16H-3, 27.5	Split core
C17n.3n–C17r	38.159	130.95–131.00	130.975	16H-3, 137.5	Split core
C17r–C18n.1n	38.449	131.55–131.65	131.600	17H-1, 50.0	Split core
C18n.1n–C18n.1r	39.554	140.35–140.40	140.375	17H-7, 27.5	Split core
C18n.1r–C18n.2n	39.602	140.75–140.80	140.775	Between Cores 17H and 18H	Split core
C18n.2n–C18r	40.084	143.02–143.12	143.070	18H-3, 70.0	Split core
C18r–C19n	41.358			Not identified	
C19n–C19r	41.510	155.30–155.40	155.350	20H-1, 125.0	Split core
C19r–C20n	42.536	159.45–159.55	159.500	20H-4, 90.0	Split core
C20n–C20r	43.789	161.50–161.70	161.600	Between Sections 20H-5 and 6	Split core

Table T25. Interstitial water data from squeezed whole-round samples, Hole U1333A. (See table notes.)

Core, section, interval (cm)	Depth CSF (m)	pH	Alkalinity (mM)	Cl^- (mM)	Na^+ (mM)	SO_4^{2-} (mM)	HPO_4^{2-} (µM)	H_4SiO_4 (µM)	Mn^{2+} (µM)	Fe^{2+} (µM)	Ca^{2+} (mM)	Mg^{2+} (mM)	B (µM)	Sr^{2+} (µM)	Ba^{2+} (µM)	Li^+ (µM)	K^+ (mM)
320-U1333A-																	
1H-2, 145–150	2.95	7.54	2.09	559	481	27.4	1.11	398	0.22	BDL	10.0	51.5	442	83.0	1.23	27.5	11.0
1H-5, 145–150	7.45	7.62	4.00	557	ND	26.3	0.58	398	ND	ND	ND	ND	ND	ND	ND	ND	ND
2H-2, 145–150	12.45	7.54	2.75	562	483	27.2	0.24	504	0.35	0.29	10.5	52.1	446	84.1	1.18	25.6	11.0
2H-5, 145–150	16.95	7.59	2.82	561	488	28.0	0.64	551	0.31	BDL	10.2	50.2	474	84.5	1.09	26.8	10.8
3H-2, 145–150	21.95	7.60	2.79	563	489	27.8	0.56	595	0.21	BDL	10.3	50.6	485	86.6	1.09	26.8	11.3
3H-5, 145–150	26.45	7.59	2.80	562	485	26.2	0.52	561	0.44	BDL	10.0	50.2	453	85.5	1.25	25.0	10.9
4H-2, 145–150	31.45	7.60	2.83	562	485	27.3	ND	622	0.49	BDL	10.4	51.1	464	85.2	1.10	24.7	11.2
4H-5, 145–150	35.95	7.60	2.83	561	480	26.6	0.50	622	0.42	BDL	10.5	52.2	458	86.8	1.19	24.9	11.3
5H-2, 145–150	40.95	7.60	2.85	565	487	26.3	1.23	598	0.21	BDL	10.2	51.3	448	85.9	1.27	23.5	11.1
5H-5, 145–150	45.45	7.64	2.98	565	485	26.7	0.34	621	0.20	BDL	10.5	52.2	476	93.0	1.31	24.5	11.2
6H-2, 145–150	50.45	7.81	2.87	563	481	25.1	0.35	602	0.51	BDL	10.4	52.1	435	86.3	1.22	22.0	11.1
6H-5, 145–150	54.95	7.51	3.48	566	488	26.3	0.74	639	0.62	BDL	10.2	51.6	453	91.7	1.32	23.4	10.8
7H-3, 140–150	61.40	7.48	4.50	565	489	26.3	0.29	681	0.17	1.27	10.3	51.0	466	92.9	1.17	23.1	10.9
8H-3, 140–150	70.70	7.51	3.02	563	481	26.9	0.54	611	0.36	BDL	10.8	53.2	454	93.4	1.14	22.5	11.2
9H-3, 140–150	80.40	7.45	1.66	562	481	26.4	0.56	639	0.84	BDL	10.5	52.0	448	91.4	1.08	21.5	11.0
10H-3, 140–150	89.90	7.46	2.37	562	481	26.2	0.57	653	0.92	BDL	10.7	52.0	450	96.8	1.16	21.9	10.8
11X-2, 140–150	97.90	7.48	3.35	563	481	25.6	0.61	676	1.24	BDL	10.9	52.0	455	99.9	1.20	22.4	10.8
12X-3, 140–150	105.10	7.46	3.21	562	479	26.1	0.63	676	1.27	BDL	11.2	52.4	448	103.4	1.21	22.2	11.0
13X-3, 140–150	114.70	7.54	3.44	564	482	25.8	0.78	714	2.18	BDL	11.3	51.8	465	104.6	1.35	23.0	10.6
14X-3, 140–150	124.40	7.47	3.22	558	480	26.9	0.65	749	0.32	BDL	11.2	51.1	465	103.5	1.23	22.2	10.6
15X-3, 140–150	134.00	7.59	2.80	562	481	25.2	0.48	852	0.34	BDL	11.3	50.7	429	95.2	1.16	21.6	10.3
16X-3, 140–150	143.60	7.60	2.79	563	482	26.1	0.77	775	2.04	0.73	11.6	51.2	422	95.0	1.28	23.2	10.5
17X-3, 140–150	153.20	7.51	3.34	564	483	25.7	0.80	786	0.58	BDL	11.4	51.5	457	105.3	1.47	25.6	10.2
18X-1, 140–150	159.80	7.56	3.63	565	484	27.0	0.67	807	3.12	0.62	11.9	52.3	454	104.0	1.61	26.4	10.6
19X-2, 140–150	170.90	7.60	3.50	566	482	25.5	0.58	737	1.25	0.91	11.7	52.3	460	104.5	1.49	24.1	10.5

Notes: ND = not determined. BDL = below detection limit (HPO_4^{2-} = 0.6 µM, Mn^{2+} = 0.17 µM, Fe^{2+} = 0.24 µM, B = 2 µM, Sr^{2+} = 0.1 µM, Ba^{2+} = 0.24 µM, Li^+ = 0.1 µM) calculated as three times the standard deviation of multiple measures of a blank. H_4SiO_4 values measured by different techniques during Expeditions 320 and 321disagree significantly, especially for low values. Therefore, caution should be used concerning the H_4SiO_4 data and comparison between the different expeditions.

Table T26. Inorganic geochemistry of solid samples, Hole U1333A. (See table notes.)

Core, section, interval (cm)	Depth CSF (m)	Major element oxide (wt%)										Trace element (ppm)							
		SiO_2	Al_2O_3	Fe_2O_3T	MnO	MgO	CaO	Na_2O	K_2O	TiO_2	P_2O_5	Ba	Cr	Cu	Sc	Sr	V	Y	Zr
320-U1333A-																			
1H-2, 65–66	2.15	44.49	6.05	3.61	0.80	2.23	18.08	4.43	1.23	0.27	0.68	6848	25.6	599	18.8	991	34.7	139.7	126.3
1H-4, 65–66	5.15	6.45	0.22	0.39	0.05	0.32	40.31	1.18	0.10	0.01	BDL	696	BDL	60	0.6	1981	BDL	16.3	15.9
4H-5, 65–66	35.15	25.53	2.29	1.51	0.30	0.98	36.47	2.30	0.62	0.11	0.32	2166	6.1	178	6.3	1779	11.3	58.1	51.8
8H-7, 35–36	75.65	7.08	0.17	0.34	0.04	0.26	40.71	1.08	0.09	0.01	0.19	786	BDL	59	BDL	1773	BDL	14.2	20.1
13X-2, 55–56	112.35	22.40	2.11	1.60	0.11	0.88	34.24	2.09	0.55	0.09	0.32	2347	BDL	177	6.1	1821	4.8	47.4	46.2
13X-4, 85–86	115.65	38.52	2.30	2.49	0.26	1.20	25.61	2.38	0.59	0.11	0.46	3189	9.4	237	7.8	989	10.4	69.1	58.3
13X-5, 65–66	116.95	65.12	2.58	3.33	0.47	1.51	9.92	2.98	0.70	0.11	0.45	4137	9.3	281	8.7	453.6	18.8	81.6	68.2
15X-3, 65–66	133.25	22.33	0.42	1.86	0.38	0.79	33.48	1.45	0.25	0.02	0.25	1904	6.0	169	1.2	1214	11.8	25.6	26.7
16X-3, 64–65	142.84	73.68	0.87	4.88	1.61	1.71	0.53	2.91	0.41	0.04	0.26	2373	5.8	357	4.2	129.5	52.8	39.2	34.4
19X-3, 36–37	171.36	74.94	0.83	5.00	1.75	2.14	0.57	2.60	0.47	0.04	0.29	3042	BDL	479	5.2	140.2	49.2	45.2	39.3
20X-CC	180.12	7.41	0.87	0.55	0.08	1.10	40.69	0.35	0.30	0.03	0.43	BDL	BDL	44	1.0	392.6	BDL	45.3	15.6

Notes: BDL = below detection limit (SiO_2 = 3.5 wt%, Al_2O_3 = 0.04 wt%, Fe_2O_3 T = 0.003 wt%, MnO = 0.0004 wt%, MgO = 0.007 wt%, CaO = 0.1 wt%, Na_2O = 0.02 wt%, K_2O = 0.004 wt%, TiO_2 = 0.001 wt%, P_2O_5 = 0.1 wt%, Ba = 28 wt%, Cr = 5 wt%, Cu = 16 wt%, Sc = 0.4 wt%, Sr = 3 wt%, V = 4 wt%, Y = 1.7 wt%, Zr = 4 wt%). See Table T9 in the "Methods" chapter for maximum values of calibration.

Table T27. Calcium carbonate and organic carbon data, Site U1333. (See table notes.)

Core, section, interval (cm)	Depth CSF (m)	Carbon (wt%)			
		$CaCO_3$	IC	TC	TOC
320-U1333A-					
1H-1, 65–66	0.65	31.41	3.77	3.34	0.05
1H-2, 65–66	2.15	26.38	3.17	ND	ND
1H-3, 65–66	3.65	68.88	8.27	ND	ND
1H-4, 65–66	5.15	88.40	10.61	ND	ND
1H-5, 65–66	6.65	81.70	9.81	ND	ND
1H-6, 65–66	8.15	84.32	10.12	ND	ND
1H-7, 45–46	9.45	87.56	10.51	ND	ND
2H-1, 65–66	10.15	90.33	10.84	ND	ND
2H-2, 65–66	11.65	93.33	11.20	10.83	BDL
2H-3, 65–66	13.15	73.77	8.86	ND	ND
2H-4, 65–66	14.65	82.37	9.89	ND	ND
2H-5, 55–56	16.05	82.64	9.92	ND	ND
2H-6, 65–66	17.65	57.81	6.94	ND	ND
2H-7, 20–21	18.70	88.27	10.60	10.08	BDL
3H-1, 65–66	19.65	83.75	10.05	9.86	0.04
3H-2, 65–66	21.15	79.08	9.49	ND	ND
3H-3, 65–66	22.65	63.72	7.65	ND	ND
3H-4, 65–66	24.15	67.62	8.12	ND	ND
3H-5, 65–66	25.65	83.05	9.97	ND	ND
3H-6, 65–66	27.15	64.95	7.80	ND	ND
3H-7, 20–21	28.20	84.50	10.14	ND	ND
4H-3, 65–66	32.15	87.93	10.56	10.21	BDL
4H-4, 65–66	33.65	71.15	8.54	ND	ND
4H-5, 65–66	35.15	63.96	7.68	ND	ND
4H-6, 65–66	36.65	85.10	10.22	ND	ND
4H-7, 65–66	38.15	89.03	10.69	ND	ND
5H-1, 99–100	38.99	88.20	10.59	ND	ND
5H-2, 99–100	40.49	81.83	9.82	ND	ND
5H-3, 99–100	41.99	92.19	11.07	ND	ND
5H-4, 99–100	43.49	88.42	10.62	ND	ND
5H-5, 99–100	44.99	91.21	10.95	ND	ND
5H-6, 99–100	46.49	91.24	10.95	10.68	0.04
5H-7, 25–26	47.25	87.11	10.46	ND	ND
6H-3, 65–66	51.15	85.74	10.29	9.97	0.04
6H-4, 65–66	52.65	86.72	10.41	ND	ND
6H-5, 85–86	54.35	96.18	11.55	ND	ND
6H-6, 65–66	55.65	85.85	10.31	ND	ND
6H-7, 20–21	56.70	88.12	10.58	ND	ND
7H-2, 65–66	59.15	87.61	10.52	ND	ND
7H-3, 65–66	60.65	88.41	10.61	ND	ND
7H-4, 65–66	62.15	92.51	11.11	10.37	0.05
7H-5, 65–66	63.65	89.02	10.69	ND	ND
7H-6, 65–66	65.15	92.24	11.07	ND	ND
7H-7, 20–21	66.20	90.30	10.84	ND	ND
8H-2, 65–66	68.45	90.63	10.88	ND	ND
8H-3, 65–66	69.95	88.70	10.65	ND	ND
8H-4, 65–66	71.45	83.33	10.00	ND	ND
8H-5, 65–66	72.95	89.58	10.75	10.35	BDL
8H-6, 65–66	74.45	92.56	11.11	ND	ND
8H-7, 35–36	75.65	90.98	10.92	ND	ND
9H-1, 65–66	76.65	92.59	11.12	ND	ND
9H-2, 65–66	78.15	89.72	10.77	ND	ND
9H-3, 65–66	79.65	85.56	10.27	ND	ND
9H-4, 65–66	81.15	89.25	10.71	ND	ND
9H-5, 65–66	82.65	91.90	11.03	ND	ND
9H-6, 65–66	84.15	91.50	10.98	ND	ND
9H-7, 45–46	85.45	82.24	9.87	9.21	0.04
10H-1, 65–66	86.15	75.53	9.07	ND	ND
10H-2, 65–66	87.65	77.95	9.36	ND	ND
10H-3, 65–66	89.15	87.57	10.51	ND	ND
10H-4, 65–66	90.65	75.60	9.08	10.40	BDL
10H-5, 65–66	92.15	82.66	9.92	ND	ND
10H-6, 65–66	93.65	81.36	9.77	ND	ND
10H-7, 31–32	94.81	83.94	10.08	ND	ND
11H-1, 110–111	96.10	87.86	10.55	ND	ND
11H-2, 65–66	97.15	85.30	10.24	9.98	BDL
11H-3, 65–66	98.65	82.74	9.93	ND	ND
11X-4, 65–66	100.15	80.62	9.68	ND	ND
12X-1, 65–66	101.35	77.50	9.30	ND	ND
12X-2, 65–66	102.85	76.78	9.22	ND	ND
12X-3, 65–66	104.35	70.33	8.44	7.73	0.04
12X-4, 65–66	105.85	83.33	10.00	ND	ND
12X-5, 65–66	107.35	77.53	9.31	9.04	0.04
13X-1, 75–76	111.05	85.65	10.28	ND	ND
13X-2, 55–56	112.35	67.42	8.09	ND	ND
13X-3, 65–66	113.95	29.14	3.50	3.24	0.04
13X-4, 85–86	115.65	43.76	5.25	ND	ND
13X-5, 65–66	116.95	12.84	1.54	ND	ND
13X-6, 65–66	118.45	29.42	3.53	ND	ND
13X-7, 25–26	119.55	59.63	7.16	6.40	BDL
14X-1, 65–66	120.65	40.89	4.91	4.84	0.03
14X-2, 65–66	122.15	39.83	4.78	ND	ND
14X-3, 65–66	123.65	27.97	3.36	ND	ND
14X-4, 65–66	125.15	12.56	1.51	1.28	0.04
14X-5, 65–66	126.65	8.79	1.05	ND	ND
14X-6, 65–66	128.15	55.52	6.67	ND	ND
14X-7, 21–22	129.21	13.92	1.67	ND	ND
15X-1, 65–66	130.25	46.20	5.55	5.44	0.03
15X-2, 65–66	131.75	74.42	8.93	ND	ND
15X-3, 65–66	133.25	68.98	8.28	ND	ND
15X-4, 65–66	134.75	35.87	4.31	4.14	0.03
15X-5, 65–66	136.25	66.00	7.92	ND	ND
15X-6, 65–66	137.75	21.86	2.62	ND	ND
16X-1, 64–65	139.84	6.10	0.73	0.46	0.04
16X-2, 64–65	141.34	5.14	0.62	ND	ND
16X-3, 64–65	142.84	0.05	0.01	ND	ND
16X-4, 64–65	144.34	10.50	1.26	1.13	0.04
16X-5, 64–65	145.84	9.61	1.15	ND	ND
16X-6, 64–65	147.34	47.84	5.74	ND	ND
17X-1, 65–66	149.45	62.72	7.53	7.39	0.04
17X-2, 65–66	150.95	62.84	7.54	ND	ND
17X-3, 65–66	152.45	61.15	7.34	ND	ND
17X-4, 65–66	153.95	57.16	6.86	6.75	0.05
17X-5, 65–66	155.45	42.76	5.13	ND	ND
17X-6, 65–66	156.95	44.08	5.29	ND	ND
17X-7, 20–21	158.00	30.74	3.69	ND	ND
18X-1, 66–67	159.06	39.41	4.73	4.67	0.04
18X-2, 66–67	160.56	45.12	5.42	ND	ND
18X-3, 66–67	161.40	16.79	2.02	ND	ND
18X-4, 66–67	162.90	61.90	7.43	7.63	BDL
19X-1, 65–66	168.65	42.66	5.12	5.20	BDL
19X-2, 65–66	170.15	22.95	2.75	ND	ND
19X-3, 36–37	171.36	0.20	0.02	ND	ND
19X-4, 58–59	173.08	75.91	9.11	9.12	0.04
19X-5, 29–30	174.29	78.98	9.48	ND	ND
20X-1, 64–65	178.24	75.95	9.12	ND	ND
20X-2, 64–65	179.74	77.89	9.35	9.45	0.03
20X-CC	180.12	90.18	10.83	ND	ND
320-U1333B-					
1H-1, 65–66	0.65	0.08	0.01	ND	ND
1H-2, 65–66	2.15	0.12	0.01	ND	ND
1H-3, 65–66	3.65	75.34	9.04	ND	ND
20X-3, 92–93	176.22	73.41	8.81	ND	ND
20X-4, 88–89	177.68	86.96	10.44	ND	ND

Notes: IC = inorganic carbon, TC = total carbon, TOC = total organic carbon determined by acidification method. BDL = below detection limit ($CaCO_3$ = <1 wt%, TOC by either method = <0.03 wt%) as determined by three times the standard deviation of replicate measures of a low concentration sample. ND = not determined.

Table T28. Moisture and density measurements, Hole U1333A.

Core, section, interval (cm)	Depth CSF (m)	Water content (%)	Density (g/cm^3)			Porosity (%)
			Wet bulk	Dry bulk	Grain	
320-U1333A-						
1H-1, 75–76	0.75	73.1	1.24	0.33	2.82	88.2
1H-2, 75–76	2.25	68.7	1.26	0.40	2.62	84.9
1H-3, 75–76	3.75	64.2	1.34	0.48	3.01	84.0
1H-4, 75–76	5.25	39.4	1.65	1.00	2.73	63.3
1H-5, 75–76	6.75	45.3	1.56	0.86	2.77	69.1
1H-6, 75–76	8.25	40.9	1.64	0.97	2.79	65.3
1H-7, 55–56	9.55	40.8	1.66	0.99	2.93	66.3
2H-1, 75–76	10.25	38.6	1.61	0.99	2.53	60.8
2H-2, 75–76	11.75	40.2	1.64	0.98	2.76	64.4
2H-3, 75–76	13.25	51.6	1.46	0.71	2.66	73.4
2H-4, 75–76	14.75	46.3	1.56	0.84	2.84	70.5
2H-5, 75–76	16.25	44.1	1.55	0.86	2.58	66.6
2H-7, 30–31	18.80	42.0	1.60	0.93	2.69	65.5
3H-1, 75–76	19.75	45.4	1.58	0.86	2.88	70.0
3H-2, 75–76	21.25	47.4	1.52	0.80	2.70	70.3
3H-3, 75–76	22.75	53.5	1.44	0.67	2.72	75.4
3H-4, 75–76	24.25	49.6	1.52	0.77	2.91	73.6
3H-5, 75–76	25.75	44.4	1.57	0.87	2.72	67.9
3H-6, 75–76	27.25	54.9	1.38	0.62	2.43	74.3
3H-7, 30–31	28.30	44.5	1.57	0.87	2.72	68.1
4H-7, 30–31	37.80	45.3	1.55	0.85	2.68	68.5
5H-1, 95–96	38.95	44.5	1.60	0.89	2.89	69.3
5H-2, 75–76	40.25	40.7	1.61	0.95	2.63	63.8
5H-3, 75–76	41.75	54.6	1.33	0.60	2.06	70.8
5H-4, 75–76	43.25	32.7	1.79	1.20	2.80	57.1
5H-5, 75–76	44.75	40.1	1.67	1.00	2.89	65.5
5H-6, 75–76	46.25	38.0	1.66	1.03	2.69	61.8
5H-7, 30–31	47.30	35.7	1.73	1.11	2.80	60.3
6H-1, 55–56	48.05	30.6	1.95	1.35	3.25	58.4
6H-2, 104–105	50.04	38.8	1.70	1.04	2.92	64.4
6H-3, 75–76	51.25	40.8	1.61	0.95	2.66	64.2
6H-4, 85–86	52.85	32.1	1.89	1.29	3.15	59.2
6H-5, 75–76	54.25	35.3	1.73	1.12	2.78	59.7
6H-6, 75–76	55.75	40.4	1.68	1.00	2.98	66.3
6H-7, 30–31	56.80	38.6	1.65	1.01	2.67	62.1
7H-3, 75–76	60.75	30.5	1.86	1.29	2.89	55.4
7H-4, 75–76	62.25	38.7	1.69	1.03	2.86	63.8
7H-5, 75–76	63.75	38.9	1.63	1.00	2.62	61.9
7H-7, 30–31	66.30	34.8	1.73	1.13	2.73	58.7
8H-2, 75–76	68.55	39.4	1.67	1.01	2.82	64.1
8H-4, 75–76	71.55	41.4	1.63	0.95	2.78	65.7
8H-5, 75–76	73.05	38.2	1.66	1.03	2.72	62.1
8H-6, 75–76	74.55	44.3	1.53	0.85	2.53	66.3
8H-7, 45–46	75.75	35.9	1.69	1.08	2.66	59.2
9H-1, 75–76	76.75	27.2	2.00	1.45	3.10	53.0
9H-2, 75–76	78.25	36.2	1.70	1.09	2.73	60.3
9H-3, 75–76	79.75	33.5	1.81	1.20	2.95	59.1
9H-4, 75–76	81.25	35.5	1.70	1.10	2.68	59.0
9H-5, 75–76	82.75	43.5	1.52	0.86	2.45	64.8
9H-6, 75–76	84.25	34.2	1.74	1.14	2.72	58.0
9H-7, 55–56	85.55	18.6	2.46	2.00	3.60	44.5
10H-1, 75–76	86.25	42.0	1.63	0.95	2.86	67.0
10H-2, 75–76	87.75	38.4	1.70	1.05	2.87	63.6
10H-3, 75–76	89.25	38.8	1.66	1.01	2.72	62.8
10H-4, 75–76	90.75	37.5	1.67	1.05	2.70	61.3
10H-5, 75–76	92.25	38.6	1.70	1.04	2.89	63.9
10H-6, 75–76	93.75	41.5	1.61	0.94	2.70	65.2
10H-7, 40–41	94.90	34.5	1.72	1.13	2.69	58.0
12X-2, 75–76	102.95	46.4	1.54	0.83	2.75	70.0
12X-3, 75–76	104.45	49.0	1.50	0.77	2.72	71.8
12X-4, 75–76	105.95	38.8	1.65	1.01	2.70	62.6
12X-5, 75–76	107.45	43.5	1.69	0.95	3.39	71.8
13X-2, 60–61	112.40	56.7	1.41	0.61	2.77	78.0
13X-3, 75–76	114.05	66.3	1.26	0.43	2.33	81.7
13X-4, 75–76	115.55	60.1	1.33	0.53	2.38	77.8
13X-5, 75–76	117.05	65.3	1.30	0.45	2.60	82.7
14X-1, 75–76	120.75	53.7	1.42	0.66	2.60	74.7
14X-2, 75–76	122.25	55.7	1.40	0.62	2.62	76.3
14X-3, 75–76	123.75	64.8	1.28	0.45	2.35	80.9
14X-4, 75–76	125.25	63.5	1.26	0.46	2.13	78.4
14X-5, 75–76	126.75	53.2	1.44	0.67	2.65	74.7
14X-6, 75–76	128.25	53.8	1.43	0.66	2.69	75.3
14X-7, 30–31	129.30	59.8	1.34	0.54	2.45	78.1
15X-1, 75–76	130.35	74.8	1.21	0.30	2.61	88.4
15X-2, 75–76	131.85	47.2	1.52	0.80	2.67	70.0
15X-3, 75–76	133.35	43.9	1.59	0.89	2.77	67.9
15X-4, 75–76	134.85	55.9	1.43	0.63	2.85	77.9
15X-5, 75–76	134.85	46.0	1.57	0.85	2.86	70.4
15X-6, 75–76	136.35	58.1	1.33	0.56	2.24	75.2
15X-7, 75–76	137.85	68.0	1.22	0.39	2.07	81.1
16X-1, 75–76	139.95	63.3	1.31	0.48	2.48	80.7
16X-2, 75–76	141.45	71.9	1.19	0.33	2.00	83.3
16X-3, 75–76	142.95	59.4	1.31	0.53	2.20	75.8
16X-4, 75–76	144.45	59.7	1.35	0.54	2.51	78.4
16X-5, 75–76	145.95	64.1	1.31	0.47	2.58	81.8
16X-7, 30–31	148.50	26.5	1.81	1.33	2.50	46.8
17X-1, 75–76	149.55	41.6	1.69	0.99	3.17	68.9
17X-2, 75–76	151.05	55.4	1.41	0.63	2.64	76.2
17X-5, 75–76	155.55	60.4	1.26	0.50	1.97	74.6
17X-6, 75–76	157.05	57.9	1.36	0.57	2.47	76.8
17X-7, 30–31	158.10	57.8	1.37	0.58	2.56	77.4
18X-2, 75–76	160.65	55.5	1.41	0.63	2.63	76.2
18X-3, 70–71	161.44	59.6	1.37	0.55	2.72	79.7
18X-4, 75–76	162.99	42.9	1.57	0.89	2.61	65.7
19X-1, 75–76	168.75	47.5	1.48	0.78	2.47	68.6
19X-2, 75–76	170.25	46.3	1.56	0.84	2.81	70.3
19X-3, 75–76	171.75	59.9	1.37	0.55	2.81	80.4
19X-4, 75–76	173.25	27.3	1.91	1.39	2.85	51.1
20X-1, 75–76	178.35	30.7	1.79	1.24	2.69	53.8

Table T29. Split-core *P*-wave velocity measurements, Hole U1333A.

Core, section	Depth CSF (m)	Velocity (m/s)		
		x-axis	*y*-axis	*z*-axis
320-U1333A-				
1H-1	1.45	1579		
1H-1	5.93	1552		
1H-5	7.30			1505
1H-5	7.39	1569		
1H-6	8.74	1570		
1H-6	8.83			1508
1H-6	8.94		1513	1848
2H-1	10.89			1509
2H-1	10.97	1580		
2H-2	12.34			1505
2H-2	12.42	1567		
2H-3	13.88		1521	
2H-3	13.94	1579		
2H-4	15.36		1518	1512
2H-4	15.45	1577		
2H-5	16.90	1568		
2H-6	18.36		1517	1504
2H-6	18.46	1608		
2H-7	19.25		1519	1512
2H-7	19.32	1575		
3H-1	20.45	1564		
3H-2	21.90	1581		
3H-3	23.34		1514	1458
3H-3	23.45	1571		
3H-4	24.88		1514	1506
3H-4	25.12	1563		
3H-5	26.40	1571		
3H-5	27.11		1514	1508
3H-6	27.85		1382	1508
3H-6	27.95	1572		
3H-7	28.59		1523	1515
4H-1	29.85		1516	1516
4H-1	29.95	1580		
4H-2	31.36		1411	
4H-2	31.42	1583		
4H-3	32.88		1517	
4H-3	32.95	1575		
4H-4	34.45	1569		
4H-5	35.82		1511	1508
4H-5	35.91	1580		
4H-6	37.38		1516	1510
4H-6	37.46	1571		
4H-7	38.26		1511	1510
4H-7	38.34	1576		
5H-1	39.37		1509	1451
5H-1	39.47	1590		
5H-2	40.85		1524	
5H-2	40.92	1606		
5H-3	42.36		1518	1521
5H-3	42.45	1571		
5H-4	43.88		1521	1514
5H-4	43.96	1585		
5H-5	45.33		1520	1514
5H-5	45.40	1584		
5H-6	46.88		1511	1509
5H-6	46.94	1577		
6H-2	50.29		1523	1512
6H-2	50.40	1577		
6H-3	51.95	1563		
6H-4	53.40		1526	1795
6H-4	53.47	1589		
6H-5	54.82		1518	1515
6H-6	56.41		1517	1513
6H-6	56.47	1583		
7H-1	58.38		1531	
7H-1	58.47	1590		
7H-2	59.85		1513	1509
7H-2	59.94	1572		
7H-3	61.26		1513	1510
7H-3	61.35	1573		
7H-4	62.87		1519	1511
7H-4	62.95	1571		
7H-5	64.32		1520	1518
7H-5	64.43	1578		
7H-6	65.86		1532	1530
8H-2	69.12		1517	1467
8H-2	69.22	1597		
8H-3	70.56		1515	1514
8H-3	70.64	1609		
8H-4	72.14		1511	1510
8H-4	72.23	1557		
8H-5	73.64		1517	1510
8H-5	73.72	1564		
8H-6	75.16		1524	1520
8H-6	75.25	1568		
9H-1	77.31		1529	1520
9H-1	77.41	1578		
9H-2	78.86		1525	1520
9H-2	78.94	1597		
9H-3	80.28		1544	1541
9H-3	80.35	1598		
9H-4	81.86		1525	1521
9H-4	81.94	1583		
9H-5	83.37		1533	1521
9H-5	83.44	1595		
9H-6	84.85		1529	1519
9H-6	84.94	1593		
10H-1	86.85		1405	1511
10H-1	86.93	1560		
10H-2	88.36		1521	1510
10H-2	88.43	1581		
10H-3	89.75		1528	1520
10H-3	89.82	1568		
10H-4	91.36		1536	1516
10H-4	91.45	1591		
10H-5	92.88		1537	1529
10H-5	92.96	1604		
10H-6	94.36		1544	1522
10H-6	94.44	1611		
11X-1	96.34		1519	1519
11X-1	96.44	1578		
11X-2	97.76		1524	1523
11X-2	97.84	1581		
11X-3	99.38			1524
11X-3	99.46	1584		
11X-4	100.82		1538	1523
11X-4	100.90	1570		
12X-1	102.08		1535	
12X-1	102.32	1602		
12X-2	103.56		1523	1520
12X-2	103.65	1580		
12X-3	104.98			
12X-3	105.04	1581		
12X-4	106.44		1419	1518
12X-4	106.65	1591		
12X-5	107.76			1477
12X-5	107.84	1603		
13X-1	111.67		1533	1526
13X-1	111.74	1600		
13X-6	119.27	1606		
14X-1	121.44	1579		
14X-2	122.94	1600		
14X-3	124.35	1609		
15X-1	130.99	1594		
15X-1	140.65	1600		
16X-2	142.08	1625		
16X-4	144.98	1611		
16X-5	146.65	1593		
16X-6	148.18	1642		
17X-1	150.25	1585		
17X-2	152.41		1541	
17X-3	153.16	1618		
17X-4	154.51	1605		
17X-5	156.25	1601		
17X-6	157.76	1634		
18X-1	159.76	1639		
18X-2	160.02	1608		
18X-3	162.08	1619		
18X-3	162.15			1498
18X-4	163.66	1606		
19X-1	169.43	1568		
19X-2	170.85	1623		
19X-3	172.44	1605		
20X-1	179.07	1606		

Table T30. Thermal conductivity, Hole U1333A.

Core, section, interval (cm)	Depth CSF (m)	Thermal conductivity (W/[m·K])
320-U1333A-		
1H-3, 115	4.15	0.824
2H-3, 115	13.65	1.080
3H-3, 115	23.15	1.048
4H-3, 115	32.65	1.127
5H-3, 115	42.15	1.307
7H-3, 115	61.15	1.177
8H-3, 115	70.45	1.205
9H-3, 115	80.15	1.344
10H-3, 115	89.65	1.215
11X-3, 115	99.15	1.129
12X-3, 115	104.85	1.083
13X-2, 115	112.95	0.993
14X-3, 115	124.15	0.830
15X-3, 115	133.75	0.974
16X-3, 115	143.35	0.780
17X-3, 115	152.95	1.046
18X-3, 115	161.89	0.830

Table T31. Shipboard core top, composite, and corrected composite depths, Site U1333.

Core	Depth CSF (m)	Offset (m)	Top depth (m)	
			CCSF-A	CCSF-B
320-U1333A-				
1H	0.00	4.66	4.66	4.05
2H	9.50	3.68	13.18	11.46
3H	19.00	6.84	25.84	22.47
4H	28.50	6.57	35.07	30.50
5H	38.00	7.80	45.80	39.83
6H	47.50	9.75	57.25	49.79
7H	57.00	11.30	68.30	59.39
8H	66.50	13.38	79.88	69.47
9H	76.00	15.73	91.73	79.77
10H	85.50	17.36	102.86	89.44
11X	95.00	18.77	113.77	98.93
12X	100.70	19.45	120.15	104.48
13X	110.30	21.65	131.95	114.74
14X	120.00	21.91	141.91	123.40
15X	129.60	21.33	150.93	131.24
16X	139.20	21.33	160.53	139.59
17X	148.80	21.33	170.13	147.94
18X	158.40	21.33	179.73	156.29
19X	168.00	21.33	189.33	164.63
20X	177.60	21.33	198.93	172.98
21X	181.60	21.33	202.93	176.46
22X	182.60	21.33	203.93	177.33
320-U1333B-				
1H	0.00	0.00	0.00	0.00
2H	7.70	0.01	7.71	6.70
3H	17.20	2.07	19.27	16.76
4H	26.70	3.18	29.88	25.99
5H	36.20	3.98	40.18	34.94
6H	45.70	5.84	51.54	44.82
7H	55.20	8.03	63.23	54.98
8H	64.70	8.77	73.47	63.88
9H	74.20	9.93	84.13	73.16
10H	83.70	13.21	96.91	84.27
11H	93.20	15.33	108.53	94.37
12H	102.70	16.80	119.50	103.91
13H	112.20	17.85	130.05	113.09
14H	121.70	19.75	141.45	123.00
15H	131.20	20.86	152.06	132.23
16H	140.70	20.86	161.56	140.49
17H	150.20	20.86	171.06	148.75
18H	159.70	20.86	180.56	157.01
19X	162.70	20.86	183.56	159.62
20X	172.30	20.86	193.16	167.96
320-U1333C-				
1H	0.00	0.00	0.00	0.00
2H	1.60	2.30	3.90	3.39
3H	11.10	2.66	13.76	11.96
4H	20.60	3.28	23.88	20.76
5H	30.10	6.55	36.65	31.87
6H	39.60	6.53	46.13	40.11
7H	49.10	9.13	58.23	50.63
8H	58.60	10.90	69.50	60.43
9H	68.10	13.24	81.34	70.73
10H	77.60	14.81	92.41	80.36
11H	87.10	14.60	101.70	88.43
12H	93.10	17.13	110.23	95.86
13H	98.10	17.00	115.10	100.09
14H	107.60	20.20	127.80	111.13
15H	117.10	20.50	137.60	119.65
16H	126.60	20.66	147.26	128.05
17H	131.10	20.63	151.73	131.94
18H	140.60	20.63	161.23	140.20
19H	150.10	20.63	170.73	148.46
20H	154.10	20.63	174.73	151.94
21H	163.20	20.63	183.83	159.85
22X	163.20	20.63	183.83	159.85
23X	172.80	20.63	193.43	168.20
24X	176.00	20.63	196.63	170.98

Table T32. Splice tie points, Site U1333. (See table notes.)

Hole, core, section, interval (cm)	Depth (m)			Hole, core, section, interval (cm)	Depth (m)	
	CSF	CCSF-A			CSF	CCSF-A
320-				320-		
U1333B-1H-5, 22	6.22	6.22	Tie to	U1333A-1H-2, 6	1.56	6.22
U1333A-1H-5, 76	6.76	11.42	Tie to	U1333B-2H-3, 71	11.41	11.42
U1333B-2H-6, 31	15.51	15.51	Tie to	U1333C-3H-2, 26	12.86	15.51
U1333C-3H-6, 63	19.23	21.88	Tie to	U1333B-3H-2, 111	19.81	21.88
U1333B-3H-6, 93	25.63	27.70	Tie to	U1333C-4H-3, 82	24.42	27.70
U1333C-4H-5, 83	27.43	30.70	Tie to	U1333B-4H-1, 82	27.52	30.70
U1333B-4H-6, 35	34.55	37.73	Tie to	U1333C-5H-1, 108	31.18	37.73
U1333C-5H-5, 98	37.08	43.63	Tie to	U1333B-5H-3, 45	39.65	43.63
U1333B-5H-5, 93	43.13	47.11	Tie to	U1333C-6H-1, 98	40.58	47.11
U1333C-6H-4, 131	45.41	51.94	Tie to	U1333B-6H-1, 40	46.10	51.94
U1333B-6H-6, 130	54.50	60.35	Tie to	U1333A-6H-3, 9	50.59	60.35
U1333A-6H-5, 106	54.56	64.32	Tie to	U1333B-7H-1, 109	56.29	64.32
U1333B-7H-6, 96	63.66	71.69	Tie to	U1333C-8H-2, 69	60.79	71.69
U1333C-8H-7, 23	67.83	78.73	Tie to	U1333B-8H-4, 76	69.96	78.73
U1333B-8H-6, 81	73.01	81.78	Tie to	U1333A-8H-2, 59	68.39	81.78
U1333A-8H-4, 46	71.26	84.65	Tie to	U1333C-9H-3, 31	71.41	84.65
U1333C-9H-4, 21	72.81	86.05	Tie to	U1333B-9H-2, 41	76.11	86.05
U1333B-9H-6, 105	82.75	92.69	Tie to	U1333A-9H-1, 95	76.95	92.69
U1333A-9H-3, 140	80.40	96.13	Tie to	U1333C-10H-3, 72	81.32	96.13
U1333C-10H-6, 29	85.39	100.21	Tie to	U1333B-10H-3, 29	86.99	100.21
U1333B-10H-6, 131	92.51	105.73	Tie to	U1333A-10H-2, 137	88.37	105.73
U1333A-10H-7, 3	94.53	111.88	Tie to	U1333B-11H-3, 36	96.56	111.88
U1333B-11H-5, 103	100.23	115.56	Tie to	U1333A-11X-2, 29	96.79	115.56
U1333A-11X-4, 14	99.64	118.40	Tie to	U1333C-13H-3, 30	101.40	118.40
U1333C-13H-7, 26	107.36	124.36	Tie to	U1333B-12H-4, 36	107.56	124.36
U1333B-12H-6, 143	111.63	128.43	Tie to	U1333C-14H-1, 63	108.23	128.43
U1333C-14H-3, 33	110.93	131.13	Tie to	U1333B-13H-1, 108	113.28	131.13
U1333B-13H-5, 146	119.66	137.51	Tie to	U1333A-13X-4, 106	115.86	137.51
U1333A-13X-6, 89	118.69	140.34	Tie to	U1333C-15H-2, 125	119.85	140.34
U1333C-15H-5, 125	124.35	144.85	Tie to	U1333B-14H-3, 40	125.10	144.85
U1333B-14H-7, 45	131.15	150.90	Append			

Notes: Spliced section ends at 150.95 m CCSF-A. Sampling below this depth will not recover a complete stratigraphic sequence and can continue in any of the holes at Site U1333 below 150.95 m CCSF-A.

Table T33. Magnetostratigraphic and biostratigraphic datums, Site U1333. (See table note.) (Continued on next page.)

Event	Age (Ma)	Depth CCSF-A (m)	Error (m)
C6n–C6r	19.722	2.61	
C6r–C6An.1n	20.040	4.14	
C6An.1n–C6An.1r	20.213	5.85	
C6An.1r–C6An.2n	20.439	6.73	
C6An.2n–C6Ar	20.709	7.88	
C6Ar–C6AAn	21.083	9.93	
C6AAn–C6AAr.1r	21.159	10.56	
C6AAr.1r–C6AAr.1n	21.403	12.67	
C6AAr.1n–C6AAr.2r	21.483	13.59	
C6AAr.2r–C6AAr.2n	21.659	15.04	
C6AAr.2n–C6AAr.3r	21.688	15.94	
C6AAr.3r–C6Bn.1n	21.767	16.54	
C6Bn.1n–C6Bn.1r	21.936	17.38	
C6Bn.1r–C6Bn.2n	21.992	17.64	
C6Bn.2n–C6Br	22.268	19.52	
C6Br–C6Cn.1n	22.564	21.62	
C6Cn.1n–C6Cn.1r	22.754	22.16	
C6Cn.1r–C6Cn.2n	22.902	23.00	
C6Cn.2n–C6Cn.2r	23.030	23.82	
C6Cn.2r–C6Cn.3n	23.278	25.62	
C6Cn.3n–C6Cr	23.340	26.21	
C6Cr–C7n.1n	24.022	30.24	
C7n.1n–C7n.1r	24.062	30.46	
C7n.1r–C7n.2n	24.147	31.04	
C7n.2n–C7r	24.459	33.09	
C7r–C7An	24.756	35.11	
C7An–C7Ar	24.984	36.23	
C7Ar–C8n.1n	25.110	37.41	
C8n.1n–C8n.1r	25.248	38.55	
C8n.1r–C8n.2n	25.306	38.85	
C8n.2n–C8r	26.032	43.31	
C8r–C9n	26.508	47.15	
C9n–C9r	27.412	55.99	
C9r–C10n.1n	27.886	61.47	
C10n.1n–C10n.1r	28.126	64.31	
C10n.1r–C10n.2n	28.164	64.93	
C10n.2n–C10r	28.318	66.19	
C10r–C11n.1n	29.166	79.00	
C11n.1n–C11n.1r	29.467	84.11	
C11n.1r–C11n.2n	29.536	84.87	
C11n.2n–C11r	29.957	90.69	
C11r–C12n	30.617	98.40	
C12n–C12r	31.021	102.02	
C12r–C13n	33.232	126.56	
C13n–C13r	33.705	133.10	
C13r–C15n	35.126	137.07	
C15n–C15r	35.254	137.40	
C15r–C16n.1n	35.328	138.50	
C16n.1n–C16n.1r	35.554	139.06	
C16n.1r–C16n.2n	35.643	139.54	
C16n.2n–C16r	36.355	143.85	
C16r–C17n.1n	36.668	145.56	
C17n.1n–C17n.1r	37.520	149.97	
C17n.2n–C17n.2r	37.907	150.13	
C17n.2r–C17n.3n	37.956	150.53	
C17n.3n–C17r	38.159	151.63	
C17r–C18n.1n	38.449	152.52	
C18n.1n–C18n.1r	39.554	160.28	
C18n.1r–C18n.2n	39.602	160.81	
C18n.2n–C18r	40.084	163.60	
C18r–C19n	41.358	173.46	
C19n–C19r	41.510	175.58	
C19r–C20n	42.536	180.01	
C20n–C20r	43.789	182.23	

Event	Age (Ma)	Depth CCSF-A (m)	Error (m)
Nannofossils			
B *Sphenolithus disbelemnos*	22.8	20.63	0.75
T *Sphenolithus delphix*	23.1	23.06	0.19
B *Sphenolithus delphix*	23.2	23.31	0.06
T *Sphenolithus ciperoensis*	24.4	42.52	0.75
X *T. longus/T. carinatus*	24.7	35.61	0.16
Tc *Cyclicargolithus abisectus*	24.7	33.29	0.75
T *Sphenolithus distentus*	26.8	48.75	0.75
T *Sphenolithus predistentus*	26.9	50.25	0.75
B *Sphenolithus ciperoensis*	27.1	52.50	1.50
T *Sphenolithus pseudoradians*	28.8	63.95	1.50
B *Sphenolithus distentus*	30.0	95.98	0.75
T *Reticulofenestra umbilicus*	32.0	119.45	0.48
T *Coccolithus formosus*	32.9	124.60	0.75
T *Discoaster saipanensis*	34.4	136.00	0.35
T *Chiasmolithus grandis*	37.1	150.91	0.80
B *Dictyococcites bisectus*	38.0	158.38	0.75
T *Chiasmolithus solitus*	40.4	166.18	0.75
T *Nannotetrina*	42.3	179.26	0.53
B *Reticulofenestra umbilicus* >14 µm	42.5	180.95	0.62
T *Nannotetrina fulgens*	43.4	184.82	0.37
B *Nannotetrina fulgens*	46.8	200.29	0.63
B *Sphenolithus furcatolithoides*	45.8	201.19	0.26
B *Nannotetrina*	48.0	201.19	0.26
Radiolarians			
B *Stichocorys delmontensis*	20.68	8.71	1.50
T *Theocyrtis annosa*	21.38	12.39	2.19
B *Calocycletta virginis*	21.39	12.39	2.19
T *Eucyrtidium mitodes*	21.95	17.22	1.50
B *Cyrtocapsella cornuta*	22.26	20.99	2.26
B *Cyrtocapsella tetrapera*	22.35	20.99	2.26
T *Artophormis gracilis*	22.62	20.99	2.26
T *Dorcadospyris cyclacantha*	22.98	27.41	0.99
T *Liriospyris longicornuta*	24.12	29.90	1.50
T *Acrocubus octopylus*	24.38	33.56	2.16
T *Lychnocanoma apodora*	24.5	33.56	2.16
B *Liriospyris longicornuta*	25.29	40.64	1.50
B *Dorcadospyris scambos*	25.33	40.64	1.50
T *Dorcadospyris circulus*	26.17	43.66	1.52
T *Eucyrtidium plesiodiaphanes*	26.4	53.41	2.05
T *Lithocyclia angusta*	27.68	62.71	1.50
T *Theocyrtis setanios*	28.21	65.62	1.41
B *Theocyrtis annosa*	28.33	75.80	2.05
Tristylospyris triceros > Dorcadospyris ateuchus	28.60	75.80	2.05
B *Eucyrtidium mitodes*	29.41	83.77	1.50
B *Dorcadospyris circulus*	29.96	95.79	1.50
T *Theocyrtis tuberosa*	30.13	102.70	1.10
T *Lithocyclia crux*	30.13	102.70	1.10
B *Eucyrtidium plesiodiaphanes*	30.37	102.70	1.10
B *Dorcadospyris spinosa*	30.84	117.73	1.50
T *Dorcadospyris pseudopaplilio*	30.84	117.73	1.50
T *Centrobotrys gravida*	30.89	119.58	0.36
T *Lithocyclia aristotelis* gr.	33.51	134.12	0.26
T *Calocyclas hispida*	33.62	134.12	0.26
T *Cryptocarpium ornatum*	33.62	133.56	0.30
T *Lophocyrtis hadra*	33.75	134.68	0.17
T *Lychnocanoma amphitrite*	33.75	134.12	0.26
T *Lychnocanoma babylonis*	33.75	134.75	0.24
Lithocyclia aristotelis > Lithocyclia angusta	33.82	134.44	0.07
B *Lithocyclia angusta*	34.13	135.36	0.36
T *Cryptocarpium azyx*	35.07	136.71	0.99
T *Thyrsocyrtis tetracantha*	35.30	137.88	0.19
B *Lophocyrtis hadra*	35.34	137.29	0.12
B *Calocyclas bandyca*	36.74	145.60	1.50

Table T33 (continued).

Event	Age (Ma)	Depth CCSF-A (m)	Error (m)
B *Lophocyrtis jacchia*	37.06	145.87	1.50
B *Cryptocarpium azyx*	37.52	149.54	2.17
T *Dorcadospyris anastasis*	38.45	152.84	1.13
B *Calocyclas turris*	38.67	152.84	1.13
B *Lithocyclia aristotelis* group	39.73	158.43	2.04
B *Podocyrtis goetheana*	40.16	164.58	1.50
T *Lophocyrtis biaurita*	40.36	171.55	1.14
T *Podocyrtis trachodes*	41.23	174.18	1.49
B *Cryptocarpium ornatum*	42.10	177.74	2.05
B *Sethochytris triconiscus*	42.40	180.24	0.45
T *Eusyringium lagena*	42.69	182.61	1.92
B *Theocyrtis perpumila*	42.97	182.61	1.92
Podocyrtis sinuosa > *Podocyrtis mitra*	43.84	187.78	2.60
T *Podocyrtis phyxis*	44.44	192.00	1.63
B *P. ampla*	44.77	192.00	1.63
Podocyrtis phyxis > *Podocyrtis ampla*	44.77	192.00	1.63
Foraminifers			
B *Paragloborotalia kugleri*	23.0	19.15	4.10
B *Paragloborotalia pseudokugleri*	25.2	26.53	0.66
T *Paragloborotalia opima*	26.9	54.96	1.62
B *Globigerina angulisuturalis*	29.2	79.16	5.40
T *Subbotina angiporoides*	29.8	86.52	0.94
T *Turborotalia ampliapertura*	30.3	83.15	6.38
B *Paragloborotalia opima*	30.8	101.25	1.50

Note: B = bottom, T = top, X = abundance crossover, Tc = top common.

Table T34. Results from APCT-3 temperature profiles, Hole U1333B. (See table notes.)

Core	Temperature (°C) Average at mudline	Minimum above mudline	Depth DSF (m)	In situ temperature (°C)	Thermal resistance (m^2K/m)
320-U1333B-					
3H	1.516	1.442	26.7	2.52	28.1
5H	1.622	1.450	45.7	3.43	44.3
7H	1.516	1.441	64.7	4.05	60.2
9H	1.509	1.436	83.7	4.55	75.5
Average:	1.541	1.442			

Notes: In situ temperatures were determined using the TP-Fit software by Martin Heesemann. Thermal resistance was calculated from thermal conductivity data (see "Physical properties") corrected for in situ conditions (see "Downhole measurements" in the "Methods" chapter).